PREDICTED RADIATION DOSE AND RISK ASSOCIATED WITH PEDIATRIC DIAGNOSTIC X-RAY PROCEDURES

By

KATHLEEN M. HINTENLANG

A DISSERTATION PRESENTED TO THE GRADUATE SCHOOL
OF THE UNIVERSITY OF FLORIDA IN PARTIAL FULFILLMENT
OF THE REQUIREMENTS FOR THE DEGREE OF
DOCTOR OF PHILOSOPHY

UNIVERSITY OF FLORIDA

1998

Copyright 1998

by

Kathleen M. Hintenlang

This dissertation is dedicated to my daughter, Lauren Lea Hintenlang, and my son, Hunter Austin Hintenlang, for bringing the goals of this research that much closer to home. To my husband David, je t'aime.

ACKNOWLEDGMENTS

The undertaking of this dissertation reminded me of the following koan:

When the mouth wants to speak about it, words fail.

When the mind seeks affinity with it, thought vanishes.

I would like to express my deepest appreciation and gratitutde to the following people who made the thoughts and words come together: to Drs. Larry Fitzgerald and Tom Crisman at the University of Florida for their unending support, to Dr. Randy Carter in Statistics, without whom statistics would be numbers with no physical meaning, and to Drs. Emmett Bolch and Jon Williams for their continual guidance. Again and always, immortalis ago gratias vobis agamque. I would also like to thank the Shands at UF radiology staff for their encouragement and assistance. Additional recognition is due Drs. Wes Bolch and David Hintenlang; with their assistance, my idea germinated into a seed and then sprouted many branches. I would like to acknowledge the support I received from the Children's Miracle Network and the Shands Medical Guild. Sincere appreciation is extended to my director in the EH&S Division, Dr. Bill Properzio, and to my assistant director, Don Munroe, not only for the professional development but also for the growth of a fast friendship. Heartfelt thanks go to my own staff in the Health Center office.

I would like to extend my greatest thanks to my family: Mom and Dad, Tom and Rachael, Rob and Terry, and Mike and Venessa, for their continued love and support.

Finally, my most sincere and personal thanks go to my husband, David, for his loving patience, understanding and staunch encouragement.

To quote the words written on a monastery wall in the Middle Ages: "The book is finished. Let the writer play."

TABLE OF CONTENTS

page

LIST OF TABLES

LIST OF FIGURES

Abstract of Dissertation Presented to the Graduate School
of the University of Florida in Partial Fulfillment of the
Requirements for the Degree of Doctor of Philosophy

PREDICTED RADIATION DOSE AND RISK ASSOCIATED WITH PEDIATRIC DIAGNOSTIC X-RAY PROCEDURES

By

Kathleen M. Hintenlang

December 1998

Chairman: W. Emmett Bolch Jr.
Major Department: Environmental Engineering Sciences

The most effective method of assessing the risks from exposure to radiation is by calculating the individual tissue absorbed doses and subsequently determining the effective dose. The absorbed dose to a specific tissue has traditionally been difficult and time consuming to measure. The effective dose and overall risk are therefore difficult to calculate directly. The problem is compounded in pediatric radiology, where the patient is particularly sensitive to radiation effects, and the body and organ sizes differ greatly from the common adult reference man.

This research developed and applied a new methodology that permitted rapid measurement of the effective dose from x-ray radiation, and the associated risks, to pediatric patients for a variety of plain film diagnostic examinations. The methodology

utilizes an anthropomorphic phantom incorporating direct reading MOSFET dosimetry, allowing the rapid and simple determination of absorbed dose to individual organs. The research integrated clinical examinations, dosimetry measurements and BEIR V risk assessment calculations using a prototype , anthropomorphic phantom of a one-year-old to quantify radiation doses delivered to pediatric patients in clinical radiology exams. Site surveys were performed in ten facilities using several standard exams to determine variations in effective dose related to clinical practice. Recommendations resulting from the site surveys were provided for the optimization of pediatric radiography procedures. Quantitative studies for a variety of examinations were performed at Shands at UF. The effective dose for these procedures ranged from 0.1 mrem for an AP skull exam that utilized thyroid shielding, to 9.2 mrem for an AP upright abdomen exam. The relative leukemia carcinogenic risk ranged from 1.000041 for the skull exam, to 1.002732 for the abdomen exam, with corresponding excess risks from 10^6 exams of 0.005 and 0.3 leukemias per year, respectively. Effective doses and risks for various cancers from all surveyed exams were quantified. These individual examinations provided a significant benefit to the patient with minimal risk. This provided the basis for continuing research to quantify long-term risk assessment to pediatric patients, as well as providing a clinical tool to evaluate the effective dose delivered to these patients from other current and emerging radiology imaging modalities.

CHAPTER 1
INTRODUCTION AND BACKGROUND

General

It is well established that diagnostic x-rays constitute the largest and most widely distributed source of man-made radiation exposure to the general population (NCRP 1987, 1989). While infants and children constitute only about 10% of the total number of radiographic examinations (NCRP 1989), they are the segment of that population at higher risk from potential radiation effects. First, their growing tissues are more susceptible to radiation effects than mature adult tissues (BEIR 1990). Second, their skeletons encompass a greater fractional distribution of active bone marrow, an organ of high radiation sensitivity (ICRP 1995). Third, the greater post-exposure lifetimes of infants and children increase the possibility for any radiation-induced effects to manifest. Fourth, children are known to have short attention spans and can be non-cooperative; as a result, they are subject to a greater number and/or longer exposures than adult patients. Finally, pediatric patients frequently have a larger portion of their anatomies located within the x-ray beam than adults in similar exams and projections.

In the course of their care, these young patients may be exposed to a wide variety of x-ray examinations. Conventional radiographs make up three quarters of pediatric radiological examinations performed (Griscom 1996). These examinations yield medical benefits and diagnostic information which must be balanced against potential risks from patient radiation exposure. With ever increasing improvements in clinical care, survival rates for prematurely born infants have risen over the past decade. As these individuals age, they frequently experience additional complications requiring a large number of x-ray

examinations from a variety of imaging modalities. Consequently, these patients may accumulate large radiation doses, the effects of which have not been evaluated since few survived in earlier years. Technological improvements that permit these newborn infants and young children to survive increase the need for clinical decision-making based on 4quantitative assessments of radiation risk.

The fundamental quantity of interest from these examinations is the cumulative absorbed dose to exposed organs. Several studies have focused on average organ doses in adult patients undergoing radiographic procedures, either through computer simulation (Rosenstein 1976a, 1976b, 1988; Jones and Wall 1985; Rosenstein et al. 1992; Stern et al. 1995) or physical measurement (Shleien 1973; Ellis et al. 1975; Chen et al. 1978). Nevertheless, very little current information exists on organ doses from pediatric radiographic projections, particularly for technique factors common to U.S. practice (Beck 1978, 1979; Rosenstein et al. 1979; Zankl et al. 1989; Hart et al. 1996).

The desire to perform a study of the current patient and examination trends in pediatric x-ray practices in the State of Florida and incorporate a direct and simple method to measure organ and effective doses in a pediatric phantom in order to perform a risk assessment was the basis for this research. An epoxy resin based anthropomorphic phantom of a one-year-old child constructed in companion research to this dissertation was utilized (Bower 1997). Site visits were performed at ten hospitals in the State of Florida. Simulated examinations of a series of plain film radiographs were performed by pediatric x-ray technologists on the phantom. Real-time Metal Oxide Semiconductor Field Effect Transistor (MOSFET) dosimeters were inserted into various organ locations in the phantom to obtain point dose measurements of the organ absorbed dose and effective dose measurements in real-time. Subsequent risk assessment calculations were performed utilizing BEIR V methodologies.

In order to facilitate the development and transfer of scientific information for the improvement in the radiologic care of children, the methods developed in this research can

then be utilized to integrate the computational and advanced experimental components and determine organ doses and assess risks to various ages of pediatric patients undergoing a variety of modern diagnostic examinations to include fluoroscopy, computed tomography, cardiac catheterization, computed radiography and digital radiography.

Pediatric Radiology as a Subspeciality

The history of pediatric radiology is the story of the emergence of pediatrics and radiology as individual medical specialties, the growth of each of these specialties, and finally the fusion of these two specialties into the new subspecialty of pediatric radiology, or Roentgenology, as it was called in the early days.

Roentgen's discovery of x-rays in November and December 1895 was announced to the world in January 1896. On February 3, 1896, a fourteen-year-old boy who was thought to have broken his wrist two weeks earlier while skating on the Connecticut River, was brought to Dartmouth College in Hanover, New Hampshire, because they supposedly had one of the best collections of vacuum tubes in the western hemisphere at that time (Spiegel 1995). His wrist was radiographed, with an exposure time of twenty minutes, and the resulting image on the emulsion-coated glass plate "showed the fracture in the ulna very distinctly." In addition to what is considered to be the first clinical radiograph in America, it was also the beginning of pediatric radiology in this hemisphere.

In March of 1896, Dr. E. P. Davis of New York City reported visualizing the trunk of a living infant and the skull of a dead fetus and also recorded images of a fetus examined in utero (Davis 1896). Shortly thereafter, the first recorded observation of disease in children probably belonged to Professor Cox of McGill University, Montreal, Canada, who used a thirty-minute exposure to find a needle embedded in the wrist of a girl of unstated age (Cox 1896). William G. Morton, at a meeting of the County of New York Medical Society held on April 27, 1986, reported that he had already seen the fetal head in

utero and predicted that the time was not far distant when the sex of the fetus in utero would be disclosed Roentgenographically (Caffey 1956). At this meeting, Morton showed lantern slides of an entire fetal skeleton and used the terms "inside-seeing or esography" for Roentgen visualization. In July, a publication listed conditions that the author had successfully shown by x-ray, including pediatric cases of dactylitis and absence of the radii (Codmam 1896).

Radiation injury to children apparently was recognized within a few weeks after the Roentgenology method was instituted, as Dr. W. V. Gage (1896, page 307) of McCook, Nebraska, reported "erythema and finally sloughing of the region penetrated by the rays, which at present is the size of the hand" in a child who was being studied for a foreign body in the stomach. Although this episode was reported in the Medical Record of August 29, 1896, Caffey stated that it is obvious that the actual Roentgen injury must have occurred many weeks earlier during the first months of 1896 (Caffey 1956). It is interesting to note that the spread of Roentgen's discovery was not just limited to large cities, but was also utilized within months of his publication in a community as medically remote as McCook, Nebraska, on the prairie which was still "frontier country" at that time (population 2,346 by the 1890 census). In many of the early reports, there appeared to be a disproportionate prevalence of pediatric cases, probably because x-rays from the available tubes at that time could not penetrate larger subjects. In addition, a majority of the researchers in the initial trial period were not physicians. Sosman (1951, page 552) observed that "by 1900, the x-ray method was being used by physicists, engineers, photographers, some charlatans and a few honest physicians". Caffey added bicycle repair men and the entrepreneurs of circus sideshows to this observation.

After this initial burst of enthusiasm after Roentgen's discovery, Caffey reports that American pediatric radiology lagged significantly behind the growth of both radiology and pediatrics and failed to progress until the 1930s, as demonstrated by the limited number of publications. In the Transactions of the American Roentgen Ray Society,

number of publications. In the Transactions of the American Roentgen Ray Society, established in 1901, no pediatric subject was discussed until 1904, when Preston M. Hickey of Detroit reported his Roentgenologic study of skeletal maturation (Hickey 1904, 1906). In addition to the decreased number of studies being reported, the majority of the case studies published represented superficial subjects. Caffey reported that in 1903, Volume 20 of the Archives of Pediatrics published a total of only four papers on Roentgenologic subjects. The most interesting one, Caffey felt, presented Roentgenologic data by A. C. Cotton purporting to show that wadding of thick diapers between the thighs produced lateral bowing of the femurs. Caffey also reported that in the first volume of the American Journal of Diseases of Children in 1911, a study by Long and Caldwell on the relationship between carpal ossification and mental development was performed with Roentgen prints of the paired hands of twenty-nine subjects, in which the authors concluded that "we can find no relation between the carpal development and the quality of mind" (Caffey 1956, page 440). Caffey noted, with some sarcasm, that this conclusion has stood the test of time. Griscom indicated that the focus was more on techniques and equipment at that time than on the medical components of the radiology of children (Griscom and Jaramillo 1995).

The 1930s, 40s and 50s showed a drastic increase in the number of x-ray studies of large numbers of healthy children from birth through adolescence. Due to the lack of normal standards, Dr. Arial George (1908, page 381) explained that "A thorough knowledge of the normal human anatomy is absolutely necessary, as are its variants. The whole study of disease in children by the Roentgen method rests on this one point. The mistakes in diagnosis by the Roentgen ray method will not be the fault of the Roentgen ray, but the fault of those who are ignorant, and who from lack of training are unable to interpret its findings ." As a result, Boyd performed studies of the normal thymus (1927). Lincoln, Hodges, and Josephi investigated cardiac size in healthy infants (Lincoln and Stillman 1928; Hodges 1933; Josephi 1935). Bouslog and Henderson studied the normal

infantile gastrointestinal tract (Bouslog 1935; Henderson 1942). The normal neonatal skull was studied Roentgenographically by Henderson and Sherman (1946). Rotch called attention to the epiphyses, as studied by x-rays, to indicate the state of bodily maturity in normal standards of growth and development for various age groups (Smith 1951). Caffey published several norms of the skeleton (Caffey 1956).

All of these early attempts to establish normal values were open to criticism as they were based on studies of groups of infants and children. It was felt that more accurate values could be obtained by longitudinal studies in which the same groups of children were investigated as they progressed from birth to maturity. So, from 1925 through 1940, Maresh and Washburn performed serial Roentgenographic observations on one hundred normal infants and children to demonstrate the variation in the size and shape of the respiratory track (Maresh and Washburn 1940). Griscom indicated that at the second meeting of the Society of Pediatric Radiology in 1959, sixteen case studies were presented (Griscom 1995). About half dealt with plain films, the remainder with intravenous urography, barium studies, nuclear medicine and dosimetry. This was the first instance where dosimetry for pediatric x-rays is mentioned in the literature. Dr. Donald Darling, from the Children's Hospital in Pittsburgh, presented a progress report entitled "Measurement of Gonadal Dose in Routine Pediatric Radiological Practice." Dr. Darling indicated that results were never published from this study (personal communication, 1998).

Rationale

The organs to be considered in radiologic risk assessment were standardized by the International Commission on Radiological Protection in 1977 with the introduction of the effective dose equivalent (EDE) (ICRP 1977). Calculations of the EDE require knowledge of the absorbed dose (total energy deposited per unit mass) to the following

tissues: breasts, lungs, reproductive tissues (ovaries or testes), thyroid, active bone marrow, skeletal endosteum and unspecified remainder tissues. These absorbed doses, or more specifically, dose equivalents,[1] are then multiplied by tissue weighting factors (w_T) which represent the fraction of total radiation risk (cancer mortality and severe genetic damage) attributed to irradiation of that tissue. The EDE is calculated as a summation of these weighted doses and thus represents a single radiation dose proportional to the total radiation risk of the exposure, regardless of whether the irradiation is uniformly or nonuniformly delivered.

This dosimetry concept was further expanded in 1990 with the introduction of the effective dose (E) in which tissue weighting factors were reassessed based on a more recent analysis of radiobiological effects (ICRP 1991). Additional weighting factors were also given for the esophagus, stomach wall, colon, liver, skin and urinary bladder wall. While originally defined for radiation protection purposes, these quantities of EDE and E have been widely reported in the medical literature for both nuclear medicine procedures and for diagnostic radiology examinations. Their intended use in medicine is to provide physicians with a unified quantity for risk communication and a quantitive means for procedure optimization. As defined in ICRP Publications 26 and 60, the tissue weighting factors are specific only to populations of adults and should not be applied in the estimation of radiation risk to individual patients (Poston 1993). For use in risk communication and/or procedure optimization, tissue weighting factors specific for children have been proposed by Almen and Mattsson (1996).

The determination of organ doses in diagnostic radiology is typically a two-step process. First, an indicator dosimetry quantity is measured in the clinical setting. Examples include the entrance skin exposure (ESE), the entrance skin dose (ESD) or the dose-area product (DAP). Second, these indicator quantities must be multiplied by an

---

[1] Dose equivalent is defined as the product of an absorbed dose and a radiation weighting factor which for photons is set to unity.

organ dose coefficient to obtain individual organ doses (i.e. mrad per R) (Rosenstein 1988). These conversion factors are obtained either through experimental measurement within physical phantoms or through computer simulations within mathematical models of the patient. The specific procedures involved in obtaining the conversion factors utilized in this research are discussed in Chapter 3, Radiation Measurement Equipment and Techniques.

Adult Organ Doses in Plain Film Radiography

The first systematic study of organ dose coefficients was published by Rosenstein in 1976 in Food and Drug Administration (FDA) Reports 76-8030 (Rosenstein 1976b) and 76-8031 (Rosenstein 1976a). In this study, the Fisher-Snyder mathematical model of the adult male was modified for use in determining organ doses for a variety of diagnostic x-ray projections. This model was previously developed for estimates of internal photon absorbed fractions needed for nuclear medicine dosimetry (Snyder et al. 1978). The model consisted of geometrical descriptions of eighteen internal organs of the adult and included three distinct tissue compositions: soft tissue, skeleton (a homogenized mixture of bone and marrow) and lung (a homogenized mixture of soft tissue and air). While the model was developed as a description of Reference Man defined in ICRP Publication 23 (1975), it was a hermaphrodite in that it included both testes and a uterus and ovaries.

In order to reduce computational requirements, the following approach was utilized. Organ doses were first determined for parallel, collimated beams of monoenergetic photons incident on the surface of the mathematical model. Each photon beam was situated on one grid of a system of 4 cm x 4 cm grid elements superimposed upon the front surface of the model (AP projection), back surface of the model (PA projection), or on a plane just inside the arm bones (lateral projection) to simulate the actual conditions of exposure in which the arm is generally moved out of the primary

beam. Organ doses for a given examination (e g AP chest) were determined by first summing the individual dose contributions from each grid element contained within the field-of-view, and then energy weighting these results for the x-ray spectrum of interest. By using this procedure, beam divergence and air scattering effects were ignored and oblique views were not accommodated. These data were subsequently used to produce a handbook providing organ doses per unit entrance skin exposure free-in-air (mrad/R) to the testes, ovaries, thyroid and active bone marrow for sixteen projections and six beam qualities (HVLs of 1.5 to 4.0 mm Al). The field size was assumed to equal the film size in this study. Limited experimental data were collected as part of the study using lithium fluoride thermoluminescent dosimeter's (LiF TLDs) in anthropomorphic phantoms.

A revision to this handbook was published in 1988 which expanded the number of projections considered to fifty-four In addition, Cancer Detriment Indices were also reported for each exam based upon risk data contained in ICRP Publication 45 (1985). In the early 1980s, Gesellschaft für Strahlen und Umweltforschung (GSF) in Germany (Kramer et al. 1982; Drexler et al. 1984) developed their own male and female adult phantoms and the British National Radiological Protection Board (NRPB) (Jones and Wall 1985) further developed the Cristy (1980) modified versions of the original Snyder Medical Internal Radiation Dosimetry (MIRD) mathematical model (Snyder et al. 1969) to assess organ doses to adults in diagnostic radiology.

Pediatric Organ Doses in Plain Film Radiography

A comprehensive and systematic investigation of organ dose coefficients for pediatric radiographic projections was published by Beck and Rosenstein in 1979 as FDA Reports 79-8078 (Beck 1978, 1979) and 79-8079 (Rosenstein et al. 1979). This study included a survey of five hospitals in the Baltimore-Washington area to determine the frequency and types of pediatric radiographic examinations performed and the various

technique factors employed in those exams such as kVp, mAs, field size, SID and beam quality. The survey data were subsequently used to perform computer simulations of the more common projections following methods similar to those employed in the adult report.

Three mathematical models developed at Oak Ridge National Laboratory by Hwang et al. were utilized representing a newborn, a one-year-old, and a five-year-old individual (1976a, 1976b, 1976c). Twenty examinations were considered, each representing at least one percent of the total number of exams in a given age group. For each exam, organ dose coefficients (mrad/R) were determined for testes, ovaries, thyroid, active bone marrow, lungs and total body at one representative source-to-image receptor distance, two field sizes (age dependent) and four beam qualities (HVLs of 2.0, 2.5, 3.0, and 3.5 mm Al). As with the adult report, limited experimental data were collected as part of the study using LiF TLDs in anthropomorphic phantoms representing a head and neck, and two phantoms corresponding to the Monte Carlo mathematical design: a one-year-old and a five-year-old. Given the experimental uncertainties in the TLD measurements and the limited number of photon histories transported (60,000), the authors concluded that good agreement was seen between the two data sets.

To date, no revisions have been made to FDA Reports 79-8078 and 79-8079, and these data are still widely used for dose estimation in pediatric radiology. Several arguments can be made for revising and expanding the research of Beck and Rosenstein. First, while mathematical models did exist for a representative ten-year-old and fifteen-year-old patient, these two groups were notably absent in the final handbook. Second, the input photon spectra used in these reports were for single phase generators, while current radiology practice employs primarily three-phase, constant potential, and high-frequency x-ray units. Third, while the pediatric models of Hwang et al. included twenty-six internal organs, dose estimates were given only for the six organs listed above, thus making calculations of EDE or E impossible. Fourth, substantial revisions and improvements have

been made to the ORNL pediatric model series over the past eighteen years, thus making the dosimetry of FDA reports 79-3030 and 79-3031 obsolete and somewhat inconsistent with current practice in radiology and in radiation protection (Cristy 1980, 1987).

In the Hwang et al. 1976 series of pediatric models, a large number of internal organs were simply scaled downward from the Fisher-Snyder adult model. In 1980, Cristy reported that this procedure resulted in "shifting and crowding" of various internal organs in a manner which did not reflect actual anatomical growth trends (Cristy 1980). As a result, a complete redesign of the ORNL pediatric model series was initiated, resulting in the publication of new pediatric models by Cristy and Eckerman in 1987. These models were subsequently adopted for radiation protection dosimetry by the ICRP in 1989 (ICRP 1989) and for nuclear medicine dosimetry in 1988 by the MIRDOSE computer code maintained by the Radiation Dosimetry Information Center in Oak Ridge, Tennessee (Stabin 1996). These models were the basis upon which a new MIRD family of mathematical models are being developed at the University of Florida in companion research to this dissertation.

Finally, no new pediatric anthropomorphic phantoms have been developed that correspond to the changes made in the MIRD mathematical models. The only other comprehensive source of organ doses for pediatric plain film exams is that produced by the NRPB in 1996 for technique factors specific to the United Kingdom and European Community utilizing the older 1987 version of the Cristy and Eckerman mathematical models (Hart et al. 1996).

Calculation of Energy Imparted in Diagnostic Radiology

One may also estimate radiation risk for diagnostic procedures by measuring the total energy imparted to the patient for a given diagnostic exam (the integral dose). Extensive studies of energy imparted in diagnostic radiology have been performed by

Huda and colleagues (Huda et al. 1989; Huda and Bissessur 1990; Atherton and Huda 1995, 1996; Huda and Atherton 1995; Gkanatsios and Huda 1997; Huda and Gkanatsios 1997). Values of energy imparted, however, in and of themselves do not provide important information on individual organ doses for a given projection or exam. In his publications, Huda proposed the use of approximate ratios of effective dose per unit energy imparted which, in combination with energy imparted on *homogeneous* phantoms, can be used to derive an estimate of the effective dose. These ratios must also be obtained from previous Monte Carlo studies such as those performed by the NRPB (Shrimpton et al. 1991; Hart et al. 1994, 1996) which use *heterogeneous* anthropomorphic models of patients. Huda has recently proposed a simple mass scaling of these ratios to yield effective doses to children undergoing CT exams (Huda et al. 1997). An important limitation of this approach is that individual organ doses can never be recovered from a single value of effective dose and the risk from different diagnostic procedures cannot be compared when different organs are exposed.

It must be remembered that the effective dose is a weighted average of the individual organ doses where the tissue weighting factors are chosen based on the current knowledge of radiation cancer risk and other detriment. This knowledge base changes with time and with changes in cancer mortality; thus the tissue weighting factors are influenced by changing success rates in cancer treatment. Consequently, the tissue weighting factors are always subject to change, whereas the individual organ dose for a specific diagnostic procedure is not. It is for these very reasons that the MIRD committee of the Society of Nuclear Medicine has always maintained a focus on individual organ absorbed dose.

Phantoms

Mathematical

In 1994, companion research to this dissertation was initiated by Dr. Wesley Bolch to couple the complete series of pediatric mathematical models of Cristy and Eckerman to the EGS4 radiation transport code (Nelson et al. 1985) for external sources of radiation. This was additionally performed as a task group effort of the Society of Nuclear Medicine's MIRD Committee to consider, for the first time, detailed transport of electrons and beta particles within internal organs for internal sources of radiation. At ORNL, the Cristy and Eckerman pediatric model series have been used extensively with ALGAM, a radiation code limited only to the consideration of photon transport (Cristy and Eckerman 1987). EGS4 allows for explicit treatment of coupled photon and electron transport (including bremsstrahlung production) and has been extensively utilized in both high energy physics and medical physics research. To verify the coding of the pediatric mathematical models within the framework of the EGS4 code system, several comparisons of specific absorbed fractions of energy were performed with the 1987 data published by Cristy and Eckerman (Kodimer 1995). Excellent agreement was seen over a wide range of photon energies, confirming the transport of photons in the Cristy and Eckerman models using EGS4.

A new mathematical model of the adult head and brain has been published (Bouchet et al. 1996). The model includes a detailed description of the skeletal system including the maxilla, teeth, mandible, cranium and cervical vertebrae. New regions in the brain model include the caudate nucleus, cerebellum, cerebral cortex, lateral ventricles, third ventricle, lentiform nucleus, thalamus and white matter. Other features include eyes and the thyroid enclosed within an explicit neck region (the original head region was modeled simply as an elliptical cylinder topped by half an ellipsoid, with no representation

photon transport, its exclusion artificially attenuates external photon sources depositing dose to the thyroid gland.

Work was initiated in late 1996 to produce a pediatric series of head and brain models based on modification of the adult model and data published on neural tissue growth trends. In June of 1997, the MIRD committee also adopted a series of revisions to the Cristy and Eckerman family of phantoms (Bolch, personal communication, 1997). These revisions included the addition of an esophagus, a prostate gland, a four-region kidney (to include a medulla, cortex, papillary, and pelvic region), a mucosal layer within walled organs (GI tract, gall bladder, and urinary bladder) and the inclusion of a rectum separate from the sigmoid colon within the current models. It is anticipated that upon completion of these revisions, future work will include the Monte Carlo-generated doses being experimentally verified against the MOSFET dosimeter measurements within the various pediatric anthropomorphic phantoms.

Anthropomorphic

ICRU Report 48 defines a phantom as a "structure that contains one or more tissue substitutes and is used to simulate radiation interactions in the body" (ICRU 1993, page 1). They are commonly used to investigate radiographic equipment image quality and dosimetric evaluations. The complexity of phantoms ranges from very simple geometries representing singles tissues such as a slab of water simulating soft tissue or a sheet of copper simulating a chest, to complex geometries with multiple realistic tissue substitutes for soft tissue, lungs and bones. Such complex phantoms are referred to as "anthropomorphic" because they simulate the size, shape and composition of a human body to provide the same attenuation and scattering characteristics.

The majority of anthropomorphic dosimetric phantoms represent an adult man (Conway et al. 1984; Constantinou et al. 1986; Conway et al. 1990; ICRU 1993). As

previously indicated in the discussion of the mathematical models, a scaled-down adult phantom is inappropriate to simulate a child, since the organ growth of a child is a complex process which cannot be described by simply scaling the anatomy of an adult. The anatomical geometry of a child varies greatly from that of an adult. The weight of the head with respect to the total body weight is greater for a child than an adult, the trunk of a child is more cylindrical compared to the elliptical adult trunk, and certain internal organs such as the thymus gland are larger (Hwang et al. 1976a). The percentage of extracellular water in children is larger and represents a higher percentage of the total body weight than in adults (Haschke et al. 1981), and the concentration of certain minerals is lower in the skeleton of children (Haschke et al. 1981; ICRP 1995). In addition, the skeleton of a child has more water and less fat than an adult skeleton (Cristy and Eckerman 1987). Furthermore, the distinction between cortical and trabecular bone and the percent distribution between yellow and red bone marrow change greatly as children age (Cristy and Eckerman 1987). The anthropomorphic pediatric phantoms developed by Chen (Chen et al. 1978) were constructed to represent identically the mathematical models of the one-year-old and the five-year old, which again, were scaled-down versions of adult models.

Due to the lack of pediatric anthropomorphic phantoms in the research community and on the commercial market, research was initiated to construct a prototype one-year-old phantom at the University of Florida (Bower 1997). The one-year-old representation was chosen because a review of the examination frequency data provided by Shands at the University of Florida from the period 1990-present indicated that the majority of pediatric diagnostic x-ray examinations are of children in their first few years of life; therefore, a phantom of a one-year-old would be fairly representative of a large class of examinations. In addition, an anthropomorphic one-year-old phantom has a mass of approximately 10 kg (21 lbs), which is easily manageable for construction and its ultimate use in field testing. The prototype one-year-old anthropomorphic phantom developed by Bower (1997)

utilized in this research is reviewed in detail in Chapter 3, Radiation Measurement Equipment and Techniques.

Radiation Detection Instrumentation

A variety of detection instrumentation has been used to measure radiation exposure or absorbed dose. These include gas filled ionization chambers, radiographic film, semiconductors and thermoluminescent detectors.

Gas Filled Ionization Chambers

Ionization chambers have a response that is proportional to absorbed energy, and, therefore, they are widely used in performing dosimetry measurements. Most ionization chambers are cylindrical with an air-equivalent wall and measure exposure. When radiation interacts with the air in the detector, ion pairs are created and collected generating a small current. Since the Roentgen is defined as the amount of ionization in air, measurement of this ionization current will indicate exposure.

The Keithley TRIAD™ Field Service Kit[2] was used in this research to perform free-in-air exposure measurements in order to calculate entrance skin exposure (ESE) at the location where the x-rays are expected to enter the patient and characterize beam quality for the simulated x-ray examinations.

Semiconductors

A semiconductor detector acts as a solid state ionization chamber, whereby the ionizing particle interacts with atoms in the sensitive volume of the detector to produce electrons by ionization. The elements in semiconductor materials form crystals that

---

[2] Radiation Measurements Division of Keithley Instruments, Inc., 28775 Aurora Road, Cleveland, Ohio, 44139, TRIAD™ Field Service Kit Model 10100A

consist of a lattice of atoms that are joined together by covalent bonds. Absorption of energy by the crystal leads to disruption of these bonds which results in a free electron and a "hole" in the position formerly occupied by the valence electron. This free electron can move about the crystal with ease. The hole can also move about in the crystal, e.g. an electron adjacent to the hole can jump into the hole and therefore leave another hole behind. Connecting the semiconductor in a closed electric circuit results in a current through the semiconductor as the electrons flow towards the positive terminal and the holes flow toward the negative terminal. The operation of a semiconductor radiation detector depends on its having either an excess of electrons or an excess of holes A semiconductor with an excess of electrons is called an *n*-type semiconductor, while one with an excess of holes is called a *p*-type semiconductor (Cember 1996).

In order to assess point estimates of organ doses in the one-year-old phantom, the Patient Dose Verification System designed by Thompson & Nielsen Electronics[3] was utilized. This system is composed of Metal Oxide Semiconductor Field Effect Transistor (MOSFET) dosimeter arrays. The MOSFET is a common microelectronic device. It is a layered device consisting of a *p*-type semiconductor separated from a metal gate by an insulating oxide layer. Ionizing radiation forms electron-hole pairs in the oxide-insulating layer of the MOSFET. The applied bias then causes the electrons to travel to the gate, while the holes migrate to the oxide silicon interface where they are trapped. The trapped positive charges cause a negative shift in the voltage required to allow conduction through the MOSFET. The shift in voltage is proportional to the radiation dose deposited, thus allowing the MOSFET to be used as a dosimeter (Hughes et al. 1988; Gladstone and Chin 1991; Vettese et al. 1996).

This system was originally designed using standard sensitivity dosimeters to measure skin doses during radiation therapy treatments. Characterization of high

---

[3] Thompson & Nielsen Electronics Ltd., 25E Northside Road, Nepean, Ontario, Canada, K2H 8S1, Patient Dose Verification System Model TN-RD-50

sensitivity dosimeters by Bower and Hintenlang (1998) for use in diagnostic radiological applications is detailed in Chapter 3, Radiation Measurement Equipment and Techniques.

Determination of Risk

Radiation risks of diagnostic radiology in the pediatric patient are either deterministic or stochastic in nature. Deterministic radiation injuries, such as tissue injury or cataract production, occur when a number of cells are involved and a threshold dose is required. Above the threshold, the severity of the injury is proportional to the dose. There is no evidence that deterministic injuries occur as a result of low-dose plain film procedures. Stochastic radiation injuries, such as genetic effects and carcinogenesis, are believed to be caused by injury to a single cell and typically a threshold dose is not required. The probability of the injury is proportional to the dose, but the severity of the injury is independent of the dose. If one assumes a linear relation without a threshold for such effects, then any amount of radiation, including low-dose plain film procedures, may potentially have an effect. A more detailed discussion of the linear, no-threshold (LNT) theory is presented in Chapter 4, Risk Asssessment.

Risk models were developed to provide a method of predicting the risk of radiation induced genetic effects and carcinogenesis in relation to the natural incidence in an unirradiated population. The epidemiological ideal of following several populations over time was not practical; therefore, statistical models were used to derive risk estimates. Radiological risk assessments and resulting risk estimates have been developed by numerous organizations, including the National Academy of Science/National Research Council's Fifth Committee on the Biological Effects of Ionizing Radiations (BEIR V, 1990), the United Nations Scientific Committee on the Effects of Atomic Radiation (UNSCEAR, 1988), the International Commission on Radiological Protection (ICRP 60,

1990) and the National Council on Radiation Protection and Measurements (NCRP 115, 1993).

The most recent reassessment of radiation-induced cancer risks from exposure to low levels of ionizing radiation was performed by the BEIR V committee, and this methodology was utilized in performing the calculation of the risk estimate from plain film procedures performed in Chapter 4, Risk Assessment. The BEIR V Report provided mathematical models to estimate risks for breast cancer, respiratory tract cancer, digestive tract cancer, leukemia, and other nonleukemia cancers. These equations include terms for dose, age at exposure, time after exposure and interaction effects. The dose term utilized in these equations is the effective dose calculated from the MOSFET organ dose determinations upon applying the dose conversion factors.

Significance and Objectives

Pediatric radiographic examinations are widely thought to yield medical benefits and/or diagnostic information which greatly exceed any potential risk from patient radiation exposure. Nevertheless, quantification of that risk is important for a number of reasons. First, it allows radiographic procedures to be optimized to maximize the medical benefit while minimizing patient risk. Second, it gives the radiologist a basis for communicating that risk to concerned patients and/or parents. Third, it allows for reconstruction of total risk for individuals who have developed radiation-associated diseases (e.g., leukemia) and who were known to have undergone high-dose or multiple radiographic procedures at an earlier age (i.e., dose reconstruction). In each case, the fundamental quantity of interest is the cumulative absorbed dose to the radiosensitive organs.

As previously discussed, several studies have focused on quantifying average organ doses in adult patients undergoing radiographic procedures, either through

computer simulation or physical measurement. Nevertheless, very little information exists on pediatric organ doses from plain film examinations, and no systematic techniques have been developed to obtain this information for pediatric dynamic procedures such as fluoroscopy, CT or cardiac catheterization. Consequently, the first objective of this research project was to establish a baseline and develop a method for assessing pediatric organ doses for the most frequent plain film procedures used in clinical practice. The second objective was to verify this method for plain film exams through the use of an anthropomorphic phantom representing a one-year-old pediatric patient and coupled to a real-time radiation dosimetry system. The third objective was to utilize the organ doses determined from the anthropomorphic phantom and calculate an effective dose for each plain film procedure. The fourth objective was to utilize the effective dose in the BEIR V methodology to calculate the risk from the procedure. The following specific aims were designed to accomplish these objectives:

1. To determine, via site survey of ten facilities, the current examination trends for one-year-old patients in pediatric x-ray practices in the State of Florida.
2. To determine, utilizing a one-year-old anthropomorphic model providing real-time radiation dosimetry, organ doses to pediatric patients undergoing the most common plain film procedures and calculate corresponding effective doses.
3. To estimate, utilizing BEIR V risk model methodology, the risk to pediatric patients of carcinogenesis from the plain film procedures.

To facilitate specific aim 1, detailed examinations were simulated at Shands at UF in order to focus the site surveys on the most prevalent examinations currently performed in pediatric practices. Technique information for these examinations were collected from all facilities. Due to the time constraint of room downtime, dosimetry data were collected at the ten facilities for the single most prevalent exam; dosimetry data were collected for all examinations simulated at Shands at UF. In specific aim 2, point estimates of organ doses were assessed by selective placement of an array of Metal Oxide Semiconductor

Field Effect Transistors (MOSFET) detectors within the phantom. These measurements for the x-ray procedures utilized the prototype one-year-old anthropomorphic phantom developed by Bower (1997). Specific aim 2 also involved the determination of dose conversions factors (organ absorbed dose per unit entrance skin exposure) for a range of radiographic projections and radiation beam qualities and the calculation of effective doses as defined by the ICRP (1977). The task associated with specific aim 3 used equations developed by BEIR V (1990) to utilize the effective dose calculated in specific aim 2 in order to predict the risk of radiation induced carcinogenesis from the simulated plain film procedures.

These tasks not only update and expand obsolete data on pediatric organ doses from plain film examinations, but establish the method to benchmark experimentally the mathematical models previously discussed and provide a baseline for the organ dose estimation computational and experimental techniques necessary to simulate dynamic pediatric exams. This research provides vital information to the pediatric radiology community in their efforts to assess organ doses and procedure risk from plain film exams both prospectively and retrospectively.

CHAPTER 2
PATIENT AND EXAMINATION TRENDS OF PEDIATRIC X-RAY PRACTICES

A general overview of the range of pediatric x-ray practices was obtained through a site survey of selected facilities within the State of Florida. Ten facilities were selected to represent their cohorts throughout the rest of the State: six facilities represented Children's Hospitals and/or Radiology Departments with dedicated pediatric radiologists, two hospitals represented community patient populations and two hospitals represented rural patient populations. Selection of the number of facilities was not based on statistical considerations, as the purpose of this survey was only to identify and characterize the examinations that are most commonly employed and not establish their precise frequencies in the U.S. population. Private practices were not included in this survey. In addition, more specific information was obtained on a single pediatric radiologic practice during in-depth investigations carried out in the Pediatric section of the Radiology Department at Shands at the University of Florida.

Shands at the University of Florida

Shands at the University of Florida is a 576-bed not-for-profit tertiary care facility. The Children's Hospital at Shands at the University of Florida is a 169-bed hospital-within-a-hospital. The Radiology Department at Shands at UF has a workload of 163,000 examinations per year, approximately six percent of which are for patients under sixteen years of age. In order to determine which examinations to include in the site surveys, examination frequency data specific for pediatrics were extracted from the Radiology Information System (RIS). The RIS provides a computerized patient record from which physicians can call up all the clinical data that they need about a given patient in

alphanumeric text. The review of the RIS ascertained, retrospectively, the frequency and types of x-ray procedures performed as a function of age, and simulations were then performed to determine the important technical parameters of each procedure.

Since the data were to be adapted to five anthropomorphic phantoms and mathematical models, five age groups were defined for the frequency data. These age groups were determined from formulae utilized for approximate average height and weight of normal infants and children that are commonly found in pediatric textbooks (Behrman and Vaughan 1987). These categories are defined in Table 2-1.

Table 2-1. Age Group Corresponding to Phantom

Phantom	Age Group
Newborn	0 to 3 months
One-Year-Old	3 months to 12 months
Five-Year-Old	1 year to 6 years
Ten-Year-Old	7 years to 12 years
Fifteen-Year-Old	13 years to 16 years

The first piece of information extracted from the RIS data was the determination of the types and frequencies of examinations as a function of age. The RIS data file listed all the pediatric radiological examinations performed at Shands at the University of Florida from January 1990 through December 1997. An additional computer program was written to extract the number of examinations performed in a given year, broken out by the age group defined in Table 2-1 from the RIS data file. The file encompassed general radiology (including ultrasound), fluoroscopy, CT, and nuclear medicine examinations. No exam technique information was contained in this file. An example of the file is presented in Table 2-2 illustrating the number of pediatric chest x-rays performed in 1997. The 1997 file in its entirety is located in Appendix A. Prior years were not included as a trend analysis indicated similar distributions of exams.

Table 2-2. Annual Number of Plain Film Chest X-Rays by Age Group

Year	Modality	Exam & Projection	Newborn	1-Year	5-Year	10-Year	15-Year
97	GENERAL	CHEST PA & LATERAL	477	474	1524	665	546
97	GENERAL	CHEST 1 VIEW	3763	797	1713	875	973
97	GENERAL	BABYGRAM (chest & abdomen)	730	30	17	0	0
97	GENERAL	CHEST DECUBITUS LEFT	31	3	18	3	9
97	GENERAL	CHEST DECUBITUS RIGHT	24	3	11	2	8

The frequency of exams was also determined from this file. The frequency is defined as the ratio of a specific exam and projection falling within a modality to the total number of examinations classified for that modality, and is expressed as a percentage. An example of the data is presented in Table 2-3 demonstrating the percent frequency of pediatric chest x-rays performed in 1997. The 1997 percent frequency file in its entirety is located in Appendix B and is tabulated from most to least frequent exam.

Table 2-3. Percent Frequency of Plain Film Chest X-Rays

Year	Modality	Exam & Projection	Newborn	1-Year	5-Year	10-Year	15-Year
97	GENERAL	CHEST PA & LATERAL	8	26	26	16	12
97	GENERAL	CHEST 1 VIEW	65	44	30	21	22
97	GENERAL	BABYGRAM (chest & abdomen)	13	1.7	0.3	0	0
97	GENERAL	CHEST DECUBITUS LEFT	0.5	0.2	0.3	0.07	0.2
97	GENERAL	CHEST DECUBITUS RIGHT	0.4	0.2	0.2	0.05	0.2

The frequency data were further segregated by the principal body region exposed in the examination: head and neck; thorax and shoulder (excluding humerus); abdomen, pelvis and hips; and extremities. The most frequent plain film exams per principal body region were chosen to be included in the dosimetry study. Table 2-4 lists the plain film exams that were surveyed at each facility based on the data for the one-year-old. Extremity examinations were not included in the dosimetry survey for the one-year-old phantom. As demonstrated in Appendix B, the frequency of these exams does not increase until the older age groups when a child has learned to walk and run, and falls occur, with subsequent damage to extremities,. Limitations of phantom design with respect to limb movement also restricted the realism with which such examinations could be simulated. Radiographic components of fluoroscopy examinations were not considered in this research, as it would be more appropriate to include such dose considerations in a

study of the overall fluoroscopic exam dose. Several additional examinations were performed at Shands at UF to investigate the effect of shielding on the resultant dose.

The RIS data file also included the projections used in the examinations. The nomenclature for projections follows that commonly used in radiology (Ballinger 1995). When referring to a radiograph of a body part as seen from the aspect of the x-ray film, this is termed a "view," in which case one refers to the side of the body, or body part, which is closest to the film. For example, in an anterior view of the chest, the patient faces the film; in a left lateral view, the patient's left side is toward the film. A left posterior oblique view is performed with the patient turned with his left back toward the film and his right front away from the film. Generally when the x-ray beam is not incident normally on the patient's front or back, "view" terminology is used, as opposed to "projection" terminology. A "projection" defines the path of the x-ray beam through the body or body part. Thus, in an Anterior-Posterior projection of the chest, the beam enters the front and exits through the back, producing what could correctly be termed a posterior view. In this research, projection orientation is used whenever the beam is normally incident on the front or back ((Anterior-Posterior (AP) or Posterior-Anterior (PA)); view orientation is used for all others, although the term projection is used for uniformity throughout.

Projections are additionally defined in terms of rotation of the patient or part, clockwise from the superior aspect beginning with the patient facing the tube. Thus an AP projection has 0 degree rotation, facing the tube; PA projection has 180 degree rotation, facing the film; LAT projection (lateral projection) has two possibilities: RLAT (right lateral) has 90 degree rotation, with the right side towards the film; and LLAT (left lateral) has 90 degree rotation, with the left side towards the film. The term decubitus is used if the patient is lying down rather than standing up. Obliques are not included in this data set, as the majority of oblique projections are associated with fluoroscopy exams. Additional nomenclature specific for skull and sinus examinations includes "Townes" and "Waters" projections, respectively. The Townes method for radiographing the skull

involves angling the x-ray tube 20 to 25 degrees caudad (beam penetration through the top of the head). The Waters method for radiographing the sinuses involves extending the patient's neck with their chin on the cassette stand.

Table 2-4 Surveyed Examinations

Exam	Projection
Skull	AP
Skull	LAT
Skull	Townes
Sinus	Waters
Sinus	LAT
Cervical spine	AP
Cervical spine	LAT
Thoracic spine	AP
Thoracic spine	LAT
Lumbar spine	AP
Lumbar spine	LAT
Abdomen	AP
Pelvis	AP
Hip	AP
Chest	LAT
Chest	AP
Chest	PA

Ten Florida Facilities

The exposure to pediatric patients during x-ray procedures would be expected to vary from facility to facility. Factors such as equipment setup and operational characteristics, patient classification and procedural techniques are of key importance. To investigate the variation that exists among facilities, a site survey of pediatric x-ray practices in ten Florida hospitals was conducted. The surveys were conducted in cooperation with the radiologist, the administrative director and the pediatric x-ray technologist of the participating facility. One or more of these personnel were present during each site visit and data collection. In addition to Shands at the University of Florida, the following facilities participated in this research:

- Tallahassee Memorial HealthCare

  Tallahassee Memorial HealthCare is located in Tallahassee, Florida and has 736 beds, with a radiology workload of 31,200 procedures per year, approximately one and a half percent of which are estimated to be pediatric.

- University Medical Center, Jacksonville

  University Medical Center is a 528-bed medical center located in Jacksonville, Florida with a radiology workload of 190,000 procedures per year, approximately eight percent of which are estimated to be pediatric.

- Shands at AGH

  Shands at AGH is located in midtown Gainesville, Florida and has 410 beds, with a radiology workload of 72,000 procedures per year, approximately four percent of which are estimated to be pediatric.

- Arnold Palmer Hospital for Children & Women

  Arnold Palmer Hospital for Children & Women is located on the downtown Orlando Regional Healthcare System campus in Orlando, Florida and has 267 beds, with a radiology workload of 33,420 procedures per year, all of which are pediatric.

- All Children's Hospital

  All Children's Hospital is located in St. Petersburg, Florida and has 236 beds, with a radiology workload of 35,930 procedures per year, all of which are pediatric.

- Wolfson Children's Hospital

  Wolfson Children's Hospital is part of the Baptist/St. Vincent's Health System located in Jacksonville, Florida and has 190 beds, with a radiology workload of 41,000 procedures per year, all of which are pediatric.

- Shands at Lake Shore

  Shands at Lake Shore is a 128-bed acute care community hospital located in Lake City, Florida with a radiology workload of 36,000 procedures per year, approximately eight percent of which are estimated to be pediatric.

- Shands at Starke

  Shands at Starke is a 49-bed acute care rural hospital located in Starke, Florida with a radiology workload of 14,780 procedures per year, approximately six percent of which are estimated to be pediatric.

- Shands at Live Oak

  Shands at Live Oak is a 30-bed acute care rural hospital located in Live Oak, Florida with a radiology workload of 18,000 procedures per year, approximately three percent of which are estimated to be pediatric.

The six facilities representing Children's Hospitals and/or Radiology Departments with dedicated pediatric radiologists were Shands at UF, Tallahassee Memorial HealthCare, University Medical Center, Arnold Palmer Hospital for Children & Women, All Children's Hospital and Wolfson Children's Hospital. The two hospitals representing community patient populations were Shands at AGH and Shands at Lake Shore. The two hospitals representing rural patient populations were Shands at Starke and Shands at Live Oak.

Exam Simulations

Per a scheduled appointment approved by the radiologist, initial contact was made with the director of radiology upon arrival at each facility. The purpose and objectives of the research were reiterated and the phantom and dosimetry system demonstrated. Copies of recent news publications about the research were also distributed. The director then assigned a x-ray room and technologist to the research project for 2.5 hours on average. The designated time was requested during appointment scheduling and was approximated based on the time required to carry out the initial characterizations performed at Shands at UF.

After initial set-up of the phantom to perform real-time dosimetry readings as described in Chapter 3, the phantom was turned over to the pediatric x-ray technologist to simulate, as close to clinical practice as possible, the exams listed in Table 2-4 for a one-year old patient. In order for the pediatric x-ray technologist to simulate the x-ray field size, shape and location on the phantom, it was necessary to indicate the locations of certain anatomical landmarks on the phantom that approximated those of an actual one-year-old patient. The anatomical landmarks, which were defined and placed on the phantom during the initial simulations at Shands at UF by Dr. J. Williams, a staff pediatric radiologist, were as follows:

1. Vertex – The top or highest part of the phantom head.
2. External acoustic meatus (EAM) – Defined to be at the horizontal level of the floor of the phantom skull.
3. Sternal Notch – Defined as the point midway between the anterior medial ends of the phantom clavicles.
4. Nipples – Defined to be located on the level midway between the top of the phantom trunk and the inferior margin of the twelfth rib; considered to be the midpoint of the thorax.
5. Xiphoid Process – Defined as the inferior margin of the sternum at the level of the seventeenth rib.
6. Umbilicus – Defined as located at the level midway between the phantom diaphragm and the bottom of the trunk. The umbilicus is considered to be at the midpoint of the abdomen and at the level of the iliac crests.
7. Symphysis Pubis – Defined as located on a level 0.086 times the vertical height of the trunk above the inferior margin of the trunk, whose relative position is taken from the vertex. This point is considered to be located at the superior margin of the pubis.
8. Hip Joint – Defined as lying on a vertical line, originating at the center of the base of the leg bone, one-third of the vertical height of the pelvis, above the floor of the trunk.

The distances of these landmarks from the base of the trunk are listed for the one-year-old phantom in Table 2-5.

Table 2-5. Defined Locations of Anatomical Landmarks on Phantom Vertical Axis with the Origin at the Base of the Trunk (cm)

Landmark	
Vertex	48.5
EAM	39.4
Sternal notch	27.5
Nipples	22.6
Xiphoid process	19.2
Umbilicus	10.6
Hip joint	1.1
Symphysis pubis	0.7

The next section of this chapter describes each exam simulation setup of the phantom patient in detail. The descriptions are based on technologist interviews and visual observations obtained of the best practices at each site for actual patient examinations, supported with the textbook by Kirks and Griscom (1998). Additional descriptions are provided by Ballinger (1995), Bontrager (1997) and Wilmot and Sharko (1987). The left lateral projection was chosen for all lateral examinations for ease in positioning. Images of these examinations are provided in Chapter 5, along with corresponding phantom images.

AP skull

The patient is positioned supine. The midsaggital plane (divides the body into right and left halves) of the skull is kept perpendicular to the tabletop. The orbitomeatal baseline is kept 15 to 20 degrees cephalad from the perpendicular by using a small sponge wedge or roll of diapers behind the patient's neck to provide some support to maintain this position. The orbitomeatal line is a frequently used positioning line located between the outer crease of the eye and the EAM. Several immobilization methods were observed, ranging from Velcro and tape to foam-backed lead "bookends" placed at both sides of the head, as shown in Figure 2-1. Typically, one-year olds are also immobilized using the

"bunny" or "mummy" technique, which consists of tightly wrapping the patient in a blanket to immobilize arms and legs The thyroid was protected by a shadow shield, which is a piece of lead attached to the tube head with an adjustable arm. Note that PA projections are not routinely obtained for this age group, as young children tend to be frightened of being face down.

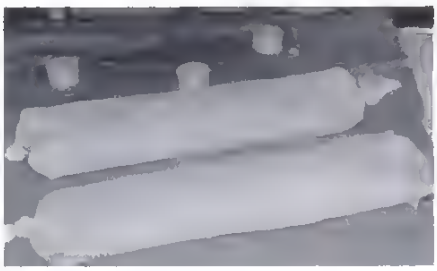

A

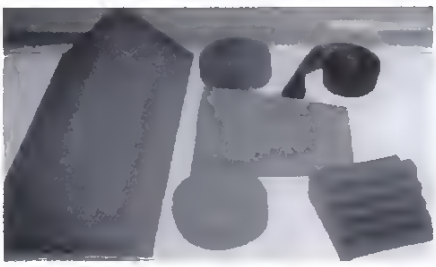

B

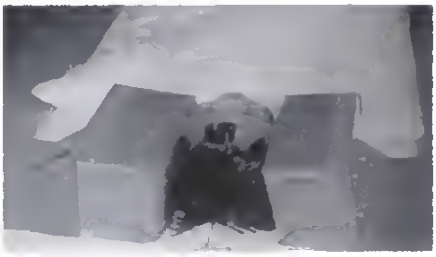

C

Figure 2-1. Items frequently used for immobilization. A: Sandbags, tape, clear Plexiglas strip. B. Sponges of various shapes and sizes, Velcro strap. C: "Bookends"; patient "mummified". Figures A and B reproduced with permission from Lippincott-Raven Publishers. Figure C reproduced with permission from Mosby-Year Book Publishers, Textbook of Radiographic Positioning and Related Anatomy, K L Bontrager (1997).

Lateral skull

The patient is positioned either semiprone or supine. If using a grid, the head is rotated so that the affected side is closest to the film. If a grid is not used, a cross table lateral is performed with a film holder. The unaffected side of the body is elevated from the tabletop using sponges under the neck and shoulders so that the coronal plane (divides

the body into anterior and posterior parts) of the body creates an angle of 45 degrees with the tabletop. The head is positioned in such a way that the midsaggital plane of the skull is parallel to the tabletop, and the interorbital line is perpendicular to the film. The interorbital line is a frequently used positioning line that connects either the pupils or the outer creases of the patient's eyes. The central ray is perpendicular to the midsaggital plane and passes midway between the glabella (the smooth raised prominence between the eyebrows just above the bridge of the nose) and the occipital protuberance (the prominent "bump" at the inferoposterior portion of the skull). Immobilization and shielding techniques were similar to those used in the AP projection, except the foam-backed lead "bookends" were not placed in the field of view.

Townes skull

The patient lies supine on the table so that the orbitomeatal baseline is perpendicular to the tabletop. Visualization of the foramen magnum (the large opening at the base of the occipital bone through which the spinal cord passes as it leaves the brain) may be improved by placing a 20 degree-angled sponge under the skull. For this age group, an additional angled sponge placed under the lower extremities may also assist in positioning by depressing the shoulders and encouraging further flexion of the neck. With the x-ray tube angled 30 to 35 degrees caudal (away from the head end of the body, toward the feet), the central ray enters the frontal bone in the midsagittal plane at the hairline passing through a line connecting both external auditory meatuses and exits through the foramen magnum. An angle of 30 degrees between the orbitomeatal line and the central ray should be achieved. Immobilization and shielding techniques were similar to those used in tbe AP projection. Due to the inability of the phantom's head to articulate for this method, the pediatric technologist compensated by angling the x-ray tube to produce the same projection.

Waters sinus

The patient is examined sitting or standing with the chin and the nose in contact with the film cassette. The patient's mouth is opened during the radiographic procedure. The neck is extended in such a way so that the orbitomeatal baseline forms a 40 to 45 degree angle with the plane of the film so that the midsaggital plane is perpendicular to the cassette. The central ray enters at the posterior sagittal suture (the joint connecting the two parietal bones) just above the occipital protuberance in the midline and runs parallel to the mentomeatle line and exits at the level where the nose and upper lip meet. The mentomeatle line is a frequently used positioning line that connects the midpoint of the chin with the EAM. Again, due to the inability of the phantom's head and jaw to articulate for this method, the pediatric technologist compensated by angling the x-ray tube to produce the same projection.

AP cervical spine

As the patient lies supine on the table, the neck is extended to bring the orbitomeatal baseline to 20 degrees cephalad (toward head end of body) to the vertical. An angled sponge under the patient's shoulders may be used in order to achieve greater extension of the neck. The central ray is kept between 10 to 20 degrees cephalad. The central ray enters at the level of C-4 or at the thyroid cartilage. The field size is adjusted so that the view includes the base of the skull as well as the T-1 vertebrae. A lead lap apron was utilized as shielding.

Lateral cervical spine

If using a grid, the patient is positioned supine. The head is in a true lateral position with the chin raised slightly. The central ray enters the C-4 vertebrae perpendicular to the film cassette. This procedure may be performed either with extension or flexion of the neck depending on the kind of functional study. The field is collimated to include the C-1 to T-2 vertebrae. If a grid is not used, a cross table lateral is performed with a film holder. The patient is placed in a reclined supine position with a sponge placed

under the shoulders. The neck is in a slightly extended position so that the inferior border of the mandible is vertical. The central ray enters approximately 2.5 cm posterior to the angle of the mandible. The field is collimated to include C-1 to T-2 vertebrae. Shielding techniques are similar to those used in the AP projection.

AP thoracic spine

The patient is placed in the supine position. The patient's head rests directly on the table without the support of a pillow. The patient's chin should be slightly raised. The hips and knees should be slightly flexed and the knees supported on a pillow so that the cervical spine will become nearly parallel to the tabletop. Additional restraint is provided by placing sandbags over the elbows and knees, and by placing Velcro restraining bands across the chest, hips, and knees. Additional sandbags may be placed along the sides of the chest and abdomen to further limit movement. The central ray enters at the level of T-6 or approximately 10 cm below the sternal notch. The field is collimated to include C-7 to L-1 vertebrae.

Lateral thoracic spine

The patient is positioned in a true lateral position with the arm closest to the table flexed to bring the hand up under the head. The upper arm also rests on the side of the head. Note that the arms in the phantom are encased in the trunk and cannot be moved. When positioning the patient for the lateral view, the head should be placed on a firm pillow to raise the head and bring the cervical spine into alignment with the thoracic spine. The hips and knees are flexed to provide stability. In order to reduce the lateral curvature and ensure that the thoracic spine is parallel to the tabletop, a sponge should be placed under the patient at the level of the lumbar spine, but above the iliac crests. The arms and legs should be restrained with sandbags and Velcro restraining bands. A bookend support should be placed against the back and against the anterior chest wall to discourage arching of the back. The central ray enters at the level of T-6 just below the inferior angle of the

scapulae. The field is collimated to include C-7 to L-1 vertebrae. The upper 2 or 3 thoracic vertebrae are not well visualized on the standard lateral view.

If upper thoracic vertebrae are of particular interest, a "swimmers" lateral view is performed. The patient is positioned as described above, but the upper arm is brought to rest behind the patient's buttocks and the shoulder is rotated slightly posteriorly. This positioning ensures that neither shoulder will be superimposed on the upper thoracic spine. The central ray enters at the level of T-2 and the field is collimated to include C-7 to T-2 vertebrae. Since the arms in the phantom are encased in the trunk and cannot be moved, this view was not performed.

A "breathing" technique was commonly employed by technologists for lateral thoracic spine radiographs. Rather than waiting for the time of expiration to take an exposure, technologists would routinely have the patient breathe normally, so that the movement would blur the lungs and ribs out.

AP lumbar spine

The patient lies supine with knees and hips flexed and the arms placed to the side. It was unnecessary for the phantom to perform this flexion, as the posterior aspect of the phantom lies immediately adjacent to the tabletop. The midsaggital plane of the body is aligned to the midline of the table. The central ray enters perpendicularly at the level of the iliac crest or at the L-4 to L-5 interspace. The techniques of immobilization already described under the discussion for positioning of the thoracic spine are equally applied in examinations of the lumbar spine.

Lateral lumbar spine

If a cross table lateral is not performed, the patient lies in a lateral recumbent position with a pillow under the head and the knees and hips flexed with support between the knees and ankles. The pelvis and the torso are in a true lateral position. The coronal

plane of the patient is aligned to the midline of the table. The central ray enters perpendicularly at the level of the iliac crest or at the level of the L-4 vertebrae.

AP abdomen

The patient lies supine on the table. The midsaggital plane of the patient is aligned with the center of the table or the film cassette. Immobilization methods that have been previously discussed were utilized, such as Velcro or tape, and foam wedges or sandbags on both sides of the abdomen. The central ray is perpendicular to the film and enters about one inch above the umbilicus for a one-year-old. The exposure should be made at the end of expiration. Upright projections of the abdomen may be clinically required and are performed with immobilization techniques similar to those utilized for upright chest radiography.

AP pelvis

The patient lies supine with legs extended and separated. The legs are internally rotated 15 to 20 degrees. Since the phantom's legs are not attached to the trunk of the body, this positioning does not change the internal anatomy of the phantom. The patient midsagittal plane is aligned with the central ray which enters a point midway between the level of the anterior superior iliac spine (prominent anterior border of the iliac crest) and the superior border of the symphysis pubis. The central ray is perpendicular to the film, and a gonad shield is utilized. It should be mentioned that a "frog-leg" pelvis view is also routinely performed for this age group. In a frog-leg view, the knees and hips are flexed as far as comfortable. Both thighs are abducted as far as possible, and plantar surfaces of the feet are placed together. This view was not performed with the phantom due to the inability of the phantom's joints to articulate.

AP bilateral hip

The patient lies supine with their arms immobilized at their sides or crossed at the chest with the pelvis as symmetrically positioned as possible. The legs are extended and

rotated internally 15 to 20 degrees when a non-trauma patient is being examined. The central ray enters the midline at a point halfway between the anterior superior iliac spine and the symphysis pubis. Both hips are always examined in the same projection on the same film.

A lateral frog-leg hip is routinely performed for this age group. The patient is laid partially oblique with a support under the affected area. The knee on the affected side is flexed, and the thigh is drawn up to a 45 degree angle position. The affected femoral neck is centered to the midpoint of the film cassette. The central ray is perpendicular to the film and enters at the level of the mid-femoral neck This view was not performed with the phantom, due to the inability of the phantom's joints to articulate.

AP, PA and lateral chest

Pediatric chest radiographs are routinely performed upright without a grid. The challenge of performing upright imaging includes preventing motion and rotation, freeing the lung fields of superimposition of chin, humeri and scapulae, and obtaining a good inspiratory radiograph. Various methods of immobilization are used, however, the most common pediatric positioner and immobilization tool utilized is the Pigg-o-stat. The Pigg-o-stat is composed of a large support base on wheels, a small adjustable seat and Plexiglas support sleeves, which come in two sizes. The seat, sleeves, and "turntable" base rotate as a unit to facilitate quick positioning from the PA to the lateral projection.

As shown in Figure 2-2, the child sits on the little bicycle type seat. The plastic support sleeves fit snugly around the sides and keeps the arms raised. The child usually cries with frustration at being confined, but the crying actually helps to obtain a good x-ray image because, at the end of a cry, the child will take a big gasp of air, and at that moment the exposure is taken. The orientation of the room, i.e., where the chest stand or film holder is located relative to the control panel, determines how well the technologist can see the child's thorax to ensure the exposure is made during inspiration. Inspiration

can also be detected by watching the child's abdomen as it extends on inspiration, watching the chest wall as the ribs will be outlined on inspiration and watching the rise and fall of the sternum. The central ray for both PA and lateral projections enters perpendicular to the film at the level of the midthorax T-6/T-7 vertebrae or mammillary (nipple) line. The collimation is adjusted so that all of the ribs are included in the radiograph and should extend from, and include, the mastoid tips to just above the iliac crests. A lead lap apron was utilized as shielding.

Figure 2-2. Infant immobilized and supported by the Pigg-o-stat device for an upright chest film. The device is then rotated 90^0 for a lateral projection. Note the presence of shielding for the pelvis. Figure reproduced with permission from Lippincott-Raven Publishers, Practical Pediatric Imaging: Diagnostic Radiology of Infants and Children, D. R. Kirks and N. T. Griscom (1998).

Radiologists that did not favor the use of the Pigg-o-stat for aesthetic reasons or because of the potential for sleeve artifacts, frequently used a supine pediatric immobilizer referred to as a Tam-em board. This one step immobilization device positions the child with the arms, head and legs immobilized with foam lined Velcro straps to a Plexiglas frame for both an AP projection (with the film located on the tabletop under the frame as

shown in Figure 2-3) and a cross table lateral projection (with the film in a holder as shown in Figure 2-4). This immobilization device was also used when upright positioning was contraindicated.

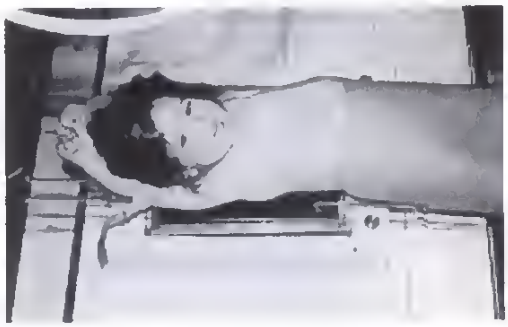

Figure 2-3. Toddler immobilized for an AP chest radiograph on the Tame-Em immobilizer. Velcro bands are placed around the arms and legs; a vinyl sheet of lead covers the lower abdomen and gonads. Figure reproduced with permission from Lippincott-Raven Publishers, Practical Pediatric Imaging: Diagnostic Radiology of Infants and Children, D. R. Kirks and N. T. Griscom (1998).

Figure 2-4. Infant immobilized for a left lateral chest radiograph on a Plexiglas immobilizer. Velcro bands are placed around the arms and head; a vinyl sheet of lead covers the lower abdomen and gonads. Figure reproduced with permission from Mosby-Year Book Publishers, Merrill's Atlas of Radiographic Positions and Radiologic Procedures, P. W. Ballinger (1995).

A variation of this device is an octagonal immobilizer, shown in Figure 2-5, which is an eight-sided immobilization tool that permits visualization in a variety of positions.

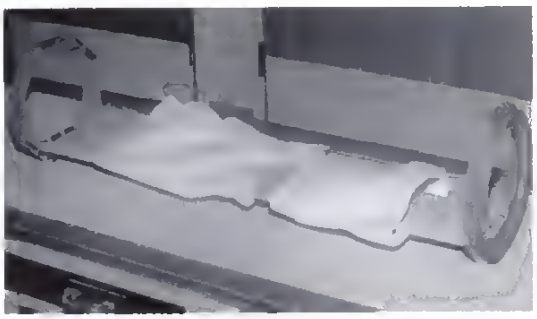

Figure 2-5. Octagon board for immobilization. Figure reproduced with permission from Lippincott-Raven Publishers, Practical Pediatric Imaging: Diagnostic Radiology of Infants and Children, D. R. Kirks and N. T. Griscom (1998).

Survey Data

For future comparison of the measured and simulated effective doses, several parameters from the survey data would need to be correlated. The most important descriptors collected during the exam simulations at each facility included the type of generator, e.g. single phase, three phase, constant potential or high frequency; the collimated size of the x-ray field; the distance from the tube focal spot to the beam entrance point on the skin or surface of the phantom (SSD); the direction of the x-ray beam with respect to the long axis of the phantom (projection); and the quality of the x-ray beam as described by the kVp and half value layer (HVL).

For comparison of technique factors among hospitals, additional parameters were collected from each facility. These parameters included the mode of operation, e.g. manual or automatic exposure controlled (AEC, also called phototiming or amplimatting); the detector configuration of ion chambers that were utilized for AEC-right (R), center (C) and/or left (L) and the density setting ((-3, -2, -1, Normal (N), +1, +2, or +3)); if scatter suppression was used; film size; film/screen speed; the distance from the tube focal spot to the image receptor distance (SID); the output of the x-ray beam as defined by the

milliamperage and time applied (mAs); the focal spot size-large (LFS) or small (SFS); and shielding used. Repeat and reject rate percentages were also collected.

In addition to recording technique parameters during the simulations, several measurements were performed. Higher than normal exposures were taken to ensure reasonable accuracy in the absorbed dose data. After the clinical exam was performed, exposures from an output of 80 mAs were performed. The accuracy of the kVp was verified prior to measuring the HVL. The exposure per mAs was measured at a variety of kVp settings at a given distance in order to compute the entrance skin exposure (ESE), which was subsequently used in the effective dose calculation. X-ray films were obtained for all the chest examinations, and the optical density of the middle of the lung fields on the chest x-rays were quantified with a densitometer and averaged to provide a measure of image quality. All measurements were performed in accordance with procedures recommended by the American Association of Physicists in Medicine (Seibert et al. 1994). The survey data in their entirety are reviewed in Chapter 5 and are tabulated for each exam and projection in Appendix C.

During the initial survey performed at Shands at UF, x-ray films and dosimetry measurements were performed for each examination listed in Table 2-4. During the subsequent site surveys, x-ray films and dosimetry measurements were only performed for the chest examinations in order to decrease room downtime. The chest examinations were chosen for comparison, as they were the most frequently performed examination at each facility.

CHAPTER 3
RADIATION MEASUREMENT EQUIPMENT AND TECHNIQUES

One-Year-Old Anthropomorphic Phantom

Bower successfully constructed a full-scale prototype of a physical heterogeneous phantom to represent the new MIRD one-year-old mathematical model, which included a revised head and neck (1997). This prototype was the phantom utilized for the measurements in the site survey study. The construction entailed several steps. First, processing techniques were developed to produce tissue equivalent materials approximating soft, lung and bone tissues which required the addition of a particulate filler with a moderately high effective atomic number, such as magnesium oxide, to an unfilled liquid resin with a low effective atomic number. The theoretical interaction coefficients (mass attenuation and mass energy-absorption coefficients) were matched between these tissue-equivalent materials and the tissue media used in the 1987 Cristy and Eckerman and MIRD models over the photon energy range 1.5 keV to 150 keV using the computer program XCOM written by Berger and Hubbell at the Center for Radiation Research, National Bureau of Standards (Hubbell 1982). The mass density was adjusted by adding a small quantity of low-density microballoons (hollow gas-filled spheres). This basic process followed that published by White (1977) and further developed by White et al. (1977, 1986) and Herman et al. (1985, 1986).

The soft tissue substitutes were made of materials providing a final elemental composition of 59.2% carbon, 20.6% oxygen, 10.5% magnesium, 7.5% hydrogen, 2.0% nitrogen and 0.10% chlorine by weight. The attenuation and mass energy-absorption coefficients of the tissue-equivalent substitutes were modeled after the atomic

compositions of soft tissue defined in the 1987 models of Cristy and Eckerman and ICRP Publication 23 (1975). These two sets of photon interaction coefficients were in agreement within $\pm$ 3% and were considerably closer at most energies. The soft tissue substitute's photon interaction coefficients were also favorably compared to those given for individual tissues given in ICRU Publication 44 (1989). The soft tissue substitute was modeled to provide the appropriate soft tissue density of 1.04 g/cm^3.

Lung-equivalent materials were manufactured using a foaming agent and a surfactant, similar to the method presented by White et al. (1986). The lung tissue substitutes were made of materials giving an elemental composition of 59.42% carbon, 17.65% oxygen, 12.06% magnesium, 8.24% hydrogen, 1.64% nitrogen, 0.84% silicon and 0.15% chlorine. The lung tissue substitute density was 0.360 g/cm^3, which approximated the lung tissue density of 0.296 g/cm^3 for the mathematical model.

A bone tissue substitute approximating the skeletal tissue of a one-year-old was also produced. Cristy and Eckerman made the following observations concerning the skeleton of the newborn: "The skeleton of the newborn contains more water, less fat, and less mineral than the adult skeleton. Furthermore, the distinction of two bone types, cortical and trabecular bone, is not evident in the newborn skeleton, and the marrow of the skeleton is all active. Thus it is clear that the elemental composition of the adult skeleton cannot be used when evaluating radiation transport in the newborn." [1987, page 42] Consequently, the authors proposed a different skeletal tissue medium for their newborn model, but utilized the adult skeletal tissue medium for all other models in the series including the one-year-old. New data on average skeletal atomic composition as a function of age available in ICRP Publication 70 (1995) were used to manufacture age-specific skeletal-equivalent materials incorporated into the one-year-old phantom. The skeleton composition (in terms of water, protein, mineral and fat by percent weight) was used to calculate an appropriate elemental composition of the bone-equivalent substitute for the one-year-old skeleton consisting of 52.98% carbon, 24.54% oxygen, 5.86%

hydrogen, 2.03% nitrogen, 5.79% chlorine and 8 81% calcium. The mineral percent by weight for a one-year-old skeleton was provided explicitly in ICRP Publication 70. The water and fat percentages were obtained from the 1995 document's data tables and the percentage of protein was obtained by subtraction. However, Bower had difficulty in producing a bone substitute that matched the density for a one-year-old, but could produce a bone substitute mixture of 1.18 g/cm^3 in 1997, which approximated Cristy and Eckerman's density of 1.22 g/cm^3 for the newborn in 1987. Since the new elemental bone composition for the one-year-old developed by Bower in 1997 was close to the newborn, and the difference in densities between the newborn and the one-year-old in ICRP Publication 70 was only 0.01 g/cm^3, he decided to use the newborn bone density of 1.18 g/cm^3 for the one-year-old.

Molds were then created for the lungs and individual skeleton components consisting of two leg bones, two arm bones, a pelvis, a spine, twelve ribs, two scapula and two clavicles. The molds were filled with the respective lung or bone liquid resin tissue substitutes and allowed to cure. The cured components were milled to final shape. Once the internal components were completed, molds were created for the external parts consisting of the trunk, legs and skull. The soft tissue substitute material was then poured into the external cylindrical trunk mold in a layered method which facilitated the correct placement of the skeletal and lung components. The legs were frustums of two soft tissue cones surrounding the leg bones. The head consisted of a skull enclosing the mandible, teeth, cranium and upper face region, as well as a neck. Guide holes were drilled into the phantom to allow placement of the dosimeters. Figure 3.1 shows the mathematical model of the one-year-old, a portion of the internal skeleton with the head model, and an external view of the completed physical prototype phantom.

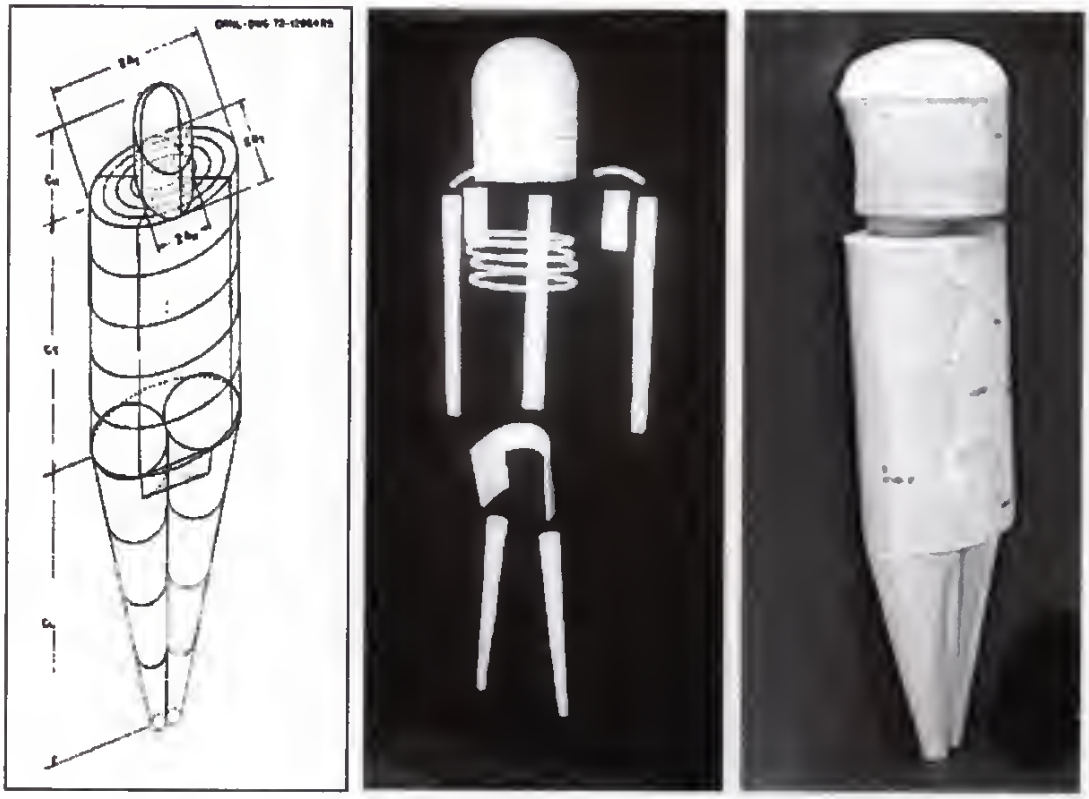

A B C

Figure 3-1. One-year-old pediatric phantom. A: Mathematical model. B: Skeletal model with 4 ribs. C: External view of physical prototype phantom.

The total mass of the one-year-old prototype is 10.2 kilograms. The length of the head, trunk and legs, respectively, is 16 cm, 32.5 cm, and 26.5 cm, for a total height of 75 cm. Several aberrations should be noted regarding the prototype phantom. The mathematical model has soft tissue eyes with a volume of 6.25 cm^3, whereas the physical prototype phantom does not have soft tissue eyes. The space for the eyes is composed of bone tissue substitute; therefore the mass of the upper face region for the physical phantom is slightly higher than the mathematical model. The upper portion of the mandible is slightly thinner in the physical phantom, however, this portion abuts against the upper face region. Therefore, when averaged together, the two regions are approximately correct in comparison with the mathematical model. The teeth are also

slightly more massive in the physical phantom, however, the total mass of the teeth is only 22 grams, and the teeth are not a chosen dosimetry monitoring location. Some of the ribs in the prototype were heavier than the theoretical masses; however, the individual ribs are thin (volume 7.28 cm^3) and are not used as a measurement location.

Metal Oxide Semiconductor Field Effect Transistor (MOSFET) Dosimetry System

Theory of Operation

The basic structure of a metal oxide semiconductor field effect transistor (MOSFET) is a sandwich-type device consisting of a p-type channel built on a n-type silicon semiconductor substrate separated from a metal gate by an insulating oxide layer. The source and the drain are on top of the positively doped silicon region. When sufficient negative bias is applied to the gate with reference to the substrate, a significant number of holes will be attracted to the oxide silicon surface. A sufficient hole population permits current to flow between the source and the drain. The gate voltage necessary to allow conduction through the MOSFET is referred to as the threshold voltage (Soubra 1994; Ramani 1997).

When the MOSFET is exposed to ionizing radiation, electron-hole pairs are formed in the oxide insulation layer. The applied positive potential to the gate causes the electrons to travel to the gate, while the holes migrate to the oxide silicon interface, where they are trapped. These trapped positive charges cause a shift in the threshold voltage. The voltage shift is proportional to the radiation dose deposited in the oxide layer. This is the basis of the MOSFET as a dosimeter. The Thomson and Nielsen Patient Dose Verification System used in this research utilizes a dual bias, dual MOSFET device design, which consists of two MOSFETs fabricated on the same chip. The threshold voltage shift magnitude is increased when the positive gate bias is raised. Since the MOSFETs are

irradiated simultaneously, the measured difference in the threshold shifts in the two sensors is representative of the absorbed dose (Soubra 1994).

Each detector of the Patient Dose Verification System consists of the matched pair of MOSFET dosimeters operated at two different positive gate biases. Each MOSFET dosimeter has an active area of 0.04 mm^2. The pair is mounted under a 1-mm layer of epoxy to a 20-cm long thin semi-opaque polyamide laminate cable encasing two gold wires. The extremely thin (0.2 mm), flexible laminate cable is attached to a sturdy 1.4-m long cable that is connected to a bias supply. The reader can accommodate up to 20 dosimeters. To facilitate monitoring of the lower absorbed doses associated with diagnostic x-rays, the model TN-RD-19 high-sensitivity bias supply is used. Grouped in sets of five, each MOSFET set is connected to a bias supply labeled "A" through "D". In this research, there were two sets of five dosimeters labeled "A" and "D", for a total of ten dosimeters. The entire dosimetry system is shown in Figure 3-2 including the reader, power supply, bias supply, a MOSFET dosimeter and the associated cabling.

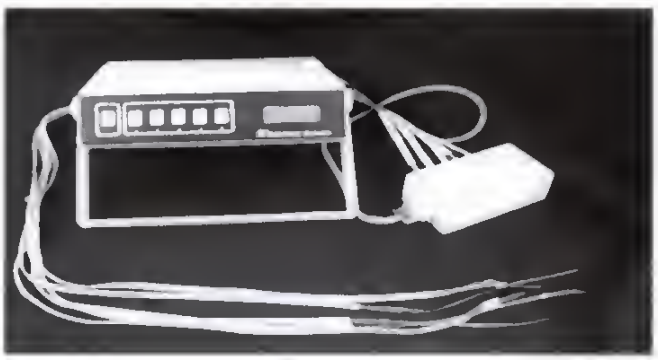

Figure 3-2. Thomson and Nielsen Electronics Ltd. MOSFET Patient Dose Verification System

Characterization of High Sensitivity MOSFET Dosimeter

The commercial Patient Dose Verification System manufactured by Thomson and Nielsen was originally designed for radiation therapy dose verification. To measure doses to organs that were outside of the primary therapy beam, Thomson and Nielsen developed high sensitivity dosimeters to measure the lower doses. Bower and Hintenlang characterized these high sensitivity dosimeters for diagnostic energies (1998). Bower measured the sensitivity, linearity, rotational angular response, multiple query response and post-exposure response of the high sensitivity MOSFETs. He determined that the high sensitivity MOSFET dosimeters had a nearly uniform angular response, good linearity, and precise sensitivities at the lower energy ranges that resulted in a standard error of $\pm$ 5% for a typical x-ray exposure. He also determined that the energy dependence of the sensitivity, the post-exposure drift and the multiple query responses were not significant limitations. Johnson performed three additional characterization tests, including a comparison of the MOSFET to TLD, a determination to see if the small air gap that surrounds the MOSFET when inserted into the phantom influences the dose measurement, and a determination of the axial angular dependence of the MOSFET (1998). She determined that the dose reported by the MOSFET is equivalent to the dose reported by the TLD inside the tissue phantoms and that the small air gap that surrounds the MOSFET when it is inserted in the holes in the phantom does not affect the reported dose. Consequently, there is no need to fill the air gap with other tissue equivalent material. She also determined that angular dependence in the axial (saggital would be a more appropriate definition) orientation of the MOSFET when placed in the phantom does not influence the measured absorbed dose. An extrapolation of these determinations for the rotational and saggital planes is that the angular dependence from a coronal orientation would also not influence the measured absorbed dose.

The MOSFET is a consumable detector. While the detector is not annealed or cleared after reading, as is the case for thermoluminescent dosimeters, the system can provide a reset between desired readings. The reset process consists of measuring the mV response and using this response as a reference value for the following measurement. The response is not completely stable over long periods of time post-exposure. Bower performed a fading study in 1997 to measure the response of the high sensitivity MOSFETs as a function of time post-exposure out to 500 hours. The dual-bias, dual-MOSFET system utilizes the stable difference in response from the two detectors for measuring absorbed dose. This method eliminates temperature and high-dose dependencies, but does not control post-exposure drift. The drift is a complicated function attributed to an array of causes. The drift is reproducible, and mathematical models and deconvolution methods have been proposed and employed (Gladstone and Chin 1995). In using this dosimeter system to monitor organ doses within the one-year-old phantom in real-time, delay times between exposure and dosimeter readout are on the order of minutes, therefore, another fading study was performed to measure the response of the MOSFET as a function of time post exposure for an immediate read, a one-minute delay, a two-minute delay and a three-minute delay. The exposure between the four reading times varied by less than 2%, so a delay time of one minute was utilized in this research to decrease the room downtime associated with the data collection, and no correction factors were necessary.

The dosimeters inserted within the physical phantom are required to have good angular response characteristics since there is no way to adjust the orientation of the detectors towards the x-ray source when simulating different views of x-ray examinations. In 1997, Bower demonstrated there is a marked angular dependence of the MOSFET dosimetry system when it is used free-in-air without an attenuating medium. The packaging of the MOSFET appears to be the main source of this angular dependence, providing different responses when exposing the flat surface (60% lower) as opposed to

the epoxy bubble side of the dosimeter. It was initially thought this difference might be attributed to insufficient material on the flat surface of the dosimeter for the establishment of electronic equilibrium. It was subsequently demonstrated that this response is not simply due to scattering from the 1-mm bubble of epoxy, since the angular response remained after material was added to the flat side of the detector to make it more symmetrical. The effect is actually due to the inherent asymmetric structure of the MOSFET itself, specifically resulting from attenuation in the silicon substrate layer. The angular dependence is much less pronounced when the dosimeter is surrounded by attenuating media. This was verified by using a tissue equivalent cylinder and measuring the angular response for the high sensitivity MOSFET dosimeter. The cylinder, with a detector inserted in the center, was irradiated in 15° increments over 360° at a tube potential of 90 kVp, 150 mAs, and a source-to-detector distance of 75 cm. The procedure was repeated for each MOSFET to obtain an average dose measurement at each increment. The response was very symmetrical, indicating excellent angular response when using this dosimeter within a phantom. The nearly uniform angular response and its small size were primary reasons the MOSFET dosimeter was chosen for the real-time dosimetry applications within the one-year-old phantom.

MOSFET Placement

The effective dose concept presented in the 1990 recommendations of the ICRP (1991) identified twelve specific tissues at risk from radiation detriment and supplied tissue weighting factors for these tissues. Several other tissues were addressed in a "remainder" term. The specific tissues and their associated weighting factors are shown in Table 3-1. The MOSFET dosimeters were placed in locations to estimate the absorbed dose in these tissues for the one-year-old phantom. For localized organs, the MOSFET was placed at the centroid of the organ to determine the dose. For distributed organs, the

dose was determined from a fractional weighting scheme applied to a specific array of MOSFET dosimeters. Standard dosimetric allowances were made for measuring the absorbed dose in both the testes and the ovaries in the hermaphrodite phantom since an actual patient would not have both types of gonads. The effective dose estimates performed in Chapter 5 are shown with the testes absorbed dose being used as the gonadal dose component for the male estimate, and the ovaries absorbed dose being used as the gonadal dose component for the female estimate. All other tissues and their corresponding tissue weighting factors were the same. A skin dose estimate was obtained by measuring the entrance and exit absorbed doses and using an average value of the two measurements. The organs defined in the remainder term were as follows: muscle, stomach wall, small intestine wall, upper large intestine wall, lower large intestine wall, kidneys, pancreas, spleen, thymus, uterus, adrenals, and bladder wall. A remainder dose estimate was calculated by averaging the measurements in the arms and the trunk of the body as representative of the overall location of the remainder organs.

Table 3-1. Tissue Weighting Factors for Calculation of Effective Dose (ICRP, 1991)

Tissue or organ	Tissue Weighting Factor (w_T)
Gonads	0.20
Bone Marrow (red)	0.12
Colon	0.12
Lung	0.12
Stomach	0.12
Bladder	0.05
Breast	0.05
Liver	0.05
Esophagus	0.05
Thyroid	0.05
Skin	0.01
Bone surface	0.01
Remainder	0.05

The MOSFET locations in the one-year-old phantom are shown in Figure 3-2 and detailed in Table 3-2. The MOSFET locations for the soft tissue organs, including the

lungs, were generally placed at the centroid of the organ. A single MOSFET location was chosen for the testes and breasts for the following reasons. In the mathematical model representing a one-year-old, the testes are outside of the trunk and are very small (1.16 cm^3). The testes are close together, and great differences were not expected between the individual testes, therefore, a single monitoring location was chosen at the point where the two legs and the trunk join. Additional soft tissue material was not added to the phantom at this representative location. The mathematical model has breasts that are again very small for the one-year-old (1.06 cm^3 including skin), so breasts were not explicitly created for the anthropomorphic phantom. The dose to the breasts is estimated with the anthropomorphic phantom by measuring the absorbed dose to the surface midway between the two breasts. The centroids of the soft tissue organs in the anthropomorphic phantom were adopted from those supplied by Cristy and Eckerman (1987; Eckerman et al. 1996) for their mathematical model with the exception of the colon and the esophagus. Representative monitoring locations were chosen for the colon and the esophagus based on the equations provided for the colon (ICRP 1995) and the esophagus (Eckerman et al. 1996). The skeletal locations were chosen using three criteria: 1) the bones selected were larger bones able to accept the MOSFET without loss of a significant percentage of the bone material, 2) the bones selected represented high concentrations of active bone marrow and 3) locations were selected to cover a major portion of the skeleton.

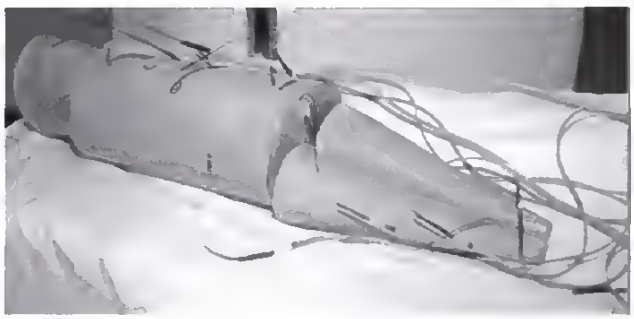

Figure 3-2. MOSFET dosimeters placed in position in prototype one-year-old phantom.

Table 3-2. Position of the MOSFET Dosimeters Within the One-Year-Old Phantom

gonads:	testes-general (left & right)
	ovaries-left
	ovaries-right
colon	
lung-left	
lung-right	
stomach	
bladder	
breasts-general (left & right)	
esophagus	
liver	
thyroid	
skeleton:	skull & facial
	spine (in head)
	spine (middle of back)
	pelvis
	leg-lower left
	leg-lower right
	arm-left
	arm-right

The MOSFETs were placed in the phantom with the epoxy bubble facing toward the x-ray tube, and the leads were taped down to prevent any movement. Initially, ten dosimeters were available for measurements. Two of the original compliment of ten failed early in the measurement series. One failed mechanically; the reason for the other failure could not be determined by the manufacturer. The simulations had to be repeated two and a half times since there are 20 different organ sites and only eight dosimeters were available. In each successive simulation, the dosimeters were placed in the 10 measurement sites that could be accessed on the top half of the phantom, and the simulation was repeated in order to measure the 10 remaining sites that were accessed on the bottom half of the patient. A full complement of dosimeters were not purchased until data collection was close to completion.

ICRP Publication 70 (1995) provides tables of the active bone marrow found in various bones as a function of age. These tables are based on work presented by Cristy

(1981) who relates the active marrow in individual bones, parts of bones, or bone groups expressed as a percentage of active marrow in the body. Weightings of the active marrow for the different phantom skeletal regions were assigned to the skeletal MOSFET locations given in Table 3-2. New active marrow percentages associated with the MOSFET location were assigned by Bower and are presented in Table 3-3.

Table 3-3 has been updated to include new bone surface percentages introduced in this research. Cristy (1981) also provides the skeletal volume for each region, from which a percentage of the total bone was calculated. Using an analagous technique, weightings of the total bone for the different skeletal regions were assigned to the same skeletal MOSFET locations, and new bone surface percentages associated with the MOSFET location were assigned.

Table 3-3. Percentage Active Bone Marrow and Bone Surface Associated with the Skeletal MOSFET Locations

Phantom Skeletal Region	% Active Marrow	% Bone	MOSFET Location	% Active Marrow Assigned to MOSFET	% Bone Surface Assigned to MOSFET
Skull (cranium & facial skeleton)	24.74	19.9	Skull & facial	14.7	11.6
Spine (upper portion)	1.88	3.2	Spine head	14.7	11.6
Arm bones upper portion	2.41	5.0	Arm bone left	7.79	9.8
Scapulae	2.73	3.2	Arm bone right	7.79	9.8
Clavicles	0.83	0.8			
Ribs	9.61	10.7			
Spine (middle portion)	9.27	8.5	Spine middle	15.88	18.5
Arm bones middle portion	2.25	5.0			
Arm bones lower portion	4.36	5.0			
Spine (lower portion)	3.37	4.1	Pelvis	21.91	21.9
Pelvis	16.47	9.3			
Leg bones upper portion	2.07	8.5			
Leg bones middle portion	3.88	8.5	Leg lower left	8.64	8.5
Leg bones lower portion	13.4	8.5	Leg lower right	8.64	8.5

Measurement of Absorbed Dose

Sensitivity has been defined as the MOSFET response per unit of exposure (mV per C kg^{-1} or mV/R) at a given tube potential; consequently the absorbed dose (rad) in the tissue may be derived as follows. The ion chamber measures exposure in air in units of roentgen (R); therefore, this unit was used in measuring the sensitivity. The exposure in air, as measured by the MOSFET dosimetry system is therefore the MOSFET dose measurement (mV) divided by the sensitivity (mV/R). Expressed symbolically in Equation 1, where X is the exposure, M is the MOSFET dose measurement and S is the sensitivity.

$$X = M * \left(\frac{1}{S}\right) \qquad \text{(Eq. 1)}$$

One roentgen produces an absorbed dose of 0.876 rad in air; therefore,

$$D_{air} = X * 0.876 \qquad \text{(Eq. 2)}$$

The absorbed dose in tissue may be then be calculated with the following equation:

$$D_{Tissue} = D_{air} * \frac{\left(\overline{\mu_{en} / \rho}\right)_{Tissue}}{\left(\overline{\mu_{en} / \rho}\right)_{air}} \qquad \text{(Eq. 3)}$$

where $\overline{\mu_{en} / \rho}$ is the average mass energy-absorption coefficient associated with the mean energy of the x-ray spectrum. Equations 1-3 may be combined into one useful equation as follows.

$$D_{Tissue} = 0.876 * \frac{\left(\overline{\mu_{en} / \rho}\right)_{oxide}}{\left(\overline{\mu_{en} / \rho}\right)_{air}} * \frac{\left(\overline{\mu_{en} / \rho}\right)_{Tissue}}{\left(\overline{\mu_{en} / \rho}\right)_{oxide}} * \left(\frac{1}{S}\right) * M \qquad \text{(Eq. 4)}$$

The value of $\overline{\mu_{en} / \rho}$ for the oxide could be removed from the equation without error; however, its inclusion indicates that the absorbed dose in the MOSFET device is an integral part of the corresponding dose value in tissue. The average mass energy-absorption coefficient ratios are effectively 1.0 for soft tissue, but increase to 3.5 for skeletal tissue at 30 keV.

The mean energy of the x-ray spectrum was estimated by utilizing the computer program XCOM5R (Nowotny and Hîfer 1985). The program is a spectrum generating program which accounts for parameters such as the tube potential, the inherent filtration, and the target materials. The program provides detailed information about the x-ray spectrum, including the mean photon energy of the spectrum. The determination of the exact mean spectrum energy is not critical for soft tissue or lungs, since the ratio of mass energy absorption coefficients is relatively constant and nearly 1.0 over the diagnostic energy range. The determination is more critical for tbe bones since that ratio is a rapidly changing with photon energy and peaks around 30 keV.

Sensitivity Analysis

MOSFET sensitivity, defined as the mV response per R exposure, is shown in Table 3-4 below for the ten high sensitivity dosimeters initially used in this research. Just prior to the completion of data collection, an additional ten dosimeters were added to the system, so during the calibration of the new dosimeters, the old dosimeters were recalibrated, as shown in column three. Exposure measurements were simultaneously made with a Keithley calibrated ion chamber. The data points were fit to obtain entrance skin exposures as a linear function of tube potential; only the most commonly used tube potential determined from the site surveys is reported.

Table 3-4. Sensitivity Calibration Factors (R/mV) at 70 kVp

MOSFET #	Calibration Factor (R/mV)	Calibration Factor (R/mV)
1	0.028	0.030
2	0.031	0.035
3	0.029	0.031
4	0.029	0.030
5	0.030	0.029
6	0.030	0.037
7	0.031	0.034
8	0.031	0.036
9	0.029	0.032
10	0.026	0.033

Table 3-4, continued.

11	0.031
12	0.029
13	0.029
14	0.030
15	0.030
16	0.030
17	0.033
18	0.030
19	0.032
20	0.033

Calibration factors needed for subsequent determination of tissue absorbed dose (R/mV) were determined from these sensitivity data and through the application of the Bragg-Gray cavity theory, as previously described. The conversion factors given in Table 3-5 contain the ratio of average mass energy absorption coefficients detailed in Appendix D and a constant for converting exposure to the absorbed dose in air, as described in Equation 4. Utilization of these conversion factors convert the exposure, obtained by multiplying the MOSFET measurement by the appropriate value in Table 3-4 to absorbed dose.

Table 3-5. Conversion Factors Converting Exposure to Absorbed Dose

Tube Potential	Soft Tissue	Lung Tissue	Bone Tissue
70	1.009	1.046	3.316

The following technique was used to assign a dose to the active bone marrow using a weighted fraction of bone marrow assigned to the MOSFET locations in the skeleton reported in Table 3-3. The active bone marrow dose was calculated by utilizing the conversion factor for soft tissue in Table 3-5 to calculate the absorbed dose of each of the skeletal components, multiplying by the fraction of active bone marrow assigned to the MOSFET (F_i) reported in Table 3-3, and then summed to get the total absorbed dose to the active marrow. Equation 5 illustrates how the dose to the active marrow is calculated.

$$D_{Active\ Marrow} = 0.876 * \frac{\left(\overline{\mu_{en}/\rho}\right)_{oxide}}{\left(\overline{\mu_{en}/\rho}\right)_{air}} * \frac{\left(\overline{\mu_{en}/\rho}\right)_{soft\ tissue}}{\left(\overline{\mu_{en}/\rho}\right)_{oxide}} * \sum_{i} \left(\frac{1}{S_i}\right) * M_i * F_i \qquad \text{(Eq. 5)}$$

A similar technique was used to assign a dose to the bone surface using a weighted fraction of bone surface assigned to the MOSFET locations in the skeleton reported in Table 3-3. The bone surface dose was calculated by utilizing the conversion factor for bone in Table 3-5 to calculate the absorbed dose of each of the skeletal, multiplying by the fraction of bone surface assigned to the MOSFET (F_i) reported in Table 3-3, and then summed to get the total absorbed dose to the bone surface. Equation 6 illustrates how the dose to the bone surface is calculated.

$$D_{Bone\ Surface} = 0.876 * \frac{\left(\overline{\mu_{en}/\rho}\right)_{oxide}}{\left(\overline{\mu_{en}/\rho}\right)_{air}} * \frac{\left(\overline{\mu_{en}/\rho}\right)_{bone\ tissue}}{\left(\overline{\mu_{en}/\rho}\right)_{oxide}} * \sum_{i} \left(\frac{1}{S_i}\right) * M_i * F_i \qquad \text{(Eq. 6)}$$

Calculation of Effective Dose

Effective dose (E) as presented by the ICRP in 1991 is the most current and comprehensive measure of radiation detriment. Effective dose equivalent (H_E) was a measure presented earlier by the ICRP in 1976. The effective dose was chosen to be calculated in this research as it evaluates the absorbed dose from more tissues than the effective dose equivalent and applies updated tissue weighting factors which are numerically different from those used with the effective dose equivalent. Various sets of tissue weighting factors were derived for children ages 0 to 9 and 10 to 19 years by Almén et al. and tested for use in the calculation of effective dose (1996). They concluded that the ICRP tissue weighting factors were applicable to children and adolescents; therefore, the ICRP tissue weighting factors were utilized in this research. The effective dose was calculated by multiplying the absorbed dose for each organ described in the previous section by its respective tissue weighting factor reported in Table 3-1. To summarize,

organ doses were determined with the MOSFET at the centroid of the organ, the active marrow and bone surface doses were determined via fractional weightings assigned to individual MOSFET locations, and the remainder dose was determined from an averaged measurement over MOSFETs located in the torso region. Since the effective dose calculation is a weighted average of the MOSFET measurement, the uncertainty in the effective dose caclulation is determined to be a maximum of $\pm$ 5%. Appendix E presents the measured organ doses and calculated effective doses utilizing the MOSFET dosimetry system and the one-year-old physical prototype phantom. The results are reviewed in Chapter 5.

CHAPTER 4
RISK ASSESSMENT

General

Risk assessment has been defined by the National Research Council (NRC) as "the characterization of the potential adverse health effects of human exposures to environmental hazards"(NRC 1983, page 18). An assessment of the risks from all types of hazards, including radiological hazards, requires all or some of the following components: i) hazard identification, which is investigated to determine whether a particular hazard has a corresponding health effect; ii) dose-response assessment, in which the relation between the magnitude of the dose and the probability that the health effect will occur is determined; iii) exposure or dose assessment, which is the determination of the extent to which humans will be exposed to the hazard; and iv) risk characterization, which describes the nature and magnitude of the human risk, including uncertainties surrounding that risk [NRC, 1983 #2254]. It is the last component of risk characterization that integrates the results of the previous three components into a risk model that includes one or more quantitative estimates (Cohrssen and Covello 1989).

Components of a Risk Model

The model used to perform a risk assessment is a function of several parameters, including populations from which data are obtained, relationships between doses and effects and methods used to project risks into the future. Due to the limited knowledge of radiation effects, there is diverse discussion about the interpretation of dose-response data and the choice of values for the other parameters.

Populations used in epidemiological studies vary among risk assessment models. Some studies provide better data than others do because some populations better represent the population of concern. In addition, differences in population characteristics such as lifestyles, cancer rates and types of exposures must be considered in transferring the results obtained from one population to another population, which is defined in a risk model as the population transfer coefficient.

The dose-response curve and dose-rate effect applied can differ. Among the possible risk models, the risk analysis techniques most commonly applied are a linear-quadratic or a linear relationship.

Risk projection models used to predict the mortality from, or incidence of, cancer and genetic disease that will occur within a given population can be of several types. Cancer risk projections use additive or multiplicative methods; genetic risk projections may use direct or indirect methods. Each method requires choices from among several additional parameters including death rates, specific causes of death, population statistics, and dose calculations.

Radiological risk assessments and resulting risk estimates have been developed by numerous organizations. Organizations such as the National Research Council's fifth committee on the Biological Effects of Ionizing Radiations (BEIR V), the United Nations Scientific Committee on the Effects of Atomic Radiation (UNSCEAR), and the International Commission on Radiological Protection (ICRP) have summarized the complex data previously discussed that are available on the effects of radiation in a form that is easily applicable. The BEIR V methodology is considered the most recent consent document for risk analysis and was utilized in this research.

BEIR V Methodology

Populations for Determining Cancer Risk

In the risk assessment by the BEIR V Committee in 1987, cancer risks were based mainly on epidemiological studies and, in large part, on the population of residents from Hiroshima and Nagasaki in 1950 (the Life Span Study). The data from this population were based on dose estimates made in 1986 (the Dosimetry System 1986 {DS86}) (Shimizu et al. 1987). To validate these assessments, additional human and animal populations were reviewed. For example, thirty-four additional studies were cited in support of the risk assessment for breast cancer.

Human Populations

The BEIR V Report estimated risks for breast cancer, respiratory tract cancer, digestive tract cancer, leukemia and other nonleukemia cancers. The human populations used in the risk assessment were chosen based on the type of cancer. For breast cancer, four populations were used: residents of Hiroshima and Nagaski in 1950 (the Life Span Study), most of whom were exposed to the atomic bomb; women examined by fluoroscopy in Canada for tuberculosis from 1930 to 1952; women examined by fluoroscopy in Massachusetts from 1930 to 1956; and women treated with radiotherapy for postpartum mastitis in New York during the 1940s and 1950s. For respiratory and digestive tract cancers, the population comprised residents of Hiroshima and Nagaski in 1950 (the Life Span Study). For leukemia, two populations were used: residents of Hiroshima and Nagaski in 1950 (the Life Span Study); and people treated with radiotherapy for ankylosing spondylitis in the United Kingdom from 1935 to 1954. A third population, women treated with radiotherapy in several countries for cervical cancer, may have been used in the leukemia risk calculations, however, the BEIR V report is

unclear on this point. For all other cancers (except leukemia), the study population was comprised of residents of Hiroshima and Nagaski in 1950 (the Life Span Study).

Animal Populations

In general, the BEIR V report cancer risk assessments considered animal populations only when necessary to validate or understand data from human populations. Animal studies raise numerous problems, including extrapolation of results obtained under experimental conditions to the conditions relevant to population exposure, such as dose rates, fractionation, and other variables; and extrapolation from an experimental organism in which radiation effects may be estimated with some confidence, to humans, because organisms differ in radiation sensitivity.

Populations for Determining Genetic Risk

The assessment for genetic risk relied on animal (especially mouse) data to supplement human data. To determine human genetic risk by extrapolating from animal data, three assumptions were made: the amount of genetic damage induced by a given type of radiation under given conditions in the animal species was the same in human germ cells; biological factors such as sex, germ cell stage, and age, and physical factors such as quality of radiation and dose rate, similarly affected genetic damage in the animal species and in humans; and the relationship between low- linear energy transfer (LET) radiation and frequency of genetic effects was linear at low doses and low dose rates. Genetic effects, by definition, require that at least one generation pass before they are expressed, and their expression is affected by the exposed population's sex, age, and probability of having children. Genetic risks determined from human data are based on the assumption that all of the exposed population was of reproductive age and wanted to have children. In the irradiation of an entire population, the reproducing people are a fraction of the total, and damage to the germ cells of the nonreproducing people in the population does not

pose a genetic risk. When the irradiation is neither random nor uniform, as is true of the available human populations utilized in the risk assessment, a reduction factor is required to adjust the genetic risk estimates.

Human Populations

The BEIR V report used several human populations, divided into three sets, to assess genetic risk. The first set consisted of people with genetic disorders resulting from spontaneous mutations. These disorders included dominant autosomal disorders, sex-linked recessive disorders, recessive autosomal disorders, chromosomal abnormalities, congenital abnormalities and other multifactorial traits. Multifactorial traits are a group of disorders about which the exact mode of inheritance is unknown and include such diseases as diabetes mellitus, gout, schizophrenia, affective psychoses, epilepsy, glaucoma, hypertension, varicose veins, asthma, psoriasis, ankylosing spondylitis and juvenile osteochondrosis of the spine. The second set consisted of people with genetic disorders resulting from several specific spontaneous mutations that were used to calculate mutation rates. The disorders included dominant autosomal disorders and recessive sex-linked disorders. The third set was the Hiroshima and Nagasaki survivors and their children, including members of a pregnancy termination study, a cytogenetic study of the children of exposed parents, an investigation of rare electrophoretic variants in children of exposed parents, and doubling dose studies.

Animal Populations

In general, mouse populations were used to assess genetic risk when human data were unavailable or inappropriate. A few data points were taken from monkey and marmoset studies. The animals in these studies displayed a specific endpoint, such as dominant and recessive lethal and visible mutations, reciprocal and heritable translocations, congenital malformations and aneuploidy.

Dose-Response Curves

A dose-response relationship, or curve, is determined by the change in effect (response, the dependent variable) with increasing amounts of radiation (dose, the independent variable). The relationship between dose and response is the primary problem in predicting the health risks of radiation (Cohrssen and Covello 1989). Determining the radiation dose has been detailed in Chapter 3. Determining the response to radiation is difficult, and the details of the process are beyond the scope of this research. Although somatic effects (such as cancer) and genetic effects are the major responses to radiation, many intermediate conditions or specific endpoints may be used as measurements. Among the many endpoints that are considered in nonhuman studies are clonogenic survival of cultured cells and formation of tumors and death in test animals. In human studies, effects such as chromosome abnormalities, enzyme aberrations, tumorigenesis and leukemia are considered.

The effects of cancer and genetic damage are presumed to be stochastic; that is, any level of irradiation increases the likelihood of inducing genetic damage or cancer (no threshold relationship). Thus, the dose-response relationship of interest presumably begins at the level of background radiation, which varies from place to place. This presumption is currently under great controversy, as a threshold relationship is becoming more frequently used. As these methodologies evolve, the quantitative risk predictions of this research may need to be revisited.

Most experimental studies are conducted using high doses, because the effects of low doses of experimentally applied radiation are indistinguishable from those of natural background radiation in small experimental populations (UNSCEAR 1986)[1]. These high doses are plotted against the responses to obtain a piece of the dose-response curve, and a mathematical relationship is used to determine the shape of the curve in the low-dose

---

[1] The UNSCEAR defines low dose as less than 0.2 Gy (20 rad).

region. Mathematical relationships explain the two differently shaped dose-response curves most commonly applied to radiation data: linear and linear-quadratic., as shown in Equations 1 and 2, respectively, where R is response, D is dose and α and β are constants.

$$LINEAR: \qquad R = \alpha D \qquad \text{(Eq. 1)}$$

$$LINEAR-QUADRATIC: \qquad R = \alpha D + \beta D^2 \qquad \text{(Eq. 2)}$$

The linear relationship extrapolates high-dose data along a straight line into the low-dose region where response is directly proportional to dose. The linear-quadratic relationship is effectively linear at low doses but begins to rise more steeply with increasing dose because of a squared term in the mathematical expression. Thus, at high doses, response is proportional to the square of the dose. At low doses, the linear relationship predicts a greater response than does the linear-quadratic relationship and is often considered as an upper limit. Thus, the linear relationship provides a conservative estimate of dose useful for radiation protection purposes.

The BEIR V committee chose a linear dose-response curve for quantifying genetic risk and most cancer risks from low doses of radiation because the epidemiological data they reviewed were best described by this model. For leukemia, however, the BEIR V committee used a linear-quadratic dose-response curve, which better fit the DS86 dosimetry data from the residents of Hiroshima and Nagasaki.

Dose-Rate Effects

Since most of the data on radiation effects come from high doses, they must be extrapolated to low doses, which describe most human irradiation, and the plain film examinations reviewed in this research. Evidence from medicine and biology suggests that as dose and dose rate decrease, the effect per unit dose also decreases for low-LET radiation (NCRP 1980). Thus, high doses and dose rates are more effective at causing

damage than low doses and dose rates. This difference is quantified by the dose-rate effectiveness factor (DREF) or dose and dose-rate effectiveness factor (DDREF).

The effect of dose rate has been studied for numerous years. For low-LET radiation, the effect depends on several factors, including repair of sublethal damage, redistribution of cells in the mitotic cycle, and compensatory proliferation of cells during protracted irradiation. For high-LET radiation, the dose-rate effect is much reduced. The effect seems to apply both to cancer and genetic endpoints, although the effect is not necessarily equal for either endpoint (BEIR 1990).

The dose rate effectiveness factor is estimated using mouse or human data. To reiterate, with a linear-quadratic relationship, the dose response curve is approximately linear at low doses at the low end of the curve. With a linear relationship, the dose-response curve continues to be linear at low doses. Since it is extrapolated from high-dose data along a straight line, it predicts greater response at a given dose than does the linear-quadratic relationship. The ratio of these two responses at low doses, which is in effect the linear extrapolation overestimation factor, approximates the dose-rate effectiveness factor (Fabrikant 1990). These two models are shown in Figure 4-1. The solid circles represent hypothetical data for an excess incidence of cancer observed at relatively high doses. Curve A represents a linear extrapolation; curve B represents a quadratic relationship between incidence and dose; curve C illustrates a threshold type of response, which was previously discussed. While all three models fit the high-dose data equally well, the risk estimates pertinent to this research in the low-dose region are quite different according to which model is chosen for the extrapolation.

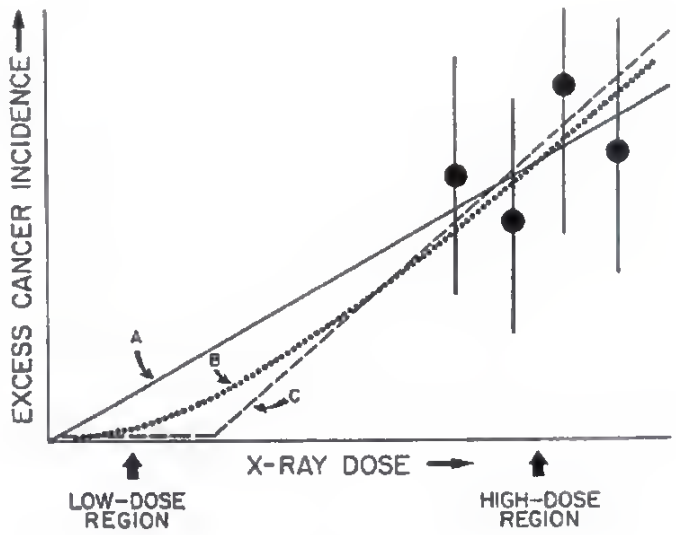

Figure 4-1. Various models used to extrapolate high-dose data on cancer incidence to the low-dose region, so that risk estimates can be performed. Redrawn from: Radiation Carcinogenesis in Man, United Nations Scientific Committee on the Effects of Atomic Radiation (1977).

The most commonly cited range for dose-rate effectiveness factor is two to ten; that is, radiation at high doses and dose rates is from two to ten times more effective at causing damage than radiation at low doses and dose rates (NCRP 1980). Dose rate effectiveness factors are applied with care. For example, as previously discussed, BEIR V used a linear-quadratic relationship to model leukemia, which would already predict reduced numbers of cases of leukemia at low doses and dose rates (BEIR 1990). The BEIR V committee also chose to fit separate dose-response curves for each cancer (Fabrikant 1990) and therefore did not use a dose-rate effectiveness factor. The factor used in assessing genetic risk, which was based on the ratio of genetic risk from high to low dose-rate irradiation of mice, was approximately three.

Population Transfer Coefficients

A number of uncertainties are involved in a risk assessment. Some sources of uncertainty can be evaluated using conventional statistical theory and are incorporated into risk assessment parameters such as dose-response relationships and risk projection

methods. Other sources of uncertainties cannot be captured by the usual statistical techniques. One important uncertainty addressed by the BEIR V report was that inherent in applying risks determined in one population to another population. Referenced in a risk model as the population transfer coefficient, this issue was of major concern because the BEIR V methodology's risk assessment was primarily based on results from the Hiroshima and Nagasaki survivors applied to U.S. populations. The extrapolation required assumptions about diets, industrial exposures, cancer rates and lifestyles in general. The BEIR V committee recognized the population transfer issue to be a fundamental problem and considerable source of uncertainty in estimating risks. The report chose to evaluate this issue by "a consensus of expert opinion as to the uncertainty, expressed in a number on a scale commensurate with ordinary statistical measures of variability" (BEIR 1990, page 220).

The committee obtained this number by judging the range within which it was believed to lie with 95 percent confidence. In this way, all types of uncertainty, both statistically calculated and estimated by consensus, were evaluated together to obtain combined measurements of standard error and confidence intervals. The committee thus estimated the uncertainty in population transfer to be 20%.

BEIR V Cancer Risk Projection Method

Lifetable analyses using standard mortality tables that were modified to include an additional incremental risk from radiation were used by the BEIR V committee to calculate lifetime cancer risks from specific irradiation. Input data for the lifetable analyses included radiation doses and parameters used in the assumed dose-response relationship (Bunger et al. 1981).

To comprehend a lifetable analysis of a standard mortality table, consider a lifetime irradiation at a constant annual rate. A lifetable analysis starts with a hypothetical

population of one million newborns, and the columns of the table provide the following information shown in Table 4-1.

Table 4-1. Lifetable Analysis of a Standard Mortality Table

Number of surviving infants	Cancer death rate	Number of cancer cases	Number of deaths from other causes

The first column gives the number of infants expected to survive each age; the second column gives the cancer death rate predicted by the dose-response curve; the third column gives the number of cases of cancer deaths (which is the product of the first and second columns); and the fourth column gives the number of deaths from causes other than radiation based on mortality rates. The number of infants surviving to each age (first column) less the number of radiogenic and nonradiogenic cancer deaths (sum of third and fourth columns) is the number of survivors at the beginning of the next age interval. This process continues with increasing age until the entire population is dead or until age one hundred (BEIR 1990).

Quantifying excess cancer deaths from radiation is the key to projecting risks. When the risk to exposed people exceeds the risk to unexposed people by the same amount at all ages, the effect of the radiation is additive, and the mathematical expression for this risk is thus an additive one. This is often called the absolute risk because at all ages the excess risk is constant. When the risk to exposed people exceeds the risk to unexposed people by a constant fraction, the effect of radiation is multiplicative. Also known as relative risk because at all ages after irradiation, the relative risk or risk ratio is constant, the multiplicative relationship is the mathematical expression of this risk (Muirhead and Darby 1987). These two models are overly simplistic in projecting risk. The BEIR V Committee permits the risk to vary as complex functions of time after exposure throughout the individual's lifetime. This is demonstrated in Figure 4-2, which illustrates the Committee's preferred risk model for leukemia.

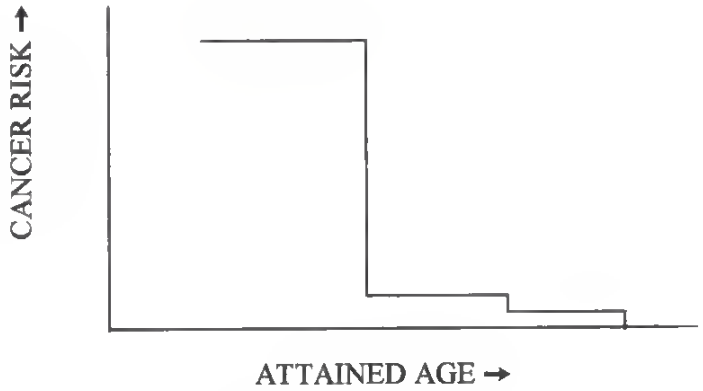

Figure 4-2. The risk of leukemia due to low LET radiation as a function of attained age.

Cancer risk projection requires knowledge of several parameters, including the relationship between excess cancer risk and relative risk, the latency period or the time from irradiation to the first expression of excess cancer risk, the plateau period or the time from the first expression of excess risk until the excess cancer risk disappears, the age distribution of the exposed population and the baseline pattern of age-specific mortality rates from all causes and from the cancers under consideration, the age at irradiation and the dose-response function. These parameters are brought together in the cancer risk projection model used by the BEIR V Committee. The report used cancer risk projection to provide several measures of risk, i.e., estimating the probability of radiation-induced cancer death expressed as a percentage, the number of projected cancer deaths expressed as deaths per thousand or million exposed people per unit dose, and the number of years of life lost in an exposed population because of radiation-induced cancers. All of these estimates, however, derive from a single measure of excess lifetime cancer risk chosen by BEIR V, as discussed in the next section.

The BEIR V Committee chose to use only multiplicative methods to project cancer risk. The measure chosen by this committee was excess lifetime cancer risk, which is the increase in the lifetime probability that a person will die from a specific cancer as a

result of a specific irradiation. The method of lifetime excess risk estimation used in the BEIR V report differs slightly from those previously used. In the BEIR V Report, separate lifetime risks are estimated for an exposed population and for an unexposed population. The unexposed population is assumed to be exposed to the same background radiation as the exposed population. The excess cancer risk is simply the difference between the two lifetime risks (BEIR 1990). The parameter estimates used for the BEIR V cancer risk projections were obtained using AMFIT, a program developed for the analysis of survival data. Further discussion of some of these parameters provides more insight into the assumptions made by the BEIR V report and are reviewed in the next sections.

Specific Cause of Death

As previously noted in the discussion on populations, the BEIR V report projected risks separately for leukemia, breast cancer, respiratory tract cancer, digestive tract cancer and other nonleukemia cancers. For leukemia deaths, the BEIR V report assumed a two-year latency period. For deaths from other cancers, a ten-year latency period was assumed.

Age of Population

The age distribution of a population at the time of irradiation must be specified in order to predict the effect of that irradiation because some of the cancers used as endpoints depend strongly on age at irradiation. For example, leukemia risks for people exposed before age 20 are much greater than leukemia risks for people exposed later in life (Vaeth and Pierce 1990) and risk varies as a complex function of age and time since irradiation (Thomas, Darby et al. 1992). For the cancers with the longer latency periods, there is more uncertainty in the application of the BEIR V risk models. Since there is nothing available that is more advanced than BEIR V, the BEIR V methodology was

utilized, recognizing that these results may need to be revised if the BEIR V models are revised.

BEIR V Genetic Risk Projection Method

The BEIR V report did not provide a direct estimate of the risk of total genetic damage, stating that these estimates were highly uncertain because they did not include allowance for genetic diseases of complex etiology that may be caused by multiple factors. The report suggested that these diseases make up the largest category of genetically related diseases and that further research was required before these probabilities could be estimated accurately. The report did provide estimates of genetic effects for other types of genetic disorders, however, the performance of these calculations are beyond the scope of this research. This research will only utilize the BEIR V methodology to estimate the risk of radiation induced cancer utilizing the equations detailed in the following section.

Calculating the Relative Cancer Risk from Pediatric Diagnostic X-Ray Procedures

The BEIR V report's general expression for calculating the total cancer risk, including natural and radiation-induced, to a population is given in Equation 3 (BEIR 1990).

$$\lambda(d) = \lambda_0 [1 + f(d)g(\beta)] \quad or \quad \lambda(d) = \lambda_0 + f(d)g(\beta)\lambda_0 \qquad \text{(Eq. 3)}$$

where λ_0 is the individual's age and gender-specific mortality rate for a given type of cancer in the absence of a radiation exposure other than natural background (or absolute age specific cancer risk to the unexposed population); $f(d)$ is a function of dose equivalent in Sievert; $g(\beta)$ is the excess risk function for a specific cancer that depends upon gender, age of the individual, age at exposure, and time since exposure; and $\lambda(d)$ represents total

fatal cancer risk. The second term on the right of Equation 3, $[1 + f(d)\, g(\beta)]$, therefore, represents the radiation-induced fatal cancer risk.

The dose-response function, $f(d)$, depends upon the type of cancer involved. The equations for $f(d)$, taken from BEIR V (BEIR 1990), are:

Leukemia:	$f(d) = 0.243d + 0.271d^2$
Respiratory cancer:	$f(d) = 0.636d$
Digestive cancer.	$f(d) = 0.809d$
Other cancer:	$f(d) = 1.22d$
Female Breast Cancer:	$f(d) = 1.22d$

Similarly, the radiation –induced cancer risk depends upon a number of factors that are incorporated into the excess risk function that has been discussed previously. In the following equations for the excess risk function $g(\beta)$, E represents the age at exposure, and T represents the number of years following exposure. Only the equations applicable to a one-year-old patient simulated in this research are presented.

For males:

A. Leukemia (latent period = two years)

$E \leq 20$; $T \leq 15$: $g(\beta) = \exp(4.885) = 132.3$

B. Respiratory cancer (latent period = ten years)

$g(\beta) = \exp[-1.437 \ln(T/20)]$

C. Digestive cancers (latent period = ten years)

$E \leq 25$: $g(\beta) = \exp(0) = 1.0$

D. Other cancers (latent period = ten years)

$E \leq 10$: $g(\beta) = 1.0$

For females:

A. Leukemia (latent period = two years)

$E \leq 20$; $T \leq 15$: $g(\beta) = \exp(4\ 885) = 132.3$

B. Respiratory cancer (latent period = ten years)

$g(\beta) = \exp[-1.437 \ln(T/20) + 0.711]$

C. Digestive cancers (latent period = ten years)

$E \leq 25$: $g(\beta) = \exp(0.553) = 1.74$

D. Other cancers (latent period = ten years)

$E \leq 10$: $g(\beta) = 1.0$

E. Breast cancers (latent period = ten years)

$E < 15$: $g(\beta) = \exp[1.385 - 0.104 \ln(T/20) - 2.21 \ln^2(T/20)]$

The values of $g(\beta)$ were determined for each gender for an exposure that occurs at an age of one year and the time post-exposure was chosen to be five years past the latency period for each different type of cancer. The five year post-latent time period was chosen by plotting $g(\beta)$ as a function of time for each cancer and gender, as shown in Figures 4-3 through 4-9. These illustrations only extend to 25 years, but the elevated risk continues further into the future. The five year post-latent time period was chosen as representative of all the cancer models but was initially based on the leukemia cancer model because that is approximately in the middle of the time interval of maximum risk for leukemia, as shown in Figure 4-3.

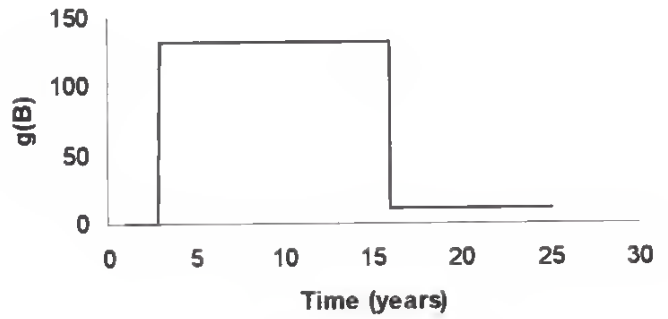

Figure 4-3. Time dependent risk for exposure at age equal to one year for both male and female leukemia models

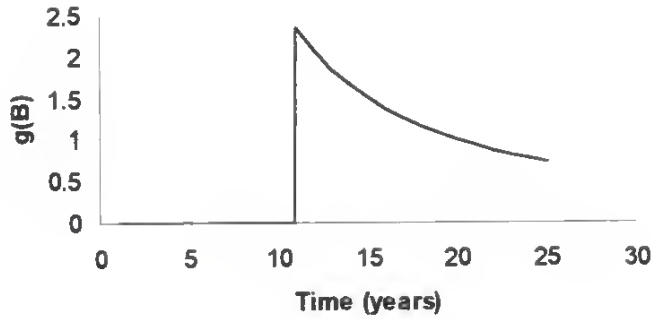

Figure 4-4. Time dependent risk for exposure at age equal to one year for male respiratory cancer model.

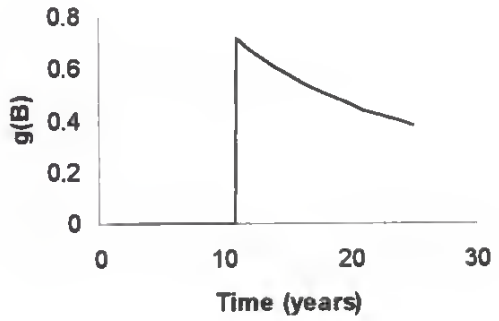

Figure 4-5. Time dependent risk for exposure at age equal to one year for female respiratory cancer model.

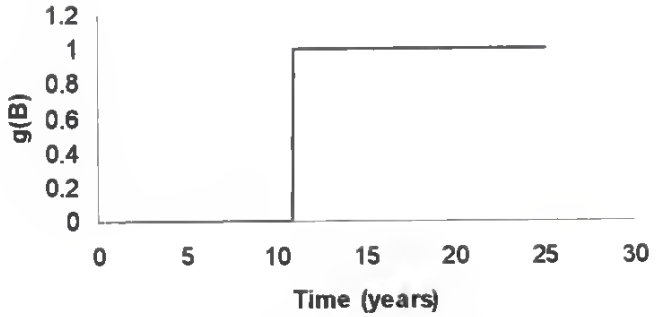

Figure 4-6. Time dependent risk for exposure at age equal to one year for male digestive cancer model.

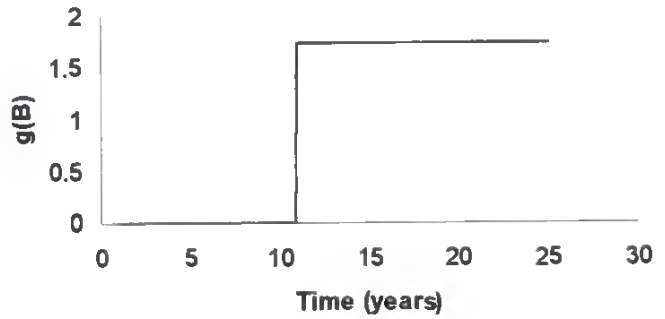

Figure 4-7. Time dependent risk for exposure at age equal to one year for female digestive cancer model.

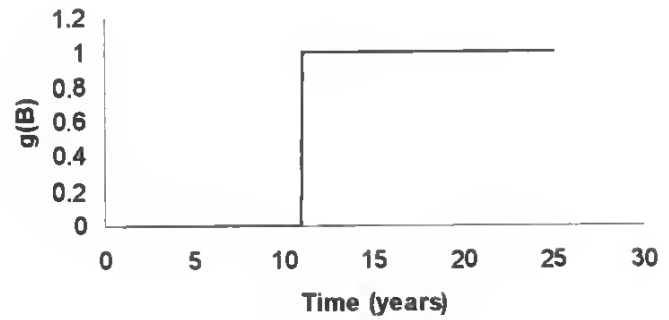

Figure 4-8. Time dependent risk for exposure at age equal to one year for both male and female other cancer models.

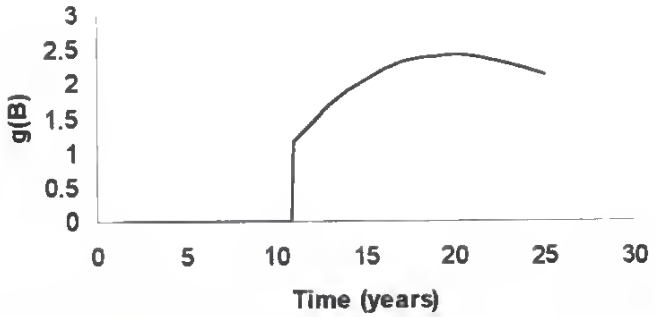

Figure 4-9. Time dependent risk for exposure at age equal to one year for female breast cancer model.

The values of $f(d)$ were determined utilizing the effective doses calculated in Chapter 3, rather than dose equivalent, since effective dose is the most current and comprehensive measure. The values of $g(\beta)$ were then multiplied by the appropriate value of $f(d)$ and the relative risk predicted by the $[1 + f(d)\ g(\beta)]$ term in Equation 1 was determined using these variables for each procedure simulated. The calculation of the relative risk for specific pediatric exams are performed in Chapter 5.

CHAPTER 5
RESULTS AND DISCUSSIONS

Facility Approach to Handling Special Concerns of Pediatric Patients

The child is not a small adult. This aphorism is a mantra for any discussion of pediatric radiology; it is particularly pertinent to the specifics of technique. Most general diagnostic radiologists and radiologic technologists are uncomfortable examining an infant or young child. Unfortunately, this uneasiness may be transmitted to the pediatric patient and frequently to the parent. The result is often an inadequate examination that is either confusing or uninterpretable and requires retakes, ultimately yielding an increase in radiation dose to the patient (Kirks and Griscom 1998). Pediatric imaging is no better than its techniques and technologists. Thus, special approaches are required to handle pediatric patients.

Children are frequently apprehensive in the hospital setting. These feelings are compounded by fear of the unknown and the pain so often associated with doctors and hospitals. As a result, not all technologists enjoy working with children; many become frustrated by the lack of cooperation of infants and by the time required for pediatric examinations, and there are, therefore, dedicated pediatric technologists. All of the pediatric technologists involved in the site surveys appeared to be conscientious and dedicated individuals who enjoyed working with children and had sufficient patience but firmness to develop the rapport to handle pediatric patients. Reducing the child's fright and obtaining his or her trust is of great benefit to the patient psyche and adds to the technologist's ability to carry out high-quality examinations.

There are many different ways of successfully approaching a child, and certain basic guidelines were observed during the site surveys that appeared to be adapted to individual technologist styles and personalities. Of greatest importance is obtaining the pediatric patient's trust. Obtaining trust can be difficult with any child but is especially difficult with a child who is ill and suddenly finds herself, or himself, in a strange environment. Creating an environment in which a child feels unthreatened and comfortable is a challenge to hospital designers. Children enjoy stimulating surroundings and require something to occupy their time while waiting for a procedure to be performed. The environment must accommodate the parent's needs in addition to those of the child. Since the first area encountered in a radiology department is usually the waiting room, furniture appropriate to both parents and children should be available. For the departments in the site survey that had dedicated pediatric facilities, an area equipped with tables and chairs to accommodate children's activities was commonly found. Unbreakable toys, puzzles, games, coloring books, crayons and storybooks were observed in all of the surveyed facilities. In the majority of surveyed facilities, the room commonly used for pediatric examinations had a mural painted on the wall or a myriad of stuffed animals on the shelves to provide a soothing, entertaining atmosphere for the child. One of the facilities visited had the x-ray equipment itself painted in a jungle motif and the table and lift decorated to resemble a boat; patients were told to relax and enjoy the jungle boat ride. Most pediatric rooms also carefully kept all medical paraphernalia out of sight but had accessory equipment such as sponges, sandbags, and restraining devices readily accessible from the tableside.

All of the pediatric technologists interviewed indicated that the key to establishing rapport with a child is truth and honesty. As children are not only inquisitive, but very perceptive, they should never be lied to. All of the technologists attempted to establish a good cooperative relationship with the child by initiating a conversation with the child about things that interested him or her. Chatting often enables the child to relax and

increases their willingness to help with the study. The technologists always explained the procedure fully to the patient no matter how young the child was, in words that could be understood. The technologists felt this knowledge not only helped to lower the patient's anxiety, but also increased their credibility. Children like to be talked to and feel reassured and comforted by participating in an interesting conversation. This technique also worked with infants, who seemed to feel more secure when they heard a friendly voice.

A major aid utilized by all the surveyed facilities to decrease parent and patient anxiety was to furnish them with a simple, printed explanation of the procedure when the appointment is initially made. The technologists felt this proved to be a great help in getting the patient to relax and be cooperative. Scheduling the appointment to coincide with the child's routine was also important, although obviously not always practical. All technologists expressed the preference to not x-ray children under the age of five between noon and 4:00 P.M., as that is when most children are eating lunch and taking naps. The technologists preferred to perform the procedures in the morning when the children were rested, refreshed, not a lot of doctors had poked at them, and nothing really overwhelming had happened to them yet. Children cannot handle the procedure as well later in the afternoon because they are tired, stressed out and they have reached their limit for the day.

In obtaining the child's cooperation, it is often helpful to give him/her a small degree of control over the circumstances. For example, a teddy bear or a security blanket may be placed as the child wishes, or the choice of a particular Band-Aid or color of hospital gown may give the child the feeling that he/she can still influence this new environment. Another method of helping children feel in control of the situation is to tell them what they're going to do during the exam. The most successful technologists observed would say "You're going to stand up here and do this, then you're going to turn around and do that, I'm going to do this, and then you're finished!" rather than "Come on in here and let's take some pictures." Another example often recalled by the technologists included emphasizing what's positive, e.g. asking a child to show them how long they

could hold still rather than telling the child "Don't move." It is worthwhile for the child to understand that he/she is an active participant in this important procedure that is being performed on his/her behalf. Children often want to help adults, and the sick child is no exception. The phrase "Now I need you to help me" was heard frequently during the site surveys.

Parent involvement in the procedure varied from site to site and appeared to be a controversial issue. At most of the facilities, parents were invited to be present in the radiography suite for all plain film examinations, as most young children are more cooperative during radiographic procedures when a parent is present. Separation from parents can be very stressful for young children and the presence of the parent may make the child more cooperative by diminishing the fear of being deserted in a strange place. During the explanation of the exam, the technologist can determine the child's response to the new environment and decide which parent will make the most effective assistant. It was common to invite only one parent to accompany the patient into the radiographic suite. A careful explanation of the procedure enhances the ability of the parent to assist the technologist and provides reassurance to the child. Parents sometimes feel guilty that their child has suffered an accident or illness and allowing them to assist may help to ease their anxiety as well. The technologists also made it clear that if the parent became upset with the procedure or were disruptive to the achievement of good rapport with the child, they would not hesitate to ask them to leave the room. The technologists indicated that the possibility that a parent may be asked to leave is often sufficient encouragement for the child to cooperate in the study, as is the thought of having to repeat the procedure. The technologist also made it clear to the child that the examination he/she is undergoing is necessary and inevitable and that he/she has no choice in the matter. The idea that the technologist is "the boss" was also made clear to the child. The technologists routinely stressed the importance of immobilization to the parent. If immobilization devices are used, the parent can assist in placing the child in the device, although most technologists

seemed to prefer to do this themselves so that the parent just provided moral support and could "come to the rescue" when the procedure was over. Parents can also demonstrate to the child what will take place during the exam. The technologists indicated that many children balk at instructions from an instinct of self-preservation, as children will not turn their backs to complete strangers in complete medical settings, especially if they have had rectal exams, lumbar punctures or shots. Getting the child into the appropriate position was often accomplished with the use of stickers on the wall at the point where children of differing heights would be looking. The children were then told to look at and count the stickers appropriate to their height. Often, animal stickers would be scattered about the mural previously discussed. The children are then instructed to try and spot as many stickers as possible and choose a favorite; they are then told to hold very still because if they move, the animal sticker will run away. Bargaining with lollipops and stickers is a common technique (however, many children possess uncanny negotiating skills). Many such games were observed. Of additional benefit to the technologist, the parent can serve as an extra set of hands and eyes to ensure the child's safety while on a radiography table or in a restraining device, since toddlers are very active.

Finally, the child needs to be rewarded for good behavior and for contributing to the success of the exam. The technologists felt this was important for symbolic value and hopefully left the child with a relatively good feeling about a potentially negative experience. Verbal praise was observed to be administered copiously throughout the procedure and subsequently in the parent's presence at the completion of the exam. To quote Mary Francis Sheppard, Supervisor of Pediatric Radiology at Shands at UF and lead pediatric radiologist, "It's of great benefit and costs nothing." All facilities also distributed a variety of stickers, lollipops, coupons, or small toys.

Younger children are sometimes inconsolable and will cry or struggle even under optimal circumstances. In these situations, it was observed that performing the exam quickly and efficiently is the best thing that can be done. Pacifiers appeared to be helpful,

as was a soothing continuously talking voice. It was observed that the technologist would always talk to the child, even if he/she was screaming, crying, looking away, or pretending to talk to someone else. Frequently, the children who seemed to be ignoring the technologist were actually paying close attention. A common ploy used by the technologist would be to keep asking the child questions during all the screaming and slide in the question if they wanted to go home and if they answered, then the technologist knew they were listening. Although most parents would tell their child to not cry, the technologist would tell them that crying is preferable to biting, kicking or spitting as a method to relieve their stress.

To consistently obtain high-quality radiographs in agitated children is a technically demanding task, but the overall observation from the site surveys was that success was possible with thought, care, time and patience. The following poem by pediatric radiologist Leonard E. Swischuk, M.D. (1997), was posted in a majority of the surveyed facilities and accurately depicts the approach a facility should follow with pediatric patients.

A bundle of movement so awkward to hold,
Crying and crying for minutes untold
Perpetual motion, so hard to contain,
Your charisma and patience, it truly can strain

Your very first thought may prompt a retreat,
You'll want to give up and concede to defeat
But before you pack up and go screaming away,
Just think for a moment, this babe needs you today.

Hold him awhile, help him adjust,
Restrain his momentum, it's almost a must.
You'll not really hurt him, if his arms you must bind,
Just stay in command, be gentle and kind.

There is nothing so fine as to take a babe home,
And nothing so hard as to leave him alone.
So help little Jack, and somebody's Jill,
Their mothers and fathers sure hope that you will.

Patient and Examination Trends

Although the workload distribution of examinations were significantly different between hospitals, the same examinations tended to predominate in each hospital. As shown by the survey data in Appendix C, the numerical workload was dominated by the data for the hospitals with the most beds and any statistical comparison among the hospitals would be of little value. Looking only at the examinations identified from the initial survey at Shands at UF, it was seen that these examinations listed in Table 2-4 were represented in each hospital sample. The purpose of this survey was only to characterize the examinations that were most commonly employed and not to establish their precise frequencies.

In adult examinations, the assumption that the field size equals the film size is usually made for organ dose calculations. This assumption is not representative of pediatric radiography, where an unexposed margin was seen on the majority of films in the various hospitals surveyed. The field sizes used on the phantom in this survey represent the fields used in actual clinical practice.

This section illustrates the exams included in the site survey in each of the figures. The left hand illustration is an actual patient x-ray obtained from Dr. Jonathan Williams' teaching and case file and the right hand illustration is the comparable view of the one-year-old anthropomorphic phantom. Note that the dosimeters, leads and drill holes are frequently visible in the phantom images.

The anatomical features shown in the projection in Figure 5-1 demonstrate the petrous ridges that are projected through the lower third of the orbits. The organs of hearing and balance are housed in the petrous pyramids. The petrous ridges are the upper border of these pyramids.

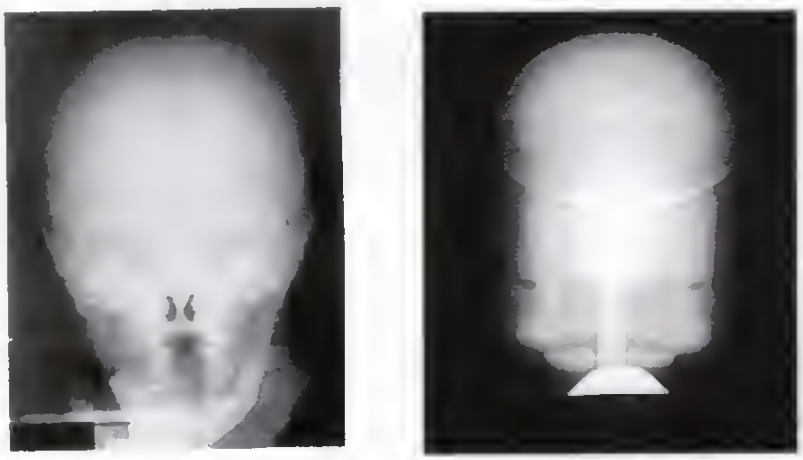

Figure 5-1. AP Skull

The anatomical features that are best shown in Figure 5-2 in lateral skull radiographs are cranial bones, facial bones, nasal sinuses, sellae turcica, anterior and posterior clinoid process, dorsum sellae, the mandible and the upper segments of the cervical spine.

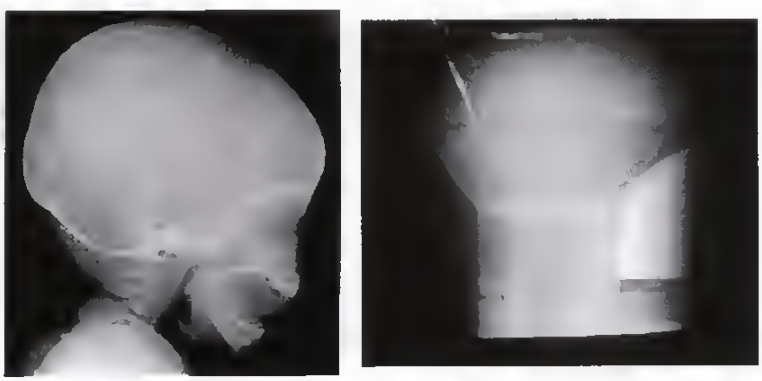

Figure 5-2. Lateral Skull

The anatomical features that are best shown in radiographs utilizing Townes view in Figure 5-3 are the occipital bone, the posterior foramen magnum, the dorsum sellae, the posterior clinoid processes, the petrous bones and the temporomandibular joint.

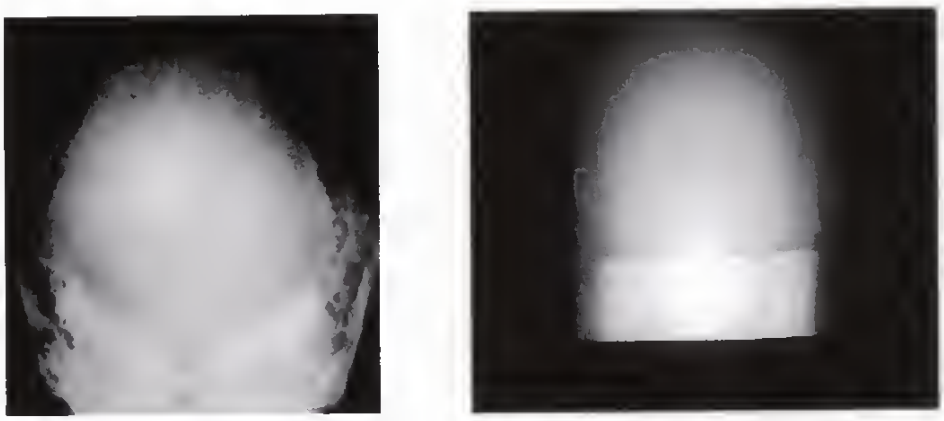

Figure 5-3. Townes Skull

Anatomical features best shown with the AP cervical spine projection in Figure 5-4 are C-3 to C-7 vertebral bodies, spaces between pedicles, intervertebral disc spaces and spinous processes.

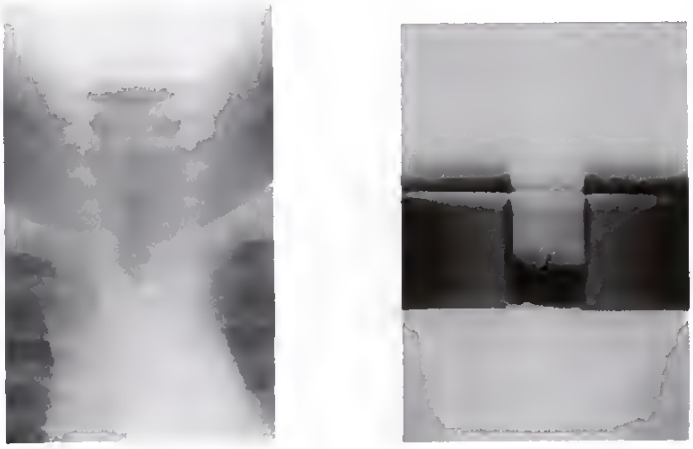

Figure 5-4. AP Cervical Spine

Cervical vertebral bodies, intervertebral joint spaces, articular pillars, spinous processes and zygapophyseal joints are shown with the lateral view in Figure 5-5.

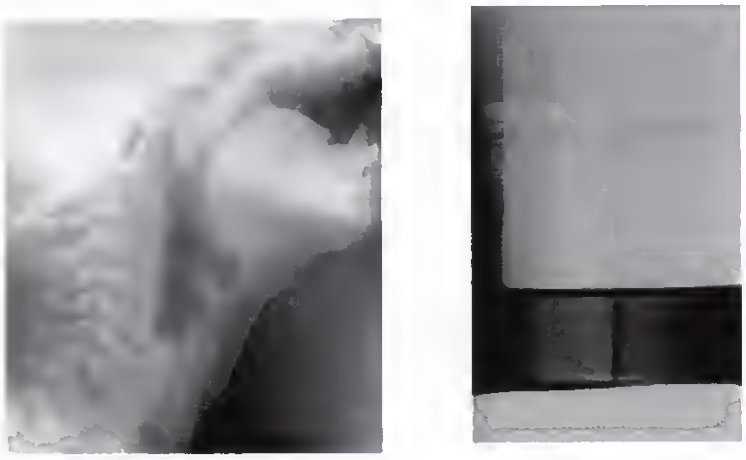

Figure 5-5. Lateral Cervical Spine

Anatomical features best shown with the AP thoracic spine projection in Figure 5-6 are thoracic vertebral bodies, intervertebral joint spaces, distance between pedicles, spinous and transverse processes, posterior ribs and costovertebral articulations.

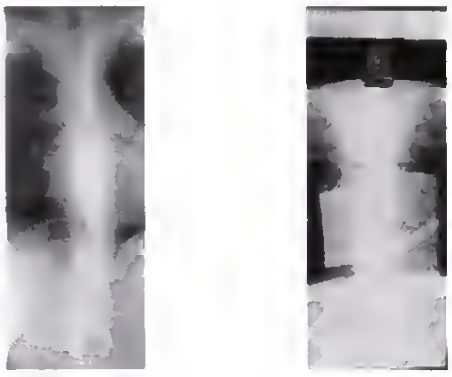

Figure 5-6. AP Thoracic Spine

Thoracic vertebral bodies, intervertebral joint spaces and intervertebral foramina are shown with the lateral breathing view in Figure 5-7.

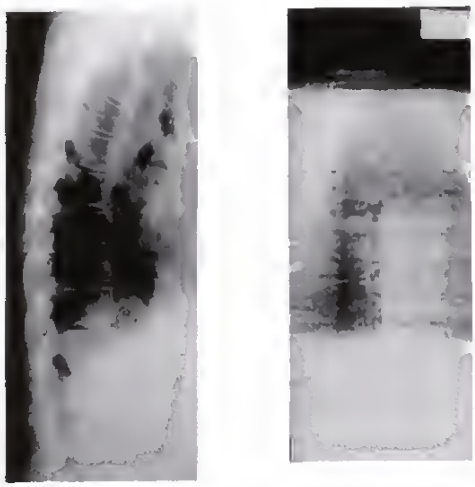

Figure 5-7. Lateral Thoracic Spine.

Anatomical features best shown with the AP lumbar spine projection in Figure 5-8 are lumbar vertebral bodies, intervertebral joints, spinous and transverse processes, laminae, and SI joints and sacrum.

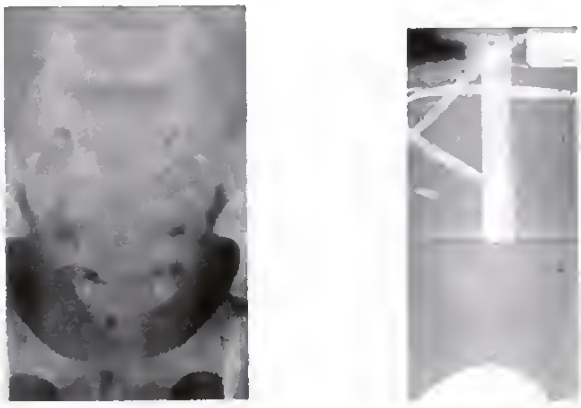

Figure 5-8. AP Lumbar Spine.

Anatomical features best shown with the lateral lumbar spine projection in Figure 5-9 are lumbar vertebral bodies, intervertebral joints, spinous processes, L-5 to S-1 junction, sacrum and first four intervertebral foramina.

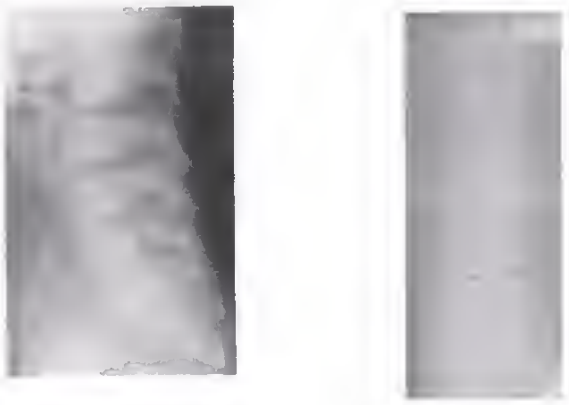

Figure 5-9. Lateral Lumbar Spine.

The anatomical structures visualized with the AP abdomen projection in Figure 5-10 are liver, spleen, kidneys, abnormal masses, calcifications or accumulations of gas, pelvis, lumbar spine, and lower ribs.

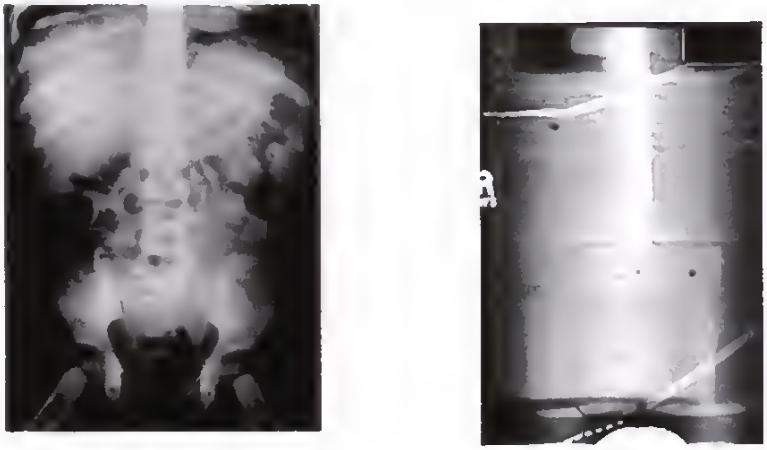

Figure 5-10. AP Abdomen.

The anatomical structures visualized with the AP pelvis projection in Figure 5-11 are the pelvic girdle, L-5, sacrum and coccyx, femoral heads, neck, and greater trochanter. The anatomical structures visualized with the AP frog-leg pelvis projection are the femoral heads, neck and greater trochanteric areas.

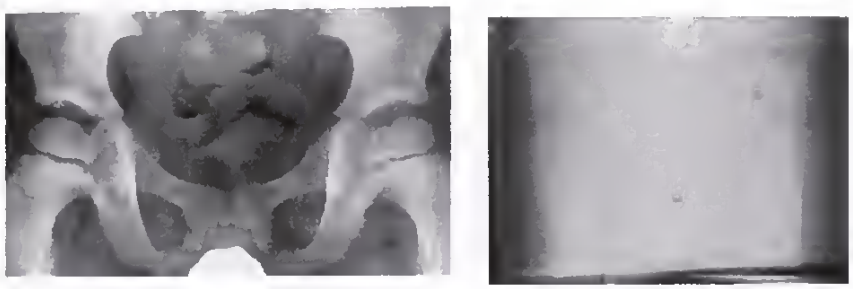

Figure 5-11. AP Pelvis.

The anatomical structures best shown with the AP hip projection in Figure 5-12 are the acetabulum, femoral head, neck, and greater trochanter. The lateral view of the acetabulum and femoral head, and the neck and trochanteric area are best shown with the frog leg hip projection.

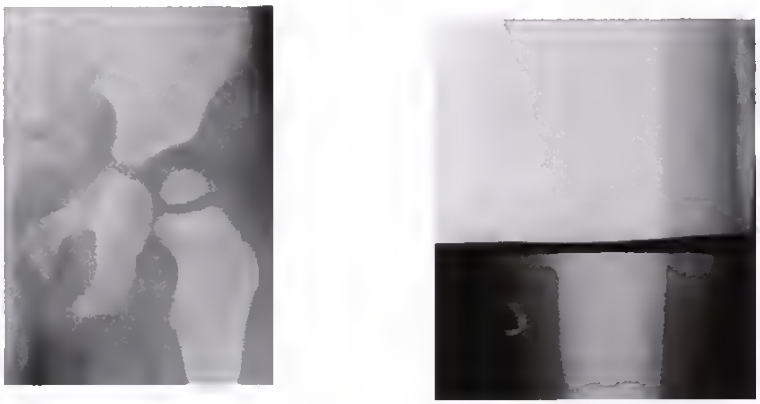

Figure 5-12. AP Left Hip.

Anatomical structures best shown with the Waters view in Figure 5-13 include frontal sinuses, the maxillary antra, the orbits and the petrous bones. The lateral sinus view shown in Figure 5-14 demonstrates all the paranasal sinuses and the nasopharynx. Imaging the sinuses in patients under the age of two appeared to be a controversial issue, as most facilities believed that the views provide very little information, although they are frequently requested. However, Swischuk states that such ideas as "sinuses are not present in patients under two years of age", "sinusitis does not occur in patients under two

years of age" and "the sinuses can be obliterated in association with crying in the infant" are all slowly being discarded since it is certain that maxillary and ethmoid sinus cavities are present in infants, and when they are opacified, they are abnormal (1997).

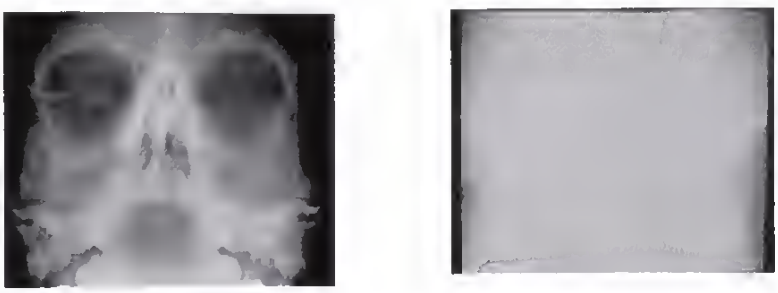

Figure 5-13. Waters Sinus.

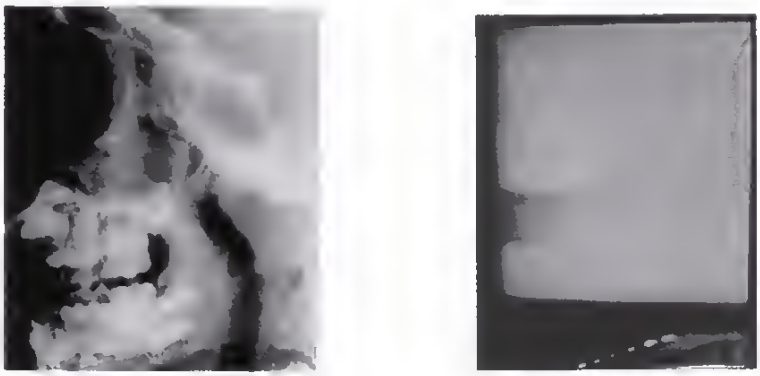

Figure 5-14. Lateral Sinus

The chest projections shown in Figures 5-15, and 5-16, respectively, reveal lungs, including apices and trachea, heart and great vessels, diaphragm (including costophrenic angles for the AP projection and the posterior costophrenic angles for the lateral projection), and bony thorax.

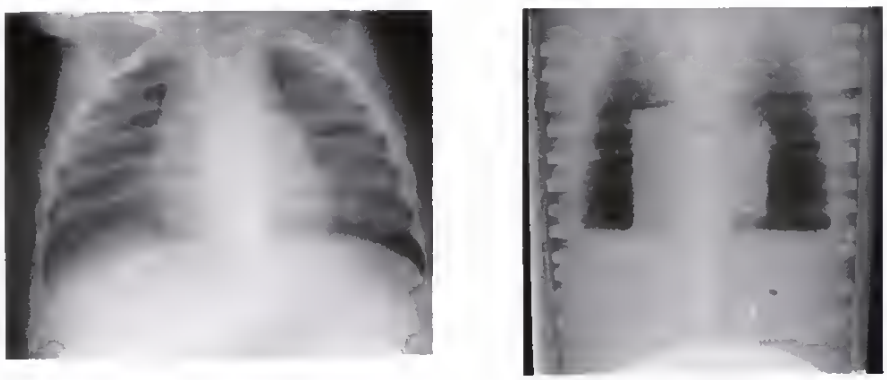

Figure 5-15. AP Chest.

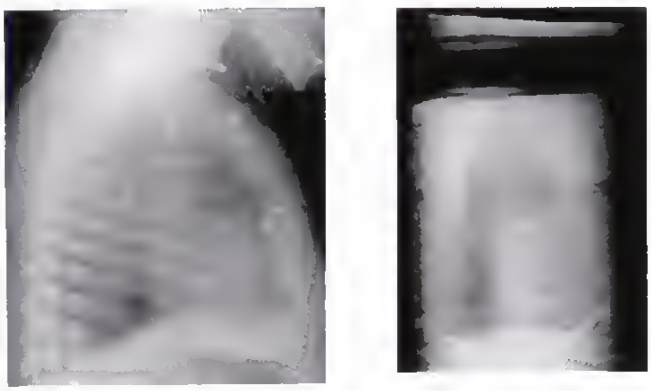

Figure 5-16. Lateral Chest.

The following sections detail the survey results and the techniques summarized in Appendix C. As has been previously stated, the image quality of a pediatric exam is no better than its radiologic technologist; however, their ability to produce quality films depends upon the equipment they have to use at their disposal.

Generators

The effective radiographic voltage depends on the type and age of the generator. Considering the very short exposure times required for pediatric examinations, a nearly rectangular radiation waveform and a minimal amount of ripple are desirable for pediatric patients. 1-, 2- and 6-pulse single phase generators cannot generally provide this. 12-

pulse three phase, high frequency or direct current constant potential high voltage generators are required. High milliamperage (400-600 mA, 800 mA maximum) permits shorter exposure times, so motion is not a problem even in the uncooperative infant or young child, yet low milliamperage settings are also required in small infants. This means that the smallest patients need the most powerful machines. As seen in Appendix C, two of the facilities in the site survey have high frequency generators, one has a single phase generator and the remainder have three phase systems. The range of kVp utilized by each facility for each exam surveyed is illustrated in Figure 5-17. These facilities were specifically chosen to survey each type of generator available. It should be noted that workload and patient flow patterns also dictate the type of equipment needed for general applications if a room is not dedicated for pediatrics

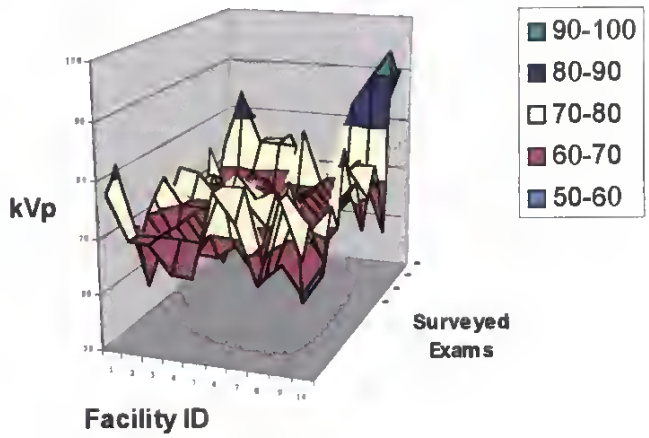

Figure 5-17. Range of kVp used for the 17 surveyed exams.

Exposure Time

In pediatric imaging, exposure times must be short, which necessitates the high mA stations previously discussed. This is only possible with powerful generators and tubes, as well as optimal rectification and accurate time switches. The various output mAs employed by each facility for each exam surveyed is illustrated in Figure 5-18.

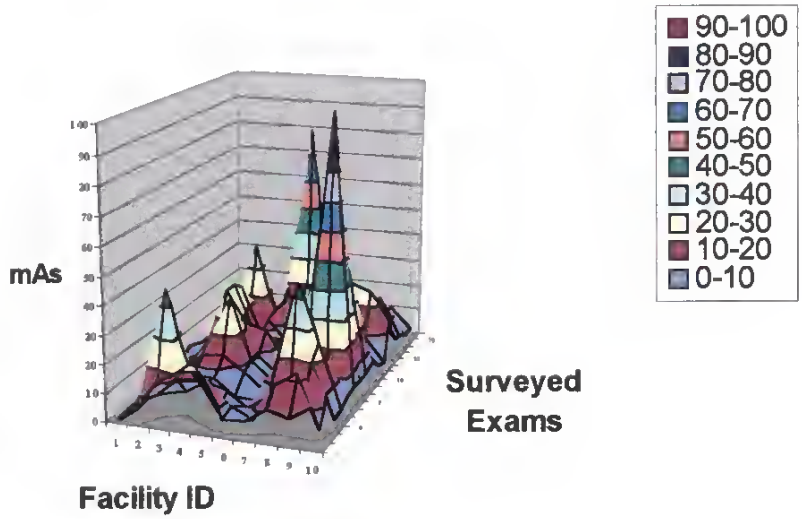

Figure 5-18. Range of mAs used for the 17 surveyed exams.

Focal Spot Size

A focal spot size between 0.6 and 1.3 mm edge length was used at all facilities; all the facilities used the small focal spot for the chest examinations. The facilities that didn't use the smaller focal spot for the remainder of the examinations were the non-dedicated pediatric facilities that had bi-focal tubes where the focal spot size that allowed the most appropriate setting of exposure time and voltage at the chosen SID most commonly used was the large.

Additional Filtration

The soft part of the radiation spectrum that is completely absorbed in the patient is useless for the production of the radiographic image and contributes unnecessarily to the patient dose. Part of it is eliminated by the inherent filtration of the tube, tube housing, and collimator, but this is insufficient. Most tubes have a minimum inherent filtration of 2.5 mm Al. Additional filtration can further reduce unproductive radiation and thus patient dose. Pediatric radiation dose should be kept low, particularly when high speed film-screen combinations are used. As previously discussed, not all generators allow the

short exposure times that are required for higher kV technique. Consequently, very low voltages were frequently observed being used for the pediatric studies surveyed. Adequate additional filtration allows the use of higher voltage with the shortest available exposure times, thus overcoming the limited capability of such equipment for short exposures. This makes the use of high speed-film combinations possible. In all of the facilities surveyed, additional filtration of up to 1 mm aluminum or 0.1 mm – 0.2 mm of copper equivalent appeared to be present, as shown in Figure 5-19.

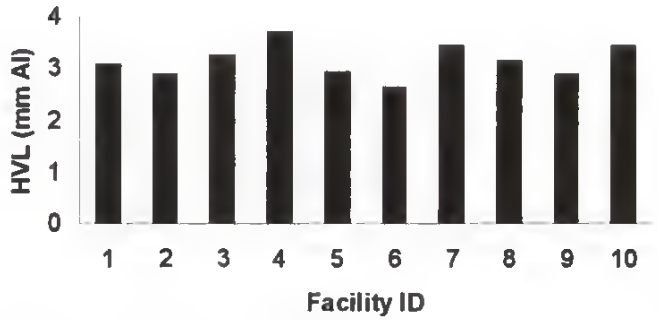

Figure 5-19. Range of HVL.

Grids

Grids are composed of alternating strips of lead and interspaces of plastic or aluminum. The lead strips are designed to attenuate the scattered radiation and the plastic or aluminum interspaces to allow the passage of the primary radiation. Grids are placed between the patient and the film and are an inherent component of either the chestboard or the table bucky. The majority of the dedicated pediatric facilities either had grids that were removable from their chestboard or shot cross-table x-rays if the exam was performed on the table and the grid was not preferred. Grids are described according to their grid ratio, which is the ratio of the height of the lead strips to the distance between them. The higher the ratio, the more radiation the grid absorbs and hence the more radiation is required to penetrate the patient and the grid to reach the film.

In pediatric patients, radiography should be performed without grids, as the tissue volume irradiated is small and there is little scatter. The radiation dose to the pediatric patient can be significantly reduced by omitting the grid. The survey showed that all chest exams were performed without a grid, except in facilities where it was impossible to remove the grid. The abdomen, pelvis, spine and skull exams were all performed with a grid. Grids with 10:1 ratios were found in most of the facilities. Facilities that used a general purpose x-ray room for their pediatric studies, in which kilovoltages of more than 100 kV were commonly used, had 12:1 linear grids installed.

Cassettes

The front of a cassette is made of a minimally attenuating material such as carbon fiber. The back of a cassette is covered on the inside with a sheet of lead foil to absorb x-rays and reduce backscatter, which would reduce image quality. Cassettes are important for providing proper film-screen contact. Poor screen contact resulting from air pockets being trapped between screens and film as the cassette is closed will spread the light emitted from the screen, and blur the recorded radiographic image. If the film-screen contact is too tight, pressure artifacts are produced and structural screen mottle is accentuated. Cassettes should be properly handled and routinely tested for film-screen contact to produce acceptable images and reduce retakes.

Because pediatric patients range in size from the newborn to the young adult, each facility had a spectrum of cassette sizes available. The cassettes most commonly used included 20 cm x 25 cm (8" x 10"), 24 cm x 30 cm (10" x 12"), 28 cm x 36 cm (11" x 14"), and 35 cm x 43 cm (14" x 17"), with various other smaller and larger sizes for special applications. A variety of cassette manufacturers were utilized in the surveyed faciltities, including Kodak, DuPont/Sterling, and Fuji.

Film-Screen Combination

Among the technical parameters, the selection of higher speed classes of the film-screen combination has the greatest impact on dose reduction. In addition, it allows shorter exposure times that minimize motion unsharpness, which is the most important cause of blurring in pediatric imaging. Only one facility utilized a 600 speed system; the remainder utilized 400 speed systems. The reduced resolution of higher speed screens is the limiting factor in the choice of higher system speed. Most facilities also had different sets of cassettes available for special indications, with screens of the lower speed and higher resolution.

Source-Image Distance (SID)

There are no differences from adult patients for this item. The SID is usually 101 cm (40") for tabletop tubes with grids and 182 cm (72") for chestboard stands. When no grid is used and the cassette is placed upon the table, the same tube-table distance as with a grid was usually observed. Slight departures from these distances were technologist preferences.

Automatic Exposure Control

Adult patients vary in size, but their variation is small compared to the range in pediatric patients. Most facilities accomodate this range by utilizing manual techniques, yet one would expect that an automatic exposure control (AEC) device would be helpful in this situation. However, many of the systems commonly available are not satisfactory for this purpose. They have relatively large and fixed ionization chambers. Neither their size, nor shape, or position is able to compensate for the many variations of body size and body proportion in pediatrics patients. In addition, the usual ionization chambers of AECs are built in behind the grid. Consequently, AEC use may be associated with the use of the grid where the grid is not removable. Specially designed pediatric AECs have been tested which utilize a small mobile ion chamber for use behind a lead-free cassette. The position of the detector can be selected with respect to the most important region of interest. This

would need to be performed extremely carefully, as even minor patient movement would throw off the detector's reading. Since the high speed of modern screens require a minimal dose at the front of the cassette, the detector behind the cassette would be required to work in a range at a fraction of the entrance dose. It has proven difficult to ensure reproducibility in this range and is an area for future research.

Manual techniques are the preferred method of radiographing pediatric patients. The majority of facilities that utilized manual techniques had generated their technique charts either through experience or through the utilization of a variety of sizes of frozen game birds, for example a game hen would mimic a neonate.

Field Size and Collimation

Inappropriate field size is the most important fault in pediatric radiographic technique. A field which is too small will immediately degrade the respective image criteria. A field which is too large will not only impair image contrast and resolution by increasing the amount of scattered radiation but also result in unnecessary irradiation of the body outside the area of interest. Consequently, the anatomical areas specified by the respective image criteria define the minimum and the maximum field sizes, although some degree of latitude is necessary to ensure that the entire field of interest is included.

Correct collimation requires proper knowledge of the external anatomical landmarks by the technologist. These differ with the age of the patient according to the varying proportions of the developing body. In addition, the size of the field of interest depends more on the nature of the underlying disease in infants and younger children than adults. For example, the lung fields may be extremely large in congestive heart failure and pulmonary diseases or the position of the diaphragm may be very high in digestive diseases. Therefore, a basic knowledge of pediatric pathology is required for technologists to ensure proper collimation in these age groups. As shown in Appendix C,

the facilities that paid strict attention to tight collimation were all dedicated pediatric facilities or conscientious technologists, although all facilities had unexposed margins.

Radiographic Film Quality

Film blackening has a major influence on image quality. For the same radiographic projection, film blackening depends on many factors: radiation dose, radiation quality, patient size, radiographic technique, image receptor sensitivity and film processing. Film blackening determines the optical densities of a radiographic film. The optimal range of the optical density (D) is between D = 0.5 and D = 2.0 (net density, i.e. over fog and base), with a mean optical density of D = 1.2. Films with a mean optical density of less than D=0.4 or more than D=2.0 usually possess inferior information content. Figure 5-20 illustrates the net lung optical densities for AP chest, PA chest and lateral chest films, respectively, performed at each facility. The majority of the facilities surveyed were in the optical density range between D=1.0 and D=2.0. It should be noted that the degree of film blackening is also subject to the personal preference of the individual radiologist.

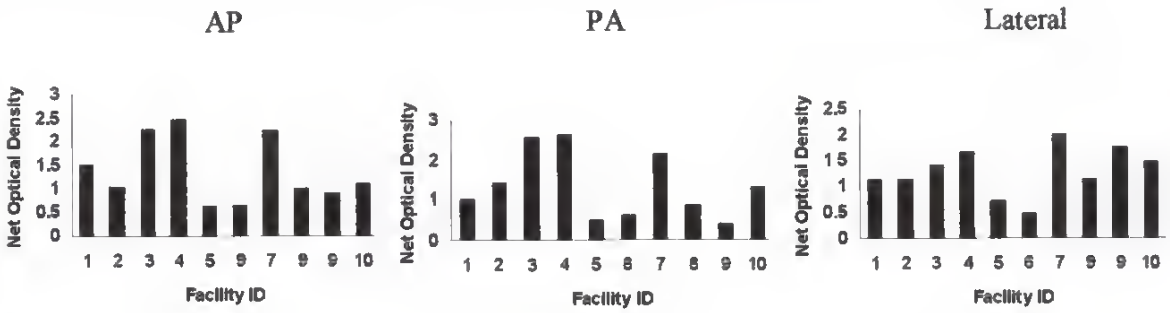

Figure 5-20. Net lung optical densities for AP chest, PA chest and lateral chest films.

Repeat Analysis

Repeat analysis involves an assessment of how many and why images are being re-taken. Most radiology departments save their spent film for silver reclamation which are periodically collected from the waste film bin and evaluated. It is important to know the time period over which the films were collected and how much total film was used in the department. The thrown out films are collated into different categories. Discarded

radiographic films with patient anatomy on them constitute the repeat category. The repeat rate is calculated as the fraction, or percentage, of films that were repeated. Repeat films are a technical concern as these films represent repeated radiation exposure to the patient. The repeated films can be broken down into subcategories such as overexposed, underexposed, motion problems and improper positioning. Retake rates in excess of 10% are cause for concern. Repeat rates for each surveyed facility are shown in Figure 5-21, none of which exceed 10%. It should be noted that one facility with a low repeat rate is filmless utilizing a computed radiography (CR) system and generally only uses film when the CR system is nonoperational. Computed radiography uses photostimulable phosphor plates to capture x-ray exposure patterns rather than screen/film combinations. CR is advantageous because it has a wide dynamic range and can therefore produce diagnostic quality films with suboptimal x-ray techniques, resulting in reduced repeats. For the purposes of this research, the facility agreed to go back to using film-screen combinations.

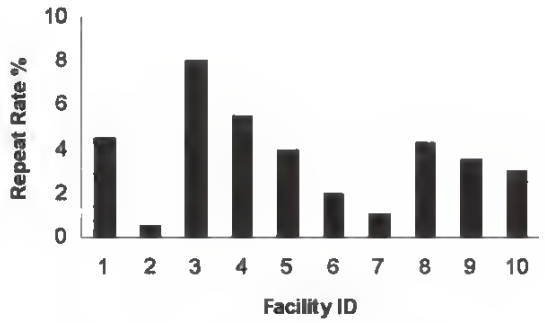

Figure 5-21. Repeat percentages per facility.

It is important to realize that the repeat rate for an institution is not necessarily a good parameter for evaluating the quality between different facilities. Radiology services that produce poor images and where the radiologists will read anything will generally have low retake rates, but may not necessarily exhibit high quality. Departments with radiologists who demand high quality images from the technologists may exhibit higher retake rates, but yield better diagnostic results.

Radiation Protection

For all examinations of pediatric patients, good radiographic technique includes lead rubber shielding of the body in the immediate proximity of the diagnostic field. The body is thus protected from external scattered and extrafocal radiation. For exposures of 60-80 kV utilized in this research, a dose reduction of about 30-40% can be achieved by shielding with 0.25 mm lead equivalent rubber 4-6 cm away from the boundary of the primary beam. This is only true when the protective device is placed correctly at the field limit. Lead-rubber covering further away away from the boundary of the primary beam is less effective, and at a distance greater than 6 cm is completely ineffective; it may have a psychological effect but provides no radiation protection at all. For pediatric chest radiography, lead shields that are appropriate to the patient's size are placed over the gonads when the study is performed with the patient in the supine position. When the child is examined in the upright position, a small lead apron is placed around the waist. For abdominal radiography, shielding should not be used for either the upright or supine studies in pediatric female patients. The gonads are shielded when studies of the abdomen are performed on male patients.

There is some controversy as to the most appropriate shielding for radiography of the hip of a child. Generally only one of the two views of the hips requires gonadal shielding for the first study on female patients; gonadal shielding is used for both views in all subsequent studies. Studies on male patients require gonadal shielding to be used for both views of the hips, including those of the first study. General studies of the female pelvis, as opposed to hip exams, do not require gonadal shielding; the male gonads are always shielded when the pelvis is radiographed. For radiography of the head, neck, cervical and thoracic spines, small lead aprons are placed over the pelvis for all of these studies in pediatric patients. No shielding can be employed for the AP lumbosacral spine in pediatric female patients. However, shielding should be used for both views of male

patients and for the lateral view of female patients. The fact that male gonads are always shielded is reflected in the effective dose results detailed in the next section.

Organ Doses per Entrance Skin Exposure and Effective Doses

The one-year-old phantom was used to evaluate the organ doses from several plain film radiographic examinations. The radiographic examinations chosen for simulation were those discussed in the previous section for projections common in pediatric radiology and are common projections performed at Shands at the University of Florida. Due to the limited time availability at each facility, dosimetry measurements were only performed for the chest series of examinations at statewide facilities.

The x-ray system utilized for the measurements performed at Shands at UF was a three phase system with 3.07 mm Al filtration. Tube potentials used were typical of what is currently used in practice at Shands at UF and other hospitals, which ranged from 60 kVp to 95 kVp.

The results for the 27 exams at Shands at UF are given in Appendix E. There are three data sheets per exam in Appendix E, except for the head series, which only has two data sheets. The first two pages and the top half of the third page of the data sheets are associated with the MOSFET dose measurements and the effective dose information, and the bottom half of the third page of the data sheets contain the risk estimation information. Correspondingly for the head series, the first page and the top half of the second page of the data sheets are associated with the MOSFET dose measurements and the effective dose information, and the bottom half of the second page of the data sheets contain the risk estimates.

Eight high sensitivity MOSFET dosimeters were available for the majority of the dose measurements. The MOSFET locations are shown in the data sheets of Appendix E. The one-year-old phantom was loaded with MOSFET dosimeters in areas applicable to

the exam being simulated. For example, the right arm, left arm, skull/facial, thyroid and spine head positions were loaded first for the skull series. The two groupings of MOSFET detectors are shown in the data sheet in the organ/position column. The first eight organ/positions correspond to the first group, and the next eight organ/positions correspond to the second group.

Areas on the data sheet without data indicate that the MOSFET measurements were not made at those locations, as the dosimeters were located well out of the field of view. If a position was monitored and a negative reading was obtained, an absorbed dose of zero was assigned. The MOSFET measurement is the difference between the voltage measurement of the MOSFET device held at a high bias and the voltage measurement of the MOSFET device held at a low bias; therefore, there is a statistical probability of obtaining small negative readings from the Patient Dose Verification System. Negative readings are actually quite common when the device has received no absorbed dose since the MOSFET device with the high bias experiences more ion recombination than the low bias device.

The last data sheet contains an effective dose calculation for each of the exams. The pediatric technologist was asked to simulate each exam as if the phantom were an actual one-year-old; technique factors specific to the exam were then obtained. The absorbed organ dose for this study was obtained by applying a ratio of the actual techniques (mAs) used for the clinical exam to the techniques used to obtain accurate absorbed dose data previously described.

Tissue weighting factors from Table 3-1, Chapter 3, were then applied. The average of the absorbed dose between the two lungs was used, multiplied by the lung tissue weighting factor for the lung contribution to the effective dose. The same procedure was applied to the left and right ovaries. The ovary dose was used for the gonad contribution to the female effective dose calculation and the testes dose was used for the gonad contribution for the male. The active marrow, bone surface, remainder and

skin doses were calculated with the procedure outlined in Chapter 3, and the respective tissue weighting factors given in Table 3-1 were applied. The effective dose is given in Table 5-1 for each procedure performed at Shands at UF and for both males and females. As expected, the exams with higher effective doses reflect the areas of the exposed body which contain more radiosensitive organs, such as the thoracic and lumbar spine, and the abdomen and pelvis. Female exams also require more attention as their resultant doses were higher than male exams in all cases but one.

A comparison of the effective doses from the chest examinations among facilities is shown in Table 5-2. Facilities #3, #4, and #7 all yielded larger effective doses than the other facilities. Some of the possible reasons for the higher effective doses include: Facilities #3 and #4 are both community hospitals whose patient population is biased towards indigent care; therefore, their protocols are not optimized for pediatric patients. Facility #4 did not utilize a dedicated pediatric technologist. The radiologist staff at Facilities #3 and #4 also prefer a higher degree of film blackening, as shown by Figure 5-20. Facility #7 utilizes the CR system and demonstrates that although collective doses may be decreased by decreased repeats, individual patient doses may be higher since technique factors are not as carefully tracked when CR's post-processing capabilities are available. Facilities #4 and #7 also did not use a manual technique but relied on the AEC system. The problems with utilizing AEC units constructed for adult anatomy on pediatric patients has been previously discussed, but would only be applicable to Facility #4 as Facility #7 has a dedicated pediatric chest unit. Modification of these practices would reduce their doses. In general, the facilities that followed the recommended practices discussed for dose reduction, did deliver lower effective doses.

Table 5-1. Effective Doses for Male and Female One-Year-Olds at Shands at UF

Examination	Effective Dose (mrem)
AP Skull	
Male or Female	0 5
AP Skull w/thyroid shield	
Male or Female	0.1
PA Skull	
Male or Female	0.2
PA Skull w/thyroid shield	
Male or Female	0.2
LAT Skull	
Male or Female	0 2
Townes Skull	
Male or Female	0.4
AP Cervical Spine	
Male or Female	1 0
LAT Cervical Spine	
Male or Female	2.1
AP Thoracic Spine	
Male or Female	4.2
LAT Thoracic Spine	
Male	6 6
Female	6.4
AP Lumbar Spine	
Male	4.3
Female	5.5
LAT Lumbar Spine	
Male	3.1
Female	4.6
AP Abdomen Supine	
Male	6.0
Female	6.9
PA Abdomen Supine	
Male or Female	2.4
AP Abdomen Upright	
Male	7 8
Female	9.2
AP Pelvis	
Male	2.4
Female	3.7
AP Hip	
Male or Female	0.7
Waters Sinus	
Male or Female	0.1
LAT Sinus	
Male or Female	0.2
AP Sinus	
Male or Female	0.2
LAT Chest	
Male or Female	0 9
AP Chest	
Male or Female	1.2
AP Chest w/bladder shield	
Male or Female	0.3
PA Chest	
Male or Female	0 4
LAO Chest	
Male or Female	1.0
RPO Chest	
Male or Female	1.3
RAO Chest	
Male or Female	1.3

Table 5-2. Comparison of Effective Doses for Male and Female One-Year-Olds Among Facilities for Chest Exams

Facility ID	AP Chest Effective Dose (mrem)	PA Chest Effective Dose (mrem)	LAT Chest Effective Dose (mrem)
Shands at UF	0.8	1.2	0.4
#2	0.7	0.4	1.1
#3	3.8	3.7	4.7
#4	5.3	4.1	6.1
#5	0.8	0.2	1.5
#6	2.7	0.6	1.3
#7	5.9	2.4	6.1
#8	1.2	0.5	1.7
#9	2.1	0.7	6.2
#10	2.2	1.3	3.1

A comparison was performed between the results of this research and that performed by the FDA and the NRPB, as these are the only two entities that have compiled data for this age group, as discussed in Chapter 1. The FDA research was performed approximately 20 years ago, and the resultant doses reflect the equipment and techniques used in that era. The NRPB study reflects European practices that may not be directly comparable to U.S. practices.

For comparison between Shands at UF with other dosimetry studies performed by the FDA, the absorbed dose data were normalized to the clinical exam entrance exposure for the thyroid, lung, bone marrow, ovaries and testes, which were the only sites included in the FDA study. Comparison of the experimental measurements performed at UF and Monte Carlo calculations performed by the FDA are shown in Table 5-3 for 12 of the 27 exams detailed in Appendix E. Direct comparison with the experimental TLD measurements performed by the FDA was not possible due to variation between the

phantoms, technique factors and equipment specifications for these studies. The FDA Handbook of Selected Organ Doses for Projections Common in Pediatric Radiology (Rosenstein et al. 1979) utilized the notation of enclosing data in parentheses when the coefficient of variation exceeded 50 percent; this notation is also included in Table 5-3. The Handbook reports single lung and ovary absorbed dose per unit exposure values; for comparison purposes, these single values were placed either in the average lung or average ovary row, as appropriate. Additionally, the head and neck model utilized by the FDA is considerably different from the head and neck model utilized in this research; therefore direct comparisons are not appropriate.

In general, the UF study's estimates of dose are lower than those given in the FDA report. The primary reason for the lower values are the different organ mass and tissue composition of the phantom and model used. For example the total lung mass in the UF anthropomorphic phantom is 150 grams compared to a total lung mass of 129 grams in the FDA mathematical model. Consequently, it is expected that even for equal values of energy deposition per unit mass to the lungs of both the phantom and the model, the UF phantom values would only be 86% of the lung doses estimated for the model in the FDA study. Additional differences would also be attributed to differences in tissue densities. The skeletal, lung and soft tissue densities in the UF phantom are 1.18 g/cm^3, 0.296 $g/cm^3$and 1.04 g/cm^3, respectively. The skeletal, lung and soft tissue densities in the FDA model are 1.4862 g/cm^3, 0.2958 $g/cm^3$and 0.9896 g/cm^3, respectively. This change in tissue density clearly affects the particle transport and therefore, the dose. The thyroid dose was appreciably higher in the UF study for exams in which the x-ray field was directly projected and the organ was not shielded, such as the AP cervical spine. This dose differential is directly attributable to the thyroid being placed in a more anatomically correct position in the UF phantom than in the FDA model, which did not have an explicit neck and included the thyroid as part of the head.

Table 5-3. Comparison of Shands at UF and FDA Absorbed Dose/ESE

Organ	View and Projection	1998 UF Absorbed Dose/ESE (rad/R)	1979 FDA Absorbed Dose/ESE (rad/R)
Thyroid	Townes Skull	0.171	(0.410)
	AP Skull	0.909	0.585
	PA Skull	0.059	0.130
	LAT Skull	0.000	0.380
	AP C-Spine	1.140	0.585
	LAT C-Spine	0.180	(0.370)
	AP Chest	0.355	0.585
	PA Chest	0.089	(0.120)
	LAT Chest	0.253	(0.380)
	AP Abdomen Supine	0.000	0.000
	PA Abdomen	0.000	(0.006)
	AP Pelvis	0.000	0.000
Average Lung	Townes Skull	0.000	0.056
	AP Skull	0.000	0.082
	PA Skull	0.000	0.078
	LAT Skull	0.000	0.029
	AP C-Spine	0.000	0.063
	LAT C-Spine	0.000	0.045
	AP Chest	0.145	0.554
	PA Chest	0.195	0.613
	LAT Chest	0.105	0.706
	AP Abdomen Supine	0.059	0.055
	PA Abdomen	0.000	0.056
	AP Pelvis	0.000	(0.006)
Active Bone Marrow	Townes Skull	0.066	0.048
	AP Skull	0.064	0.054
	PA Skull	0.021	0.072
	LAT Skull	0.073	0.051
	AP C-Spine	0.000	0.030
	LAT C-Spine	0.030	0.035
	AP Chest	0.021	0.101
	PA Chest	0.061	0.169
	LAT Chest	0.045	0.150
	AP Abdomen Supine	0.036	0.112
	PA Abdomen	0.000	0.214
	AP Pelvis	0.000	0.104

Table 5-3, continued.

Organ	View and Projection	1998 UF Absorbed Dose/ESE (rad/R)	1979 FDA Absorbed Dose/ESE (rad/R)
Average Ovary	Townes Skull	0.000	0.000
	AP Skull	0.000	0.000
	PA Skull	0.000	0.000
	LAT Skull	0.000	0.000
	AP C-Spine	0.000	0.000
	LAT C-Spine	0.000	0.000
	AP Chest	0.000	(0.019)
	PA Chest	0.000	(0.002)
	LAT Chest	0.000	(0.013)
	AP Abdomen Supine	0.254	0.400
	PA Abdomen	0.000	0.400
	AP Pelvis	0.363	0.400
Testes	Townes Skull	0.000	0.000
	AP Skull	0.000	0.000
	PA Skull	0.000	0.000
	LAT Skull	0.000	0.000
	AP C-Spine	0.000	0.000
	LAT C-Spine	0.000	0.000
	AP Chest	0.000	0.000
	PA Chest	0.000	0.000
	LAT Chest	0.000	0.000
	AP Abdomen Supine	0.000	0.105
	PA Abdomen	0.000	0.047
	AP Pelvis	0.000	(1.070)

In order to compare the doses delivered at the surveyed facilities with dosimetry studies performed by the NRPB, the effective dose data were normalized to the clinical exam entrance skin absorbed dose. Comparison results between experimental measurements performed at the facilities and Monte Carlo calculations performed by the NRPB are shown in Table 5-4 for the chest exams detailed in Appendix E. The NRPB Report of Coefficients for Estimating Effective Doses from Pediatric X-Ray Examinations (Hart et al. 1996) utilizes the previous generation Cristy and Eckerman mathematical pediatric models. The NRPB modified these phantoms by adding their own esophagus and neck, and further modified the composition of the breast tissue to reflect a higher fat content. These modifications are not published in detail, and the head model utilized by

the NRPB is considerably different from the prototype head model utilized in this research; therefore direct comparisons are not possible.

Table 5-4. Comparison Among All Facilities and NRPB Effective Dose/ESD

Facility ID	AP Chest 1998 UF Effective Dose/ESD (rem/rad)	AP Chest 1996 NRPB Effective Dose/ESD (rem/rad)	PA Chest 1998 UF Effective Dose/ESD (rem/rad)	PA Chest 1996 NRPB Effective Dose/ESD (rem/rad)	LAT Chest 1998 UF Effective Dose/ESD (rem/rad)	LAT Chest 1996 NRPB Effective Dose/ESD (rem/rad)
Shands at UF	0.508	0.168	0.162	0.103	0.117	0.113
#2	0.133	0.182	0.064	0.109	0.105	0.118
#3	1.348	0.188	1.157	0.115	1.639	0.123
#4	0.243	0.200	0.142	0.126	0.202	0.133
#5	0.303	0.153	0.076	0.096	0.461	0.107
#6	0.382	0.146	0.088	0.090	0.095	0.101
#7	0.378	0.188	0.186	0.115	0.246	0.123
#8	0.442	0.182	0.187	0.109	0.291	0.118
#9	0.123	0.194	0.043	0.121	0.102	0.128
#10	0.416	0.210	0.190	0.137	0.208	0.142

A comparison of the data indicates that the effective doses received from the observed clinical procedures are generally consistent with the effective doses predicted from the Monte Carlo calculations. There are, however, several sites with large discrepancies. It is difficult to attribute these discrepancies to any particular features of the exams, because the NRPB normalized their doses to entrance skin absorbed dose rather than entrance skin exposure, and do not provide a detailed explanation of how they calculate their entrance skin absorbed dose. This provides strong motivation for performing the detailed comparison of experimental and computer simulations that will be performed at UF in future work, utilizing a mathematical model that is as identical as possible to the anthropomorphic phantom.

Relative Risk

The BEIR V report's general expression for calculating the total cancer risk, including natural and radiation-induced, to a population was utilized to determine relative risks. The values of $g(\beta)$ were determined for each gender for an exposure that occurs at

an age of one year, and the time post-exposure was chosen to be five years past the latency period for each different type of cancer. The values of $f(d)$ were determined utilizing the effective doses calculated in Chapter 3. Numerical values of $g(\beta)$ and $f(d)$ are shown in Appendix E, and were multiplied to determine the relative risk predicted by: $[1 + f(d)\, g(\beta)]$. This general expression was evaluated using these variables for each procedure simulated at Shands at UF, as shown in Table 5-5 and for the chest examinations at all of the facilities as shown in Table 5-6.

Table 5-5. Relative Risk for Shands at UF Examinations

Exam	Leukemia	Male Respiratory	Female Respiratory	Male Digestive	Female Digestive	Other	Female Breast
AP Skull	1.000157	1.000023	1.000046	1.000004	1.000007	1.000006	1.000000
AP Skull w/shield	1.000041	1.000006	1.000012	1.000001	1.000002	1.000002	1.000000
PA Skull	1.000067	1.000010	1.000020	1.000002	1.000003	1.000003	1.000000
PA Skull w/shield	1.000065	1.000009	1.000019	1.000002	1.000003	1.000002	1.000000
LAT Skull	1.000055	1.000008	1.000016	1.000001	1.000002	1.000002	1.000000
Townes Skull	1.000131	1.000019	1.000039	1.000003	1.000006	1.000005	1.000000
AP C-Spine	1.000308	1.000045	1.000091	1.000008	1.000013	1.000012	1.000001
LAT C-Spine	1.000672	1.000097	1.000198	1.000017	1.000029	1.000025	1.000002
AP T-Spine	1.001343	1.000195	1.000397	1.000034	1.000059	1.000051	1.000003
LAT T-Spine	1.002096	1.000299	1.000628	1.000052	1.000093	1.000080	1.000005
AP L-Spine	1.001584	1.000203	1.000523	1.000035	1.000078	1.000060	1.000003
LAT L-Spine	1.001584	1.000146	1.000433	1.000025	1.000064	1.000047	1.000003
AP Abdomen Supine	1.002073	1.000279	1.000657	1.000048	1.000097	1.000079	1.000005
PA Abdomen Supine	1.000769	1.000112	1.000227	1.000019	1.000034	1.000029	1.000002
AP Abdomen Upright	1.002732	1.000362	1.000876	1.000063	1.000130	1.000104	1.000006
AP Pelvis	1.000970	1.000110	1.000349	1.000019	1.000052	1.000037	1.000002
AP Hip	1.000219	1.000032	1.000065	1.000006	1.000010	1.000008	1.000001
Waters Sinus	1.000044	1.000006	1.000013	1.000001	1.000002	1.000002	1.000000
LAT Sinus	1.000080	1.000012	1.000024	1.000002	1.000003	1.000003	1.000000
AP Sinus	1.000050	1.000007	1.000015	1.000001	1.000002	1.000002	1.000000
AP Chest w/shield	1.000107	1.000016	1.000032	1.000003	1.000005	1.000004	1.000000
LAO Chest	1.000323	1.000047	1.000096	1.000008	1.000014	1.000012	1.000001
RPO Chest	1.000433	1.000063	1.000128	1.000011	1.000019	1.000016	1.000001
RAO Chest	1.000423	1.000061	1.000125	1.000011	1.000019	1.000016	1.000001

Table 5-6. Relative Risk for Chest Examinations Among All Facilities

AP Chest							
Facility ID	Leukemia	Male Respiratory	Female Respiratory	Male Digestive	Female Digestive	Other	Female Breast
Shands at UF	1.000384	1.000056	1.000113	1.000010	1.000017	1.000015	1.000001
#2	1.000230	1.000034	1.000068	1.000006	1.000010	1.000009	1.000001
#3	1.001237	1.000179	1.000365	1.000031	1.000054	1.000047	1.000003
#4	1.001694	1.000246	1.000499	1.000043	1.000074	1.000064	1.000004
#5	1.000238	1.000034	1.000072	1.000006	1.000011	1.000009	1.000001
#6	1.000832	1.000117	1.000253	1.000020	1.000038	1.000032	1.000002
#7	1.001895	1.000276	1.000558	1.000048	1.000083	1.000072	1.000005
#8	1.000382	1.000055	1.000113	1.000010	1.000017	1.000014	1.000001
#9	1.000633	1.000084	1.000204	1.000015	1.000030	1.000024	1.000001
#10	1.000719	1.000104	1.000212	1.000018	1.000031	1.000027	1.000002
PA Chest							
Facility ID	Leukemia	Male Respiratory	Female Respiratory	Male Digestive	Female Digestive	Other	Female Breast
Shands at UF	1.000123	1.000018	1.000036	1.000003	1.000005	1.000005	1.000000
#2	1.000138	1.000020	1.000041	1.000003	1.000006	1.000005	1.000000
#3	1.001189	1.000173	1.000350	1.000030	1.000052	1.000045	1.000003
#4	1.001314	1.000193	1.000384	1.000033	1.000057	1.000050	1.000003
#5	1.000062	1.000009	1.000018	1.000002	1.000003	1.000002	1.000000
#6	1.000199	1.000029	1.000059	1.000005	1.000009	1.000008	1.000000
#7	1.000777	1.000113	1.000229	1.000020	1.000034	1.000029	1.000002
#8	1.000150	1.000020	1.000048	1.000003	1.000007	1.000006	1.000000
#9	1.000235	1.000034	1.000069	1.000006	1.000010	1.000009	1.000001
#10	1.000412	1.000060	1.000121	1.000010	1.000018	1.000016	1.000001
LAT Chest							
Facility ID	Leukemia	Male Respiratory	Female Respiratory	Male Digestive	Female Digestive	Other	Female Breast
Shands at UF	1.000281	1.000040	1.000084	1.000007	1.000012	1.000011	1.000001
#2	1.000361	1.000052	1.000108	1.000009	1.000016	1.000014	1.000001
#3	1.001500	1.000217	1.000444	1.000038	1.000066	1.000057	1.000004
#4	1.001958	1.000284	1.000578	1.000049	1.000086	1.000074	1.000005
#5	1.000495	1.000071	1.000147	1.000012	1.000022	1.000019	1.000001
#6	1.000422	1.000061	1.000126	1.000011	1.000019	1.000016	1.000001
#7	1.001945	1.000281	1.000576	1.000049	1.000085	1.000074	1.000005
#8	1.000550	1.000080	1.000162	1.000014	1.000024	1.000021	1.000001
#9	1.001981	1.000287	1.000586	1.000050	1.000087	1.000075	1.000005
#10	1.000900	1.000118	1.000292	1.000020	1.000043	1.000034	1.000002

The values of relative risk show that the examinations that yielded higher effective doses and had the most radiosensitive tissues in the field of view, e.g. the abdomen, thoracic spine and lumbar spine, also yielded the highest risk. These values of relative risk can also be used to predict excess risks that may be more meaningful to members of the general public. For example, from Table 5-5 for an AP abdomen upright exam, the

relative risk for leukemia is 1.002732. Recall from Chapter 4 that λ_0 is the cancer risk to the unexposed population. According to the American Cancer Society (Murphy et al. 1995), λ_0 for leukemia is 28,600 cases in 1994. For the U.S. population of 259.5×10^6, as determined by an average of the 1990 - 1998 U.S. census (BC 1998), this results in an incidence rate of 1.10×10^{-4} leukemias/person-year. For 10^6 individual examinations, the excess cancers predicted by BEIR V would be $(1.002732 - 1)(1.10 \times 10^{-4}$ leukemias/person-year$)(10^6$ persons$) = 0.3$ leukemias per year. The risk from this single examination is quite low and provides a significant benefit to the patient. This methodology may be similarly extended to additional cancers and to cases where a patient is subjected to a series of multiple examinations, resulting in a significantly greater risk which may be of concern. There are several limitations to this approach. The first is that the effective dose from the exam performed at Shands at UF is not necessarily representative of exams performed in the entire U.S. It would obviously be better to have a relative risk that is representative of the exams administered throughout the U.S. The FDA has recently initiated an effort to collect representative data on pediatric exams performed in the U.S. through their Nationwide Examination of X-Ray Trends (NEXT) survey, which should be available in several years. The second is that the BEIR V and American Cancer Society parameters apply to the entire population and do not separate out those specific to pediatric patients. The availability of pediatric specific data and models would permit more accurate risk evaluations for this population.

The great advantage of this methodology is that it can be readily updated to incorporate future revised data. As research into pediatric cancer and radiation exposure continues, tissue and radiation weighting factors specific to each age range for pediatric patients may be determined, or pediatric specific risk models may be developed. These revisions can then be easily combined with the existing organ dose measurements to obtain improved values of effective dose and prediction of risk.

CHAPTER 6
CONCLUSIONS

Site Surveys

Detailed studies in the Shands at UF pediatric section of the radiology department and site surveys in nine other Florida facilities have confirmed that radiation protection is particularly important for the pediatric patient. While radiological examinations are indispensable throughout childhood from birth to adolescence, the justification and optimization, which provide the basis for radiation protection, are of far greater importance in these age groups than in adults. Justification of the examination is the most effective radiation protection in pediatric patients. Every examination should result in a net benefit for the patient. This is only applicable if it is anticipated that the examination will influence the efficacy of the decision of the referring physician with respect to diagnosis, patient management and treatment, and final outcome for the patient.

To minimize risks and maximize diagnostic benefit from any imaging examination, the radiologic procedure must be tailored to the specific clinical problem. This approach is particularly valid in pediatric radiology because of the radiation dose delivered. Radiologists assume responsibility for determining what imaging modalities are indicated for diagnostic evaluation, subsequent therapy, and follow-up. They must determine if requested examinations are indicated, the examination that should be performed, what views should be obtained, what sequence of examinations should be selected, and if other imaging modalities are required. All of the radiologists who participated in the survey were keenly interested in quantifying the doses they were delivering to their patients and what they could do to improve the quality of their care.

The radiologic technologist, preferably a dedicated pediatric technologist, plays the central and critical role in the diagnostic imaging process and is responsible for providing high quality films. In order to limit patient exposure as low as practicable without losing its benefits, the following recommendations resulting from the site surveys are made for optimization of pediatric diagnostic radiography:

Accurate exposure charts should be utilized corresponding to radiographic technique and the patient's weight when x-raying the trunk of the body, or the patient's age when x-raying the extremities. In the future, small computers and utilization of the various ages of anthropomorphic phantoms could incorporate such multifactorial parameters as machine specifics to provide prospectively the dose from a variety of exams to aid the radiologist in his clinical choice

This study demonstrated that due to the small body size and volume of young children, a large portion of their total body is exposed to the radiation beam that would cover only a small area in the adult. Therefore, confining the x-ray beam to the smallest area commensurate with adequate illumination of the field of interest not only improves detailed discrimination of radiographic images, but can reduce patient dosage and decrease the scattered radiation dose to attending personnel and technologists.

Radiography depends on the fact that a small portion of the radiation energy impinging on the patient emerges on the other side of the body and then selectively blackens the x-ray film. The difference in energy between the entry and exit radiation, constituting the greater part of the total radiation, is either absorbed by the skin and deep tissue structures or scattered to surrounding areas. The input radiation may be dramatically reduced without loss of the necessary exit radiation required to produce the film image in the following ways: Increased filtration at the x-ray tube head up to 1 mm Al plus 0.1 – 0.2 mm Cu or similar materials should be used. Since low energy photons generally cannot pass through the patient's body, they contribute little to producing an image on the x-ray film. The filter will selectively absorb these lower energy photons.

Thus, the added filtration reduces the entry dose to the patient without sacrificing detail of the film image. The use of high-speed intensifying screens and high speed film can also reduce the patient dose without loss of the quality of image on the x-ray film.

The judicious use of clinical x-ray examinations of pediatric patients, avoiding as far as possible, unnecessary repetitive diagnostic radiography and technically nondiagnostic radiography, is desirable. Technically unsatisfactory x-rays are a waste of time, effort and money. Moreover, every nondiagnostic film requires a retake and thus a doubling of patient dose and associated risk. To this end, proper immobilization techniques improve image quality, decrease the length of the examination, and decrease the need for repeat studies.

When not contraindicated, gonadal shielding is always recommended for most diagnostic procedures. It is not currently known if genetic damage occurs as a result of low-dose diagnostic radiologic procedures. However, if one assumes a linear relation without a threshold for genetic effects in which any amount of radiation has a response, it would be appropriate to shield the gonads of pediatric patients. Thyroid shielding should also be used where applicable.

Future improvements in x-ray technology such as computed or digital radiography must be used with care. As demonstrated with the one facility in the survey that is filmless, the potential for abuse is high where post-processing capabilities are available.

In summary, radiation dose and corresponding risk may be decreased by performing only examinations that are clinically indicated, tailoring the examination, decreasing exposure with increased filtration and fast film-screen combinations, using correct techniques, shielding the patient's gonads and thyroid when possible, preventing repeat exposures due to motion with proper immobilization, and using low-dose digital radiography or nonionizing imaging modalities such as ultrasonography or magnetic resonance imaging, for definitive diagnosis whenever feasible.

Phantom Measurements

The organ doses calculated from the point dose measurements, excluding the thyroid, range from 15% to 143 % of the previously published FDA Monte Carlo data. Direct comparison of the data is difficult since the mathematical models have evolved, especially with the addition of the head and neck model. This is demonstrated by the thyroid organ doses which ranged from 42% to 195 % of the values generated by the FDA. The FDA models did not explicitly contain a neck, and the head itself was less realistically represented. The corresponding effective doses also ranged in agreement with the recently published NRPB Monte Carlo data in some cases by a factor of ten. Again, direct comparison of the data is difficult because the NRPB mathematical pediatric models are substantially different from the current mathematical models from which the anthropomorphic phantom was constructed. This distinctly points out the need to perform future work at UF utilizing a mathematical model that is as identical as possible to the anthropomorphic phantom.

Tbe phantom-dosimetry system used in this study has some practical limitations, especially in the determination of the dose to the bone marrow. First, a homogenous bone mixture is used similar to that used in prior Monte Carlo calculations. A heterogenous bone and soft tissue mixture would be more realistic of pediatric anatomy, both in the anthropomorphic phantom and the mathematical model. Second, the system only measures the bone dose in six locations and determines a marrow dose from this limited information. The location of the field of view with respect to the MOSFET locations could skew the final marrow dose calculation depending on whether the MOSFET dosimeters were in the primary field or not. A similar limitation is seen in the larger organs such as the lungs. If the entire lung is either in the primary beam or outside the primary beam, then the organ dose estimate calculated from the point dose measurement should be accurate; however, if only the edge of the primary beam intersects the lung, the

absorbed dose estimate will either be overestimated if the MOSFET is located within the field of view, or underestimated if the MOSFET is located outside the field of view.

The initial lack of an external funding source limited the full expansion of the system. Ideally 20 high sensitivity MOSFET dosimeters would be utilized to measure all the point doses simultaneously and read out immediately into a laptop computer. For the majority of this work, only eight high sensitivity dosimeters were available; therefore multiple exposures were necessary for each view. The time required to collect the data was also increased. A full complement of dosimeters would reduce the workload and provide instant dose calculations via computer interface, making the real-time aspects of the system more evident.

The phantom-dosimetry system is very simple to use and provides real-time dose estimates. It is expected the system could be used for dose reconstruction work, dose estimates from typical exams, as well as in situations which are difficult to simulate mathematically such as fluoroscopy. Since the real-time point dose estimates are a good measure of the organ doses in typical plain film examinations, it is expected that they will prove valuable in the verification of the more difficult simulations using oblique views. This type of benchmarking for the Monte Carlo simulations is an extremely important step in the ensuring the validity of the results.

The development of a newborn anthropomorphic phantom is a high priority. As shown by the data in Appendix A, thousands of exams are performed on newborns annually. Patients born with complications are routinely subjected to a series of multiple examinations, resulting in a significantly greater cumulative dose and risk which may be of concern, and where the methodology developed in this research will prove to be most useful.

Effective Dose and Risk Predictions

The results of this research provide the effective dose and relative carcinogenic risks for several commonly performed plain film diagnostic procedures. The measured effective doses ranged from a low of 0.1 mrem for an AP skull exam that utilized thyroid shielding, to a high of 9.2 mrem for an AP upright abdomen exam on a female. Correspondingly, the relative leukemia carcinogenic risk ranged from 1.000041 for an AP skull exam that utilized thyroid shielding, to a high of 1.002732 for an AP upright abdomen exam, with corresponding estimates of excess risks based on 10^6 exams of 0.005 and 0.3 leukemias per year, respectively. The risk from these individual examinations are quite low and probably provide a significant benefit to the patient. Future research into tissue and radiation weighting factors specific to each age range for pediatric patients, or pediatric specific risk models is needed in cases where a patient is subjected to a series of multiple examinations, such as the newborn patient population previously discussed.

The methods developed in this research can now be utilized to facilitate the development and transfer of scientific information for the improvement in the radiologic care of children. The techniques can be integrated with the computational and advanced experimental interfaces being developed to quickly assess the organ doses and risks to various ages of pediatric patients undergoing a variety of modern diagnostic examinations. Such automated systems will permit the ready extension of these techniques to advanced radiological procedures including fluoroscopy, computed tomography, cardiac catheterization, computed radiography and digital radiography.

APPENDIX A
NUMBER OF EXAMS FOR PEDIATRIC PATIENTS UNDER 16 YEARS OF AGE
For the Time Period 01/01/97-12/31/97
at Shands at the University of Florida Radiology Department

The following data indicate number and type of exam for all imaging modalities.

Year	Modality	RIS #	Exam & View	Newborn	1-Year	5-Year	10-Year	15-Year
97	CT	1000	ABDOMEN W/OU CONTRAST - CT	0	1	1	2	2
97	CT	1001	ABDOMEN W/O CONTRAST EXT - CT	0	0	0	0	0
97	CT	1005	ABDOMEN WITH CONTRAST - CT	2	2	3	27	98
97	CT	1006	ABDOMEN W/CONTRAST EXTENDED -C	0	0	0	0	1
97	CT	1010	ANGIO - CT	0	0	0	0	0
97	CT	1015	ABDOMEN W & W/O CONTRAST - CT	0	0	0	1	8
97	CT	1020	BIOPSY 0 – 30 MINUTES - CT	0	0	0	0	0
97	CT	1025	BIOPSY 30 MINUTES - 1 HOUR - CT	0	0	0	1	0
97	CT	1030	BIOPSY OVER 1 HOUR - CT	0	0	0	1	0
97	CT	1035	BRW STEREOTACT LOCATION - CT	0	0	1	1	0
97	CT	1036	BRW STEREOTACTIC LOCATION - EX	0	0	1	5	3
97	CT	1040	DRAINAGE 30 MINUTES - 1 HOUR-	0	0	0	0	0
97	CT	1045	CHEST W/OUT CONTRAST - CT	0	0	2	14	53
97	CT	1046	CHEST W/O CONTRAST EXT - CT	0	0	0	1	2
97	CT	1050	DRAINAGE OVER 1 HOUR - CT	0	0	0	0	1
97	CT	1055	CHEST WITH CONTRAST - CT	0	0	3	3	33
97	CT	1056	CHEST W/CONTRAST EXTENDED - CT	0	0	0	0	0
97	CT	1060	HEAD W/OUT CONTRAST - CT	138	87	226	173	173
97	CT	1061	HEAD W/O CONTRAST EXTENDED - CT	2	2	4	1	4
97	CT	1065	CHEST W & W/O CONTRAST - CT	0	0	0	0	0
97	CT	1070	HEAD WITH CONTRAST - CT	1	4	8	10	5
97	CT	1071	HEAD W/CONTRAST EXTENDED - CT	0	0	1	0	0
97	CT	1075	DRAINAGE 0 – 30 MINUTES - CT	0	0	0	0	0
97	CT	1080	HEAD WITH & WITHOUT CONTRAST - C	10	9	53	33	35
97	CT	1081	HEAD W/&W/O CONTRAST EXTENDED	0	0	1	4	0
97	CT	1084	CORONAL HEAD - CT	2	0	0	0	1
97	CT	1085	MAXILLO FACIAL PROJ W/O CON – CT	4	0	5	6	5
97	CT	1086	MAXILLO FACIAL 1PROJ W/O CON EX	1	0	3	4	3
97	CT	1087	CT MAXILLO FACIAL LIMITED	1	1	4	3	4
97	CT	1090	ORBITS 1PROJ W/CONTRAST - CT	0	0	0	0	0
97	CT	1091	ORBITS 1PROJ W/CONTRAST EXT - CT	0	0	0	0	0
97	CT	1095	MAXILLO FACIAL 1PROJ W/CONTRAST 1	0	6	4	1	
97	CT	1096	MAXILLO FACIAL 1PROJ W/CON EXT	0	1	1	0	0
97	CT	1097	MAXILLO FACIAL 1PROJ W/&W/O CO	0	0	0	1	0
97	CT	1100	ORBITS 2 PROJ W/OUT CONTRAST-CT	0	0	2	8	6
97	CT	1101	ORBITS 2 PROJ W/O CONTRAST EXT	0	0	0	0	0
97	CT	1105	MAXILLO FACIAL 2 PROJ W/O CON	0	0	21	21	16
97	CT	1106	MAXILLOFACIAL 2PROJ W/O CON EX	1	0	1	1	0
97	CT	1110	ORBITS 2 PROJ WITH CONTRAST - CT	1	0	4	1	0
97	CT	1111	ORBITS 2PROJ W/CONTRAST EXT - CT	0	0	0	0	1
97	CT	1115	MAXILLO FACIAL 2 PROJ W/CON - CT	0	1	11	8	4
97	CT	1116	MAXILLOFACIAL 2PROJ W/CON EXT	0	0	0	0	0
97	CT	1117	MAXILLO FACIAL 2PROJ W/&W/O CO	0	0	1	0	0
97	CT	1125	ORBITS 1 PROJ W/OUT CONTRAST-CT	0	0	1	0	0
97	CT	1126	ORBITS 1PROJ W/O CONTRAST EXT	0	0	0	0	0
97	CT	1130	SELLA 1 PROJ W/OUT CONTRAST - CT	0	0	0	0	1
97	CT	1135	SELLA 1 PROJ WITH CONTRAST - CT	0	0	0	0	1
97	CT	1137	SELLA 1PROJ W/&W/O CONTRAST - CT	0	0	0	0	0

Year	Modality	RIS #	Exam & View	Newborn	1-Year	5-Year	10-Year	15-Year
97	CT	1140	TEMPORAL BONE 2 PROJ W/O CON - CT	2	3	36	27	12
97	CT	1141	TEMPORAL BONE 2PROJ W/O CON EX	0	0	0	0	1
97	CT	1146	SELLA 2PROJ W/O CON EXT - CT	0	0	0	0	1
97	CT	1150	TEMPORAL BONE 2 PROJ W/CON - CT	0	2	7	3	2
97	CT	1151	TEMPORAL BONE 2PROJ W/CON EXT	0	0	0	0	1
97	CT	1155	SELLA 2 PROJ WITH CONTRAST - CT	0	0	0	1	1
97	CT	1157	SELLA 2PROJ W/&W/O CON - CT	0	1	0	0	2
97	CT	1161	POSTERIOR FOSSA W/O CONTRAST - CT	1	1	1	0	0
97	CT	1162	POSTERIOR FOSSA W/CONTRAST - CT	0	1	2	2	0
97	CT	1163	POSTERIOR FOSSA W/&W/O CONTRAS	0	0	1	1	0
97	CT	1165	TEMPORAL BONE 1 PROJ W/O CON - CT	2	0	8	1	0
97	CT	1166	TEMPORAL BONE 1PROJ W/O CON EX	0	0	1	0	0
97	CT	1175	TEMPORAL BONE 1 PROJ W/CON – CT	0	0	1	1	0
97	CT	1176	TEMPORAL BONE 1PROJ W/CON EXT	0	0	0	0	0
97	CT	1180	LOWER EXTREMITY W/OUT CON - CT	0	0	0	2	10
97	CT	1181	LOWER EXTREMITY W/O CON EXT - CT	0	0	0	1	2
97	CT	1185	LOWER EXTREMITY WITH CONTRAST-C	0	0	3	2	2
97	CT	1186	LOWER EXTREMITY W/CONTRAST EXT	0	0	0	0	1
97	CT	1190	UPPER EXTREMITY W & W/O CON - CT	0	0	0	1	0
97	CT	1195	LOWER EXTREMITY W & W/O CON - CT	0	0	0	1	6
97	CT	1200	UPPER EXTREMITY WIT2H AIR - CT	0	0	0	0	0
97	CT	1205	LOWER EXTREMITY - CT WIT2H AIR	0	0	0	0	0
97	CT	1210	UPPER EXTREMITY W/OUT CON - CT	0	0	0	3	3
97	CT	1211	UPPER EXTREMITY W/O CON EXT - CT	0	0	0	0	1
97	CT	1215	PELVIS W/OUT CONTRAST - CT	0	0	0	1	3
97	CT	1216	PELVIS W/O CONTRAST EXTENDED - CT	0	0	1	0	0
97	CT	1220	UPPER EXTREMITY WITH CONTRAST-	0	0	0	1	0
97	CT	1225	PELVIS WITH CONTRAST - CT	1	1	1	26	83
97	CT	1226	PELVIS W/CONTRAST EXTENDED - CT	0	0	0	0	5
97	CT	1230	PELVIS W & W/OUT CONTRAST - CT	0	0	0	0	0
97	CT	1235	SOFT TISSUE NECK W/ CONTRAST - CT	1	3	24	16	16
97	CT	1236	SOFT TISSUE NECK W/CON EXT - CT	0	0	0	0	0
97	CT	1240	RADIATION THERAPY PLANNING - CT	0	0	0	0	0
97	CT	1245	SOFT TISSUE NECK W & W/O CON - CT	0	0	0	0	1
97	CT	1255	CERVICAL SPINE W/OUT CONTRAST-	1	0	3	6	10
97	CT	1256	CERVICAL SPINE W/O CON EXT - CT	0	0	0	0	3
97	CT	1265	CERVICAL SPINE WITH CONTRAST - CT	0	0	0	0	0
97	CT	1266	CERVICAL SPINE W/CONTRAST EXT	0	0	0	0	0
97	CT	1267	CERVICAL SPINE W/&W/O CON - CT	0	0	0	0	0
97	CT	1270	SOFT TISSUE NECK W/O CONTRAST-	1	0	2	0	2
97	CT	1271	SOFT TISSUE NECT W/O CON EXT - CT	0	0	0	0	0
97	CT	1275	CERVICAL SPINE POST MYELOGRAM-	0	0	0	0	0
97	CT	1276	CERVICAL SPINE POST MYELO EXT	0	0	0	0	0
97	CT	1280	LUMBAR SPINE W/OUT CONTRAST-CT	0	0	2	3	4
97	CT	1281	LUMBAR SPINE W/O CONTRAST EXT	0	0	1	0	0
97	CT	1285	THORACIC SPINE POST MYELOGRAM-	0	0	0	0	0
97	CT	1286	THORACIC SPINE POST MYELO EXT	0	0	0	0	0
97	CT	1290	LUMBAR SPINE WITH CONTRAST - CT	0	0	1	0	0
97	CT	1291	LUMBAR SPINE W/CONTRAST EXT - CT	0	0	0	0	1
97	CT	1300	LUMBAR SPINE POST MYELOGRAM - CT	0	0	0	0	0
97	CT	1301	LUMBAR SPINE POST MYELO EXT - CT	0	0	0	0	0
97	CT	1310	THORACIC SPINE W/OUT CONTRAST-	0	0	0	2	1
97	CT	1311	THORACIC SPINE W/O CON EXT – CT	0	0	0	1	0
97	CT	1315	3D RECONSTRUCTION - CT	1	1	2	2	3
97	CT	1320	THORACIC SPINE WITH CONTRAST - CT	0	0	0	0	1
97	CT	1321	THORACIC SPINE W/CONTRAST EXT	0	0	0	0	0
97	CT	1322	THORACIC SPINE W/&W/O CONTRAST	0	0	0	1	0
97	CT	1325	CT CALL BACK	17	5	48	19	39
97	CT	1330	NON-IONIC CONTRAST 1 UNIT - CT	35	27	191	28	1
97	CT	1335	NON-IONIC CONTRAST 3 UNITS - CT	0	0	0	10	70
97	CT	1336	NON-IONIC CONTRAST 4 UNITS CT	0	0	0	0	1
97	CT	1340	NON-IONIC CONTRAST 2 UNITS - CT	0	0	10	52	49
97	CT	1345	PELVIS -LIMITED STUDY CT	0	0	0	0	1
97	CT	1350	L-SPINE WIT2H & W/O CONTRAST -C	0	0	0	0	0
97	CT	1400	PELVIMETRY -CT	0	0	0	0	0
97	CT	1410	MULTI-PLANAR REFORMATIONS	6	0	22	17	33
97	CT	1411	DENTAL VIEW - LIMITED - CT	0	0	0	0	1
97	CT	1413	MPR - DENTAL - CT	0	0	0	0	1

Year	Modality	RIS #	Exam & View	Newborn	1-Year	5-Year	10-Year	15-Year
97	CT	1490	PARAVERTEBRAL NERVE INJ – SING	0	0	0	0	0
97	CT	1491	PARAVERTEBRAL NERVE INJ - MULT	0	0	0	0	0
97	CT	1492	FACET INJECTION - SINGLE - CT	0	0	0	0	0
97	CT	1493	FACET INJECTION - ADDITIONAL -	0	0	0	0	0
97	CT	1500	ABDOMEN -LIMITED STUDY CT	0	0	0	1	0
97	CT	1505	CHEST -LIMITED STUDY CT	0	0	2	0	1
97	CT	1510	NECK-LIMITED STUDY CT	0	0	0	4	4
97	CT	1515	HEAD-LIMITED STUDY CT	0	0	0	1	0
97	CT	1520	T-SPINE -LIMITED STUDY CT	0	0	0	1	0
97	CT	1525	C-SPINE -LIMITED STUDY CT	0	0	0	1	1
97	CT	1530	L-SPINE -LIMITED STUDY CT	0	0	0	0	0
97	CT	1535	LOWER EXTREMITY -LIMITED STUDY	0	0	0	0	0
97	CT	1540	UPPER EXTREMITY -LIMITED STUDY	0	0	0	0	0
97	CT	1600	BIOPSY MUSCLE DEEP - CT	0	0	0	0	0
97	CT	1602	BIO NECK/THORAX SOFTTISSUE - CT	0	0	0	1	0
97	CT	1603	BIO BACK OR FLANK SOFT TISSUE	0	0	0	0	0
97	CT	1604	BIO BACK AREA DEEP TISSUE - CT	0	0	0	0	0
97	CT	1605	BIO SHOULDER SUPERFICIAL - CT	0	0	0	0	0
97	CT	1606	BIO SHOULDER DEEP - CT	0	0	0	0	0
97	CT	1607	BIO PELVIS/HIP SUPERFICIAL - CT	0	0	0	0	0
97	CT	1608	BIO PELVIS/HIP DEEP - CT	0	0	0	0	0
97	CT	1609	BIO THIGH/KNEE DEEP - CT	0	0	0	0	0
97	CT	1611	BIO PERCUTANEOUS LUNG -CT	0	0	0	1	0
97	CT	1612	BIO LYMP2H NODE DEEP W/NEEDLE - C	0	0	0	0	0
97	CT	1613	BIO DEEP AXILLARY NODE - CT	0	0	0	0	0
97	CT	1617	BIOPSY LIVER - CT	0	0	0	0	0
97	CT	1618	BIO PANCREAS PERCUTANEOUS - CT	0	0	0	0	0
97	CT	1619	BIOPSY KIDNEY - CT	0	0	0	0	0
97	CT	1626	BIOPSY UPPER ARM DEEP - CT	0	0	0	0	0
97	CT	1630	BIOPSY LOWER LEG DEEP - CT	0	0	0	0	0
97	CT	1632	BIOPSY FEMUR DEEP - CT	0	0	0	0	1
97	CT	1634	BIOPSY ABDOMINAL/RETROPERITONE	0	0	0	0	0
97	CT	1645	DRNG SOFT TISSUE/NECK - CT	0	0	0	0	0
97	CT	1646	DRNG BURSA/KNEE/THIGH - CT	0	0	0	0	0
97	CT	1647	DRNG PERITONEAL - CT	0	0	0	0	1
97	CT	1648	DRNG SUBDIAOHRAGMATIC - CT	0	0	0	0	0
97	CT	1649	DRNG RETROPERITONEAL - CT	0	0	0	0	0
97	CT	1650	DRNG PERITONEOCENTESIS - CT	0	0	0	0	0
97	CT	1651	DRNG RENAL/PERIRENAL - CT	0	0	0	0	0
97	CT	1652	DRAINAGE PANCREATIC PSEUDOCYST	0	0	0	0	0
97	CT	1654	THORACOSTOMY EMPYEMA - CT	0	0	0	0	0
97	CT	1655	DRAINAGE PANCREAS - CT	0	0	0	0	0
97	CT	1656	DRAINAGE LIVER - CT	0	0	0	0	0
97	CT	1700	ASPIRATION 0-30 MIN - CT	0	0	0	0	0
97	CT	1701	ASPIRATION 30-60 MIN - CT	0	0	0	0	0
97	CT	1702	ASPIRATION OVER 1 HOUR - CT	0	0	0	0	1
97	CT	1710	ASPIRATION KIDNEY/PELVIC CYST	0	0	0	0	0
97	CT	1711	ASPIRATION LUNG - CT	0	0	0	0	0
97	CT	1712	ASPIRATION PLEURAL CAVITY - CT	0	0	0	0	0
97	CT	1713	ASPIRATION PNEUMOTHORAX - CT	0	0	0	0	0
97	CT	1714	ASPIRATION INTERVERTEBRAL DISK	0	0	0	0	0
97	CT	1900	PEDS ABDOMEN W/O CONTRAST - CT	1	0	1	2	0
97	CT	1901	PEDS ABDOMEN W/CONTRAST - CT	9	5	92	30	0
97	CT	1902	PEDS ABDOMEN W/&W/O CONTRAST – C	5	2	11	4	0
97	CT	1910	PEDS PELVIS W/O CONTRAST - CT	0	1	1	0	0
97	CT	1911	PEDS PELVIS W/CONTRAST - CT	7	4	76	25	0
97	CT	1912	PEDS PELVIS W/&W/O CONTRAST - CT	0	1	2	0	0
97	CT	1920	PEDS CHEST W/O CONTRAST - CT	5	5	28	11	1
97	CT	1921	PEDS CHEST W/CONTRAST - CT	7	3	36	13	0
97	CT	1922	PEDS CHEST W/&W/O CONTRAST - CT	2	1	0	1	0
97	CT	8290	MYELOGRAM LUMBOSACRAL – LUMBAR	0	0	0	0	0
97	FLUORO	1275	CERVICAL SPINE POST MYELOGRAM-	0	0	0	0	0
97	FLUORO	2000	ABDOMEN 1VIEW	0	0	0	0	0
97	FLUORO	2010	ABDOMEN SUPINE & UPRIGHT	0	0	0	0	0
97	FLUORO	2020	KUB	1	0	0	0	0
97	FLUORO	2100	CHEST PA & LATERAL	0	0	0	0	0

Year	Modality	RIS #	Exam & View	Newborn	1-Year	5-Year	10-Year	15-Year
97	FLUORO	2105	CHEST 1VIEW	2	1	0	0	0
97	FLUORO	2115	CHEST DECUBITUS LEFT	0	0	0	0	0
97	FLUORO	2120	CHEST DECUBITUS RIGHT	0	0	0	0	0
97	FLUORO	2200	INTRAVENOUS PYELOGRAM	0	0	0	0	5
97	FLUORO	2205	CYSTOGRAM WITH RADIOLOGIST	0	0	0	0	0
97	FLUORO	2210	INTRAVENOUS PYELOGRAM W/TOMOGR	0	0	0	0	0
97	FLUORO	2215	CYSTOGRAM – VOIDINO	11	2	5	5	4
97	FLUORO	2220	IVP ABBREVIATED	0	0	0	0	1
97	FLUORO	2230	ANTEGRADE PYELOGRAM	0	0	4	0	3
97	FLUORO	2240	RETROGRADE PYELOGRAM	0	0	0	1	3
97	FLUORO	2245	RETROGRADE URETHROGRAM	0	0	0	0	2
97	FLUORO	2255	LOGPOGRAM	0	0	0	0	0
97	FLUORO	3050	TOMOGRAPHY	0	0	0	0	0
97	FLUORO	3320	SHOULDER RIGHT	0	0	0	0	0
97	FLUORO	3500	CERVICAL SPINE	0	0	0	0	0
97	FLUORO	3530	C-SPINE FLEXION & EXTENSION ON	0	0	0	0	1
97	FLUORO	3540	LUMBAR SPINE	0	0	0	0	0
97	FLUORO	4090	ESOPHAGEAL SWALLOW - NUCMED	0	0	0	0	0
97	FLUORO	6160	CATHETER MANIPULATIONS	0	0	0	0	0
97	FLUORO	6180	CATHETER PLACEMENT	0	0	0	0	0
97	FLUORO	6200	CHOLANGIOGRAM - T/TUBE	0	0	0	0	0
97	FLUORO	6245	PERCUTANEOUS OASTROSTOMY	0	0	0	0	0
97	FLUORO	6500	LUMBAR PUNCTURE	0	0	0	0	0
97	FLUORO	6770	PARAVERTEBRAL NERVE BLOCK	0	0	0	0	0
97	FLUORO	8000	GI SERIES	32	6	18	4	3
97	FLUORO	8005	ESOPHOGRAM	6	8	5	2	4
97	FLUORO	8010	GI W/SMALL BOWEL SERIES	1	1	2	2	4
97	FLUORO	8015	ESOPHOGRAM W/HYPOPHARNYX	0	0	0	0	0
97	FLUORO	8025	REHAB BARIUM SWALLOW	1	0	1	1	2
97	FLUORO	8030	SMALL BOWEL SERIES ONLY	2	0	1	1	3
97	FLUORO	8035	BARIUM ENEMA	11	2	4	3	2
97	FLUORO	8040	ENTEROCLYSIS STUDY	0	0	0	0	0
97	FLUORO	8045	BARIUM ENEMA WITH/AIR	2	0	3	0	0
97	FLUORO	8050	CHOLANGIOGRAM	0	0	0	0	0
97	FLUORO	8055	HYSTEROSALPINGOGRAM	0	0	0	0	0
97	FLUORO	8070	ERCP	0	0	1	1	3
97	FLUORO	8085	SINEOGRAM - FISTULAGRAM	0	0	0	1	0
97	FLUORO	8090	FLUOROSCOPY	1	1	1	2	0
97	FLUORO	8095	SPEECH CINE EXAM	0	0	0	0	0
97	FLUORO	8100	CHEST – FLUORO ONLY	0	1	1	0	1
97	FLUORO	8110	CHEST W/FLUOROSCOPY	0	0	0	0	1
97	FLUORO	8125	VENOGRAM LEG RIGHT	0	0	0	1	0
97	FLUORO	8140	GI TUBE PLACEMENT	2	0	3	1	0
97	FLUORO	8141	GI TUBE REPOSITION	1	2	1	0	0
97	FLUORO	8145	ARTHROGRAM-WRIST	0	0	0	0	0
97	FLUORO	8146	ARTHROGRAM WRIST - LIMITED	0	0	0	0	0
97	FLUORO	8150	ARTHROGRAM – SHOULDER	0	0	0	0	1
97	FLUORO	8151	ARTHROGRAM SHOULDER - LIMITED	0	0	0	0	5
97	FLUORO	8156	ARTHROGRAM ANKLE - LIMITED	0	0	0	0	0
97	FLUORO	8165	ARTHROGRAM – ELBOW	0	0	0	0	1
97	FLUORO	8166	ARTHROGRAM ELBOW – LIMITED	0	0	0	0	1
97	FLUORO	8175	ARTHROGRAM – HIP	0	0	0	0	1
97	FLUORO	8176	ARTHROGRAM HIP – LIMITED	0	0	2	2	1
97	FLUORO	8200	FLUORO W/RADIOLOGIST	3	2	2	3	3
97	FLUORO	8201	FLUORO – ER	0	0	3	1	1
97	FLUORO	8210	FOREIGN BODY REMOVAL –ESOPHAGE	0	3	7	1	0
97	FLUORO	8224	FACET INJECTION-SINGLE-LUMBAR	0	0	0	0	0
97	FLUORO	8225	FACET INJECTION ADDITIONAL LE	0	0	0	0	0
97	FLUORO	8230	BE INTUSSUSCEPTION	4	2	2	1	0
97	FLUORO	8240	NON-IONIC CONTRAST -1 UNIT	0	0	0	1	0
97	FLUORO	8250	DEFECOGRAPHY	0	0	0	0	0
97	FLUORO	8280	MYELOGRAM CERVICAL – LUMBAR PU	0	0	0	0	0
97	FLUORO	8283	MYELOGRAM CERVICAL – C1-2 PUNC	0	0	0	0	0
97	FLUORO	8285	MYELOGRAM THORACIC - LUMBAR PU	0	0	0	0	0
97	FLUORO	8290	MYELOGRAM LUMBOSACRAL - LUMBAR	0	0	0	0	0

Year	Modality	RIS #	Exam & View	Newborn	1-Year	5-Year	10-Year	15-Year
97	FLUORO	8295	MYELOGRAM SPINE CANAL – LUMBAR	0	0	0	0	0
97	FLUORO	8304	C1-2 PUNCTURE – DIAGNOSTIC	0	0	1	0	1
97	FLUORO	8305	LUMBAR PUNCTURE - DIAGNOSTIC	0	0	0	0	5
97	FLUORO	8306	LUMBAR PUNCTURE - THERAPEUTIC	0	0	0	0	14
97	FLUORO	8307	EPIDURAL INJECTION	0	0	0	0	0
97	FLUORO	8310	PARAVERTEBRAL NERVE BLOCK - S1	0	0	0	0	0
97	FLUORO	8311	PARAVERTEBRAL NERVE BLOCK – RE	0	0	0	0	0
97	FLUORO	9155	FLUOROSCOPY - 1 HOUR	0	0	0	0	0
97	FLUORO	9160	FLUOROSCOPY - PER ½ HOUR	0	0	0	0	0
97	FLUORO	9626	NO EXAM PERFORMED	0	0	0	0	0
97	FLUORO	9920	INJ EPIDURAL STEROID	0	0	0	0	0
97	OENERAL	2000	ABDOMEN 1 VIEW	203	82	257	115	83
97	GENERAL	2010	ABDOMEN SUPINE & UPRIGHT	8	7	83	88	51
97	GENERAL	2015	ABDOMEN DECUBITUS LEFT	288	16	40	25	15
97	GENERAL	2020	KUB	491	74	134	69	67
97	GENERAL	2021	KUB – FLAT & UPRIGHT	2	0	10	4	4
97	GENERAL	2025	ABDOMEN DECUBITUS RIGHT	3	0	0	0	2
97	GENERAL	2100	CHEST PA & LATERAL	477	474	1524	665	546
97	GENERAL	2105	CHEST 1 VIEW	3763	797	1713	875	973
97	GENERAL	2106	BABYGRAM - CHEST & ABDOMEN	730	30	17	0	0
97	GENERAL	2115	CHEST DECUBITUS LEFT	31	3	18	3	9
97	GENERAL	2120	CHEST DECUBITUS RIGHT	24	3	11	2	8
97	GENERAL	2125	CHEST PA & LATERAL WITH BARIUM	0	0	0	0	1
97	OENERAL	2135	CHEST PA/LAT& BILATERAL OBLIQ	0	0	0	0	0
97	GENERAL	2140	CHEST OBLIQUE ONLY	0	0	0	0	0
97	GENERAL	2145	CHEST APICAL LORDOTIC	0	0	0	0	0
97	GENERAL	2150	CHEST 3VIEWS	0	0	0	1	0
97	GENERAL	2200	INTRAVENOUS PYELOGRAM	1	0	2	3	2
97	GENERAL	2205	CYSTOGRAM WITH RADIOLOGIST	0	2	6	12	3
97	GENERAL	2206	CYSTOGRAM IN CYSTO	0	0	0	0	0
97	GENERAL	2210	INTRAVENOUS PYELOGRAM W/TOMOGR	0	0	0	1	2
97	GENERAL	2215	CYSTOGRAM - VOIDING	93	51	269	78	21
97	GENERAL	2220	IVP ABBREVIATED	0	0	0	0	1
97	GENERAL	2225	KIDNEY IN THE OR	0	0	0	0	0
97	GENERAL	2230	ANTEGRADE PYELOGRAM	10	2	5	4	0
97	GENERAL	2240	RETROGRADE PYELOGRAM	0	0	0	0	1
97	GENERAL	2245	RETROGRADE URETHROGRAM	0	0	0	1	1
97	GENERAL	2250	ABDOMEN W/OBLIQUES	0	0	0	0	6
97	GENERAL	2255	LOOPOGRAM	0	0	0	0	1
97	GENERAL	2400	SKULL SERIES	10	23	17	10	3
97	GENERAL	2405	MANDIBLE	0	0	3	4	15
97	GENERAL	2406	PANOREX	0	0	0	5	6
97	GENERAL	2410	SKULL 2VIEWS FOLLOW UP ONLY	13	6	16	14	11
97	GENERAL	2415	TMJ - TEMPORAL MANDIBULAR JOIN	0	0	0	0	2
97	GENERAL	2420	SINUSES	0	0	30	29	20
97	GENERAL	2425	MASTOIDS	0	1	2	3	1
97	GENERAL	2430	FACIAL BONES	0	0	4	10	12
97	GENERAL	2440	NASAL BONES – NOSE	0	0	3	5	7
97	GENERAL	2455	EYE FOREIGN BODY	0	0	1	0	0
97	GENERAL	2460	ORBIT – EYE	0	0	2	2	4
97	GENERAL	2605	KNEE 4 VIEWS RIGHT	0	0	1	19	82
97	GENERAL	2610	FEMUR LEFT	6	0	38	39	20
97	GENERAL	2620	FEMUR RIGHT	9	6	32	41	35
97	GENERAL	2625	KNEE AP & LAT LEFT	1	0	14	43	73
97	OENERAL	2635	KNEE AP & LAT RIGHT	1	1	16	48	56
97	GENERAL	2640	KNEE 4 VIEWS LEFT	0	0	2	17	84
97	GENERAL	2645	KNEES BILATERAL AP ONLY	1	0	0	2	2
97	GENERAL	2655	LOW LEG - TIBIA - RIGHT	0	4	28	21	73
97	GENERAL	2660	TIBIA LOW LEG - LEFT	1	1	4	13	17
97	GENERAL	2665	LEGS AP – HIP TO ANKLE BILATER	0	0	19	7	6
97	GENERAL	2670	TIBIA LOW LEG - RIGHT	2	1	5	5	16
97	GENERAL	2675	LEG AP & LAT-HIP TO ANKLE LEF	4	3	15	8	14
97	GENERAL	2685	LEG-AP & LAT – HIP TO ANKLE R	5	3	12	11	13
97	GENERAL	2690	LOW LEG - TIBIA - LEFT	3	2	34	40	59
97	GENERAL	2695	LEG LENOTH - SCANOGRAM	0	0	13	31	17
97	GENERAL	2705	FOGT RIGHT	18	4	38	50	48

Year	Modality	RIS #	Exam & View	Newborn	1-Year	5-Year	10-Year	15-Year
97	GENERAL	2710	ANKLE LEFT	0	1	14	67	65
97	GENERAL	2720	ANKLE RIGHT	0	0	25	55	120
97	GENERAL	2725	HEEL LEFT	0	0	3	2	3
97	GENERAL	2735	HEEL RIGHT	0	0	2	3	2
97	GENERAL	2740	FOOT LEFT	16	1	34	55	46
97	GENERAL	2750	TOES LEFT FOOT	0	0	2	8	1
97	GENERAL	2755	TOES RIGHT FOOT	0	0	3	7	8
97	GENERAL	2900	MAMMOGRAM BILATERAL	0	0	0	0	0
97	GENERAL	2901	MAMMOGRAM BILATERAL LIMITED	0	0	0	0	0
97	OENERAL	2902	MAMMOGRAM BILATERAL W/IMPLANTS	0	0	0	0	0
97	GENERAL	2906	BREAST LESION LOCALIZATION - L	0	0	0	0	0
97	GENERAL	2907	BREAST LESION LOCALIZATION – R	0	0	0	0	0
97	GENERAL	2908	BREAST LESION LOCALIZATION - U	0	0	0	0	0
97	GENERAL	2910	MAMMOGRAM UNILATERAL LEFT	0	0	0	0	0
97	GENERAL	2911	MAMMOGRAM UNILATERAL LEFT LIMI	0	0	0	0	0
97	GENERAL	2912	MAMMOGRAM UNILATERAL LEFT W/IM	0	0	0	0	0
97	GENERAL	2915	MAMMOGRAM – SCREENING	0	0	0	0	0
97	GENERAL	2916	MAMM - SCREENING – PARK AVE	1	0	0	0	0
97	GENERAL	2920	MAMMOGRAM UNILATERAL RIGHT	0	0	0	0	0
97	GENERAL	2921	MAMMOGRAM UNILATERAL RIGHT LIM	0	0	0	0	0
97	GENERAL	2922	MAMMOGRAM UNILATERAL RIGHT W/I	0	0	0	0	0
97	GENERAL	2925	MAMMOGRAPHIC DUCTOGRAM – SINGL	0	0	0	0	0
97	GENERAL	2930	BREAST LESION - ADDITIONAL LOC	0	0	0	0	0
97	GENERAL	2935	BREAST SURGICAL SPECIMEN	0	0	0	0	0
97	GENERAL	2941	BREAST CYST ASPIRATION - LEFT	0	0	0	0	0
97	GENERAL	2942	BREAST CYST ASPIRATION - RIGHT	0	0	0	0	0
97	GENERAL	2943	BREAST CYST ASPIRATION - US	0	0	0	0	0
97	GENERAL	2944	BREAST CYST ASPIRATION - ADD'L	0	0	0	0	0
97	GENERAL	2945	MAMMOGRAM - ULTRASOUND	0	0	0	2	4
97	GENERAL	2946	MAMMOGRAM - ULTRASOUND - LIMIT	0	0	0	0	0
97	GENERAL	2950	MAMMOGRAPHIC DUCTOGRAM - MULTI	0	0	0	0	0
97	GENERAL	2955	BREAST CORE BIOPSY - LEFT	0	0	0	0	0
97	GENERAL	2956	BREAST CORE BIOPSY - RIGHT	0	0	0	0	0
97	GENERAL	2957	BREAST CORE BIOPSY - US	0	0	0	0	0
97	GENERAL	2960	BREAST NEEDLE BIOPSY - LEFT	0	0	0	0	0
97	GENERAL	2965	STEREOTACTIC BREAST BIOPSY – L	0	0	0	0	0
97	GENERAL	2966	STEREOTACTIC BREAST BIOPSY - R	0	0	0	0	0
97	GENERAL	2975	BREAST ABSCESS DRAINAGE - LEFT	0	0	0	0	0
97	GENERAL	2976	BREAST ABSCESS DRAINAGE - RIG2H	0	0	0	0	0
97	GENERAL	2999	OUTSIDE READING - MAMMS	0	0	0	0	0
97	GENERAL	3000	BONE AGE	5	4	66	126	69
97	OENERAL	3010	CHOLANGIOGRAM – OR	2	1	2	0	2
97	GENERAL	3015	NECK - SOFT TISSUE	13	14	26	9	9
97	GENERAL	3050	TOMOGRAPHY	0	0	0	0	0
97	GENERAL	3100	PELVIS AP 1 VIEW	8	23	72	59	89
97	GENERAL	3101	PELVIS INLET/OUTLET VIEWS	0	0	0	2	4
97	GENERAL	3102	PELVIS – JUDET VIEWS	0	0	0	1	2
97	GENERAL	3105	HIP AP& LATERAL RIGHT	1	0	4	3	5
97	GENERAL	3110	PELVIS - ORTHO FOR THA	0	0	3	0	3
97	GENERAL	3120	PELVIS WIT2H LATERAL HIPS	4	4	75	62	50
97	GENERAL	3125	HIP AP ONLY LEFT	0	0	0	0	0
97	GENERAL	3135	HIPAP ONLY RIGHT	0	0	1	1	0
97	GENERAL	3140	HIP AP & LATERAL LEFT	0	0	5	5	3
97	GENERAL	3150	PELVIS -ORTHO W/LAT HIPS FOR T	0	0	0	1	1
97	GENERAL	3200	RIBS BILATERAL	0	0	0	1	1
97	GENERAL	3205	RIBS UNILATERAL LEFT	0	0	0	3	3
97	GENERAL	3210	RIBS BILATERAL WITH CHEST	0	0	1	0	0
97	GENERAL	3215	RIBS UNILATERAL RIGHT	0	0	1	2	4
97	GENERAL	3305	SCAPULA RIGHT	0	0	0	1	2
97	GENERAL	3310	SHOULDER LEFT	0	2	7	20	37
97	GENERAL	3320	SHOULDER RIGHT	0	5	6	20	40
97	GENERAL	3325	CLAVICLE LEFT	1	1	7	14	17
97	GENERAL	3335	CLAVICLE RIGHT	2	2	9	10	7
97	OENERAL	3340	SCAPULA LEFT	1	0	0	0	2
97	GENERAL	3345	ACROMIOCLAVICULAR JOINTS	0	0	1	0	3
97	GENERAL	3350	STERNO - CLAVICULAR JOINTS	0	0	0	1	0

Year	Modality	RIS #	Exam & View	Newborn	1-Year	5-Year	10-Year	15-Year
97	GENERAL	3355	STERNUM	0	1	0	0	0
97	GENERAL	3500	CERVICAL SPINE	7	5	77	90	139
97	GENERAL	3505	LUMBAR SPINE LATERAL ONLY	0	0	0	2	5
97	GENERAL	3510	CERVICAL SPINE LATERAL ONLY	0	1	4	4	10
97	GENERAL	3515	LUMBAR SPINE WIT2H OBLIQUES	0	0	0	2	16
97	GENERAL	3520	CERVICAL SPINE WIT2H OBLIQUES	0	1	0	3	5
97	GENERAL	3525	L-SPINE FLEXION & EXTENSION ON	0	0	0	0	2
97	GENERAL	3530	C-SPINE FLEXION & EXTENSION ON	0	0	9	27	40
97	GENERAL	3540	LUMBAR SPINE	4	1	23	28	76
97	GENERAL	3545	LUMBAR SPINE BENDING ONLY	0	0	0	0	0
97	GENERAL	3550	THORACIC SPINE	2	0	14	29	48
97	GENERAL	3555	SPINE – 1 VIEW ONLY	4	1	2	2	0
97	GENERAL	3560	THORACIC SPINE AP ONLY	0	0	1	2	3
97	GENERAL	3565	SCOLIOTIC SERIES	0	0	0	1	3
97	GENERAL	3570	SACRUM	1	0	1	1	2
97	GENERAL	3575	SCOLIOTIC AP ONLY	0	0	2	0	1
97	GENERAL	3580	SACROILIAC JOINTS	0	0	0	4	7
97	GENERAL	3585	SCOLIOTIC AP & LAT	0	4	41	125	223
97	GENERAL	3590	COCCYX	0	0	0	1	1
97	GENERAL	3595	THORACOLUMBAR SPINE	0	0	6	6	6
97	GENERAL	3700	LONG BONE SURVEY	4	0	2	0	0
97	GENERAL	3705	SHUNT SERIES	4	5	28	40	16
97	GENERAL	3710	METASTATIC SURVEY	0	0	0	0	0
97	GENERAL	3715	SILVERMAN SERIES	14	20	26	0	0
97	GENERAL	3720	SKELETAL SURVEY - ADULT	0	0	0	0	0
97	GENERAL	3730	SKELETAL SURVEY - CHILD	3	5	9	1	1
97	GENERAL	3805	ELBOW RIGHT	1	1	42	29	37
97	GENERAL	3806	ELBOW-RIGHT-STRESS VIEWS	0	0	0	0	1
97	GENERAL	3810	HUMERUS - UPPER ARM LEFT	1	1	10	20	19
97	GENERAL	3820	HUMERUS - UPPER ARM RIGHT	3	3	10	21	21
97	GENERAL	3825	FOREARM LEFT	5	1	88	111	45
97	GENERAL	3835	FOREARM RIOHT	8	4	73	80	34
97	GENERAL	3840	ELBOW LEFT	0	2	76	46	38
97	GENERAL	3841	ELBOW-LEFT-STRESS VIEWS	0	0	0	0	1
97	GENERAL	3850	WRIST LEFT	2	0	57	131	70
97	GENERAL	3855	HAND LEFT	4	3	24	47	31
97	GENERAL	3860	WRIST RIGHT	4	1	47	96	82
97	GENERAL	3865	HAND RIGHT	5	3	23	47	87
97	GENERAL	3870	WRIST ORTHO SERIES 7 VIEWS LE	0	0	0	0	0
97	GENERAL	3875	HANDS AP BILATERAL 1VIEW	1	0	0	0	1
97	GENERAL	3880	WRIST ORTHO SERIES 7 VIEWS RIG	0	0	0	0	0
97	GENERAL	3885	FINGERS LEFT HAND	1	1	17	60	36
97	GENERAL	3895	FINGERS RIGHT HAND	0	0	23	50	39
97	GENERAL	6180	CATHETER PLACEMENT	0	0	0	1	0
97	GENERAL	6545	VENOGRAM - UPPER EXTREMITY LEF	4	0	0	0	0
97	GENERAL	7000	ABDOMEN - ULTRASOUND	51	4	10	3	7
97	GENERAL	7015	CHEST - ULTRASOUND	3	0	1	0	0
97	GENERAL	7020	GUIDANCE ONLY - ULTRASOUND	0	0	3	3	1
97	GENERAL	7025	DOPPLER - ULTRASOUND	6	1	10	0	1
97	OENERAL	7035	BILAT LOWER EXTREMITY DOPPLER	0	0	1	0	1
97	GENERAL	7036	UNILAT LOWER EXTREMITY DOPPLER	2	0	0	0	0
97	GENERAL	7037	BILAT UPPER EXTREMITY DOPPLER	0	0	1	0	0
97	GENERAL	7038	UNILAT UPPER EXTREMITY DOPPLER	0	0	1	1	0
97	GENERAL	7045	HIPS - ULTRASOUND	3	0	0	0	0
97	GENERAL	7055	INTRAOPERATIVE - ULTRASOUND	0	0	0	1	0
97	GENERAL	7056	ENDOSCOPIC ULTRASOUND	0	0	0	0	0
97	GENERAL	7085	RENAL TRANSPLANT - ULTRASOUND	0	0	0	0	0
97	GENERAL	7090	HEAD SCAN - ULTRASOUND	305	0	0	0	0
97	GENERAL	7100	SCROTUM - ULTRASOUND	0	1	0	0	0
97	GENERAL	7110	SOFT TISSUE - ULTRASOUND	1	0	0	0	1
97	GENERAL	7111	THYROID - US	0	0	0	0	0
97	GENERAL	7115	CALL BACK - ULTRASOUND	9	0	6	0	2
97	GENERAL	7125	LIMITED STUDY - ULTRASOUND	12	4	7	2	5
97	GENERAL	7126	LIMITED RUQ - US	3	0	2	2	2
97	GENERAL	7127	LIMITED RENAL - US	19	2	5	0	2
97	GENERAL	7128	LIMITED OALLBLADDER - US	0	0	1	0	0
97	GENERAL	7136	TRANSRECTAL VOLUME STUDY - US	0	0	0	0	0

Year	Modality	RIS #	Exam & View	Newborn	1-Year	5-Year	10-Year	15-Year
97	GENERAL	7137	RADIOELEMENT APPLICATION - US	0	0	0	0	0
97	GENERAL	7219	BIOPSY KIDNEY - US	0	0	0	0	0
97	GENERAL	7247	DRNG PERITONEAL - US	0	0	0	0	0
97	GENERAL	7250	DRNG PARACENTESIS - US	0	0	0	0	0
97	GENERAL	8000	GI SERIES	67	31	51	28	12
97	GENERAL	8005	ESOPHOGRAM	33	13	30	12	10
97	GENERAL	8010	GI W/SMALL BOWEL SERIES	9	6	7	17	11
97	GENERAL	8015	ESOPHOGRAM W/HYPOPHARNYX	0	0	0	1	0
97	GENERAL	8025	REHAB BARIUM SWALLOW	3	2	18	7	2
97	GENERAL	8035	BARIUM ENEMA	22	3	7	16	2
97	GENERAL	8040	ENTEROCLYSIS STUDY	0	0	1	0	3
97	GENERAL	8045	BARIUM ENEMA WITH/AIR	1	0	3	1	0
97	GENERAL	8050	CHOLANGIOGRAM	0	0	0	0	0
97	GENERAL	8070	ERCP	0	0	1	3	2
97	GENERAL	8085	SINEOGRAM - FISTULAGRAM	0	0	1	4	0
97	GENERAL	8090	FLUORO SCOPY	1	1	2	1	0
97	GENERAL	8095	SPEECH CINE EXAM	0	0	4	4	1
97	GENERAL	8100	CHEST - FLUORO ONLY	0	0	1	1	0
97	GENERAL	8140	GI TUBE PLACEMENT	23	13	9	5	4
97	GENERAL	8141	GI TUBE REPOSITION	4	1	1	0	1
97	GENERAL	8176	ARTHROGRAM HIP - LIMITED	0	0	0	0	0
97	GENERAL	8185	FLUOROSCOPY (OR)	47	32	75	55	46
97	GENERAL	8190	FLUOROSCOPY (1HR OR)	2	1	14	12	21
97	GENERAL	8195	FLUOROSCOPY (1.5HR OR)	0	0	0	1	4
97	GENERAL	8200	FLUORO W/RADIOLOGIST	2	3	5	8	4
97	GENERAL	8201	FLUORO – ER	0	0	3	3	3
97	GENERAL	8210	FOREIGN BODY REMOVAL -ESOPHAGE	0	0	5	0	0
97	GENERAL	8230	BE INTUSSUSCEPTION	4	1	1	0	0
97	GENERAL	8305	LUMBAR PUNCTURE - DIAGNOSTIC	0	0	0	0	1
97	GENERAL	8306	LUMBAR PUNCTURE - THERAPEUTIC	0	0	0	0	2
97	GENERAL	9160	FLUOROSCOPY - PER ½ HOUR	0	0	0	0	0
97	GENERAL	9190	OUTSIDE FILM READING	0	0	1	1	0
97	GENERAL	9195	CONSULTATION-OUTPT-EXPANDED	0	2	6	6	6
97	GENERAL	9197	CONSULTATION-INITIAL INPT-MODE	2	0	5	4	2
97	GENERAL	9199	CONSULTATION-FOLLOW UP-INPT	0	1	2	0	3
97	NUCMED	4000	BILIARY SCAN	7	1	0	1	0
97	NUCMED	4005	LIVER HEMANGIOMA /SPECT	0	0	0	0	0
97	NUCMED	4015	SPLEEN SCAN	0	0	1	0	1
97	NUCMED	4030	HEPATIC TUMOR - MAA SPECT	0	0	0	0	0
97	NUCMED	4040	LIVER -SPECT	1	0	0	0	0
97	NUCMED	4050	GASTRIC/REFLUX & ASPIRATION	0	1	0	0	0
97	NUCMED	4060	GASTRIC EMPTYING	6	7	19	8	16
97	NUCMED	4065	RENAL GFR QUANTIFICATION	10	6	31	9	12
97	NUCMED	4070	GI BLEED – BLOOD LOSS	0	0	0	0	1
97	NUCMED	4075	RENAL SCAN – CAPTOPRIL	1	0	3	1	1
97	NUCMED	4080	GI BLEED - MECKEL'S	1	0	2	1	3
97	NUCMED	4085	RENAL DTPA LASIX	16	5	32	7	8
97	NUCMED	4090	ESOPHAGEAL SWALLOW - NUCMED	0	0	1	0	2
97	NUCMED	4095	RENAL SCAN – DTPA	2	2	3	1	5
97	NUCMED	4100	RENOGRAM LASIX	0	0	0	0	1
97	NUCMED	4105	LUNG SCAN VENTILATION XENON	0	0	0	0	0
97	NUCMED	4110	RENOGRAM	1	1	3	2	1
97	NUCMED	4115	LUNG VENTILATION /AER	0	0	0	5	6
97	NUCMED	4120	CYSTOGRAM NUCLEAR MEDICINE	1	2	8	3	0
97	NUCMED	4125	SPLIT LUNG SCAN	0	0	0	0	0
97	NUCMED	4130	LUNG SCAN – PERFUSION	1	0	3	5	6
97	NUCMED	4155	BRAIN SCAN	0	0	2	2	2
97	NUCMED	4160	MYOCARDIAL FUNCTION - REST IV	0	0	4	6	11
97	NUCMED	4165	BONE IMAGING - SPECT	1	1	3	10	19
97	NUCMED	4170	MYOCARDIAL FUNCTION - STRESS	0	0	0	0	0
97	NUCMED	4175	BRAIN FUNCTION SCAN - SPECT	0	1	17	10	13
97	NUCMED	4180	MYOCARDIAL REST MULTIVIEW	0	0	0	0	0
97	NUCMED	4185	CISTERNOGRAM – DTPA	0	0	0	0	0
97	NUCMED	4190	MYOCAR PERFUSION - REST & STRE	0	0	0	0	0
97	NUCMED	4195	CISTERNOGRAM CSF LEAK	0	0	0	0	0
97	NUCMED	4205	TUMOR LOCALIZATION -WHOLE BODY	1	2	2	8	8
97	NUCMED	4206	TUMOR LOCALIZATION - PROSTASCI	0	0	0	0	0

Year	Modality	RIS #	Exam & View	Newborn	1-Year	5-Year	10-Year	15-Year
97	NUCMED	4207	PROSTASCINT - SPECT	0	0	0	0	0
97	NUCMED	4210	BONE SCAN	0	1	5	3	1
97	NUCMED	4215	TUMOR LOCALIZATION -SPECT	0	2	2	8	12
97	NUCMED	4216	ABSCESS LOCALIZATION SPECT	2	0	5	6	12
97	NUCMED	4217	ABSCESS LOCALIZATION - LIMITED	0	0	0	0	0
97	NUCMED	4220	BONE SCAN - 3PHASE	6	2	28	30	54
97	NUCMED	4225	ABSCESS LOCALIZATION - WHOLE B	4	0	7	5	15
97	NUCMED	4235	TOTAL BODY SCAN 1311	0	0	0	0	1
97	NUCMED	4245	THERAPY STRONTIUM BONE PAIN	0	0	0	0	0
97	NUCMED	4260	PARATHYROID SCAN NUCMED	0	0	0	0	0
97	NUCMED	4270	THYROID SCAN	0	0	0	0	1
97	NUCMED	4275	THER I131 HYPERTHYROID 10-20	0	0	1	1	4
97	NUCMED	4280	THYROID UPTAKE	0	0	0	0	0
97	NUCMED	4285	THER.I131 HYPERTHYROID 20-30	0	0	0	0	0
97	NUCMED	4290	THYROIDUPTAKE & SCAN	0	0	1	1	5
97	NUCMED	4295	THER I131 HYPERTHYROID50-110	0	0	0	0	0
97	NUCMED	4300	THER.I131 HYPERTHYROID111-200	0	0	0	0	0
97	NUCMED	4305	RADIONUCLIDE ANGIOGRAPHY	0	0	0	0	0
97	NUCMED	4310	LYMPHATIC SCAN	0	0	0	0	0
97	NUCMED	4315	SHUNT PATENCY-NUCLEAR MEDICI	0	0	0	0	0
97	NUCMED	4325	TESTICULAR SCAN NUCMED	0	0	0	1	0
97	NUCMED	4330	VENOGRAM BILATERAL NUCMED	0	0	0	1	0
97	NUCMED	4340	PLATELETSURVIVAL SCAN	1	0	0	0	0
97	NUCMED	4350	ISOTOPES - CATEGORY 1	0	0	0	0	0
97	NUCMED	4360	ISOTOPES - CATEGORY II	0	0	0	0	0
97	NUCMED	4375	DATA PROCESSING SIMPLE <30MI	16	9	37	14	24
97	NUCMED	4385	DATA PROCESSING COMPLEX >30M	46	27	121	59	50
97	NUCMED	4405	SCHILLINGS STAGE	1	0	0	0	0
97	NUCMED	4410	CALL BACK - NUCLEAR MEDICINE	2	3	6	3	3
97	NUCMED	4420	REDBLOOD CELL SURVIVAL	0	0	0	0	0
97	NUCMED	4430	RED BLOOD CELL TECHNETIUM TAG	0	0	1	0	1
97	NUCMED	4435	BRAIN 18-FDG	0	0	1	0	1
97	NUCMED	4436	F-18 FDG TUMOR LOCALIZATION	0	1	7	0	2
97	NUCMED	4440	RED BLOOD CELL VOLUME	0	0	0	0	0
97	NUCMED	4450	KIDNEY STATIC DMSA	43	26	109	41	22
97	NUCMED	4455	BONE MARROW (WHOLE BODY)	0	0	0	0	0
97	NUCMED	4460	STRESS TEST – TREADMILL	0	0	0	0	0
97	NUCMED	4465	ADRENAL IMAOINO	0	0	0	0	0
97	NUCMED	4466	SOMATSTATIN	0	0	0	0	0
97	NUCMED	4467	MIBG	0	0	0	0	0
97	NUCMED	4481	P32 THERAPY INTRA-ARTICULAR	0	0	0	0	1
97	NUCMED	4485	MYOCARDIAL PERFUSION REST CAR	0	0	1	0	0
97	NUCMED	4500	MYOCARDIAL 18-FDG	0	0	0	0	0
97	NUCMED	4505	MYOCARDIAL PERFUSION ADENOSIN	0	0	0	0	0
97	NUCMED	4510	RADIONUCLIDE ADMINISTRATION	0	0	0	0	0
97	NUCMED	7025	DOPPLER - ULTRASOUND	0	0	0	0	0
97	NUCMED	7085	RENAL TRANSPLANT - ULTRASOUND	0	0	0	0	0
97	NUCMED	9625	NO SHOW	0	0	1	0	0
97	NUCMED	9626	NO EXAM PERFORMED	0	0	0	0	0

APPENDIX B
EXAM FREQUENCY FOR PEDIATRIC PATIENTS UNDER 16 YEARS OF AGE
For the Time Period 01/01/97-12/31/97
at Shands at the University of Florida Radiology Department

The following data indicate exam frequency for the general radiology modality.

Examination	0-3 months	% frequency	3-12 months	% frequency	1-6 years	% frequency	7-12 years	% frequency	13-16 years	% frequency
Chest 1 view	3763	54.36	797	43.46	1713	29.46	875	20.59	973	22.26
Babygram	730	10.55	474	25.85	1524	26.21	665	15.65	546	12.49
KUB	491	7 09	82	4 47	269	4.63	131	3.08	223	5.10
Chest PA and Lateral	477	6 89	74	4 03	257	4.42	126	2.97	139	3.18
Head Scan - Ultrasound	305	4 41	51	2.78	134	2.30	125	2.94	120	2.75
Abdomen Decubitus Left	288	4.16	32	1.74	88	1.51	115	2.71	89	2.04
Abdomen 1 View	203	2 93	31	1.69	83	1.43	111	2.61	87	1.99
Cystogram - Voiding	93	1.34	30	1.64	77	1.32	96	2 26	84	1.92
GI Series	67	0.97	23	1.25	76	1.31	90	2.12	83	1.90
Abdomen - Ultrasound	51	0.74	23	1 25	75	1 29	88	2 07	82	1.88
Fluoroscopy (OR)	47	0.68	20	1.09	75	1.29	80	1.88	82	1.88
Esophogram	33	0.48	16	0.87	73	1.26	78	1.84	76	1.74
Chest Decubitus Left	31	0.45	14	0.76	72	1.24	69	1.62	73	1.67
Chest Decubitus Right	24	0 35	13	0 71	66	1.14	67	1.58	73	1.67
GI Tube Placement	23	0 33	13	0.71	57	0.98	62	1.46	70	1.60
Barium Enema	22	0 32	7	0.38	51	0.88	60	1.41	69	1 58
Foot Right	18	0 26	6	0.33	47	0.81	59	1 39	67	1 53
Foot Left	16	0.23	6	0.33	42	0.72	55	1.29	65	1.49
Silverman Series	14	0.20	6	0.33	41	0.71	55	1.29	59	1.35
Skull 2 Views Follow Up Only	13	0.19	5	0.27	40	0.69	55	1.29	56	1.28
Neck - Soft Tissue	13	0 19	5	0.27	38	0.65	50	1.18	51	1.17
Limited Study - Ultrasound	12	0.17	5	0.27	38	0.65	50	1.18	50	1.14
Skull Series	10	0.14	5	0.27	34	0 58	48	1.13	48	1.10
Antegrade Pyelogram	10	0 14	4	0.22	34	0.58	47	1.11	48	1 10
GI w/Small Bowel Series	9	0.13	4	0.22	32	0.55	47	1.11	46	1.05
Femur Right	9	0.13	4	0 22	30	0.52	46	1.08	46	1.05
Pelvis AP 1 View	8	0.12	4	0.22	30	0.52	43	1.01	45	1.03
Abdomen Supine and Upright	8	0.12	4	0 22	28	0.48	41	0.96	40	0.92

Examination	0-3 months	% frequency	3-12 months	% frequency	1-6 years	% frequency	7-12 years	% frequency	13-16 years	% frequency
Forearm Right	8	0.12	4	0.22	28	0.48	40	0.94	40	0.92
Cervical Spine	7	0.10	4	0.22	26	0.45	40	0.94	39	0.89
Femur Left	6	0.09	4	0.22	26	0.45	39	0.92	38	0.87
Doppler - Ultrasound	6	0.09	3	0.16	25	0.43	31	0.73	37	0.85
Leg AP and Lat - Hip to Ankle Right	5	0.07	3	0.16	24	0.41	29	0.68	37	0.85
Forearm Left	5	0.07	3	0.16	23	0.40	29	0.68	36	0.82
Hand Right	5	0.07	3	0.16	23	0.40	29	0.68	35	0.80
Bone Age	5	0.07	3	0.16	23	0.40	28	0.66	34	0.78
Shunt Series	4	0.06	3	0.16	19	0.33	28	0.66	31	0.71
Pelvis with Lateral Hips	4	0.06	3	0.16	18	0.31	27	0.64	21	0.48
Lumbar Spine	4	0.06	3	0.16	18	0.31	25	0.59	21	0.48
Hand Left	4	0.06	3	0.16	17	0.29	21	0.49	21	0.48
GI Tube Reposition	4	0.06	2	0.11	17	0.29	21	0.49	20	0.46
Leg AP and Lat - Hip to Ankle Left	4	0.06	2	0.11	17	0.29	20	0.47	20	0.46
Spine - 1 View Only	4	0.06	2	0.11	16	0.28	20	0.47	19	0.43
Long Bone Survey	4	0.06	2	0.11	16	0.28	20	0.47	17	0.39
Wrist Right	4	0.06	2	0.11	15	0.26	19	0.45	17	0.39
BE Intussusception	4	0.06	2	0.11	14	0.24	17	0.40	17	0.39
Low Leg - Tibia - Left	3	0.04	2	0.11	14	0.24	17	0.40	16	0.37
Skeletal Survey - Child	3	0.04	1	0.05	14	0.24	16	0.38	16	0.37
Humerus - Upper Arm Right	3	0.04	1	0.05	14	0.24	14	0.33	16	0.37
Abdomen Decubitus Right	3	0.04	1	0.05	13	0.22	14	0.33	15	0.34
Rehab Barium Swallow	3	0.04	1	0.05	12	0.21	13	0.31	15	0.34
Fluoro w/Radiologist	2	0.03	1	0.05	11	0.19	12	0.28	14	0.32
KUB - Flat and Upright	2	0.03	1	0.05	10	0.17	12	0.28	13	0.30
Wrist Left	2	0.03	1	0.05	10	0.17	12	0.28	12	0.27
Thoracic Spine	2	0.03	1	0.05	10	0.17	11	0.26	12	0.27
Tibia Low Leg - Right	2	0.03	1	0.05	10	0.17	10	0.24	11	0.25
Clavicle Right	2	0.03	1	0.05	10	0.17	10	0.24	11	0.25
Cholangiogram - OR	2	0.03	1	0.05	9	0.15	10	0.24	10	0.23
Fluoroscopy (1HR OR)	2	0.03	1	0.05	9	0.15	9	0.21	10	0.23
Sacrum	1	0.01	1	0.05	9	0.15	8	0.19	9	0.21
Knee AP and Lat Right	1	0.01	1	0.05	9	0.15	8	0.19	9	0.21
Clavicle Left	1	0.01	1	0.05	7	0.12	8	0.19	8	0.18
Humerus - Upper Arm Left	1	0.01	1	0.05	7	0.12	7	0.16	8	0.18
Knee AP and Lat Left	1	0.01	1	0.05	7	0.12	7	0.16	7	0.16
Barium Enema with Air	1	0.01	1	0.05	7	0.12	7	0.16	7	0.16
Elbow Right	1	0.01	1	0.05	7	0.12	6	0.14	7	0.16
Hands AP Bilateral 1 View	1	0.01	1	0.05	6	0.10	5	0.12	7	0.16

Examination	0-3 months	% frequency	3-12 months	% frequency	1-6 years	% frequency	7-12 years	% frequency	13-16 years	% frequency
Intravenous Pyelogram	1	0.01	1	0.05	6	0.10	5	0 12	6	0 14
Knees Bilateral AP Only	1	0.01	1	0.05	6	0.10	5	0.12	6	0.14
Tibia - Low Leg - Left	1	0.01	1	0.05	6	0.10	5	0 12	6	0.14
Mammogram - Park Avenue	1	0.01	0	0 00	5	0.09	4	0.09	5	0.11
Hip AP and Lateral Right	1	0.01	0	0.00	5	0.09	4	0.09	5	0.11
Scapula Left	1	0.01	0	0.00	5	0.09	4	0.09	5	0.11
Fingers Left Hand	1	0.01	0	0.00	5	0.09	4	0 09	5	0.11
Fluoroscopy	1	0.01	0	0.00	5	0.09	4	0.09	4	0.09
Low Leg - Tibia - Right	0	0 00	0	0.00	4	0.07	4	0.09	4	0.09
Shoulder Left	0	0.00	0	0.00	4	0.07	4	0.09	4	0 09
Cystogram with Radiologist	0	0.00	0	0.00	4	0.07	3	0.07	4	0.09
Retrograde Urethrogram	0	0.00	0	0.00	4	0.07	3	0.07	4	0.09
Legs AP - Hip to Ankle Bilateral	0	0.00	0	0.00	4	0 07	3	0.07	4	0.09
Ankle Left	0	0.00	0	0 00	3	0.05	3	0.07	4	0.09
Ankle Right	0	0.00	0	0.00	3	0.05	3	0.07	4	0.09
Toes Right Foot	0	0 00	0	0.00	3	0.05	3	0.07	3	0.07
Hip AP and Lateral Left	0	0.00	0	0.00	3	0.05	3	0.07	3	0.07
Shoulder Right	0	0.00	0	0.00	3	0.05	3	0.07	3	0.07
Scoliotic AP and Lat	0	0.00	0	0.00	3	0.05	3	0.07	3	0.07
Thoracolumbar Spine	0	0.00	0	0.00	3	0.05	3	0.07	3	0.07
Call Back - Ultrasound	0	0.00	0	0.00	2	0.03	2	0.05	3	0.07
Abdomen Decubitus Bilateral	0	0.00	0	0 00	2	0.03	2	0.05	3	0 07
Chest PA/Lat and Bilateral Oblique	0	0.00	0	0.00	2	0.03	2	0.05	3	0.07
Chest Oblique Only	0	0.00	0	0.00	2	0.03	2	0.05	3	0.07
Chest Apical Lordotic	0	0.00	0	0.00	2	0.03	2	0.05	3	0.07
Chest 3 Views	0	0.00	0	0.00	2	0.03	2	0.05	2	0.05
Cystogram in Cysto	0	0.00	0	0.00	2	0.03	2	0.05	2	0.05
Intravenous Pyelogram w/Tomogra	0	0.00	0	0.00	2	0.03	2	0.05	2	0.05
IVP Abbreviated	0	0 00	0	0.00	2	0.03	2	0.05	2	0.05
Retrograde Pyelogram	0	0 00	0	0.00	2	0.03	2	0.05	2	0.05
Abdomen w/Obliques	0	0.00	0	0 00	2	0.03	2	0.05	2	0.05
Mandible	0	0 00	0	0 00	1	0.02	2	0.05	2	0.05
TMJ - Temporal Mandibular Joint	0	0 00	0	0.00	1	0.02	1	0.02	2	0.05
Sinuses	0	0.00	0	0.00	1	0.02	1	0.02	2	0.05
Mastoids	0	0 00	0	0 00	1	0.02	1	0.02	2	0.05
Facial Bones	0	0 00	0	0.00	1	0.02	1	0.02	2	0.05
Sella Turcica	0	0.00	0	0.00	1	0.02	1	0.02	2	0.05
Nasal Bones - Nose	0	0.00	0	0.00	1	0.02	1	0.02	2	0.05
Eye Foreign Body	0	0.00	0	0.00	1	0.02	1	0.02	2	0.05
Orbit - Eye	0	0.00	0	0.00	1	0.02	1	0.02	2	0.05

Examination	0-3 months	% frequency	3-12 months	% frequency	1-6 years	% frequency	7-12 years	% frequency	13-16 years	% frequency
Knee 4 Views Right	0	0.00	0	0.00	1	0.02	1	0.02	2	0 05
Knee - Left - 2V - Stress	0	0.00	0	0.00	1	0 02	1	0.02	1	0.02
Knee - Right - 2V -Stress	0	0 00	0	0.00	1	0.02	1	0.02	1	0.02
Knee 4 Views Left	0	0 00	0	0 00	1	0.02	1	0.02	1	0 02
Leg Length - Scanogram	0	0.00	0	0.00	1	0.02	1	0.02	1	0.02
Ankle Left - Stress Views	0	0.00	0	0.00	0	0.00	1	0.02	1	0.02
Ankle Right - Stress Views	0	0.00	0	0.00	0	0.00	1	0.02	1	0.02
Heel Left	0	0.00	0	0.00	0	0.00	1	0.02	1	0.02
Heel Right	0	0.00	0	0.00	0	0.00	1	0.02	1	0.02
Toes Left Foot	0	0 00	0	0 00	0	0.00	1	0.02	1	0.02
Mammogram Bilateral	0	0.00	0	0.00	0	0.00	1	0.02	1	0.02
Mammogram Bilateral Limited	0	0.00	0	0.00	0	0.00	0	0.00	1	0.02
Mammogram Bilateral w/Implants	0	0.00	0	0.00	0	0.00	0	0.00	1	0.02
Breast Lesion Localization - L	0	0.00	0	0.00	0	0.00	0	0.00	1	0.02
Breast Lesion Localization - R	0	0 00	0	0 00	0	0.00	0	0.00	1	0.02
Breast Lesion Localization - U	0	0 00	0	0.00	0	0.00	0	0.00	1	0.02
Mammogram Unilateral Left	0	0.00	0	0.00	0	0.00	0	0.00	1	0.02
Mammogram Unilateral Left Limited	0	0.00	0	0.00	0	0.00	0	0.00	0	0.00
Mammogram - Screening	0	0.00	0	0.00	0	0.00	0	0.00	0	0.00
Bone Densitometry	0	0.00	0	0.00	0	0.00	0	0.00	0	0.00
Mammogram Unilateral Right	0	0.00	0	0.00	0	0.00	0	0.00	0	0.00
Mammogram Unilateral Right Limited	0	0.00	0	0.00	0	0.00	0	0.00	0	0.00
Mammographic Ductogram - Single	0	0.00	0	0.00	0	0.00	0	0.00	0	0.00
Breast Lesion - Additional Loc	0	0.00	0	0.00	0	0.00	0	0.00	0	0.00
Breast Surgical Specimen	0	0.00	0	0.00	0	0.00	0	0.00	0	0 00
Breast Cyst Aspiration - Left	0	0.00	0	0.00	0	0 00	0	0.00	0	0.00
Breast Cyst Aspiration - Right	0	0.00	0	0.00	0	0.00	0	0.00	0	0.00
Breast Cyst Aspiration - US	0	0.00	0	0.00	0	0.00	0	0.00	0	0.00
Breast Cyst Aspiration - Add'l	0	0.00	0	0.00	0	0.00	0	0.00	0	0.00
Mammogram - Ultrasound	0	0.00	0	0.00	0	0.00	0	0.00	0	0.00
Mammogram - Ultrasound Limited	0	0.00	0	0.00	0	0.00	0	0.00	0	0.00
Breast Core Biopsy - Left	0	0.00	0	0.00	0	0.00	0	0.00	0	0.00
Breast Core Biopsy - Right	0	0.00	0	0.00	0	0.00	0	0.00	0	0.00
Breast Core Biopsy - US	0	0 00	0	0 00	0	0.00	0	0.00	0	0.00
Stereotactic Breast Biopsy - L	0	0.00	0	0.00	0	0.00	0	0.00	0	0.00
Stereotactic Breast Biopsy - R	0	0.00	0	0 00	0	0.00	0	0 00	0	0.00
Xeromammogram	0	0.00	0	0.00	0	0 00	0	0.00	0	0.00
Breast Abscess Drainage - Left	0	0.00	0	0 00	0	0.00	0	0.00	0	0.00
Breast Abscess Drainage - Right	0	0.00	0	0 00	0	0 00	0	0.00	0	0.00

Examination	0-3 months	% frequency	3-12 months	% frequency	1-6 years	% frequency	7-12 years	% frequency	13-16 years	% frequency
Lymphangiogram - Bilateral	0	0 00	0	0.00	0	0.00	0	0 00	0	0.00
Pelvis Inlet/Outlet Views	0	0.00	0	0.00	0	0.00	0	0.00	0	0.00
Pelvis - Judet Views	0	0.00	0	0 00	0	0 00	0	0.00	0	0.00
Pelvis - Ortho For Tha	0	0 00	0	0.00	0	0.00	0	0.00	0	0.00
Hip AP Only Left	0	0.00	0	0 00	0	0.00	0	0.00	0	0.00
Hip AP Only Right	0	0.00	0	0 00	0	0.00	0	0.00	0	0.00
Pelvis - Ortho w/Lat Hips for T	0	0 00	0	0.00	0	0.00	0	0.00	0	0.00
Ribs Bilateral	0	0 00	0	0.00	0	0.00	0	0.00	0	0.00
Ribs Unilateral Left	0	0.00	0	0.00	0	0.00	0	0.00	0	0.00
Ribs Bilateral with Chest	0	0.00	0	0.00	0	0.00	0	0.00	0	0 00
Ribs Unilateral Right	0	0.00	0	0 00	0	0.00	0	0.00	0	0 00
Scapula Right	0	0.00	0	0.00	0	0.00	0	0.00	0	0.00
Acromioclavicular Joints	0	0.00	0	0.00	0	0.00	0	0 00	0	0.00
Sterno-Clavicular Joints	0	0 00	0	0.00	0	0.00	0	0.00	0	0 00
Sternum	0	0 00	0	0.00	0	0.00	0	0 00	0	0.00
Lumbar Spine Lateral Only	0	0.00	0	0.00	0	0.00	0	0.00	0	0.00
Cervical Spine Lateral Only	0	0.00	0	0.00	0	0.00	0	0.00	0	0.00
Lumbar Spine with Obliques	0	0.00	0	0 00	0	0.00	0	0 00	0	0.00
Cervical Spine with Obliques	0	0.00	0	0.00	0	0.00	0	0.00	0	0.00
L-Spine Flexion and Extension On	0	0.00	0	0.00	0	0 00	0	0.00	0	0.00
Cervical Sp Flexion and Extension	0	0.00	0	0.00	0	0.00	0	0.00	0	0.00
Lumbar Spine Bending Only	0	0.00	0	0.00	0	0.00	0	0.00	0	0.00
Thoracic Spine AP Only	0	0.00	0	0.00	0	0.00	0	0.00	0	0.00
Scoliotic Series	0	0.00	0	0.00	0	0.00	0	0.00	0	0.00
Scoliotic AP Only	0	0.00	0	0 00	0	0.00	0	0.00	0	0 00
Sacroiliac Joints	0	0.00	0	0.00	0	0.00	0	0.00	0	0.00
Coccyx	0	0.00	0	0.00	0	0.00	0	0.00	0	0.00
Metastatic Survey	0	0.00	0	0.00	0	0 00	0	0 00	0	0.00
Skeletal Survey - Adult	0	0.00	0	0.00	0	0.00	0	0.00	0	0.00
Elbow Left	0	0.00	0	0.00	0	0.00	0	0.00	0	0.00
Wrist Ortho Series 7 Views Left	0	0.00	0	0.00	0	0.00	0	0.00	0	0.00
Wrist Ortho Series 7 Views Right	0	0.00	0	0 00	0	0.00	0	0 00	0	0.00
Fingers Right Hand	0	0.00	0	0.00	0	0.00	0	0.00	0	0.00
Cholagiogram - T/Tube	0	0.00	0	0 00	0	0.00	0	0.00	0	0.00
Lumbar Puncture	0	0.00	0	0 00	0	0.00	0	0.00	0	0.00
Guidance Only - Ultrasound	0	0.00	0	0.00	0	0.00	0	0.00	0	0.00
Doppler Study/Peripheral - Us	0	0 00	0	0.00	0	0.00	0	0.00	0	0.00
Blood Vessels - Ultrasound	0	0 00	0	0.00	0	0 00	0	0.00	0	0.00
Renal Transplant - Ultrasound	0	0.00	0	0.00	0	0.00	0	0 00	0	0 00

Examination	0-3 months	% frequency	3-12 months	% frequency	1-6 years	% frequency	7-12 years	% frequency	13-16 years	% frequency
Tube Thoracostomy - Us	0	0.00	0	0.00	0	0.00	0	0.00	0	0.00
Dmg Soft Tissue/Neck - Us	0	0.00	0	0.00	0	0.00	0	0.00	0	0.00
Esophogram w/Hypopharynx	0	0.00	0	0.00	0	0.00	0	0.00	0	0.00
Small Bowel Series Only	0	0.00	0	0.00	0	0.00	0	0.00	0	0.00
Cholangiogram	0	0.00	0	0.00	0	0.00	0	0.00	0	0.00
ERCP	0	0.00	0	0.00	0	0.00	0	0.00	0	0.00
Sinogram - Fistulagram	0	0.00	0	0.00	0	0.00	0	0.00	0	0.00
Speech Cine Exam	0	0.00	0	0.00	0	0.00	0	0.00	0	0.00
Chest - Fluoro Only	0	0.00	0	0.00	0	0.00	0	0.00	0	0.00
Fluoroscopy (1.5HR OR)	0	0.00	0	0.00	0	0.00	0	0.00	0	0.00
Foreign Body Removal - Esophogus	0	0.00	0	0.00	0	0.00	0	0.00	0	0.00
Defecography	0	0.00	0	0.00	0	0.00	0	0.00	0	0.00
Myelogram Cervical	0	0.00	0	0.00	0	0.00	0	0.00	0	0.00
Myelogram Thoracic	0	0.00	0	0.00	0	0.00	0	0.00	0	0.00
Myelogram Lumbosacral	0	0.00	0	0.00	0	0.00	0	0.00	0	0.00
Fluoroscopy - Per 1/2 Hour	0	0.00	0	0.00	0	0.00	0	0.00	0	0.00
Outside Film Reading	0	0.00	0	0.00	0	0.00	0	0.00	0	0.00
Consultation - Outpt - Minor	0	0.00	0	0.00	0	0.00	0	0.00	0	0.00
No Exam Performed	0	0.00	0	0.00	0	0.00	0	0.00	0	0.00
Chest Pa and Lateral with Barium	0	0.00	0	0.00	0	0.00	0	0.00	0	0.00
Chest w/Fluoroscopy	0	0.00	0	0.00	0	0.00	0	0.00	0	0.00
Total	**6922**	**100**	**1834**	**100**	**5814**	**100**	**4249**	**100**	**4371**	**100**

APPENDIX C

EXAM CHARACTERISTICS DETERMINED FROM FACILITY SITE SURVEYS

Table C-1. AP Skull

Facility ID	Relative Speed	Generator Type	Mode of Operation	Detector Config for AEC	AEC Density Setting	Scatter Suppress	SID	Film Size	Field Size	kVp	mA	time (msec)	mAs	Focal Spot Size	Shield Used
Facility #1	600	3 phase	manual	na	na	yes	40	18x24	17x24	78	250	5	1.25	small	yes
Facility #2	400	3 phase	manual	na	na	yes	40	24x30	16x23	70	100	64	6.40	small	yes
Facility #3	400	3 phase	AEC	C	N	yes	40	24x24	14x23	70	125	136	17.00	large	yes
Facility #4	400	high frequency	AEC	C	-1	yes	40	24x30	19x23	65	ng	ng	21.00	large	no
Facility #5	400	3 phase	AEC	C	N	yes	44	24x30	17x23	65	250	ng	21.70	small	no
Facility #6	400	3 phase	manual	na	na	yes	40	24x30	19x20	80	400	ng	6.40	small	no
Facility #7	400	3 phase	AEC	C	N	yes	40	24x30	14x19	75	250	18	4.50	large	no
Facility #8	400	high frequency	AEC	C	N	yes	40	24x30	18x23	65	500	23.5	11.70	small	no
Facility #9	400	1 phase	AEC	C	N	yes	40	24x30	18X24	80	200	ng	10.00	large	no
Facility #10	400	3 phase	AEC	C	N	yes	72	24x30	10x15	70	400	36	14.40	large	no

Table C-2. Townes Skull

Facility ID	Relative Speed	Generator Type	Mode of Operation	Detector Config for AEC	AEC Density Setting	Scatter Suppress	SID	Film Size	Field Size	kVp	mA	time (msec)	MAs	Focal Spot Size	Shield Used
Facility #1	600	3 phase	manual	na	na	yes	40	18x24	10x10	82	250	7	1.75	small	yes
Facility #2	400	3 phase	manual	na	na	yes	40	24x30	17x11	70	100	64	6.40	small	yes
Facility #3	400	3 phase	AEC	C	N	yes	40	24x24	23x13	70	125	368	46.00	large	yes
Facility #4	400	high frequency	AEC	C	-1	yes	40	24x30	23x15	70	ng	ng	20.80	large	no
Facility #5	400	3 phase	AEC	C	N	yes	38	24x30	25x18	70	250	ng	11.62	small	no
Facility #6	400	3 phase	manual	na	na	yes	40	24x30	20x19	80	400	ng	8.00	small	no
Facility #7	400	3 phase	AEC	C	N	yes	40	24x30	20x15	80	250	12	3.00	large	no
Facility #8	400	high frequency	AEC	C	N	yes	40	24x30	23x15	65	500	34.3	17.10	small	no
Facility #9	400	1 phase	AEC	C	N	yes	40	24x30	22X20	80	200	ng	22.00	large	no
Facility #10	400	3 phase	AEC	C	N	yes	40	24x30	24x23	75	400	10	4.00	large	no

Table C-3. Lateral Skull

Facility ID	Relative Speed	Generator Type	Mode of Operation	Detector Config for AEC	AEC Density Setting	Scatter Suppress	SID	Film Size	Field Size	kVp	mA	time (msec)	mAs	Focal Spot Size	Shield Used
Facility #1	600	3 phase	manual	na	na	yes	40	18x24	19x22	73	250	7	1.75	small	yes
Facility #2	400	3 phase	manual	na	na	no	40	24x30	20x20	60	100	50	5.00	small	yes
Facility #3	400	3 phase	AEC	C	N	yes	40	24x24	18x20	70	125	96	12.00	large	yes
Facility #4	400	high frequency	AEC	C	-1	yes	40	24x30	22x22	65	ng	ng	12.40	large	no
Facility #5	400	3 phase	manual	na	na	no	38	24x30	25x23	70	250	10	2.50	small	no
Facility #6	400	3 phase	manual	na	na	yes	40	24x30	23x20	70	400	ng	5.00	small	no
Facility #7	400	3 phase	AEC	C	N	yes	40	24x30	18x18	65	250	15	3.75	large	no
Facility #8	400	high frequency	AEC	C	N	yes	40	24x30	20x20	65	500	13.9	6.95	small	no
Facility #9	400	1 phase	AEC	C	N	yes	40	24x30	22X22	75	200	ng	12.00	large	no
Facility #10	400	3 phase	AEC	C	N	yes	72	24x30	15x10	70	400	33	13.20	large	no

Table C-4. AP Cervical Spine

Facility ID	Relative Speed	Generator Type	Mode of Operation	Detector Config for AEC	AEC Density Setting	Scatter Suppress	SID	Film Size	Field Size	kVp	mA	time (msec)	mAs	Focal Spot Size	Shield Used
Facility #1	600	3 phase	manual	na	na	yes	40	18x24	10x10	65	250	15	3.75	small	yes
Facility #2	400	3 phase	manual	na	na	yes	40	24x30	10x20	65	60	50	3.00	small	yes
Facility #3	400	3 phase	AEC	C	N	yes	40	24x24	10x23	70	125	40	5.00	large	yes
Facility #4	400	high frequency	AEC	C	N	yes	40	24x30	10x18	65	ng	ng	9.10	large	no
Facility #5	400	3 phase	AEC	C	N	yes	38	18x24	10x25	65	250	ng	8.80	small	no
Facility #6	400	3 phase	manual	na	na	no	40	24x30	10x22	68	400	ng	2.00	small	no
Facility #7	400	3 phase	AEC	C	N	yes	40	24x30	10x15	65	250	18	4.50	large	no
Facility #8	400	high frequancy	AEC	C	N	yes	40	24x30	13x20	65	500	8.4	4.20	small	no
Facility #9	400	1 phase	manual	na	na	yes	40	24x30	15X19	60	200	100	20.00	large	no
Facility #10	400	3 phase	AEC	C	-1	yes	40	24x30	24x30	66	400	5	2.00	large	no

Table C-5. Lateral Cervical Spine

Facility ID	Relative Speed	Generator Type	Mode of Operation	Detector Config for AEC	AEC Density Setting	Scatter Suppress	SID	Film Size	Field Size	kVp	mA	time (msec)	mAs	Focal Spot Size	Shield Used
Facility #1	600	3 phase	manual	Na	na	yes	40	18x24	10x20	70	250	25	8.25	small	yes
Facility #2	400	3 phase	manual	Na	na	no	40	24x30	10x21	65	100	40	4.00	small	yes
Facility #3	400	3 phase	AEC	C	N	yes	40	24x24	8x18	70	125	64	8.00	large	yes
Facility #4	400	high frequency	AEC	C	-1	yes	40	24x30	10x17	65	ng	ng	8.01	large	no
Facility #5	400	3 phase	manual	na	na	no	38	18x24	10x25	67	250	8	2.00	small	no
Facility #6	400	3 phase	manual	na	na	no	40	24x30	10x20	74	400	ng	1.60	small	no
Facility #7	400	3 phase	AEC	C	N	yes	72	24x30	12.5x18	70	250	40	10.00	large	no
Facility #8	400	high frequency	AEC	C	N	yes	72	24x30	10x18	65	500	90.2	45.10	small	no
Facility #9	400	1 phase	manual	na	na	yes	40	24x30	12X24	70	200	125	25.00	large	no
Facility #10	400	3 phase	AEC	C	N	yes	40	24x30	15x25	75	400	6	2.40	large	no

Table C-6. AP Thoracic Spine

Facility ID	Relative Speed	Generator Type	Mode of Operation	Detector Config for AEC	AEC Denalty Setting	Scatter Suppress	SID	Film Size	Field Size	kVp	mA	time (msec)	mAa	Focal Spot Size	Shield Used
Facility #1	600	3 phase	manual	na	na	yes	40	18x24	13x23	72	250	15	3.75	small	yes
Facility #2	400	3 phaae	manual	na	na	yes	40	24x30	11x24	65	100	50	5.00	small	yes
Facility #3	400	3 phase	AEC	C	N	yes	40	24x24	10x23	70	125	104	13.00	large	yes
Facility #4	400	high frequency	AEC	C	N	yes	40	24x30	15x25	65	ng	ng	14.00	large	no
Facility #5	400	3 phase	AEC	C	N	yes	38	30x35	10x28	70	250	ng	6 35	small	no
Facility #6	400	3 phase	manual	Na	na	yes	40	24x30	10x22	68	400	ng	2.00	small	no
Facility #7	400	3 phase	AEC	C	N	yes	40	24x30	10x20	75	250	39	9.75	large	no
Facility #8	400	high frequency	manual	Na	na	yes	40	24x30	13x23	65	500	1D 7	5 35	small	no
Facility #9	400	1 phase	manual	Na	na	yes	40	24x30	13x23	65	500	10.7	5.35	large	no
Facility #10	400	3 phase	AEC	C	-1	yes	40	24x30	14x24	70	400	9	3 60	large	no

Table C-7. Lateral Thoracic Spine

Facility ID	Relative Speed	Generator Type	Mode of Operation	Detector Config for AEC	AEC Denalty Setting	Scatter Suppress	SID	Film Size	Field Size	kVp	mA	time (msec)	Maa	Focal Spot Size	Shield Used
Facility #1	600	3 phase	manual	na	na	yes	40	18x24	11x22	75	250	25	8.25	small	yes
Facility #2	400	3 phase	manual	na	na	yes	40	24x30	10x22	70	100	64	6 40	small	yes
Facility #3	400	3 phase	AEC	C	N	yes	40	24x24	8x20	70	125	128	16 00	large	yes
Facility #4	400	high frequency	AEC	C	N	yes	40	24x30	13x22	60	ng	ng	32.10	large	no
Facility #5	400	3 phase	AEC	C	N	yes	38	30x35	13x30	70	250	ng	9.72	small	no
Facility #6	400	3 phase	manual	na	na	yes	40	24x30	10x19	68	400	ng	4.00	small	no
Facility #7	400	3 phase	AEC	C	N	yes	40	24x30	10x16	70	250	41.5	1D.38	large	no
Facility #8	400	high frequency	manual	na	na	yes	40	24x30	13x23	54	32	1250	40 00	small	no
Facility #9	400	1 phase	manual	na	na	yes	40	24x30	13x27	60	100	1000	100.00	large	no
Facility #1D	400	3 phase	AEC	C	N	yes	40	24x30	15x25	83	400	13	5 20	large	no

Table C-8. AP Lumbar Spine

Facility ID	Relative Speed	Generator Type	Mode of Operation	Detector Config for AEC	AEC Density Setting	Scatter Suppress	SID	Film Size	Field Size	kVp	mA	time (msec)	Mas	Focal Spot Size	Shield Used
Facility #1	600	3 phase	manual	na	na	yes	40	18x24	13x23	72	250	15	3.75	small	yes
Facility #2	400	3 phase	manual	na	na	yes	40	24x30	11x24	70	100	64	6.40	small	yes
Facility #3	400	3 phase	AEC	C	N	yes	40	24x24	10x23	70	125	128	16.00	large	yes
Facility #4	400	high frequency	AEC	C	-1	yes	40	24x30	18x25	70	ng	ng	9.63	large	no
Facility #5	400	3 phase	AEC	C	N	yes	38	30x35	10x28	70	250	ng	9.02	small	no
Facility #6	400	3 phase	manual	na	na	yes	40	24x30	10x22	68	400	ng	3.20	small	no
Facility #7	400	3 phase	AEC	C	N	yes	40	24x30	10x20	75	250	47	11.75	large	no
Facility #8	400	high frequency	manual	na	na	yes	40	24x30	13x23	65	500	16.8	9.40	small	no
Facility #9	400	1 phase	AEC	na	N	yes	40	24x30	10x22.5	70	200	ng	30.00	large	no
Facility #10	400	3 phase	AEC	C	-1	yes	40	24x30	14x24	75	400	10	4.00	large	no

Table C-9. Lateral Lumbar Spine

Facility ID	Relative Speed	Generator Type	Mode of Operation	Detector Config for AEC	AEC Density Setting	Scatter Suppress	SID	Film Size	Field Size	kVp	mA	time (msec)	MAs	Focal Spot Size	Shield Used
Facility #1	600	3 phase	AEC	C	N	yes	40	24x30	14x19	75	400	16	7.20	small	yes
Facility #2	400	3 phase	manual	na	na	yes	40	24x30	10x22	74	100	100	10.00	small	yes
Facility #3	400	3 phase	AEC	C	N	yes	40	24x24	10x23	70	125	240	30.00	large	yes
Facility #4	400	high frequency	AEC	C	N	yes	40	24x30	11x23	75	ng	ng	18.50	large	no
Facility #5	400	3 phase	AEC	C	N	yes	38	30x35	10x28	70	250	ng	16.22	small	no
Facility #6	400	3 phase	manual	na	na	yes	40	24x30	10x19	68	400	ng	6.00	small	no
Facility #7	400	3 phase	AEC	C	N	yes	40	24x30	10x20	70	250	88	22.00	large	no
Facility #8	400	high frequency	AEC	C	1	yes	40	24x30	10x23	65	500	55.6	27.90	small	no
Facility #9	400	1 phase	AEC	C	N	yes	40	24x30	12x24	70	200	ng	45.00	large	no
Facility #10	400	3 phase	AEC	C	N	yes	40	24x30	15x25	75	400	12	4.80	large	no

Table C-10. AP Abdomen

Facility ID	Relative Speed	Generator Type	Mode of Operation	Detector Config for AEC	AEC Density Setting	Scatter Suppress	SID	Film Size	Field Size	kVp	mA	time (msec)	MAs	Focal Spot Size	Shield Used
Facility #1	600	3 phase	manual	na	na	yes	40	24x30	22x22	70	250	15	3.75	small	yes
Facility #2	400	3 phase	manual	na	na	yes	40	24x30	19x23	68	100	40	4.00	small	yes
Facility #3	400	3 phase	AEC	C	N	yes	40	24x24	18x25	60	250	120	30.00	large	yes
Facility #4	400	high frequency	AEC	C	-1	yes	40	24x30	20x28	70	ng	ng	12.60	large	no
Facility #5	400	3 phase	AEC	C	N	yes	38	30x35	22x28	70	250	ng	8.45	small	no
Facility #6	400	3 phase	manual	na	na	no	40	24x30	23x27	68	400	ng	3.20	small	no
Facility #7	400	3 phase	AEC	C	N	yes	40	24x30	15x21	70	250	44	11.00	large	no
Facility #8	400	high frequency	AEC	C	N	yes	40	24x30	18x27	66	500	16.1	8.05	small	no
Facility #9	400	1 phase	AEC	RCL	N	yes	40	24x30	23X30	75	200	ng	10.00	large	no
Facility #10	400	3 phase	AEC	C	N	yes	40	24x30	24x30	65	400	16	6.40	large	no

Table C-11. AP Pelvis

Facility ID	Relative Speed	Generator Type	Mode of Operation	Detector Config for AEC	AEC Density Setting	Scatter Suppress	SID	Film Size	Field Size	kVp	mA	time (msec)	MAs	Focal Spot Size	Shield Used
Facility #1	600	3 phase	manual	na	na	yes	40	18x24	14x20	70	250	15	3.75	small	yes
Facility #2	400	3 phase	manual	na	na	yes	40	30x24	22x18	72	100	50	5.00	small	no
Facility #3	400	3 phase	AEC	C	N	yes	40	24x24	18x18	60	250	108	27.00	large	no
Facility #4	400	high frequency	AEC	C	-1	yes	40	30x24	23x20	70	ng	ng	8.87	large	no
Facility #5	400	3 phase	AEC	C	N	yes	38	18x24	18x20	70	250	ng	7.55	small	no
Facility #6	400	3 phase	manual	na	Na	no	40	24x30	19x24	68	400	ng	3.20	small	no
Facility #7	400	3 phase	AEC	C	N	yes	40	24x30	15x18	70	250	14	3.50	large	no
Facility #8	400	high frequency	AEC	C	N	yes	40	30x24	23x20	66	500	14.3	7.15	small	no
Facility #9	400	1 phase	AEC	RCL	N	yes	40	30X24	24X22	75	200	ng	10.00	large	no
Facility #10	400	3 phase	AEC	C	-1	yes	40	24x30	18x24	70	400	5	2.00	large	no

Table C-12. AP Hip

Facility ID	Relative Speed	Generator Type	Mode of Operation	Detector Config for AEC	AEC Density Setting	Scatter Suppress	SID	Film Size	Field Size	kVp	mA	time (msec)	MAs	Focal Spot Size	Shield Used
Facility #1	600	3 phase	manual	na	na	yes	40	18x24	12x11	65	250	15	3.75	small	yes
Facility #2	400	3 phase	manual	na	na	yes	40	24x30	13x20	70	100	50	5.00	small	no
Facility #3	400	3 phase	AEC	C	N	yes	40	24x24	8x18	60	250	36	9.00	large	no
Facility #4	400	high frequency	AEC	C	-1	yes	40	30x24	10x13	65	ng	ng	12.10	large	no
Facility #5	400	3 phase	AEC	C	N	yes	38	18x24	10x24	65	250	ng	4.50	small	no
Facility #6	400	3 phase	manual	na	na	yes	40	24x30	24x19	68	400	ng	3.20	small	no
Facility #7	400	3 phase	AEC	C	N	yes	40	24x30	15x16	70	250	14	3.50	large	no
Facility #8	400	high frequency	AEC	C	N	yes	40	30x24	18x10	66	500	3.6	1.80	small	no
Facility #9	400	1 phase	AEC	RCL	N	yes	40	18X24	13X18	75	200	ng	10.00	large	no
Facility #10	400	3 phase	AEC	C	-1	yes	40	24x30	20x15	75	400	2	0.80	large	no

Table C-13. Waters Sinus

Facility ID	Relative Speed	Generator Type	Mode of Operation	Detector Config for AEC	AEC Density Setting	Scatter Suppress	SID	Film Size	Field Size	KVp	mA	time (msec)	mAs	Focal Spot Size	Shield Used
Facility #1	600	3 phase	manual	na	na	yes	40	18x24	12x15	75	250	7	1.75	small	yes
Facility #2	400	3 phase	manual	na	na	yes	40	24x30	11x17	65	100	64	6.40	small	yes
Facility #3	400	3 phase	AEC	C	-1	yes	40	24x24	13x15	70	125	304	38.00	large	yes
Facility #4	400	high frequency	AEC	C	N	yes	40	24x30	13x15	70	ng	ng	14.20	large	no
Facility #5	400	3 phase	AEC	C	N	yes	38	18x24	13x13	65	250	ng	20.40	small	no
Facility #6	400	3 phase	manual	na	na	yes	40	24x30	13x13	80	400	ng	8.00	small	no
Facility #7	400	3 phase	AEC	C	N	yes	72	24x30	14x19	70	250	116	29.00	large	no
Facility #8	400	high frequency	AEC	C	N	yes	40	24x30	18x20	65	500	55.6	27.80	small	no
Facility #9	400	1 phase	AEC	C	N	yes	72	24x30	12X18	75	200	ng	25.00	large	no
Facility #10	400	3 phase	AEC	C	-2	yes	40	24x30	13x16	70	400	36	14.40	large	no

Table C-14. Lateral Sinus

Facility ID	Relative Speed	Generator Type	Mode of Operation	Detector Config for AEC	AEC Density Setting	Scatter Suppress	SID	Film Size	Field Size	kVp	mA	time (msec)	MAs	Focal Spot Size	Shield Used
Facility #1	600	3 phase	manual	na	Na	yes	40	18x24	15x14	68	250	7	1.75	small	yes
Facility #2	400	3 phase	manual	na	Na	no	40	24x30	20x20	80	100	50	5.00	small	yes
Facility #3	400	3 phass	AEC	C	-1	yes	40	24x24	8x15	70	125	16	2.00	large	yes
Facility #4	400	high frequency	AEC	C	N	yes	40	24x30	10x14	65	ng	ng	10.30	large	no
Facility #5	400	3 phase	manual	na	Na	no	38	18x24	13x13	65	250	6.4	1.80	small	no
Facility #6	400	3 phase	manual	na	Na	yes	40	24x30	13x13	70	400	ng	5.00	small	no
Facility #7	400	3 phase	AEC	C	N	yes	72	24x30	13.5x16	70	250	44	11.00	large	no
Facility #8	400	high frequency	AEC	C	N	yes	40	24x30	18x20	65	500	41.3	20.60	small	no
Facility #9	400	1 phase	AEC	C	N	yes	40	24x30	12X18	70	200	ng	17.50	large	no
Facility #10	400	3 phase	AEC	C	-1	yes	40	24x30	13x16	60	400	12	4.80	large	no

Table C-15. Lateral Chest

Facility ID	Relative Speed	Generator Type	Mode of Operation	Detector Config for AEC	AEC Density Setting	Scatter Suppress	SID	Film Size	Field Size	kVp	mA	time (msec)	mAs	Focal Spot Size	Shield Used
Facility #1	600	3 phase	manual	na	na	No	72	18x24	13x11	74	250	15	3.75	small	yes
Facility #2	400	3 phase	manual	na	na	No	72	24x30	12x11	85	100	40	4.00	small	yes
Facility #3	400	3 phase	manual	na	na	No	72	24x30	23x15	75	125	14	1.70	small	yes
Facility #4	400	high frequency	AEC	C	N	yes	72	24x30	25x20	75	ng	ng	17.90	small	no
Facility #5	400	3 phase	manual	na	na	no	60	24x30	25x20	75	250	8	2.00	small	no
Facility #6	400	3 phase	manual	na	na	no	42	24x30	23x18	58	400	ng	3.20	small	no
Facility #7	400	3 phase	AEC	C	N	yes	72	24x30	16x15 5	70	250	49	12.25	small	no
Facility #8	400	high frequency	manual	na	na	no	72	24x30	20x18	84	400	6 25	2.50	small	no
Facility #9	400	1 phase	AEC	RCL	N	yes	72	24x30	21x14	90	200	ng	18.00	small	no
Facility #10	400	3 phase	AEC	RCL	N	yes	72	24x30	15x10	95	400	10	4.00	small	no

Table C-16. AP Chest

Facility ID	Relative Speed	Generator Type	Mode of Operation	Detector Config for AEC	AEC Density Setting	Scatter Suppress	SID	Film Size	Field Size	kVp	mA	time (msec)	mAs	Focal Spot Size	Shield Used
Facility #1	600	3 phase	manual	na	na	No	72	18x24	12x12	66	250	7	1 75	small	yes
Facility #2	400	3 phase	manual	na	na	No	72	24x30	12x12	70	100	32	3.20	small	yes
Facility #3	400	3 phase	manual	na	na	No	72	24x30	18x20	75	125	14	1 70	small	yes
Facility #4	400	high frequency	AEC	C	-2	Yes	72	24x30	20x25	75	ng	ng	12 90	small	no
Facility #5	400	3 phase	manual	na	na	No	61	24x30	20x25	62	250	5	1.25	small	no
Facility #6	400	3 phase	manual	na	na	No	40	24x30	19x23	58	400	ng	1.60	small	no
Facility #7	400	3 phase	AEC	C	N	Yes	72	24x30	19x20	70	250	37	9 25	small	no
Facility #8	400	high frequency	manual	na	na	No	72	24x30	23x29	68	500	4	2.00	small	no
Facility #9	400	1 phase	AEC	RL	N	Yes	72	24x30	18X18	60	200	ng	10.00	small	no
Facility #10	400	3 phase	AEC	RCL	-1	Yes	72	24x30	11 5x12 5	90	400	4	1.60	small	no

Table C-17. PA Chest

Facility ID	Relative Speed	Generator Type	Mode of Operation	Detector Config for AEC	AEC Density Setting	Scatter Suppress	SID	Film Size	Field Size	KVp	mA	time (msec)	mAs	Focal Spot Size	Shield Used
Facility #1	600	3 phase	manual	na	na	no	72	18x24	12x12	66	250	7	1.75	small	yes
Facility #2	400	3 phase	manual	na	na	no	72	24x30	11x12	72	100	40	4.00	small	yes
Facility #3	400	3 phase	manual	na	na	no	72	24x30	18x18	68	160	12	1.90	small	yes
Facility #4	400	high frequency	AEC	C	-2	yes	72	24x30	20x25	75	ng	ng	17.00	small	no
Facility #5	400	3 phase	manual	na	na	no	72	24x30	20x25	67	250	5	1.25	small	no
Facility #6	400	3 phase	manual	na	na	no	40	24x30	19x23	58	400	ng	1.60	small	no
Facility #7	400	3 phase	AEC	C	N	yes	72	24x30	19x20	70	250	31	7.75	small	no
Facility #8	400	high frequency	manual	na	na	no	72	24x30	23x23	68	500	4	2.00	small	no
Facility #9	400	1 phase	AEC	RL	N	yes	72	24x30	18X18	80	200	ng	10.00	small	no
Facility #10	400	3 phase	AEC	RCL	-1	Yes	72	24x30	11.5x12.5	90	400	5	2.00	small	no

Table C-18. Non-Exam Specific Operational Data

Facility ID	HVL	Grid Ratio	Avg. Lung OD AP Chest	Avg. Lung OD PA Chest	Avg. Lung OD Lateral Chest	Repeat Rate %
Facility #1	3.07	10:1	1.495	1.015	1.115	4.5
Facility #2	2.89	12:1	1.03	1.4	1.11	0.5
Facility #3	3.28	12:1	2.235	2.57	1.415	8.0
Facility #4	3.72	12:1	2.44	2.655	1.665	5.5
Facility #5	2.94	10:1	0.625	0.475	0.715	4.0
Facility #6	2.66	10:1	0.65	0.595	0.47	2.0
Facility #7	3.46	10:1	2.215	2.16	1.995	1.0
Facility #8	3.16	12:1	0.99	0.84	1.125	4.3
Facility #9	2.91	12:1	0.875	0.425	1.735	3.5
Facility #10	3.44	12:1	1.1	1.295	1.48	3.0

APPENDIX D
AVERAGE MASS ENERGY ABSORPTION COEFFICIENTS

Calculation of the average mass energy absorption coefficients
for air, soft tissue, bone and lung at 70 kVp
using the x-ray spectrum generated by XCOMP5R

	# of	% of	Air	Soft Tissue	Bone	Lung				
keV	Photons	Spectrum	μ_{en}/ρ	$\%*\mu_{en}/\rho$	μ_{en}/ρ	$\%*\mu_{en}/\rho$	μ_{en}/ρ	$\%*\mu_{en}/\rho$	μ_{en}/ρ	$\%*\mu_{en}/\rho$
1	*0*	0	3616	0	1170	0	978	0	1150	0
2	*0*	0	529.1	0	531	0	436	0	539	0
3	*0*	0	160.8	0	170	0	206	0	172	0
4	*0*	0	75.97	0	73.9	0	92.5	0	75	0
5	*0*	0	38.96	0	38.2	0	90.9	0	38.9	0
6	*0*	0	22.42	0	22.1	0	55.6	0	22.5	0
7	*0*	0	7.563	0	7.62	0	22.75	0	7.765	0
8	*0*	0	9.246	0	9.24	0	25.20	0	9.430	0
9	*0*	0	7.785	0	7.755	0	20.525	0	7.923	0
10	*0*	0	4.640	0	4.650	0	13.400	0	4.750	0
11	*0*	0	3.972	0	3.982	0	11.550	0	4.070	0
12	*0*	0	3.304	0	3.314	0	9.700	0	3.390	0
13	*0*	0	2.636	0	2.646	0	7.850	0	2.710	0
14	*2*	2.00E-05	1.968E+00	3.94E-05	1.978	3.96E-05	6.000	1.20E-04	2.030	4.06E-05
15	*8*	8.00E-05	1.300E+00	1.04E-04	1.310	1.05E-04	4.150	3.32E-04	1.350	1.08E-04
16	*30*	3.00E-04	1.145E+00	3.44E-04	1.155	3.46E-04	3.674	1.10E-03	1.189	3.57E-04
17	*80*	8.00E-04	9.902E-01	7.92E-04	0.999	7.99E-04	3.198	2.56E-03	1.028	8.23E-04
18	*176*	1.76E-03	8.353E-01	1.47E-03	0.844	1.49E-03	2.722	4.79E-03	0.868	1.53E-03
19	*327*	3.27E-03	6.804E-01	2.22E-03	0.688	2.25E-03	2.246	7.34E-03	0.707	2.31E-03
20	*537*	5.37E-03	5.255E-01	2.82E-03	0.533	2.86E-03	1.770	9.51E-03	0.546	2.93E-03
21	*785*	7.85E-03	4 880E-01	3.83E-03	0.495	3.89E-03	1.646	1.29E-02	0.507	3.98E-03
22	*1062*	1.06E-02	4.504E-01	4.78E-03	0.457	4.85E-03	1.521	1.62E-02	0.468	4.97E-03
23	*1358*	1.36E-02	4.129E-01	5.61E-03	0.419	5.69E-03	1.397	1.90E-02	0.429	5.83E-03
24	*1658*	1.66E-02	3.753E-01	6.22E-03	0.381	6.32E-03	1.272	2.11E-02	0.390	6.47E-03
25	*1949*	1.95E-02	3.378E-01	6.58E-03	0.343	6.69E-03	1.148	2.24E-02	0.352	6.85E-03
26	*2223*	2.22E-02	3.003E-01	6.67E-03	0.305	6.78E-03	1.024	2.28E-02	0.313	6.95E-03
27	*2472*	2.47E-02	2.627E-01	6.49E-03	0.267	6.60E-03	0.899	2.22E-02	0.274	6.77E-03
28	*2691*	2.69E-02	2.252E-01	6.06E-03	0.229	6.16E-03	0.775	2.09E-02	0.235	6.32E-03
29	*2879*	2.88E-02	1.876E-01	5.40E-03	0.191	5.50E-03	0.650	1.87E-02	0.196	5.64E-03
30	*3035*	3.04E-02	1.501E-01	4.56E-03	0.153	4.64E-03	0.526	1.60E-02	0.157	4.77E-03
31	*3132*	3.13E-02	1.420E-01	4.45E-03	0.145	4.53E-03	0.496	1.55E-02	0.149	4.66E-03
32	*3195*	3.20E-02	1.340E-01	4.28E-03	0.136	4.35E-03	0.466	1.49E-02	0.141	4.49E-03
33	*3236*	3.24E-02	1.259E-01	4.07E-03	0.128	4.13E-03	0.436	1.41E-02	0.132	4.28E-03
34	*3257*	3.26E-02	1.178E-01	3.84E-03	0.119	3.89E-03	0.406	1.32E-02	0.124	4.05E-03
35	*3260*	3.26E-02	1.098E-01	3.58E-03	0.111	3.61E-03	0.376	1.22E-02	0.116	3.78E-03
36	*3247*	3.25E-02	1.017E-01	3.30E-03	0.102	3.33E-03	0.345	1.12E-02	0.108	3.50E-03
37	*3221*	3.22E-02	9.361E-02	3.02E-03	0.094	3.03E-03	0.315	1.02E-02	0.100	3.21E-03
38	*3182*	3.18E-02	8.554E-02	2.72E-03	0.086	2.72E-03	0.285	9.08E-03	0.091	2.91E-03
39	*3133*	3.13E-02	7.747E-02	2.43E-03	0.077	2.42E-03	0.255	7.99E-03	0.083	2.61E-03
40	*3075*	3.08E-02	6.940E-02	2.13E-03	0.069	2.11E-03	0.225	6.92E-03	0.075	2.31E-03
41	*2998*	3.00E-02	6.676E-02	2.00E-03	0.066	1.98E-03	0.215	6.43E-03	0.072	2.15E-03
42	*2912*	2.91E-02	6.412E-02	1.87E-03	0.063	1.84E-03	0.204	5.94E-03	0.069	2.00E-03

43	*2823*	2.82E-02	6.148E-02	1.74E-03	0.061	1.71E-03	0.194	5.46E-03	0.065	1.84E-03
44	*2731*	2.73E-02	5.884E-02	1.61E-03	0.058	1.58E-03	0.183	5.00E-03	0.062	1.70E-03
45	*2637*	2.64E-02	5.621E-02	1.48E-03	0.055	1.46E-03	0.173	4.55E-03	0.059	1.55E-03
46	*2541*	2.54E-02	5.357E-02	1.36E-03	0.053	1.33E-03	0.162	4.12E-03	0.056	1.41E-03
47	*2443*	2.44E-02	5.093E-02	1.24E-03	0.050	1.22E-03	0.152	3.70E-03	0.052	1.28E-03
48	*2344*	2.34E-02	4.829E-02	1.13E-03	0.047	1.10E-03	0.141	3.31E-03	0.049	1.15E-03
49	*2244*	2.24E-02	4.565E-02	1.02E-03	0.044	9.96E-04	0.131	2.93E-03	0.046	1.03E-03
50	*2143*	2.14E-02	4.301E-02	9.22E-04	0.042	8.94E-04	0.120	2.57E-03	0.043	9.15E-04
51	*2038*	2.04E-02	4 171E-02	8.50E-04	0.041	8.29E-04	0.116	2.36E-03	0.042	8.49E-04
52	*1931*	1.93E-02	4.042E-02	7.80E-04	0.040	7.65E-04	0.111	2.15E-03	0.041	7.84E-04
53	*1824*	1.82E-02	3.912E-02	7.14E-04	0.039	7.04E-04	0.107	1.95E-03	0.040	7.21E-04
54	*1718*	1.72E-02	3.782E-02	6.50E-04	0.038	6.46E-04	0.102	1.76E-03	0.038	6.61E-04
55	*1613*	1.61E-02	3.653E-02	5.89E-04	0.037	5.90E-04	0.098	1.58E-03	0.037	6.03E-04
56	*1508*	1.51E-02	3.523E-02	5.31E-04	0.036	5.36E-04	0.094	1.41E-03	0.036	5.48E-04
57	*1403*	1.40E-02	3.393E-02	4.76E-04	0.034	4.84E-04	0.089	1.25E-03	0.035	4.95E-04
58	*1298*	1.30E-02	3.263E-02	4.24E-04	0.033	4.34E-04	0.085	1.10E-03	0.034	4.44E-04
59	*1200*	1.20E-02	3.134E-02	3.76E-04	0.032	3.89E-04	0.080	9.65E-04	0.033	3.98E-04
60	*1100*	1.10E-02	3.004E-02	3.30E-04	0.031	3.45E-04	0.076	8.36E-04	0.032	3.53E-04
61	*987*	9.87E-03	2.974E-02	2.93E-04	0.031	3.07E-04	0.074	7.34E-04	0.032	3.14E-04
62	*883*	8.83E-03	2.943E-02	2.60E-04	0.031	2.72E-04	0.073	6.42E-04	0.031	2.78E-04
63	*781*	7.81E-03	2.913E-02	2.27E-04	0.031	2.38E-04	0.071	5.55E-04	0.031	2.43E-04
64	*679*	6.79E-03	2.882E-02	1.96E-04	0.030	2.05E-04	0.069	4.72E-04	0.031	2.09E-04
65	*579*	5.79E-03	2.852E-02	1.65E-04	0.030	1.73E-04	0.068	3.93E-04	0.031	1.77E-04
66	*479*	4.79E-03	2.821E-02	1.35E-04	0.030	1.42E-04	0.066	3.17E-04	0.030	1.45E-04
67	*381*	3.81E-03	2.791E-02	1.06E-04	0.029	1.12E-04	0.065	2.46E-04	0.030	1.14E-04
68	*287*	2.87E-03	2.760E-02	7.92E-05	0.029	8.32E-05	0.063	1.81E-04	0.030	8.49E-05
69	*188*	1.88E-03	2.730E-02	5.13E-05	0.029	5.40E-05	0.061	1.15E-04	0.029	5.50E-05
70	*94*	9.40E-04	2.699E-02	2.54E-05	0.028	2.67E-05	0.060	5.61E-05	0.029	2.72E-05

70 kVp	Air	Soft Tissue	Bone	Lung
Sum of %*μ_{en}/ρ	1.19E-01	1.21E-01	3.96E-01	1.25E-01
Average μ_{en}/ρ	1.71E-03	1.72E-03	5.66E-03	1.79E-03

APPENDIX E

EFFECTIVE DOSE AND RISK CALCULATIONS

Table E-1. AP Skull

Organ/ Position	MOSFETs	mV at 40 mAs	exam mAs	mV at Exam mAs	CF [mV/R]	DCF	Absorbed Dose [rad]	Tissue Weigbting Factor	Effective Dose [rem]
Thyroid	A3	9	1.25	0.28125	34.60	1 009	0.0072	0.05	0.0004
Active Bone Marrow							0.0005	0.12	0.0001
Bone surface							0.0013	0.01	0.0000
Remainder							0.0000	0.05	0.0000
Skin							0.0055	0.01	0.0001

Calculation of dose to active marrow

Organ/ Position	MOSFETs	mV 40 mAs	exam mAs	mV at exam mAs	CF [mV/R]	DCF	Absorbed Dose [rad]	Fract. Active marrow assigned to MOSFET	Fract. * Absorbed dose [rad]
Head Spine	A1	0	1.25	0	36.10	1.009	0.0000	0.1470	0.0000
Skull	A2	4	1.25	0.125	32.20	1.009	0.0034	0.1470	0.0005
Rt Arm	A4	0	1.25	0	34 80	1.009	0.0000	0.0779	0.0000
Lt Arm	A5	0	1.25	0	33.30	1.009	0.0000	0.0779	0.0000
						Total dose (rad) to active marrow			***0.0005***

Calculation of dose to bone surface

Organ/ Position	MOSFETs	mV 40 mAs	exam mAs	mV at exam mAs	CF [mV/R]	DCF	Absorbed Dose [rad]	Fract. Bone assigned to MOSFET	Fract. * Absorbed dose [rad]
Head Spine	A1	0	1.25	0	36.10	3.316	0.0000	0.1160	0.0000
Skull	A2	4	1.25	0.125	32.20	3.316	0.0113	0.1160	0.0013
Rt Arm	A4	0	1.25	0	34.80	3.316	0.0000	0.0980	0.0000
Lt Arm	A5	0	1.25	0	33.30	3.316	0.0000	0.0980	0.0000
						Total dose (rad) to bone surface			***0.0013***

Calculation of dose to remainder

Organ/ Position	MOSFETs	mV 40 mAs	exam mAs	mV at exam mAs	CF [mV/R]	DCF	Absorbed Dose [rad]
Rt Arm	A4	0	1.25	0	34.80	1.009	0.0000
Lt Arm	A5	0	1.25	0	33.30	1.009	0.0000
		Total dose (rod) to remoinder					***0.0000***

Colculation of dose to skin

Position	MOSFETs	mV 80 mAs	exam mAs	mV at exam mAs	CF [mV/R]	DCF	Absorbed Dose [rad]
Entrance	A1	25	1.25	0.390625	32.90	1.009	0.0105
Exit	A2	1	1.25	0.015625	28.80	1.009	0.0005
		Total dose (rod) to skin					***0.0055***

Total effective dose **0.0005 rem**
ESE AP Skull 0.0079 R

	f(d)	g(b)
Leukemia	1.185E-06	132.3
Male Respiratory	3.102E-06	7.3309492
Female Respiratory	3.102E-06	14.926005
Male Digestive	3.946E-06	1
Female Digestive	3.946E-06	1.74
Other	5.950E-06	1
Female Breast	5.950E-06	0.0660047

Relative Risk

Male Respiratory	Female Respiratory	Male Digestive	Female Digestive	Other	Female Breast
1.000023	1.000046	1.000004	1.000007	1.000006	1.000000

Table E-2. AP Skull with Thyroid Shield

Organ/ Position	MOSFETs	mV at 40 mAs	exam mAs	mV at exam mAs	CF [mV/R]	DCF	Absorbed Dose [rad]	Tissue Weigbting Factor	Effective Dose [rem]
Thyroid	A3	0	1.25	0	34.60	1.009	0.0000	0.05	0.0000
Active Bone Marrow							0.0005	0.12	0.0001
Bone surface							0.0013	0.01	0.0000
Remainder							0.0000	0.05	0.0000
Skin							0.0055	0.01	0.0001

Calculation of dose to active marrow

Organ/ Position	MOSFETs	mV 40 mAs	exam mAs	mV at exam mAs	CF [mV/R]	DCF	Absorbed Dose [rad]	Fract. Active marrow assigned to MOSFET	Fract. * Absorbed dose [rad]
Head Spine	A1	1	1.25	0.03125	36.10	1.009	0.0008	0.1470	0.0001
Skull	A2	3	1.25	0.09375	32.20	1.009	0.0026	0.1470	0.0004
Rt Arm	A4	0	1.25	0	34.80	1.009	0.0000	0.0779	0.0000
Lt Arm	A5	0	1.25	0	33.30	1.009	0.0000	0.0779	0.0000
						Total dose (rad) to active marrow			***0.0005***

Calculation of dose to bone surface

Organ/ Position	MOSFETs	mV 40 mAs	exam mAs	mV at exam mAs	CF [mV/R]	DCF	Absorbed Dose [rad]	Fract. Bone assigned to MOSFET	Fract. * Absorbed dose [rad]
Head Spine	A2	0	1.25	0	36.10	3.316	0.0000	0.1160	0.0000
Skull	A1	4	1.25	0.125	32.20	3.316	0.0113	0.1160	0.0013
Rt Arm	A4	0	1.25	0	34.80	3.316	0.0000	0.0980	0.0000
Lt Arm	A5	0	1.25	0	33.30	3.316	0.0000	0.0980	0.0000
						Total dose (rad) to bone surface			***0.0013***

Calculation of dose to remainder

Organ/ Position	MOSFETs	mV 40 mAs	exam mAs	mV at exam mAs	CF [mV/R]	DCF	Absorbed Dose [rad]
Rt Arm	A4	0	1.25	0	34.80	1.009	0.0000
Lt Arm	A5	0	1.25	0	33.30	1.009	0.0000
		Total dose (rad) to remainder					***0.0000***

Calculation of dose to skin

Position	MOSFETs	mV 80 mAs	exam mAs	mV at exam mAs	CF [mV/R]	DCF	Absorbed Dose [rad]
Entrance	A1	25	1.25	0.390625	32.90	1.009	0.0105
Exit	A2	1	1.25	0.015625	28.80	1.009	0.0005
		Total dose (rad) to skin					***0.0055***

Total effective dose **0.0001 rem**
ESE AP Skull 0.0079 R

	f(d)	g(b)
Leukemia	3.082E-07	132.3
Male Respiratory	8.067E-07	7.330949
Female Respiratory	8.067E-07	14.92601
Male Digestive	1.026E-06	1
Female Digestive	1.026E-06	1.74
Other	1.547E-06	1
Female Breast	1.547E-06	0.066005

Relative Risk

Leukemia	Male Respiratory	Female Respiratory	Male Digestive	Female Digestive	Other	Female Breast
1.000041	1.000006	1.000012	1.000001	1.000002	1.000002	1.000000

Table E-3. PA Skull

Organ/ Position	MOSFETs	mV at 42 mAs	exam mAs	mV at exam mAs	CF [mV/R]	DCF	Absorbed Dose [rad]	Tissue Weighting Factor	Effective Dose [rem]
Thyroid	A3	2	1.25	0.059524	34.60	1.009	0.0015	0.05	0.0001
Active Bone Marrow							0.0005	0.12	0.0001
Bone surface							0.0014	0.01	0.0000
Remainder							0.0000	0.05	0.0000
Skin							0.0055	0.01	0.0001

Calculation of dose to active marrow

Organ/ Position	MOSFETs	mV 42 mAs	exam mAs	mV at exam mAs	CF [mV/R]	DCF	Absorbed Dose [rad]	Fract. Active marrow assigned to MOSFET	Fract. * Absorbed dose [rad]
Head Spine	A1	5	1.25	0.14881	36.10	1.009	0.0036	0.1470	0.0005
Skull	A2	0	1.25	0	32.20	1.009	0.0000	0.1470	0.0000
Rt Arm	A4	0	1.25	0	34.80	1.009	0.0000	0.0779	0.0000
Lt Arm	A5	0	1.25	0	33.30	1.009	0.0000	0.0779	0.0000
						Total dose (rad) to active marrow			***0.0005***

Calculation of dose to bone surface

Organ/ Position	MOSFETs	mV 42 mAs	exam mAs	mV at exam mAs	CF [mV/R]	DCF	Absorbed Dose [rad]	Fract. Bone assigned to MOSFET	Fract. * Absorbed dose [rad]
Head Spine	A1	5	1.25	0.14881	36.10	3.316	0.0120	0.1160	0.0014
Skull	A2	0	1.25	0	32.20	3.316	0.0000	0.1160	0.0000
Rt Arm	A4	0	1.25	0	34.80	3.316	0.0000	0.0980	0.0000
Lt Arm	A5	0	1.25	0	33.30	3.316	0.0000	0.0980	0.0000
						Total dose (rad) to bone surface			***0.0014***

Calculation of dose to remainder

Organ/ Position	MOSFETs	mV 42 mAs	exam mAs	mV at exam mAs	CF [mV/R]	DCF	Absorbed Dose [rad]
Rt Arm	A4	0	1.25	0	34.80	1.009	0.0000
Lt Arm	A5	0	1.25	0	33.30	1.009	0.0000
		Total dose (rad) to remainder					***0.0000***

Calculation of dose to skin

Position	MOSFETs	mV 80 mAs	exam mAs	mV at exam mAs	CF [mV/R]	DCF	Absorbed Dose [rad]
Entrance	A1	25	1.25	0.390625	32.90	1.009	0.0105
Exit	A2	1	1.25	0.015625	28.80	1.009	0.0005
		Total dose (rad) to skin					***0.0055***

Total effective dose 0.0002 **rem**
ESE PA Skull 0.0258 R

	f(d)	g(b)
Leukemia	5.080E-07	132.3
Male Respiratory	1.330E-06	7.330949
Female Respiratory	1.330E-06	14.92601
Male Digestive	1.691E-06	1
Female Digestive	1.691E-06	1.74
Other	2.551E-06	1
Female Breast	2.551E-06	0.066005

Relative Risk

Leukemia	Male Respiratory	Female Respiratory	Male Digestive	Female Digestive	Other	Female Breast
1.000067	1.000010	1.000020	1.000002	1.000003	1.000003	1.000000

Table E-4. PA Skull with Thyroid Shield

Organ/ Position	MOSFETs	mV at 42 mAs	exam mAs	mV at Exam mAs	CF [mV/R]	DCF	Absorbed Dose [rad]	Tissue Weigbting Factor	Effective Dose [rem]
Thyroid	A3	1	1.25	0.029762	34.60	1.009	0.0008	0.05	0.0000
Active Bone Marrow							0.0007	0.12	0.0001
Bone surface							0.0019	0.01	0.0000
Remainder							0.0000	0.05	0.0000
Skin							0.0055	0.01	0.0001

Calculation of dose to active marrow

Organ/ Position	MOSFETs	mV 42 mAs	exam mAs	mV at Exam mAs	CF [mV/R]	DCF	Absorbed Dose [rad]	Fract. Active marrow assigned to MOSFET	Fract. * Absorbed dose [rad]
Head Spine	A1	7	1.25	0.208333	36.10	1.009	0.0051	0.1470	0.0007
Skull	A2	0	1.25	0	32.20	1.009	0.0000	0.1470	0.0000
Rt Arm	A4	0	1.25	0	34.80	1.009	0.0000	0.0779	0.0000
Lt Arm	A5	0	1.25	0	33.30	1.009	0.0000	0.0779	0.0000
						Total dose (rad) to active marrow			***0.0007***

Calculation of dose to bone surface

Organ/ Position	MOSFETs	mV 42 mAs	exam mAs	mV at Exam mAs	CF [mV/R]	DCF	Absorbed Dose [rad]	Fract. Bone assigned to MOSFET	Fract. * Absorbed dose [rad]
Head Spine	A1	7	1.25	0.208333	36.10	3.316	0.0168	0.1160	0.0019
Skull	A2	0	1.25	0	32.20	3.316	0.0000	0.1160	0.0000
Rt Arm	A4	0	1.25	0	34.80	3.316	0.0000	0.0980	0.0000
Lt Arm	A5	0	1.25	0	33.30	3.316	0.0000	0.0980	0.0000
						Total dose (rad) to bone surface			***0.0019***

Calculation of dose to remainder

Organ/ Position	MOSFETs	mV 42 mAs	exam mAs	mV at Exam mAs	CF [mV/R]	DCF	Absorbed Dose [rad]
Rt Arm	A4	0	1.25	0	34.80	1.009	0.0000
Lt Arm	A5	0	1.25	0	33.30	1.009	0.0000
		Total dose (rad) to remainder					***0.0000***

Calculation of dose to skin

Position	MOSFETs	mV 80 mAs	exam mAs	mV at Exam mAs	CF [mV/R]	DCF	Absorbed Dose [rad]
Entrance	A1	25	1.25	0.390625	32.90	1.009	0.0105
Exit	A2	1	1.25	0.015625	28.80	1.009	0.0005
		Total dose (rad) to skin					***0.0055***

Total effective dose **0.0002 rem**
ESE PA Skull 0.0258 R

	f(d)	g(b)
Leukemia	4.916E-07	132.3
Male Respiratory	1.287E-06	7.330949
Female Respiratory	1.287E-06	14.92601
Male Digestive	1.637E-06	1
Female Digestive	1.637E-06	1.74
Other	2.468E-06	1
Female Breast	2.468E-06	0.066005

Relative Risk

Leukemia	Male Respiratory	Female Respiratory	Male Digestive	Female Digestive	Other	Female Breast
1.000065	1.000009	1.000019	1.000002	1.000003	1.000002	1.000000

Table E-5. Lateral Skull

Organ/ Position	MOSFETs	mV at 40 mAs	exam mAs	mV at exam mAs	CF [mV/R]	DCF	Absorbed Dose [rad]	Tissue Weighting Factor	Effective Dose [rem]
Thyroid	A3	0	1.75	0	34.60	1.009	0.0000	0.05	0.0000
Active Bone Marrow							0.0007	0.12	0.0001
Bone surface							0.0017	0.01	0.0000
Remainder							0.0000	0.05	0.0000
Skin							0.0074	0.01	0.0001

Calculation of dose to active marrow

Organ/ Position	MOSFETs	mV 40 mAs	exam mAs	mV at exam mAs	CF [mV/R]	DCF	Absorbed Dose [rad]	Fract. Active marrow assigned to MOSFET	Fract. * Absorbed dose [rad]
Head Spine	A1	2	1.75	0.0875	36.10	1.009	0.0021	0.1470	0.0003
Skull	A2	2	1.75	0.0875	32.20	1.009	0.0024	0.1470	0.0004
Rt Arm	A4	0	1.75	0	34.80	1.009	0.0000	0.0779	0.0000
Lt Arm	A5	0	1.75	0	33.30	1.009	0.0000	0.0779	0.0000
						Total dose (rad) to active marrow			***0.0007***

Calculation of dose to bone surface

Organ/ Position	MOSFETs	mV 40 mAs	exam mAs	mV at exam mAs	CF [mV/R]	DCF	Absorbed Dose [rad]	Fract. Bone assigned to MOSFET	Fract. * Absorbed dose [rad]
Head Spine	A1	2	1.75	0.0875	36.10	3.316	0.0070	0.1160	0.0008
Skull	A2	2	1.75	0.0875	32.20	3.316	0.0079	0.1160	0.0009
Rt Arm	A4	0	1.75	0	34.80	3.316	0.0000	0.0980	0.0000
Lt Arm	A5	0	1.75	0	33.30	3.316	0.0000	0.0980	0.0000
						Total dose (rad) to bone surface			***0.0017***

Calculation of dose to remainder

Organ/ Position	MOSFETs	mV 40 mAs	exam mAs	mV at exam mAs	CF [mV/R]	DCF	Absorbed Dose [rad]
Rt Arm	A4	0	1.75	0	34.80	1.009	0.0000
Lt Arm	A5	0	1.75	0	33.30	1.009	0.0000
		Total dose (rad) to remainder					***0.0000***

Calculation of dose to skin

Position	MOSFETs	mV 80 mAs	exam mAs	mV at exam mAs	CF [mV/R]	DCF	Absorbed Dose [rad]
Entrance	A1	24	1.75	0.525	32.90	1.009	0.0141
Exit	A2	1	1.75	0.021875	28.80	1.009	0.0007
		Total dose (rad) to skin					***0.0074***

Total effective dose **0.0002 rem**
ESE LAT Skull 0.0091 R

	f(d)	g(b)
Leukemia	4.164E-07	132.3
Male Respiratory	1.090E-06	7.330949
Female Respiratory	1.090E-06	14.92601
Male Digestive	1.386E-06	1
Female Digestive	1.386E-06	1.74
Other	2.091E-06	1
Female Breast	2.091E-06	0.066005

Relative Risk

Leukemia	Male Respiratory	Female Respiratory	Male Digestive	Female Digestive	Other	Female Breast
1.000055	1.000008	1.000016	1.000001	1.000002	1.000002	1.000000

Table E-6. Townes Skull

Organ/ Position	MOSFETs	mV at 40 mAs	exam mAs	mV at exam mAs	CF [mV/R]	DCF	Absorbed Dose [rad]	Tissue Weighting Factor	Effective Dose [rem]
Thyroid	A3	2	1.75	0.0875	34.60	1.009	0.0022	0.05	0.0001
Active Bone Marrow							0.0009	0.12	0.0001
Bone surface							0.0025	0.01	0.0000
Remainder							0.0012	0.05	0.0001
Skin							0.0109	0.01	0.0001

Calculation of dose to active marrow

Organ/ Position	MOSFETs	mV 40 mAs	exam mAs	mV at exam mAs	CF [mV/R]	DCF	Absorbed Dose [rad]	Fract. Active marrow assigned to MOSFET	Fract. * Absorbed dose [rad]
Head Spine	A1	1	1.75	0.04375	36.10	1.009	0.0011	0.1470	0.0002
Skull	A2	3	1.75	0.13125	32.20	1.009	0.0036	0.1470	0.0005
Rt Arm	A4	0	1.75	0	34.80	1.009	0.0000	0.0779	0.0000
Lt Arm	A5	2	1.75	0.0875	33.30	1.009	0.0023	0.0779	0.0002
							Total dose (rad) to active marrow		***0.0009***

Calculation of dose to bone surface

Organ/ Position	MOSFETs	mV 40 mAs	exam mAs	mV at exam mAs	CF [mV/R]	DCF	Absorbed Dose [rad]	Fract. Bone assigned to MOSFET	Fract. * Absorbed dose [rad]
Head Spine	A1	1	1.75	0.04375	36.10	3.316	0.0035	0.1160	0.0004
Skull	A2	3	1.75	0.13125	32.20	3.316	0.0118	0.1160	0.0014
Rt Arm	A4	0	1.75	0	34.80	3.316	0.0000	0.0980	0.0000
Lt Arm	A5	2	1.75	0.0875	33.30	3.316	0.0076	0.0980	0.0007
							Total dose (rad) to bone surface		***0.0025***

Calculation of dose to remainder

Organ/ Position	MOSFETs	mV 40 mAs	exam mAs	mV at exam mAs	CF [mV/R]	DCF	Absorbed Dose [rad]
Rt Arm	A4	0	1.75	0	34.80	1.009	0.0000
Lt Arm	A5	2	1.75	0.0875	33.30	1.009	0.0023
		Total dose (rad) to remainder					***0.0012***

Calculation of dose to skin

Position	MOSFETs	mV 80 mAs	exam mAs	mV at exam mAs	CF [mV/R]	DCF	Absorbed Dose [rad]
Entrance	A1	36	1.75	0.7875	32.90	1.009	0.0212
Exit	A2	1	1.75	0.021875	28.80	1.009	0.0007
		Total dose (rad) to skin					***0.0109***

Total effective dose **0.0004 rem**
ESE Townes Skull 0.0131 R

	f(d)	g(b)
Leukemia	9.925E-07	132.3
Male Respiratory	2.598E-06	7.330949
Female Respiratory	2.598E-06	14.92601
Male Digestive	3.304E-06	1
Female Digestive	3.304E-06	1.74
Other	4.983E-06	1
Female Breast	4.983E-06	0.066005

Relative Risk

Leukemia	Male Respiratory	Female Respiratory	Male Digestive	Female Digestive	Other	Female Breast
1.000131	1.000019	1.000039	1.000003	1.000006	1.000005	1.000000

Table E-7. AP Cervical Spine

Organ/ Position	MOSFETs	mV at 40 mAs	exam mAs	mV at exam mAs	CF [mV/R]	DCF	Absorbed Dose [rad]	Tissue Weighting Factor	Effective Dose [rem]
Esophagus	D4	0	3.75	0	34.80	1.009	0.0000	0.05	0.0000
Thyroid	A3	7	3.75	0.65625	34.60	1.009	0.0168	0.05	0.0008
Breast	D2	0	3.75	0	32.70	1.009	0.0000	0.05	0.0000
Average Lung							0.0000	0.12	0.0000
Rt Lung	D3	0	3.75	0	32.00	1.046	0.0000		
Lt Lung	D1	0	3.75	0	33.30	1.046	0.0000		
Stomach	D5	0	3.75	0	38.50	1.009	0.0000	0.12	0.0000
Liver	NM		3.75	0	31.98	1.009	0.0000	0.05	0.0000
Bladder	NM		3.75	0	32.91	1.009	0.0000	0.05	0.0000
Colon	NM		3.75	0	31.98	1.009	0.0000	0.12	0.0000
Active Bone Marrow							0.0000	0.12	0.0000
Bone surface							0.0000	0.01	0.0000
Skin							0.0121	0.01	0.0001
Average Ovary							0.0000	0.20	0.0000
Rt Ovary	NM		3.75	0	33.44	1.009	0.0000		
Lt Ovary	NM		3.75	0	31.18	1.009	0.0000		
Testes	NM		3.75	0	33.04	1.009	0.0000	0.20	0.0000
Remainder-F							0.0000	0.05	0.0000
Remainder-M							0.0000	0.05	0.0000

Calculation of dose to active marrow

Organ/ Position	MOSFETs	mV at 40 mAs	exam mAs	mV at exam mAs	CF [mV/R]	DCF	Absorbed Dose [rads]	Fract. Active marrow assigned to MOSFET	Fract. * Absorbed dose [rad]
Head Spine	A1	0	3.75	0	36.10	1.009	0.0000	0.1470	0.0000
Skull	A2	0	3.75	0	32.20	1.009	0.0000	0.1470	0.0000
Rt Arm	A5	0	3.75	0	33.30	1.009	0.0000	0.0779	0.0000
Lt Arm	A4	0	3.75	0	34.80	1.009	0.0000	0.0779	0.0000
						Total dose (rad) to active marrow			***0.0000***

Calculation of dose to bone surface

Organ/ Position	MOSFETs	mV at 40 mAs	exam mAs	mV at exam mAs	CF [mV/R]	DCF	Absorbed Dose [rad]	Fract. Bone assigned to MOSFET	Fract. * Absorbed dose [rad]
Head Spine	A1	0	3.75	0	36.10	3.316	0.0000	0.1160	0.0000
Skull	A2	0	3.75	0	32.20	3.316	0.0000	0.1160	0.0000
Rt Arm	A5	0	3.75	0	33.30	3.316	0.0000	0.0980	0.0000
Lt Arm	A4	0	3.75	0	34.80	3.316	0.0000	0.0980	0.0000
							Total dose (rad) to bone surface		***0.0000***

Calculation of dose to remainder

Organ/ Position	MOSFETs	mV at 40 mAs	exam mAs	mV at exam mAs	CF [mV/R]	DCF	Absorbed Dose [rad]	
Rt Arm	A5	0	3.75	0	33.30	1.009	0.0000	
Lt Arm	A4	0	3.75	0	34.80	1.009	0.0000	
Esophagus	D4	0	3.75	0	34.80	1.009	0.0000	
Breast	D2	0	3.75	0	32.70	1.009	0.0000	
Stomach	D5	0	3.75	0	38.50	1.009	0.0000	
Liver	NM		3.75	0	31.98	1.009	0.0000	
Bladder	NM		3.75	0	32.91	1.009	0.0000	
Colon	NM		3.75	0	31.98	1.009	0.0000	
Average Lung							0.0000	
Rt Lung	D3	0	3.75	0	32.00	1.046	0.0000	
Lt Lung	D1	0	3.75	0	33.30	1.046	0.0000	
Average Ovary							0.0000	
Rt Ovary	NM		3.75	0	33.44	1.009	0.0000	
Lt Ovary	NM		3.75	0	31.18	1.009	0.0000	
Testes	NM		3.75	0	33.04	1.009	0.0000	
							Total dose (rad) to remainder-F	***0.0000***
							Total dose (rad) to remainder-M	***0.0000***

Calculation of dose to skin

Position	MOSFETs	mV at 80 mAs	exam mAs	mV at exam mAs	CF [mV/R]	DCF	Absorbed Dose [rad]
Entrance	A1	18	3.75	0.84375	32.90	1.009	0.0227
Exit	A2	1	3.75	0.046875	28.80	1.009	0.0014
				Total dose (rad) to skin			*0.0121*

Subtotal Effective Dose ***0.0010*** ***rem***

Female Effective Dose ***0.0010*** rem
Male Effective Dose ***0.0010*** rem

ESE AP C-Spine 0.0147 R

	f(d)	g(b)
Leukemia	2.330E-06	132.3
Male Respiratory	6.098E-06	7.330949
Female Respiratory	6.098E-06	14.92601
Male Digestive	7.756E-06	1
Female Digestive	7.756E-06	1.74
Other	1.170E-05	1
Female Breast	1.170E-05	0.066005

Relative Risk

Leukemia	Male Respiratory	Female Respiratory	Male Digestive	Female Digestive	Other	Female Breast
1.000308	1.000045	1.000091	1.000008	1.000013	1.000012	1.000001

Table E-8. Lateral Cervical Spine

Organ/ Position	MOSFETs	mV at 40 mAs	exam mAs	MV at exam mAs	CF [mV/R]	DCF	Absorbed Dose [rad]	Tissue Weighting Factor	Effective Dose [rem]
Esophagus	D4	1	6.25	0.15625	34.80	1.009	0.0040	0.05	0.0002
Thyroid	A3	5	6.25	0.78125	34.60	1.009	0.0200	0.05	0.0010
Breast	D2	0	6.25	0	32.70	1.009	0.0000	0.05	0.0000
Average Lung							0.0000	0.12	0.0000
Rt Lung	D3	0	6.25	0	32.00	1.046	0.0000		
Lt Lung	D1	0	6.25	0	33.30	1.046	0.0000		
Stomach	D5	0	6.25	0	38.50	1.009	0.0000	0.12	0.0000
Liver	NM		6.25	0	31.98	1.009	0.0000	0.05	0.0000
Bladder	NM		6.25	0	32.91	1.009	0.0000	0.05	0.0000
Colon	NM		6.25	0	31.98	1.009	0.0000	0.12	0.0000
Active Bone Marrow							0.0033	0.12	0.0004
Bone surface							0.0119	0.01	0.0001
Skin							0.0220	0.01	0.0002
Average Ovary							0.0000	0.20	0.0000
Rt Ovary	NM		6.25	0	33.44	1.009	0.0000		
Lt Ovary	NM		6.25	0	31.18	1.009	0.0000		
Testes	NM		6.25	0	33.04	1.009	0.0000	0.20	0.0000
Remainder-F							0.0032	0.05	0.0002
Remainder-M							0.0032	0.05	0.0002

Calculation of dose to active marrow

Organ/ Position	MOSFETs	mV at 40 mAs	exam mAs	mV at exam mAs	CF [mV/R]	DCF	Absorbed Dose [rads]	Fract. Active marrow assigned to MOSFET	Fract. * Absorbed dose [rad]
Head Spine	A1	2	6.25	0.3125	36.10	1.009	0.0077	0.1470	0.0011
Skull	A2	0	6.25	0	32.20	1.009	0.0000	0.1470	0.0000
Rt Arm	A5	0	6.25	0	33.30	1.009	0.0000	0.0779	0.0000
Lt Arm	A4	7	6.25	1.09375	34 80	1.009	0.0278	0.0779	0.0022
						Total dose (rad) to active marrow			***0.0033***

Calculation of dose to bone surface

Organ/ Position	MOSFETs	mV at 40 mAs	exam mAs	mV at exam mAs	CF [mV/R]	DCF	Absorbed Dose [rad]	Fract. Bone assigned to MOSFET	Fract. * Absorbed dose [rad]
Head Spine	A1	2	6.25	0.3125	36.10	3.316	0.0251	0.1160	0.0029
Skull	A2	0	6.25	0	32.20	3.316	0.0000	0.1160	0.0000
Rt Arm	A5	0	6.25	0	33.30	3.316	0.0000	0.0980	0.0000
Lt Arm	A4	7	6.25	1.09375	34.80	3.316	0.0913	0.0980	0.0089
						Total dose (rad) to bone surface			***0.0119***

Calculation of dose to remainder

Organ/ Position	MOSFETs	mV at 40 mAs	exam mAs	mV at exam mAs	CF [mV/R]	DCF	Absorbed Dose [rad]	
Rt Arm	A5	0	6.25	0	33.30	1.009	0.0000	
Lt Arm	A4	7	6.25	1.09375	34.80	1.009	0.0278	
Esophagus	D4	1	6.25	0.15625	34 80	1.009	0.0040	
Breast	D2	0	6.25	0	32.70	1.009	0.0000	
Stomach	D5	0	6.25	0	38.50	1.009	0.0000	
Liver	NM		6.25	0	31.98	1.009	0.0000	
Bladder	NM		6.25	0	32.91	1.009	0.0000	
Colon	NM		6.25	0	31.98	1.009	0.0000	
Average Lung							0.0000	
Rt Lung	D3	0	6.25	0	32.00	1.046	0.0000	
Lt Lung	D1	0	6.25	0	33.30	1.046	0.0000	
Average Ovary							0.0000	
Rt Ovary	NM		6.25	0	33.44	1.009	0.0000	
Lt Ovary	NM		6.25	0	31.18	1.009	0.0000	
Testes	NM		6.25	0	33.04	1.009	0.0000	
						Total dose (rad) to remainder-F		***0.0032***
						Total dose (rad) to remainder-M		***0.0032***

Calculation of dose to skin

Position	MOSFETs	mV at 80 mAs	exam mAs	mV at exam mAs	CF [mV/R]	DCF	Absorbed Dose [rad]
Entrance	A1	21	6.25	1.640625	32.90	1.009	0.0441
Exit	A2	0	6.25	0	28.80	1.009	0.0000
				Total dose (rad) to skin			***0.0220***

Subtotal Effective Dose ***0.0019*** ***rem***

Female Effective Dose ***0.0021*** rem
Male Effective Dose ***0.0021*** rem

ESE LAT C-Spine 0.1111 R

	f(d)	g(b)
Leukemia	5.076E-06	132.3
Male Respiratory	1.328E-05	7.330949
Female Respiratory	1.328E-05	14.92601
Male Digestive	1.690E-05	1
Female Digestive	1.690E-05	1.74
Other	2.548E-05	1
Female Breast	2.548E-05	0.066005

Relative Risk

Leukemia	Male Respiratory	Female Respiratory	Male Digestive	Female Digestive	Other	Female Breast
1.000672	1.000097	1.000198	1.000017	1.000029	1.000025	1.000002

Table E-9. AP Thoracic Spine

Organ/ Position	MOSFETs	mV at 80 mAs	exam mAs	mV at exam mAs	CF [mV/R]	DCF	Absorbed Dose [rad]	Tissue Weighting Factor	Effective Dose [rem]
Esophagus	B3	3	3.75	0.140625	27.50	1.009	0.0045	0.05	0.0002
Thyroid	A3	2	3.75	0.09375	31.90	1.009	0.0026	0.05	0.0001
Breast	A2	22	3.75	1.03125	28.80	1.009	0.0316	0.05	0.0016
Average Lung							0.0071	0.12	0.0008
Rt Lung	C3	5	3.75	0.234375	34.00	1.046	0.0063		
Lt Lung	C4	6	3.75	0.28125	33.10	1.046	0.0078		
Stomach	C1	2	3.75	0.09375	32.30	1.009	0.0026	0.12	0.0003
Liver	A2	2	3.75	0.09375	28.80	1.009	0.0029	0.05	0.0001
Bladder	C2	0	3.75	0	34.20	1.009	0.0000	0.05	0.0000
Colon	D5	0	3.75	0	29.90	1.009	0.0000	0.12	0.0000
Active Bone Marrow							0.0013	0.12	0.0002
Bone surface							0.0051	0.01	0.0001
Skin							0.0152	0.01	0.0002
Average Ovary							0.0000	0.20	0.0000
Rt Ovary	B5	0	3.75	0	30.60	1.009	0.0000		
Lt Ovary	B1	0	3.75	0	27.00	1.009	0.0000		
Testes	D2	0	3.75	0	30.30	1.009	0.0000	0.20	0.0000
Remainder-F							0.0118	0.05	0.0006
Remainder-M							0.0118	0.05	0.0006

Calculation of dose to active marrow

Organ/ Position	MOSFETs	mV at 80 mAs	exam mAs	mV at exam mAs	CF [mV/R]	DCF	Absorbed Dose [rads]	Fract. Active marrow assigned to MOSFET	Fract. * Absorbed dose [rad]
Spine middle	A1	1	3.75	0.046875	32.90	1.009	0.0013	0.1588	0.0002
Rt Arm	A5	5	3.75	0.234375	34.60	1.009	0.0060	0.0779	0.0005
Lt Arm	A4	6	3.75	0.28125	33.10	1.009	0.0075	0.0779	0.0006
Pelvis	D3	0	3.75	0	33.50	1.009	0.0000	0.2191	0.0000
						Total dose (rad) to active marrow			***0.0013***

Calculation of dose to bone surface

Organ/ Position	MOSFETs	mV at 80 mAs	exam mAs	mV at exam mAs	CF [mV/R]	DCF	Absorbed Dose [rad]	Fract. Bone assigned to MOSFET	Fract. * Absorbed dose [rad]
Spine middle	A1	1	3.75	0.046875	32.90	3.316	0.0041	0.1850	0.0008
Rt Arm	A5	5	3.75	0.234375	34.60	3.316	0.0197	0.0980	0.0019
Lt Arm	A4	6	3.75	0.28125	33.10	3.316	0.0247	0.0980	0.0024
Pelvis	D3	0	3.75	0	33.50	3.316	0.0000	0.2190	0.0000
						Total dose (rad) to bone surface			***0.0051***

Calculation of dose to remainder

Organ/ Position	MOSFETs	mV at 80 mAs	exam mAs	mV at exam mAs	CF [mV/R]	DCF	Absorbed Dose [rad]	
Rt Arm	A4	5	3.75	0.234375	33.10	1.009	0.0063	
Lt Arm	A5	6	3.75	0.28125	34.60	1.009	0.0072	
Esophagus	B3	3	3.75	0.140625	27.50	1.009	0.0045	
Breast	B4	22	3.75	1.03125	31.70	1.009	0.0288	
Stomach	C1	2	3.75	0.09375	32.30	1.009	0.0026	
Liver	A2	2	3.75	0.09375	28.80	1.009	0.0614	
Bladder	C2	0	3.75	0	34.20	1.009	0.0000	
Colon	D5	0	3.75	0	29.90	1.009	0.0000	
Average Lung							0.0071	
Rt Lung	C3	5	3.75	0.234375	34.00	1.046	0.0063	
Lt Lung	C4	6	3.75	0.28125	33.10	1.046	0.0078	
Average Ovary							0.0000	
Rt Ovary	B5	0	3.75	0	30.60	1.009	0.0000	
Lt Ovary	B1	0	3.75	0	27.00	1.009	0.0000	
Testes	D2	0	3.75	0	30.30	1.009	0.0000	
						Total dose (rad) to remainder-F		***0.0118***
						Total dose (rad) to remainder-M		***0.0118***

Calculation of dose to skin

Position	MOSFETs	mV at 80 mAs	exam mAs	mV at exam mAs	CF [mV/R]	DCF	Absorbed Dose [rad]
Entrance	A1	23	3.75	1.078125	32.90	1.009	0.0290
Exit	A2	1	3.75	0.046875	28.80	1.009	0.0014
				Total dose (rad) to skin			*0.0152*

Subtotal Effective Dose ***0.0036*** ***rem***

Female Effective Dose ***0.0042*** rem
Male Effective Dose ***0.0042*** rem

ESE AP T-Spine 0.0190 R

	f(d)	g(b)
Leukemia	1.015E-05	132.3
Male Respiratory	2.657E-05	7.330949
Female Respiratory	2.657E-05	14.92601
Male Digestive	3.380E-05	1
Female Digestive	3.380E-05	1.74
Other	5.097E-05	1
Female Breast	5.098E-05	0.066005

Relative Risk

Leukemia	Male Respiratory	Female Respiratory	Male Digestive	Female Digestive	Other	Female Breast
1.001343	1.000195	1.000397	1.000034	1.000059	1.000051	1.000003

Table E-10. Lateral Thoracic Spine

Organ/ Position	MOSFETs	mV at 80 mAs	exam mAs	mV at exam mAs	CF [mV/R]	DCF	Absorbed Dose [rad]	Tissue Weighting Factor	Effective Dose [rem]
Esophagus	B3	0	24	0	27.50	1.009	0.0000	0.05	0.0000
Thyroid	A3	3	24	0.9	31.90	1.009	0.0249	0.05	0.0012
Breast	A2	0	24	0	28.80	1.009	0.0000	0.05	0.0000
Average Lung							0.0162	0.12	0.0019
Rt Lung	C3	4	24	1.2	34.00	1.046	0.0323		
Lt Lung	C4	0	24	0	33.10	1.046	0.0000		
Stomach	C1	0	24	0	32.30	1.009	0.0000	0.12	0.0000
Liver	A2	2	24	0.6	32.90	1.009	0.0161	0.05	0.0008
Bladder	C2	0	24	0	34.20	1.009	0.0000	0.05	0.0000
Colon	D5	0	24	0	29.90	1.009	0.0000	0.12	0.0000
Active Bone Marrow							0.0079	0.12	0.0010
Bone surface							0.0320	0.01	0.0003
Skin							0.0604	0.01	0.0006
Average Ovary							0.0000	0.20	0.0000
Rt Ovary	B5	0	24	0	30.60	1.009	0.0000		
Lt Ovary	B1	0	24	0	27.00	1.009	0.0000		
Testes	D2	0	24	0	30.30	1.009	0.0000	0.20	0.0000
Remainder-F							0.0150	0.05	0.0007
Remainder-M							0.0110	0.05	0.0005

Calculation of dose to active marrow

Organ/ Position	MOSFETs	mV at 80 mAs	exam mAs	mV at exam mAs	CF [mV/R]	DCF	Absorbed Dose [rads]	Fract. Active marrow assigned to MOSFET	Fract. * Absorbed dose [rad]
Spine middle	A1	2	24	0.6	32.90	1.009	0.0161	0.1588	0.0026
Rt Arm	A5	9	24	2.7	34.60	1.009	0.0690	0.0779	0.0054
Lt Arm	A4	0	24	0	33.10	1.009	0.0000	0.0779	0.0000
Pelvis	D3	0	24	0	33.50	1.009	0.0000	0.2191	0.0000
							Total dose (rad) to active marrow		***0.0079***

Calculation of dose to bone surface

Organ/ Position	MOSFETs	mV at 80 mAs	exam mAs	mV at exam mAs	CF [mV/R]	DCF	Absorbed Dose [rad]	Fract. Bone assigned to MOSFET	Fract. * Absorbed dose [rad]
Spine middle	A1	2	24	0.6	32.90	3.316	0.0530	0.1850	0.0098
Rt Arm	A5	9	24	2.7	34.60	3.316	0.2267	0.0980	0.0222
Lt Arm	A4	0	24	0	33.10	3.316	0.0000	0.0980	0.0000
Pelvis	D3	0	24	0	33.50	3.316	0.0000	0.2190	0.0000
						Total dose (rad) to bone surface			***0.0320***

Calculation of dose to remainder

Organ/ Position	MOSFETs	mV at 80 mAs	exam mAs	mV at exam mAs	CF [mV/R]	DCF	Absorbed Dose [rad]	
Rt Arm	A4	9	24	2.7	33.10	1.009	0.0721	
Lt Arm	A5	0	24	0	34.60	1.009	0.0000	
Esophagus	B3	0	24	0	27.50	1.009	0.0000	
Breast	B4	0	24	0	31.70	1.009	0.0000	
Stomach	C1	0	24	0	32.30	1.009	0.0000	
Liver	A2	2	24	0.6	28.80	1.009	0.0614	
Bladder	C2	0	24	0	34.20	1.009	0.0000	
Colon	D5	0	24	0	29.90	1.009	0.0000	
Average Lung							0.0162	
Rt Lung	C3	4	24	1.2	34.00	1.046	0.0323	
Lt Lung	C4	0	24	0	33.10	1.046	0.0000	
Average Ovary							0.0000	
Rt Ovary	B5	0	24	0	30.60	1.009	0.0000	
Lt Ovary	B1	0	24	0	27.00	1.009	0.0000	
Testes	D2	0	24	0	30.30	1.009	0.0000	
						Total dose (rad) to remainder-F		***0.0150***
						Total dose (rad) to remainder-M		***0.0110***

Calculation of dose to skin

Position	MOSFETs	mV at 80 mAs	exam mAs	mV at exam mAs	CF [mV/R]	DCF	Absorbed Dose [rad]
Entrance	A1	15	24	4.5	32.90	1.009	0.1209
Exit	A2	0	24	0	28.80	1.009	0.0000
				Total dose (rad) to skin			*0.0604*

Subtotal Effective Dose ***0.0059*** ***rem***

Female Effective Dose ***0.0066*** rem
Male Effective Dose ***0.0064*** rem

ESE LAT T-Spine 0.0842 R

	f(d)	g(b)
Leukemia	1.584E-05	132.3
Male Respiratory	4.083E-05	7.330949
Female Respiratory	4.209E-05	14.92601
Male Digestive	5.193E-05	1
Female Digestive	5.354E-05	1.74
Other	7.953E-05	1
Female Breast	7.831E-05	0.066005

Relative Risk

Leukemia	Male Respiratory	Female Respiratory	Male Digestive	Female Digestive	Other	Female Breast
1.002096	1.000299	1.000628	1.000052	1.000093	1.000080	1.000005

Table E-11. AP Lumbar Spine

Organ/ Position	MOSFETs	mV at 80 mAs	exam mAs	mV at exam mAs	CF [mV/R]	DCF	Absorbed Dose [rad]	Tissue Weighting Factor	Effective Dose [rem]
Esophagus	B3	0	3.75	0	27.50	1.009	0.0000	0.05	0.0000
Thyroid	A3	0	3.75	0	31.90	1.009	0.0000	0.05	0.0000
Breast	A2	0	3.75	0	28.80	1.009	0.0000	0.05	0.0000
Average Lung							0.0000	0.12	0.0000
Rt Lung	C3	0	3.75	0	34.00	1.046	0.0000		
Lt Lung	C4	0	3.75	0	33.10	1.046	0.0000		
Stomach	C1	7	3.75	0.328125	32.30	1.009	0.0090	0.12	0.0011
Liver	A2	5	3.75	0.234375	32.90	1.009	0.0063	0.05	0.0003
Bladder	C2	7	3.75	0.328125	34.20	1.009	0.0085	0.05	0.0004
Colon	D5	2	3.75	0.09375	29.90	1.009	0.0028	0.12	0.0003
Active Bone Marrow							0.0002	0.12	0.0000
Bone surface							0.0008	0.01	0.0000
Skin							0.0152	0.01	0.0002
Average Ovary							0.0057	0.20	0.0011
Rt Ovary	B5	5	3.75	0.234375	30.60	1.009	0.0068		
Lt Ovary	B1	3	3.75	0.140625	27.00	1.009	0.0046		
Testes	D2	0	3.75	0	30.30	1.009	0.0000	0.20	0.0000
Remainder-F							0.0408	0.05	0.0020
Remainder-M							0.0402	0.05	0.0020

Calculation of dose to active marrow

Organ/ Position	MOSFETs	mV at 80 mAs	exam mAs	mV at exam mAs	CF [mV/R]	DCF	Absorbed Dose [rads]	Fract. Active marrow assigned to MOSFET	Fract. * Absorbed dose [rad]
Spine middle	A1	1	3.75	0.046875	32.90	1.009	0.0013	0.1588	0.0002
Rt Arm	A5	0	3.75	0	34.60	1.009	0.0000	0.0779	0.0000
Lt Arm	A4	0	3.75	0	33.10	1.009	0.0000	0.0779	0.0000
Pelvis	D3	1	3.75	0.046875	33.50	1.009	0.0012	0.2191	0.0003
						Total dose (rad) to active marrow			***0.0002***

Calculation of dose to bone surface

Organ/ Position	MOSFETs	mV at 80 mAs	exam mAs	mV at exam mAs	CF [mV/R]	DCF	Absorbed Dose [rad]	Fract. Bone assigned to MOSFET	Fract. * Absorbed dose [rad]
Spine middle	A1	1	3.75	0.046875	32.90	3.316	0.0041	0.1850	0.0008
Rt Arm	A5	0	3.75	0	34.60	3.316	0.0000	0.0980	0.0000
Lt Arm	A4	0	3.75	0	33.10	3.316	0.0000	0.0980	0.0000
Pelvis	D3	1	3.75	0.046875	33.50	3.316	0.0041	0.2190	0.0009
						Total dose (rad) to bone surface			*0.0008*

Calculation of dose to remainder

Organ/ Position	MOSFETs	mV at 80 mAs	exam mAs	mV at exam mAs	CF [mV/R]	DCF	Absorbed Dose [rad]	
Rt Arm	A4	0	3.75	0	33.10	1.009	0.0000	
Lt Arm	A5	0	3.75	0	34.60	1.009	0.0000	
Esophagus	B3	0	3.75	0	27.50	1.009	0.0000	
Breast	B4	0	3.75	0	31.70	1.009	0.0000	
Stomach	C1	7	3.75	0.328125	32.30	1.009	0.0090	
Liver	A2	5	3.75	0.234375	28 80	1.009	0.1535	
Bladder	C2	7	3.75	0.328125	34.20	1.009	0.1809	
Colon	D5	2	3.75	0.09375	29.90	1.009	0.0591	
Average Lung							0.0000	
Rt Lung	C3	0	3.75	0	34.00	1.046	0.0000	
Lt Lung	C4	0	3.75	0	33.10	1.046	0.0000	
Average Ovary							0.0057	
Rt Ovary	B5	5	3.75	0.234375	30.60	1.009	0.0068	
Lt Ovary	B1	3	3.75	0.140625	27.00	1.009	0.0046	
Testes	D2	0	3.75	0	30.30	1.009	0.0000	
						Total dose (rad) to remainder-F		*0.0408*
						Total dose (rad) to remainder-M		*0.0402*

Calculation of dose to skin

Position	MOSFETs	mV at 80 mAs	exam mAs	mV at exam mAs	CF [mV/R]	DCF	Absorbed Dose [rad]
Entrance	A1	23	3.75	1.078125	32.90	1.009	0.0290
Exit	A2	1	3.75	0.046875	28.80	1.009	0.0014
				Total dose (rad) to skin			*0.0152*

Subtotal Effective Dose	***0.0023***	rem
Female Effective Dose	***0.0055***	rem
Male Effective Dose	***0.0043***	rem

ESE AP L-Spine 0.0190 R

	f(d)	g(b)
Leukemia	1.198E-05	132.3
Male Respiratory	2.763E-05	7.330949
Female Respiratory	3.505E-05	14.92601
Male Digestive	3.515E-05	1
Female Digestive	4.458E-05	1.74
Other	6.012E-05	1
Female Breast	5.301E-05	0.066005

Relative Risk

Leukemia	Male Respiratory	Female Respiratory	Male Digestive	Female Digestive	Other	Female Breast
1.001584	1.000203	1.000523	1.000035	1.000078	1.000060	1.000003

Table E-12. Lateral Lumbar Spine

Organ/ Position	MOSFETs	mV at 80 mAs	exam mAs	mV at exam mAs	CF [mV/R]	DCF	Absorbed Dose [rad]	Tissue Weigbting Factor	Effective Dose [rem]
Esophagus	B3	0	6.25	0	27.50	1.014	0.0000	0.05	0.0000
Thyroid	A3	0	6.25	0	31.90	1.014	0.0000	0.05	0.0000
Breast	A2	0	6.25	0	28.80	1.014	0.0000	0.05	0.0000
Average Lung							0.0000	0.12	0.0000
Rt Lung	C3	0	6.25	0	34.00	1.046	0.0000		
Lt Lung	C4	0	6.25	0	33.10	1.046	0.0000		
Stomach	C1	1	6.25	0.078125	32.30	1.014	0.0021	0.12	0.0003
Liver	A2	5	6.25	0.390625	32.90	1.014	0.0105	0.05	0.0005
Bladder	C2	2	6.25	0.15625	34.20	1.014	0.0041	0.05	0.0002
Colon	D5	2	6.25	0.15625	29.90	1.014	0.0046	0.12	0.0006
Active Bone Marrow							0.0000	0.12	0.0000
Bone surface							0.0000	0.01	0.0000
Skin							0.0253	0.01	0.0003
Average Ovary							0.0070	0.20	0.0014
Rt Ovary	B5	5	6.25	0.390625	30.60	1.014	0.0113		
Lt Ovary	B1	1	6.25	0.078125	27.00	1.014	0.0026		
Testes	D2	0	6.25	0	30.30	1.014	0.0000	0.20	0.0000
Remainder-F							0.0275	0.05	0.0014
Remainder-M							0.0268	0.05	0.0013

Calculation of dose to active marrow

Organ/ Position	MOSFETs	mV at 80 mAs	exam mAs	mV at exam mAs	CF [mV/R]	DCF	Absorbed Dose [rads]	Fract. Active marrow assigned to MOSFET	Fract. * Absorbed dose [rad]
Spine middle	A1	0	6.25	0	32.90	1.014	0.0000	0.1588	0.0000
Rt Arm	A5	0	6.25	0	34.60	1.014	0.0000	0.0779	0.0000
Lt Arm	A4	0	6.25	0	33.10	1.014	0.0000	0.0779	0.0000
Pelvis	D3	2	6.25	0.15625	33.50	1.014	0.0041	0.2191	0.0009
							Total dose (rad) to active marrow		***0.0000***

Calculation of dose to bone surface

Organ/ Position	MOSFETs	mV at 80 mAs	exam mAs	mV at exam mAs	CF [mV/R]	DCF	Absorbed Dose [rad]	Fract. Bone assigned to MOSFET	Fract. * Absorbed dose [rad]
Spine middle	A1	0	6.25	0	32.90	3.316	0.0000	0.1850	0.0000
Rt Arm	A5	0	6.25	0	34.60	3.316	0.0000	0.0980	0.0000
Lt Arm	A4	0	6.25	0	33.10	3.316	0.0000	0.0980	0.0000
Pelvis	D3	0	6.25	0	33.50	3.316	0.0000	0.2190	0.0000
						Total dose (rad) to bone surface			***0.0000***

Calculation of dose to remainder

Organ/ Position	MOSFETs	mV at 80 mAs	exam mAs	mV at exam mAs	CF [mV/R]	DCF	Absorbed Dose [rad]	
Rt Arm	A4	0	6.25	0	33.10	1.014	0.0000	
Lt Arm	A5	0	6.25	0	34.60	1.014	0.0000	
Esophagus	B3	0	6.25	0	27.50	1.014	0.0000	
Breast	B4	0	6.25	0	31.70	1.014	0.0000	
Stomach	C1	1	6.25	0.078125	32.30	1.014	0.0021	
Liver	A2	5	6.25	0.390625	28.80	1.014	0.1542	
Bladder	C2	2	6.25	0.15625	34.20	1.014	0.0519	
Colon	D5	2	6.25	0.15625	29.90	1.014	0.0594	
Average Lung							0.0000	
Rt Lung	C3	0	6.25	0	34.00	1.046	0.0000	
Lt Lung	C4	0	6.25	0	33.10	1.046	0.0000	
Average Ovary							0.0070	
Rt Ovary	B5	5	6.25	0.390625	30.60	1.014	0.0113	
Lt Ovary	B1	1	6.25	0.078125	27.00	1.014	0.0026	
Testes	D2	0	6.25	0	30.30	1.014	0.0000	
						Total dose (rad) to remainder-F		***0.0275***
						Total dose (rad) to remainder-M		***0.0268***

Calculation of dose to skin

Position	MOSFETs	mV at 80 mAs	exam mAs	mV at exam mAs	CF [mV/R]	DCF	Absorbed Dose [rad]
Entrance	A1	24	6.25	1.875	32.90	1.014	0.0506
Exit	A2	0	6.25	0	28.80	1.014	0.0000
				Total dose (rad) to skin			***0.0253***

Subtotal Effective Dose ***0.0018*** rem

Female Effective Dose ***0.0046*** rem
Male Effective Dose ***0.0031*** rem

ESE LAT L-Spine 0.0389 R

	f(d)	g(b)
Leukemia	9.355E-06	132.3
Male Respiratory	1.995E-05	7.330949
Female Respiratory	2.902E-05	14.92601
Male Digestive	2.538E-05	1
Female Digestive	3.691E-05	1.74
Other	4.697E-05	1
Female Breast	3.827E-05	0.066005

Relative Risk

Leukemia	Male Respiratory	Female Respiratory	Male Digestive	Female Digestive	Other	Female Breast
1.001238	1.000146	1.000433	1.000025	1.000064	1.000047	1.000003

Table E-13. AP Abdomen Supine

Organ/ Position	MOSFETs	mV at 80 mAs	exam mAs	mV at exam mAs	CF [mV/R]	DCF	Absorbed Dose [rad]	Tissue Weighting Factor	Effective Dose [rem]
Esophagus	B3	0	6.25	0	27.50	1.009	0.0000	0.05	0.0000
Thyroid	A3	0	6.25	0	31.90	1.009	0.0000	0.05	0.0000
Breast	A2	0	6.25	0	28.80	1.009	0.0000	0.05	0.0000
Average Lung							0.0011	0.12	0.0001
Rt Lung	C3	1	6.25	0.078125	34.00	1.046	0.0021		
Lt Lung	C4	0	6.25	0	33.10	1.046	0.0000		
Stomach	C1	11	6.25	0.859375	32.30	1.009	0.0235	0.12	0.0028
Liver	A2	0	6.25	0	32.90	1.009	0.0000	0.05	0.0000
Bladder	C2	11	6.25	0.859375	34.20	1.009	0.0222	0.05	0.0011
Colon	D5	0	6.25	0	29.90	1.009	0.0000	0.12	0.0000
Active Bone Marrow							0.0006	0.12	0.0001
Bone surface							0.0026	0.01	0.0000
Skin							0.0264	0.01	0.0003
Average Ovary							0.0045	0.20	0.0009
Rt Ovary	B5	4	6.25	0.3125	30.60	1.009	0.0090		
Lt Ovary	B1	0	6.25	0	27.00	1.009	0.0000		
Testes	D2	0	6.25	0	30.30	1.009	0.0000	0.20	0.0000
Remainder-F							0.0318	0.05	0.0016
Remainder-M							0.0311	0.05	0.0016

Calculation of dose to active marrow

Organ/ Position	MOSFETs	mV at 80 mAs	exam mAs	mV at exam mAs	CF [mV/R]	DCF	Absorbed Dose [rads]	Fract. Active marrow assigned to MOSFET	Fract. * Absorbed dose [rad]
Spine middle	A1	1	6.25	0.078125	32.90	1.009	0.0021	0.1588	0.0003
Rt Arm	A5	2	6.25	0.15625	34.60	1.009	0.0040	0.0779	0.0003
Lt Arm	A4	0	6.25	0	33.10	1.009	0.0000	0.0779	0.0000
Pelvis	D3	0	6.25	0	33.50	1.009	0.0000	0.2191	0.0000
							Total dose (rad) to active marrow		***0.0006***

Calculation of dose to bone surface

Organ/ Position	MOSFETs	mV at 80 mAs	exam mAs	mV at exam mAs	CF [mV/R]	DCF	Absorbed Dose [rad]	Fract. Bone assigned to MOSFET	Fract. * Absorbed dose [rad]
Spine middle	A1	1	6.25	0.078125	32.90	3.316	0.0069	0.1850	0.0013
Rt Arm	A5	2	6.25	0.15625	34.60	3.316	0.0131	0.0980	0.0013
Lt Arm	A4	0	6.25	0	33.10	3.316	0.0000	0.0980	0.0000
Pelvis	D3	0	6.25	0	33.50	3.316	0.0000	0.2190	0.0000
						Total dose (rad) to bone surface			***0.0026***

Calculation of dose to remainder

Organ/ Position	MOSFETs	mV at 80 mAs	exam mAs	mV at exam mAs	CF [mV/R]	DCF	Absorbed Dose [rad]	
Rt Arm	A4	2	6.25	0.15625	33.10	1.009	0.0042	
Lt Arm	A5	0	6.25	0	34.60	1.009	0.0000	
Esophagus	B3	0	6.25	0	27.50	1.009	0.0000	
Breast	B4	0	6.25	0	31.70	1.009	0.0000	
Stomach	C1	11	6.25	0.859375	32.30	1.009	0.0235	
Liver	A2	0	6.25	0	28.80	1.009	0.0000	
Bladder	C2	11	6.25	0.859375	34.20	1.009	0.2843	
Colon	D5	0	6.25	0	29.90	1.009	0.0000	
Average Lung							0.0011	
Rt Lung	C3	1	6.25	0.078125	34.00	1.046	0.0021	
Lt Lung	C4	0	6.25	0	33.10	1.046	0.0000	
Average Ovary							0.0045	
Rt Ovary	B5	4	6.25	0.3125	30.60	1.009	0.0090	
Lt Ovary	B1	0	6.25	0	27.00	1.009	0.0000	
Testes	D2	0	6.25	0	30.30	1.009	0.0000	
						Total dose (rad) to remainder-F		***0.0318***
						Total dose (rad) to remainder-M		***0.0311***

Calculation of dose to skin

Position	MOSFETs	mV at 80 mAs	exam mAs	mV at exam mAs	CF [mV/R]	DCF	Absorbed Dose [rad]
Entrance	A1	24	6.25	1.875	32.90	1.009	0.0504
Exit	A2	1	6.25	0.078125	28.80	1.009	0.0024
				Total dose (rad) to skin			***0.0264***

Subtotal Effective Dose ***0.0044*** rem

Female Effective Dose ***0.0069*** rem

Male Effective Dose ***0.0060*** rem

ESE AP Abdomen 0.0178 R

	f(d)	g(b)
Leukemia	1.567E-05	132.3
Male Respiratory	3.804E-05	7.330949
Female Respiratory	4.399E-05	14.92601
Male Digestive	4.838E-05	1
Female Digestive	5.595E-05	1.74
Other	7.867E-05	1
Female Breast	7.296E-05	0.066005

Relative Risk

Leukemia	Male Respiratory	Female Respiratory	Male Digestive	Female Digestive	Other	Female Breast
1.002073	1.000279	1.000657	1.000048	1.000097	1.000079	1.000005

Table E-14 PA Abdomen Supine

Organ/ Position	MOSFETs	mV at 80 mAs	exam mAs	mV at exam mAs	CF [mV/R]	DCF	Absorbed Dose [rad]	Tissue Weigbting Factor	Effective Dose [rem]
Esophagus	B3	0	6.25	0	27.50	1.009	0.0000	0.05	0.0000
Thyroid	A3	0	6.25	0	31.90	1.009	0.0000	0.05	0.0000
Breast	A2	0	6.25	0	28.80	1.009	0.0000	0.05	0.0000
Average Lung							0.0000	0.12	0.0000
Rt Lung	C3	0	6.25	0	34.00	1.046	0.0000		
Lt Lung	C4	0	6.25	0	33.10	1.046	0.0000		
Stomach	C1	0	6.25	0	32.30	1.009	0.0000	0.12	0.0000
Liver	A2	2	6.25	0.15625	32.90	1.009	0.0042	0.05	0.0002
Bladder	C2	7	6.25	0.546875	34.20	1.009	0.0141	0.05	0.0007
Colon	D5	0	6.25	0	29.90	1.009	0.0000	0.12	0.0000
Active Bone Marrow							0.0000	0.12	0.0000
Bone surface							0.0000	0.01	0.0000
Skin							0.0264	0.01	0.0003
Average Ovary							0.0000	0.20	0.0000
Rt Ovary	B5	0	6.25	0	30.60	1.009	0.0000		
Lt Ovary	B1	0	6.25	0	27.00	1.009	0.0000		
Testes	D2	0	6.25	0	30.30	1.009	0.0000	0.20	0.0000
Remainder-F							0.0242	0.05	0.0012
Remainder-M							0.0242	0.05	0.0012

Calculation of dose to active marrow

Organ/ Position	MOSFETs	mV at 80 mAs	exam mAs	mV at exam mAs	CF [mV/R]	DCF	Absorbed Dose [rads]	Fract. Active marrow assigned to MOSFET	Fract. * Absorbed dose [rad]
Spine middle	A1	0	6.25	0	32.90	1.009	0.0000	0.1588	0.0000
Rt Arm	A5	0	6.25	0	34.60	1.009	0.0000	0.0779	0.0000
Lt Arm	A4	0	6.25	0	33.10	1.009	0.0000	0.0779	0.0000
Pelvis	D3	0	6.25	0	33.50	1.009	0.0000	0.2191	0.0000
							Total dose (rad) to active marrow		***0.0000***

Calculation of dose to bone surface

Organ/ Position	MOSFETs	mV at 80 mAs	exam mAs	mV at exam mAs	CF [mV/R]	DCF	Absorbed Dose [rad]	Fract. Bone assigned to MOSFET	Fract. * Absorbed dose [rad]
Spine middle	A1	0	6.25	0	32.90	3.316	0.0000	0.1850	0.0000
Rt Arm	A5	0	6.25	0	34.60	3.316	0.0000	0.0980	0.0000
Lt Arm	A4	0	6.25	0	33.10	3.316	0.0000	0.0980	0.0000
Pelvis	D3	0	6.25	0	33.50	3.316	0.0000	0.2190	0.0000
						Total dose (rad) to bone surface			***0.0000***

Calculation of dose to remainder

Organ/ Position	MOSFETs	mV at 80 mAs	exam mAs	mV at exam mAs	CF [mV/R]	DCF	Absorbed Dose [rad]	
Rt Arm	A4	0	6.25	0	33.10	1.009	0.0000	
Lt Arm	A5	0	6.25	0	34.60	1.009	0.0000	
Esophagus	B3	0	6.25	0	27.50	1.009	0.0000	
Breast	B4	0	6.25	0	31.70	1.009	0.0000	
Stomach	C1	0	6.25	0	32.30	1.009	0.0000	
Liver	A2	2	6.25	0.15625	28.80	1.009	0.0614	
Bladder	C2	7	6.25	0.546875	34.20	1.009	0.1809	
Colon	D5	0	6.25	0	29.90	1.009	0.0000	
Average Lung							0.0000	
Rt Lung	C3	0	6.25	0	34.00	1.046	0.0000	
Lt Lung	C4	0	6.25	0	33.10	1.046	0.0000	
Average Ovary							0.0000	
Rt Ovary	B5	0	6.25	0	30.60	1.009	0.0000	
Lt Ovary	B1	0	6.25	0	27.00	1.009	0.0000	
Testes	D2	0	6.25	0	30.30	1.009	0.0000	
						Total dose (rad) to remainder-F		***0.0242***
						Total dose (rad) to remainder-M		***0.0242***

Calculation of dose to skin

Position	MOSFETs	mV at 80 mAs	exam mAs	mV at exam mAs	CF [mV/R]	DCF	Absorbed Dose [rad]
Entrance	A1	24	6.25	1.875	32.90	1.009	0.0504
Exit	A2	1	6.25	0.078125	28.80	1.009	0.0024
				Total dose (rad) to skin			***0.0264***

Subtotal Effective Dose ***0.0012*** rem

Female Effective Dose ***0.0024*** rem
Male Effective Dose ***0.0024*** rem

ESE PA Abdomen 0.0178 R

	f(d)	g(b)
Leukemia	5.812E-06	132.3
Male Respiratory	1.521E-05	7.330949
Female Respiratory	1.521E-05	14.92601
Male Digestive	1.935E-05	1
Female Digestive	1.935E-05	1.74
Other	2 918E-05	1
Female Breast	2.918E-05	0.066005

Relative Risk

Leukemia	Male Respiratory	Female Respiratory	Male Digestive	Female Digestive	Other	Female Breast
1.000769	1.000112	1.000227	1.000019	1.000034	1.000029	1.000002

Table E-15. AP Abdomen Upright

Organ/ Position	MOSFETs	mV at 80 mAs	exam mAs	mV at exam mAs	CF [mV/R]	DCF	Absorbed Dose [rad]	Tissue Weighting Factor	Effective Dose [rem]
Esophagus	B3	0	6.25	0	27.50	1.009	0.0000	0.05	0.0000
Thyroid	A3	0	6.25	0	31.90	1.009	0.0000	0.05	0.0000
Breast	A2	4	6.25	0.3125	28.80	1.009	0.0096	0.05	0.0005
Average Lung							0.0000	0.12	0.0000
Rt Lung	C3	0	6.25	0	34.00	1.046	0.0000		
Lt Lung	C4	0	6.25	0	33.10	1.046	0.0000		
Stomach	C1	8	6.25	0.625	32.30	1.009	0.0171	0.12	0.0021
Liver	A2	3	6.25	0.234375	32.90	1.009	0.0063	0.05	0.0003
Bladder	C2	11	6.25	0.859375	34.20	1.009	0.0222	0.05	0.0011
Colon	D5	3	6.25	0.234375	29.90	1.009	0.0069	0.12	0.0008
Active Bone Marrow							0.0016	0.12	0.0002
Bone surface							0.0064	0.01	0.0001
Skin							0.0264	0.01	0.0003
Average Ovary							0.0068	0.20	0.0014
Rt Ovary	B5	6	6.25	0.46875	30.60	1.009	0.0135		
Lt Ovary	B1	0	6.25	0	27.00	1.009	0.0000		
Testes	D2	0	6.25	0	30.30	1.009	0.0000	0.20	0.0000
Remainder-F							0.0514	0.05	0.0026
Remainder-M							0.0491	0.05	0.0025

Calculation of dose to active marrow

Organ/ Position	MOSFETs	mV at 80 mAs	exam mAs	mV at exam mAs	CF [mV/R]	DCF	Absorbed Dose [rads]	Fract. Active marrow assigned to MOSFET	Fract. * Absorbed dose [rad]
Spine middle	A1	1	6.25	0.078125	32.90	1.009	0.0021	0.1588	0.0003
Rt Arm	A5	8	6.25	0.625	34.60	1.009	0.0160	0.0779	0.0012
Lt Arm	A4	0	6.25	0	33.10	1.009	0.0000	0.0779	0.0000
Pelvis	D3	0	6.25	0	33.50	1.009	0.0000	0.2191	0.0000
						Total dose (rad) to active marrow			***0.0016***

Calculation of dose to bone surface

Organ/ Position	MOSFETs	mV at 80 mAs	exam mAs	mV at exam mAs	CF [mV/R]	DCF	Absorbed Dose [rad]	Fract. Bone assigned to MOSFET	Fract. * Absorbed dose [rad]
Spine middle	A1	1	6.25	0.078125	32.90	3.316	0.0069	0.1850	0.0013
Rt Arm	A5	8	6.25	0.625	34.60	3.316	0.0525	0.0980	0.0051
Lt Arm	A4	0	6.25	0	33.10	3.316	0.0000	0.0980	0.0000
Pelvis	D3	0	6.25	0	33.50	3.316	0.0000	0.2190	0.0000
						Total dose (rad) to bone surface			***0.0064***

Calculation of dose to remainder

Organ/ Position	MOSFETs	mV at 80 mAs	exam mAs	mV at exam mAs	CF [mV/R]	DCF	Absorbed Dose [rad]	
Rt Arm	A4	8	6.25	0.625	33.10	1.009	0.0167	
Lt Arm	A5	0	6.25	0	34.60	1.009	0.0000	
Esophagus	B3	0	6.25	0	27.50	1.009	0.0000	
Breast	B4	4	6.25	0.3125	31.70	1.009	0.0087	
Stomach	C1	8	6.25	0.625	32.30	1.009	0.0171	
Liver	A2	3	6.25	0.234375	28.80	1.009	0.0921	
Bladder	C2	11	6.25	0.859375	34.20	1.009	0.2843	
Colon	D5	3	6.25	0.234375	29.90	1.009	0.0887	
Average Lung							0.0000	
Rt Lung	C3	0	6.25	0	34.00	1.046	0.0000	
Lt Lung	C4	0	6.25	0	33.10	1.046	0.0000	
Average Ovary							0.0068	
Rt Ovary	B5	6	6.25	0.46875	30.60	1.009	0.0135	
Lt Ovary	B1	0	6.25	0	27.00	1.009	0.0000	
Testes	D2	0	6.25	0	30.30	1.009	0.0000	
						Total dose (rad) to remainder-F		***0.0514***
						Total dose (rad) to remainder-M		***0.0491***

Calculation of dose to skin

Position	MOSFETs	mV at 80 mAs	exam mAs	mV at exam mAs	CF [mV/R]	DCF	Absorbed Dose [rad]
Entrance	A1	24	6.25	1.875	32.90	1.009	0.0504
Exit	A2	1	6.25	0.078125	28.80	1.009	0.0024
				Total dose (rad) to skin			***0.0264***

Subtotal Effective Dose ***0.0053*** rem

Female Effective Dose ***0.0092*** rem
Male Effective Dose ***0.0078*** rem

ESE AP Abdomen 0.0178 R

	f(d)	g(b)
Leukemia	2.065E-05	132.3
Male Respiratory	4.936E-05	7.330949
Female Respiratory	5.871E-05	14.92601
Male Digestive	6.278E-05	1
Female Digestive	7.468E-05	1.74
Other	1.036E-04	1
Female Breast	9.468E-05	0.066005

Relative Risk

Leukemia	Male Respiratory	Female Respiratory	Male Digestive	Female Digestive	Other	Female Breast
1.002732	1.000362	1.000876	1.000063	1.000130	1.000104	1.000006

Table E-16. AP Pelvis

Organ/ Position	MOSFETs	mV at 80 mAs	exam mAs	mV at exam mAs	CF [mV/R]	DCF	Absorbed Dose [rad]	Tissue Weighting Factor	Effective Dose [rem]
Esophagus	B3	0	3.75	0	27.50	1.009	0.0000	0.05	0.0000
Thyroid	A3	0	3.75	0	31.90	1.009	0.0000	0.05	0.0000
Breast	A2	0	3.75	0	28.80	1.009	0.0000	0.05	0.0000
Average Lung							0.0000	0.12	0.0000
Rt Lung	C3	0	3.75	0	34.00	1.046	0.0000		
Lt Lung	C4	0	3.75	0	33.10	1.046	0.0000		
Stomach	C1	1	3.75	0.046875	32.30	1.009	0.0013	0.12	0.0002
Liver	A2	0	3.75	0	32.90	1.009	0.0000	0.05	0.0000
Bladder	C2	6	3.75	0.28125	34.20	1.009	0.0073	0.05	0.0004
Colon	D5	3	3.75	0.140625	29.90	1.009	0.0042	0.12	0.0005
Active Bone Marrow							0.0000	0.12	0.0000
Bone surface							0.0000	0.01	0.0000
Skin							0.0113	0.01	0.0001
Average Ovary							0.0065	0.20	0.0013
Rt Ovary	B5	5	3.75	0.234375	30.60	1.009	0.0068		
Lt Ovary	B1	4	3.75	0.1875	27.00	1.009	0.0061		
Testes	D2	0	3.75	0	30.30	1.009	0.0000	0.20	0.0000
Remainder-F							0.0251	0.05	0.0013
Remainder-M							0.0245	0.05	0.0012

Calculation of dose to active marrow

Organ/ Position	MOSFETs	mV at 80 mAs	exam mAs	mV at exam mAs	CF [mV/R]	DCF	Absorbed Dose [rads]	Fract. Active marrow assigned to MOSFET	Fract. * Absorbed dose [rad]
Spine middle	A1	0	3.75	0	32.90	1.009	0.0000	0.1588	0.0000
Rt Arm	A5	0	3.75	0	34.60	1.009	0.0000	0.0779	0.0000
Lt Arm	A4	0	3.75	0	33.10	1.009	0.0000	0.0779	0.0000
Pelvis	D3	1	3.75	0.046875	33.50	1.009	0.0012	0.2191	0.0003
							Total dose (rad) to active marrow		***0.0000***

Calculation of dose to bone surface

Organ/ Position	MOSFETs	mV at 80 mAs	exam mAs	mV at exam mAs	CF [mV/R]	DCF	Absorbed Dose [rad]	Fract. Bone assigned to MOSFET	Fract. * Absorbed dose [rad]
Spine middle	A1	0	3.75	0	32.90	3.316	0.0000	0.1850	0.0000
Rt Arm	A5	0	3.75	0	34.60	3.316	0.0000	0.0980	0.0000
Lt Arm	A4	0	3.75	0	33.10	3.316	0.0000	0.0980	0.0000
Pelvis	D3	1	3.75	0.046875	33.50	3.316	0.0041	0.2190	0.0009
						Total dose (rad) to bone surface			***0.0000***

Calculation of dose to remainder

Organ/ Position	MOSFETs	mV at 80 mAs	exam mAs	mV at exam mAs	CF [mV/R]	DCF	Absorbed Dose [rad]	
Rt Arm	A4	0	3.75	0	33.10	1.009	0.0000	
Lt Arm	A5	0	3.75	0	34.60	1.009	0.0000	
Esophagus	B3	0	3.75	0	27.50	1.009	0.0000	
Breast	B4	0	3.75	0	31.70	1.009	0.0000	
Stomach	C1	1	3.75	0.046875	32.30	1.009	0.0013	
Liver	A2	0	3.75	0	28.80	1.009	0.0000	
Bladder	C2	6	3.75	0.28125	34.20	1.009	0.1551	
Colon	D5	3	3.75	0.140625	29.90	1.009	0.0887	
Average Lung							0.0000	
Rt Lung	C3	0	3.75	0	34.00	1.046	0.0000	
Lt Lung	C4	0	3.75	0	33.10	1.046	0.0000	
Average Ovary							0.0065	
Rt Ovary	B5	5	3.75	0.234375	30.60	1.009	0.0068	
Lt Ovary	B1	4	3.75	0.1875	27.00	1.009	0.0061	
Testes	D2	0	3.75	0	30.30	1.009	0.0000	
						Total dose (rad) to remainder-F		***0.0251***
						Total dose (rad) to remainder-M		***0.0245***

Calculation of dose to skin

Position	MOSFETs	mV at 80 mAs	exam mAs	mV at exam mAs	CF [mV/R]	DCF	Absorbed Dose [rad]
Entrance	A1	18	3.75	0.84375	32.90	1.009	0.0227
Exit	A2	0	3.75	0	28.80	1.009	0.0000
				Total dose (rad) to skin			***0.0113***

Subtotal Effective Dose ***0.0011*** rem

Female Effective Dose ***0.0037*** rem
Male Effective Dose ***0.0024*** rem

ESE AP Pelvis 0.0178 R

	f(d)	g(b)
Leukemia	7.330E-06	132.3
Male Respiratory	1.498E-05	7.330949
Female Respiratory	2.339E-05	14.92601
Male Digestive	1.905E-05	1
Female Digestive	2.975E-05	1.74
Other	3.680E-05	1
Female Breast	2.873E-05	0.066005

Relative Risk

Leukemia	Male Respiratory	Female Respiratory	Male Digestive	Female Digestive	Other	Female Breast
1.000970	1.000110	1.000349	1.000019	1.000052	1.000037	1.000002

Table E-17. AP Hip

Organ/ Position	MOSFETs	mV at 80 mAs	exam mAs	mV at exam mAs	CF [mV/R]	DCF	Absorbed Dose [rad]	Tissue Weighting Factor	Effective Dose [rem]
Esophagus	B3	0	3.75	0	27.50	1.009	0.0000	0.05	0.0000
Thyroid	A3	0	3.75	0	31.90	1.009	0.0000	0.05	0.0000
Breast	A2	0	3.75	0	28.80	1.009	0.0000	0.05	0.0000
Average Lung							0.0000	0.12	0.0000
Rt Lung	C3	0	3.75	0	34.00	1.046	0.0000		
Lt Lung	C4	0	3.75	0	33.10	1.046	0.0000		
Stomach	C1	0	3.75	0	32.30	1.009	0.0000	0.12	0.0000
Liver	A2	0	3.75	0	32.90	1.009	0.0000	0.05	0.0000
Bladder	C2	3	3.75	0.140625	34.20	1.009	0.0036	0.05	0.0002
Colon	D5	0	3.75	0	29.90	1.009	0.0000	0.12	0.0000
Active Bone Marrow							0.0000	0.12	0.0000
Bone surface							0.0000	0.01	0.0000
Skin							0.0113	0.01	0.0001
Average Ovary							0.0000	0.20	0.0000
Rt Ovary	B5	0	3.75	0	30.60	1.009	0.0000		
Lt Ovary	B1	0	3.75	0	27.00	1.009	0.0000		
Testes	D2	0	3.75	0	30.30	1.009	0.0000	0.20	0.0000
Remainder-F							0.0078	0.05	0.0004
Remainder-M							0.0078	0.05	0.0004

Calculation of dose to active marrow

Organ/ Position	MOSFETs	mV at 80 mAs	exam mAs	mV at exam mAs	CF [mV/R]	DCF	Absorbed Dose [rads]	Fract. Active marrow assigned to MOSFET	Fract. * Absorbed dose [rad]
Spine middle	A1	0	3.75	0	32.90	3.316	0.0000	0.1588	0.0000
Rt Arm	A5	0	3.75	0	34.60	3.316	0.0000	0.0779	0.0000
Lt Arm	A4	0	3.75	0	33.10	3.316	0.0000	0.0779	0.0000
Pelvis	D3	1	3.75	0.046875	33.50	3.316	0.0041	0.2191	0.0009
						Total dose (rad) to active marrow			***0.0000***

Calculation of dose to bone surface

Organ/ Position	MOSFETs	mV at 80 mAs	exam mAs	mV at exam mAs	CF [mV/R]	DCF	Absorbed Dose [rad]	Fract. Bone assigned to MOSFET	Fract. * Absorbed dose [rad]
Spine middle	A1	0	3.75	0	32.90	1.009	0.0000	0.1850	0.0000
Rt Arm	A5	0	3.75	0	34.60	1.009	0.0000	0.0980	0.0000
Lt Arm	A4	0	3.75	0	33.10	1.009	0.0000	0.0980	0.0000
Pelvis	D3	1	3.75	0.046875	33.50	1.009	0.0012	0.2190	0.0003
						Total dose (rad) to bone surface			*0.0000*

Calculation of dose to remainder

Organ/ Position	MOSFETs	mV at 80 mAs	exam mAs	mV at exam mAs	CF [mV/R]	DCF	Absorbed Dose [rad]	
Rt Arm	A4	0	3.75	0	33.10	1.009	0.0000	
Lt Arm	A5	0	3.75	0	34.60	1.009	0.0000	
Esophagus	B3	0	3.75	0	27.50	1.009	0.0000	
Breast	B4	0	3.75	0	31.70	1.009	0.0000	
Stomach	C1	0	3.75	0	32.30	1.009	0.0000	
Liver	A2	0	3.75	0	28.80	1.009	0.0000	
Bladder	C2	3	3.75	0.140625	34.20	1.009	0.0775	
Colon	D5	0	3.75	0	29.90	1.009	0.0000	
Average Lung							0.0000	
Rt Lung	C3	0	3.75	0	34.00	1.046	0.0000	
Lt Lung	C4	0	3.75	0	33.10	1.046	0.0000	
Average Ovary							0.0000	
Rt Ovary	B5	0	3.75	0	30.60	1.009	0.0000	
Lt Ovary	B1	0	3.75	0	27.00	1.009	0.0000	
Testes	D2	0	3.75	0	30.30	1.009	0.0000	
					Total dose (rad) to remainder-F			*0.0078*
					Total dose (rad) to remainder-M			*0.0078*

Calculation of dose to skin

Position	MOSFETs	mV at 80 mAs	exam mAs	mV at exam mAs	CF [mV/R]	DCF	Absorbed Dose [rad]
Entrance	A1	18	3.75	0.84375	32.90	1.009	0.0227
Exit	A2	0	3.75	0	28.80	1.009	0.0000
				Total dose (rad) to skin			***0.0113***

Subtotal Effective Dose ***0.0003*** rem

Female Effective Dose ***0.0007*** rem
Male Effective Dose ***0.0007*** rem

ESE AP Hip 0.0147 R

	f(d)	g(b)
Leukemia	1.659E-06	132.3
Male Respiratory	4.342E-06	7.330949
Female Respiratory	4.342E-06	14.92601
Male Digestive	5.523E-06	1
Female Digestive	5.523E-06	1.74
Other	8.329E-06	1
Female Breast	8.329E-06	0.066005

Relative Risk

Leukemia	Male Respiratory	Female Respiratory	Male Digestive	Female Digestive	Other	Female Breast
1.000219	1.000032	1.000065	1.000006	1.000010	1.000008	1.000001

Table E-18. Waters Sinus

Organ/ Position	MOSFETs	mV at 80 mAs	exam mAs	mV at exam mAs	CF [mV/R]	DCF	Absorbed Dose [rad]	Tissue Weighting Factor	Effective Dose [rem]
Thyroid	A3	0	1.75	0	34 60	1.009	0.0000	0.05	0.0000
Active Bone Marrow							0.0004	0.12	0.0001
Bone surface							0.0011	0.01	0.0000
Remainder							0.0000	0.05	0.0000
Skin							0.0074	0.01	0.0001

Calculation of dose to active marrow

Organ/ Position	MOSFETs	mV 80 mAs	exam mAs	mV at exam mAs	CF [mV/R]	DCF	Absorbed Dose [rad]	Fract. Active marrow assigned to MOSFET	Fract. * Absorbed dose [rad]
Head Spine	A1	1	1.75	0.021875	36.10	1.009	0.0005	0.1470	0.0001
Skull	A2	4	1.75	0.0875	32.20	1.009	0.0024	0.1470	0.0004
Rt Arm	A4	0	1.75	0	34.80	1.009	0.0000	0.0779	0.0000
Lt Arm	A5	0	1.75	0	33.30	1.009	0.0000	0.0779	0.0000
						Total dose (rad) to active marrow			***0.0004***

Calculation of dose to bone surface

Organ/ Position	MOSFETs	mV 80 mAs	exam mAs	mV at exam mAs	CF [mV/R]	DCF	Absorbed Dose [rad]	Fract. Bone assigned to MOSFET	Fract. * Absorbed dose [rad]
Head Spine	A1	1	1.75	0.021875	36.10	3.316	0.0018	0.1160	0.0002
Skull	A2	4	1.75	0.0875	32.20	3.316	0.0079	0.1160	0.0009
Rt Arm	A4	0	1.75	0	34.80	3.316	0.0000	0.0980	0.0000
Lt Arm	A5	0	1.75	0	33.30	3.316	0.0000	0.0980	0.0000
						Total dose (rad) to bone surface			***0.0011***

Calculation of dose to remainder

Organ/ Position	MOSFETs	mV 80 mAs	exam mAs	mV at exam mAs	CF [mV/R]	DCF	Absorbed Dose [rad]
Rt Arm	A4	0	1.75	0	34.80	1.009	0.0000
Lt Arm	A5	0	1.75	0	33.30	1.009	0.0000
		Total dose (rad) to remainder					***0.0000***

Calculation of dose to skin

Position	MOSFETs	mV 80 mAs	exam mAs	mV at exam mAs	CF [mV/R]	DCF	Absorbed Dose [rad]
Entrance	A1	24	1.75	0.525	32.90	1.009	0.0141
Exit	A2	1	1.75	0.021875	28.80	1.009	0.0007
		Total dose (rad) to skin					***0.0074***

Total effective dose **0.0001 rem**
ESE Waters Sinus 0.0099 R

	f(d)	g(b)
Leukemia	3.327E-07	132.3
Male Respiratory	8.706E-07	7.330949
Female Respiratory	8.706E-07	14.92601
Male Digestive	1.107E-06	1
Female Digestive	1.107E-06	1.74
Other	1.670E-06	1
Female Breast	1.670E-06	0.066005

Relative Risk

Leukemia	Male Respiratory	Female Respiratory	Male Digestive	Female Digestive	Other	Female Breast
1.000044	1.000006	1.000013	1.000001	1.000002	1.000002	1.000000

Table E-19. Lateral Sinus

Organ/ Position	MOSFETs	mV at 80 mAs	exam mAs	mV at exam mAs	CF [mV/R]	DCF	Absorbed Dose [rad]	Tissue Weigbting Factor	Effective Dose [rem]
Thyroid	A3	6	1.75	0.13125	34.60	1.009	0.0034	0.05	0.0002
Active Bone Marrow							0.0002	0.12	0.0000
Bone surface							0.0004	0.01	0.0000
Remainder							0.0000	0.05	0.0000
Skin							0.0056	0.01	0.0001

Calculation of dose to active marrow

Organ/ Position	MOSFETs	mV 80 mAs	exam mAs	mV at exam mAs	CF [mV/R]	DCF	Absorbed Dose [rad]	Fract. Active marrow assigned to MOSFET	Fract. * Absorbed dose [rad]
Head Spine	A1	1	1.75	0.021875	36.10	1.009	0.0005	0.1470	0.0001
Skull	A2	1	1.75	0.021875	32.20	1.009	0.0006	0.1470	0.0001
Rt Arm	A4	0	1.75	0	34.80	1.009	0.0000	0.0779	0.0000
Lt Arm	A5	0	1.75	0	33.30	1.009	0.0000	0.0779	0.0000
						Total dose (rad) to active marrow			***0.0002***

Calculation of dose to bone surface

Organ/ Position	MOSFETs	mV 80 mAs	exam mAs	mV at exam mAs	CF [mV/R]	DCF	Absorbed Dose [rad]	Fract. Bone assigned to MOSFET	Fract. * Absorbed dose [rad]
Head Spine	A1	1	1.75	0.021875	36.10	3.316	0.0018	0.1160	0.0002
Skull	A2	1	1.75	0.021875	32.20	3.316	0.0020	0.1160	0.0002
Rt Arm	A4	0	1.75	0	34.80	3.316	0.0000	0.0980	0.0000
Lt Arm	A5	0	1.75	0	33.30	3.316	0.0000	0.0980	0.0000
						Total dose (rad) to bone surface			***0.0004***

Calculation of dose to remainder

Organ/ Position	MOSFETs	mV 80 mAs	exam mAs	mV at exam mAs	CF [mV/R]	DCF	Absorbed Dose [rad]
Rt Arm	A4	0	1.75	0	34.80	1.009	0.0000
Lt Arm	A5	0	1.75	0	33.30	1.009	0.0000
		Total dose (rad) to remainder					***0.0000***

Calculation of dose to skin

Position	MOSFETs	mV 80 mAs	exam mAs	mV at exam mAs	CF [mV/R]	DCF	Absorbed Dose [rad]
Entrance	A1	18	1.75	0.39375	32.90	1.009	0.0106
Exit	A2	1	1.75	0.021875	28.80	1.009	0.0007
		Total dose (rad) to skin					***0.0056***

Total effective dose **0.0002 rem**
ESE LAT Sinus 0.0079 R

	f(d)	g(b)
Leukemia	6.033E-07	132.3
Male Respiratory	1.579E-06	7.330949
Female Respiratory	1.579E-06	14.92601
Male Digestive	2.008E-06	1
Female Digestive	2.008E-06	1.74
Other	3.029E-06	1
Female Breast	3.029E-06	0.066005

Relative Risk

Leukemia	Male Respiratory	Female Respiratory	Male Digestive	Female Digestive	Other	Female Breast
1.000080	1.000012	1.000024	1.000002	1.000003	1.000003	1.000000

Table E-20. AP Sinus

Organ/ Position	MOSFETs	mV at 80 mAs	exam mAs	mV at exam mAs	CF [mV/R]	DCF	Absorbed Dose [rad]	Tissue Weighting Factor	Effective Dose [rem]
Thyroid	A3	1	1.75	0.021875	34.60	1.009	0.0006	0.05	0.0000
Active Bone Marrow							0.0004	0.12	0.0001
Bone surface							0.0011	0.01	0.0000
Remainder							0.0000	0.05	0.0000
Skin							0.0065	0.01	0.0001

Colculation of dose to active morrow

Organ/ Position	MOSFETs	mV 80 mAs	exam mAs	mV at exam mAs	CF [mV/R]	DCF	Absorbed Dose [rad]	Fract. Active marrow assigned to MOSFET	Fract. * Absorbed dose [rad]
Head Spine	A1	1	1.75	0.021875	36.10	1.009	0.0005	0.1470	0.0001
Skull	A2	4	1.75	0.0875	32.20	1.009	0.0024	0.1470	0.0004
Rt Arm	A4	0	1.75	0	34.80	1.009	0.0000	0.0779	0.0000
Lt Arm	A5	0	1.75	0	33.30	1.009	0.0000	0.0779	0.0000
							Total dose (rad) to active marrow		***0.0004***

Calculation of dose to bone surface

Organ/ Position	MOSFETs	mV 80 mAs	exam mAs	mV at exam mAs	CF [mV/R]	DCF	Absorbed Dose [rad]	Fract. Bone assigned to MOSFET	Fract. * Absorbed dose [rad]
Head Spine	A1	1	1.75	0.021875	36.10	3.316	0.0018	0.1160	0.0002
Skull	A2	4	1.75	0.0875	32.20	3.316	0.0079	0.1160	0.0009
Rt Arm	A4	0	1.75	0	34.80	3.316	0.0000	0.0980	0.0000
Lt Arm	A5	0	1.75	0	33.30	3.316	0.0000	0.0980	0.0000
							Totol dose (rad) to bone surface		***0.0011***

Calculation of dose to remainder

Organ/ Position	MOSFETs	mV 80 mAs	exam mAs	mV at exam mAs	CF [mV/R]	DCF	Absorbed Dose [rad]
Rt Arm	A4	0	1.75	0	34 80	1.009	0.0000
Lt Arm	A5	0	1.75	0	33.30	1.009	0.0000
		Total dose (rad) to remainder					***0.0000***

Calculation of dose to skin

Position	MOSFETs	mV 80 mAs	exam mAs	mV at exam mAs	CF [mV/R]	DCF	Absorbed Dose [rad]
Entrance	A1	22	1.75	0.48125	32.90	1.009	0.0129
Exit	A2	0	1.75	0	28 80	1.009	0.0000
		Total dose (rad) to skin					***0.0065***

Total effective dose **0.0002 rem**
ESE AP Sinus 0.0091 R

	f(d)	g(b)
Leukemia	3.781E-07	132.3
Male Respiratory	9.896E-07	7.330949
Female Respiratory	9.896E-07	14.92601
Male Digestive	1.259E-06	1
Female Digestive	1.259E-06	1.74
Other	1.898E-06	1
Female Breast	1.898E-06	0.066005

Relative Risk

Leukemia	Male Respiratory	Female Respiratory	Male Digestive	Female Digestive	Other	Female Breast
1.000050	1.000007	1.000015	1.000001	1.000002	1.000002	1.000000

Table E-21. AP Chest

Organ/ Position	MOSFETs	mV at 80 mAs	exam mAs	mV at exam mAs	CF [mV/R]	DCF	Absorbed Dose [rad]	Tissue Weighting Factor	Effective Dose [rem]
Esophagus	D4	1	1.75	0.021875	34.80	1.009	0.0006	0.05	0.0000
Thyroid	A3	4	1.75	0.0875	34.60	1.009	0.0022	0.05	0.0001
Breast	D5	2	1.75	0.04375	38.50	1.009	0.0010	0.05	0.0001
Average Lung							0.0009	0.12	0.0001
Rt Lung	D3	1	1.75	0.021875	32.00	1.046	0.0006		
Lt Lung	D1	2	1.75	0.04375	33.30	1.046	0.0012		
Stomach	D5	2	1.75	0.04375	38.50	1.009	0.0010	0.12	0.0001
Liver	A2	2	1.75	0.04375	32.20	1.009	0.0012	0.05	0.0001
Bladder	A4	0	1.75	0	34.80	1.009	0.0000	0.05	0.0000
Colon	NM		1.75	0	31.98	1.009	0.0000	0.12	0.0000
Active Bone Marrow							0.0001	0.12	0.0000
Bone surface							0.0005	0.01	0.0000
Skin							0.0012	0.01	0.0000
Average Ovary							0.0000	0.20	0.0000
Rt Ovary	A2	0	1.75	0	32.20	1.009	0.0000		
Lt Ovary	NM		1.75	0	31.18	1.009	0.0000		
Testes	NM		1.75	0	33.04	1.009	0.0000	0.20	0.0000
Remainder-F							0.0136	0.05	0.0007
Remainder-M							0.0136	0.05	0.0007

Calculation of dose to active marrow

Organ/ Position	MOSFETs	mV at 80 mAs	exam mAs	mV at exam mAs	CF [mV/R]	DCF	Absorbed Dose [rads]	Fract. Active marrow assigned to MOSFET	Fract. * Absorbed dose [rad]
Spine middle	A1	0	1.75	0	36.10	1.009	0.0000	0.1588	0.0000
Rt Arm	A5	1	1.75	0.021875	33.30	1.009	0.0006	0.0779	0.0000
Lt Arm	A4	2	1.75	0.04375	34.80	1.009	0.0011	0.0779	0.0001
Pelvis	NM		1.75	0	32.20	1.009	0.0000	0.2191	0.0000
							Total dose (rad) to active marrow		***0.0001***

Calculation of dose to bone surface

Organ/ Position	MOSFETs	mV at 80 mAs	exam mAs	mV at exam mAs	CF [mV/R]	DCF	Absorbed Dose [rad]	Fract. Bone assigned to MOSFET	Fract. * Absorbed dose [rad]
Spine middle	A1	0	1.75	0	36.10	3.316	0.0000	0.1850	0.0000
Rt Arm	A5	1	1.75	0.021875	33.30	3.316	0.0019	0.0980	0.0002
Lt Arm	A4	2	1.75	0.04375	34.80	3.316	0.0037	0.0980	0.0004
Pelvis	NM		1.75	0	32.20	3.316	0.0000	0.2190	0.0000
						Total dose (rad) to bone surface			***0.0005***

Calculation of dose to remainder

Organ/ Position	MOSFETs	mV at 80 mAs	exam mAs	mV at exam mAs	CF [mV/R]	DCF	Absorbed Dose [rad]	
Rt Arm	A5	1	1.75	0.021875	33.30	1.009	0.0006	
Lt Arm	A4	2	1.75	0.04375	34.80	1.009	0.0011	
Esophagus	D4	1	1.75	0.021875	34.80	1.009	0.0006	
Breast	D5	2	1.75	0.04375	38.50	1.009	0.0010	
Stomach	D5	2	1.75	0.04375	38.50	1.009	0.0010	
Liver	A2	2	1.75	0.04375	32.20	1.009	0.0549	
Bladder	A4	3	1.75	0.065625	34.80	1.009	0.0762	
Colon	NM		1.75	0	31.98	1.009	0.0000	
Average Lung							0.0009	
Rt Lung	D3	1	1.75	0.021875	32.00	1.046	0.0006	
Lt Lung	D1	2	1.75	0.04375	33.30	1.046	0.0012	
Average Ovary							0.0000	
Rt Ovary	A2	0	1.75	0	32.20	1.009	0.0000	
Lt Ovary	NM		1.75	0	31.18	1.009	0.0000	
Testes	NM		1.75	0	33.04	1.009	0.0000	
						Total dose (rad) to remainder-F		***0.0136***
						Total dose (rad) to remainder-M		***0.0136***

Calculation of dose to skin

Position	MOSFETs	mV at 80 mAs	exam mAs	mV at exam mAs	CF [mV/R]	DCF	Absorbed Dose [rad]
Entrance	A1	4	1.75	0.0875	32.90	1.009	0.0024
Exit	A2	0	1.75	0	28.80	1.009	0.0000
				Total dose (rad) to skin			***0.0012***

Subtotal Effective Dose ***0.0005*** rem

Female Effective Dose ***0.0012*** rem
Male Effective Dose ***0.0012*** rem

ESE AP Chest 0.0063 R

	f(d)	g(b)
Leukemia	2.903E-06	132.3
Male Respiratory	7.599E-06	7.330949
Female Respiratory	7.597E-06	14.92601
Male Digestive	9.665E-06	1
Female Digestive	9.664E-06	1.74
Other	1.457E-05	1
Female Breast	1.458E-05	0.066005

Relative Risk

Leukemia	Male Respiratory	Female Respiratory	Male Digestive	Female Digestive	Other	Female Breast
1.000384	1.000056	1.000113	1.000010	1.000017	1.000015	1.000001

Table E-22. AP Chest with Thyroid Shield

Organ/ Position	MOSFETs	mV at 80 mAs	exam mAs	mV at exam mAs	CF [mV/R]	DCF	Absorbed Dose [rad]	Tissue Weighting Factor	Effective Dose [rem]
Esophagus	D4	0	1.75	0	34.80	1.009	0.0000	0.05	0.0000
Thyroid	A3	3	1.75	0.065625	34.60	1.009	0.0017	0.05	0.0001
Breast	D5	4	1.75	0.0875	38.50	1.009	0.0020	0.05	0.0001
Average Lung							0.0009	0.12	0.0001
Rt Lung	D3	2	1.75	0.04375	32.00	1.046	0.0013		
Lt Lung	D1	1	1.75	0.021875	33.30	1.046	0.0006		
Stomach	NM		1.75	0	38.50	1.009	0.0000	0.12	0.0000
Liver	NM		1.75	0	32.20	1.009	0.0000	0.05	0.0000
Bladder	A4	0	1.75	0	34.80	1.009	0.0000	0.05	0.0000
Colon	NM		1.75	0	31.98	1.009	0.0000	0.12	0.0000
Active Bone Marrow							0.0000	0.12	0.0000
Bone surface							0.0002	0.01	0.0000
Skin							0.0012	0.01	0.0000
Average Ovary							0.0000	0.20	0.0000
Rt Ovary	A2	0	1.75	0	32.20	1.009	0.0000		
Lt Ovary	NM		1.75	0	31.18	1.009	0.0000		
Testes	NM		1.75	0	33.04	1.009	0.0000	0.20	0.0000
Remainder-F							0.0004	0.05	0.0000
Remainder-M							0.0004	0.05	0.0000

Calculation of dose to active marrow

Organ/ Position	MOSFETs	mV at 80 mAs	exam mAs	mV at exam mAs	CF [mV/R]	DCF	Absorbed Dose [rads]	Fract. Active marrow assigned to MOSFET	Fract. * Absorbed dose [rad]
Spine middle	A1	0	1.75	0	36.10	1.009	0.0000	0.1588	0.0000
Rt Arm	A5	1	1.75	0.021875	33.30	1.009	0.0006	0.0779	0.0000
Lt Arm	A4	0	1.75	0	34.80	1.009	0.0000	0.0779	0.0000
Pelvis	NM		1.75	0	32.20	1.009	0.0000	0.2191	0.0000
							Total dose (rad) to active marrow		***0.0000***

Calculation of dose to bone surface

Organ/ Position	MOSFETs	mV at 80 mAs	exam mAs	mV at exam mAs	CF [mV/R]	DCF	Absorbed Dose [rad]	Fract. Bone assigned to MOSFET	Fract. * Absorbed dose [rad]
Spine middle	A1	0	1.75	0	36.10	3.316	0.0000	0.1850	0.0000
Rt Arm	A5	1	1.75	0.021875	33.30	3.316	0.0019	0.0980	0.0002
Lt Arm	A4	0	1.75	0	34.80	3.316	0.0000	0.0980	0.0000
Pelvis	NM		1.75	0	32.20	3.316	0.0000	0.2190	0.0000
						Total dose (rad) to bone surface			***0.0002***

Calculation of dose to remainder

Organ/ Position	MOSFETs	mV at 80 mAs	exam mAs	mV at exam mAs	CF [mV/R]	DCF	Absorbed Dose [rad]	
Rt Arm	A5	1	1.75	0.021875	33.30	1.009	0.0006	
Lt Arm	A4	0	1.75	0	34.80	1.009	0.0000	
Esophagus	D4	0	1.75	0	34.80	1.009	0.0000	
Breast	D5	4	1.75	0.0875	38.50	1.009	0.0020	
Stomach	NM		1.75	0	38.50	1.009	0.0000	
Liver	NM		1.75	0	32.20	1.009	0.0000	
Bladder	A4	0	1.75	0	34.80	1.009	0.0000	
Colon	NM		1.75	0	31.98	1.009	0.0000	
Average Lung							0.0009	
Rt Lung	D3	2	1.75	0.04375	32.00	1.046	0.0013	
Lt Lung	D1	1	1.75	0.021875	33.30	1.046	0.0006	
Average Ovary							0.0000	
Rt Ovary	A2	0	1.75	0	32.20	1.009	0.0000	
Lt Ovary	NM		1.75	0	31.18	1.009	0.0000	
Testes	NM		1.75	0	33.04	1.009	0.0000	
						Total dose (rad) to remainder-F		***0.0004***
						Total dose (rad) to remainder-M		***0.0004***

Calculation of dose to skin

Position	MOSFETs	mV at 80 mAs	exam mAs	mV at exam mAs	CF [mV/R]	DCF	Absorbed Dose [rad]
Entrance	A1	4	1.75	0.0875	32.90	1.009	0.0024
Exit	A2	0	1.75	0	28.80	1.009	0.0000
				Total dose (rad) to skin			***0.0012***

Subtotal Effective Dose ***0.0003*** rem

Female Effective Dose ***0.0003*** rem

Male Effective Dose ***0.0003*** rem

ESE AP Chest 0.0063 R

	f(d)	g(b)
Leukemia	8.113E-07	132.3
Male Respiratory	2.134E-06	7.330949
Female Respiratory	2.113E-06	14.92601
Male Digestive	2.715E-06	1
Female Digestive	2.687E-06	1.74
Other	4.073E-06	1
Female Breast	4.094E-06	0.066005

Relative Risk

Leukemia	Male Respiratory	Female Respiratory	Male Digestive	Female Digestive	Other	Female Breast
1.000107	1.000016	1.000032	1.000003	1.000005	1.000004	1.000000

Table E-23. PA Chest

Organ/ Position	MOSFETs	mV at 80 mAs	exam mAs	mV at exam mAs	CF [mV/R]	DCF	Absorbed Dose [rad]	Tissue Weighting Factor	Effective Dose [rem]
Esophagus	D4	2	1.75	0.04375	34 80	1.009	0.0011	0.05	0.0001
Thyroid	A3	1	1.75	0.021875	34.60	1.009	0.0006	0.05	0.0000
Breast	D5	0	1.75	0	38.50	1.009	0.0000	0.05	0.0000
Average Lung							0.0012	0.12	0.0001
Rt Lung	D3	2	1.75	0.04375	32.00	1.046	0.0013		
Lt Lung	D1	2	1.75	0.04375	33.30	1.046	0.0012		
Stomach	A2	1	1.75	0.021875	38.50	1.009	0.0005	0.12	0.0001
Liver	NM		1.75	0	32.20	1.009	0.0000	0.05	0.0000
Bladder	A4	0	1.75	0	34.80	1.009	0.0000	0.05	0.0000
Colon	NM		1.75	0	31.98	1.009	0.0000	0.12	0.0000
Active Bone Marrow							0.0004	0.12	0.0000
Bone surface							0.0015	0.01	0.0000
Skin							0.0012	0.01	0.0000
Average Ovary							0.0000	0.20	0.0000
Rt Ovary	A2	0	1.75	0	32.20	1.009	0.0000		
Lt Ovary	NM		1.75	0	31.18	1.009	0.0000		
Testes	NM		1.75	0	33.04	1.009	0.0000	0.20	0.0000
Remainder-F							0.0003	0.05	0.0000
Remainder-M							0.0004	0.05	0.0000

Calculation of dose to active marrow

Organ/ Position	MOSFETs	mV at 80 mAs	exam mAs	mV at exam mAs	CF [mV/R]	DCF	Absorbed Dose [rads]	Fract. Active marrow assigned to MOSFET	Fract. * Absorbed dose [rad]
Spine middle	A1	4	1.75	0.0875	36.10	1.009	0.0021	0.1588	0.0003
Rt Arm	A5	1	1.75	0.021875	33.30	1.009	0.0006	0.0779	0.0000
Lt Arm	A4	0	1.75	0	34.80	1.009	0.0000	0.0779	0.0000
Pelvis	NM		1.75	0	32.20	1.009	0.0000	0.2191	0.0000
							Total dose (rad) to active marrow		***0.0004***

Calculation of dose to bone surface

Organ/ Position	MOSFETs	mV at 80 mAs	exam mAs	mV at exam mAs	CF [mV/R]	DCF	Absorbed Dose [rad]	Fract. Bone assigned to MOSFET	Fract. * Absorbed dose [rad]
Spine middle	A1	4	1.75	0.0875	36.10	3.316	0.0070	0.1850	0.0013
Rt Arm	A5	1	1.75	0.021875	33.30	3.316	0.0019	0.0980	0.0002
Lt Arm	A4	0	1.75	0	34.80	3.316	0.0000	0.0980	0.0000
Pelvis	NM	0	1.75	0	32.20	3.316	0.0000	0.2190	0.0000
						Total dose (rad) to bone surface			***0.0015***

Calculation of dose to remainder

Organ/ Position	MOSFETs	mV at 80 mAs	exam mAs	mV at exam mAs	CF [mV/R]	DCF	Absorbed Dose [rad]	
Rt Arm	A5	1	1.75	0.021875	33.30	1.009	0.0006	
Lt Arm	A4	0	1.75	0	34.80	1.009	0.0000	
Esophagus	D4	2	1.75	0.04375	34.80	1.009	0.0011	
Breast	D5	0	1.75	0	38.50	1.009	0.0000	
Stomach	A2	1	1.75	0.021875	38.50	1.009	0.0005	
Liver	NM		1.75	0	32.20	1.009	0.0000	
Bladder	A4	0	1.75	0	34.80	1.009	0.0000	
Colon	NM		1.75	0	31.98	1.009	0.0000	
Average Lung							0.0012	
Rt Lung	D3	2	1.75	0.04375	32.00	1.046	0.0013	
Lt Lung	D1	2	1.75	0.04375	33.30	1.046	0.0012	
Average Ovary							0.0000	
Rt Ovary	A2	0	1.75	0	32.20	1.009	0.0000	
Lt Ovary	NM		1.75	0	31.18	1.009	0.0000	
Testes	NM		1.75	0	33.04	1.009	0.0000	
						Total dose (rad) to remainder-F		***0.0003***
						Total dose (rad) to remainder-M		***0.0004***

Calculation of dose to skin

Position	MOSFETs	mV at 80 mAs	exam mAs	mV at exam mAs	CF [mV/R]	DCF	Absorbed Dose [rad]
Entrance	A1	4	1.75	0.0875	32.90	1.009	0.0024
Exit	A2	0	1.75	0	28.80	1.009	0.0000
				Total dose (rad) to skin			***0.0012***

Subtotal Effective Dose ***0.0004*** rem

Female Effective Dose ***0.0004*** rem
Male Effective Dose ***0.0004*** rem

ESE PA Chest 0.0063 R

	f(d)	g(b)
Leukemia	9.303E-07	132.3
Male Respiratory	2.446E-06	7.330949
Female Respiratory	2.424E-06	14.92601
Male Digestive	3.111E-06	1
Female Digestive	3.084E-06	1.74
Other	4.671E-06	1
Female Breast	4.691E-06	0.066005

Relative Risk

Leukemia	Male Respiratory	Female Respiratory	Male Digestive	Female Digestive	Other	Female Breast
1.000123	1.000018	1.000036	1.000003	1.000005	1.000005	1.000000

Table E-24 Lateral Chest

Organ/ Position	MOSFETs	mV at 80 mAs	exam mAs	mV at exam mAs	CF [mV/R]	DCF	Absorbed Dose [rad]	Tissue Weighting Factor	Effective Dose [rem]
Esophagus	D4	2	3.75	0.09375	34 80	1.009	0.0024	0.05	0.0001
Thyroid	A3	4	3.75	0.1875	34.60	1.009	0.0048	0.05	0.0002
Breast	D5	1	3.75	0.046875	38.50	1.009	0.0011	0.05	0.0001
Average Lung							0.0020	0.12	0.0002
Rt Lung	D3	2	3.75	0.09375	32.00	1.046	0.0027		
Lt Lung	D1	1	3.75	0.046875	33.30	1.046	0.0013		
Stomach	A2	0	3.75	0	38.50	1.009	0.0000	0.12	0.0000
Liver	NM		3.75	0	32.20	1.009	0.0000	0.05	0.0000
Bladder	A4	0	3.75	0	34.80	1.009	0.0000	0.05	0.0000
Colon	NM		3.75	0	31.98	1.009	0.0000	0.12	0.0000
Active Bone Marrow							0.0008	0.12	0.0001
Bone surface							0.0034	0.01	0.0000
Skin							0.0038	0.01	0.0000
Average Ovary							0.0000	0.20	0.0000
Rt Ovary	A2	0	3.75	0	32.20	1.009	0.0000		
Lt Ovary	NM		3.75	0	31.18	1.009	0.0000		
Testes	NM		3.75	0	33.04	1.009	0.0000	0.20	0.0000
Remainder-F							0.0012	0.05	0.0001
Remainder-M							0.0008	0.05	0.0000

Calculation of dose to active marrow

Organ/ Position	MOSFETs	mV at 80 mAs	exam mAs	mV at exam mAs	CF [mV/R]	DCF	Absorbed Dose [rads]	Fract. Active marrow assigned to MOSFET	Fract. * Absorbed dose [rad]
Spine middle	A1	2	3.75	0.09375	36.10	1.009	0.0023	0.1588	0.0004
Rt Arm	A5	5	3.75	0.234375	33.30	1.009	0.0062	0.0779	0.0005
Lt Arm	A4	0	3.75	0	34.80	1.009	0.0000	0.0779	0.0000
Pelvis	NM		3.75	0	32.20	1.009	0.0000	0.2191	0.0000
							Total dose (rad) to active marrow		***0.0008***

Calculation of dose to bone surface

Organ/ Position	MOSFETs	mV at 80 mAs	exam mAs	mV at exam mAs	CF [mV/R]	DCF	Absorbed Dose [rad]	Fract. Bone assigned to MOSFET	Fract. * Absorbed dose [rad]
Spine middle	A1	2	3.75	0.09375	36.10	3.316	0.0075	0.1850	0.0014
Rt Arm	A5	5	3.75	0.234375	33.30	3.316	0.0204	0.0980	0.0020
Lt Arm	A4	0	3.75	0	34.80	3.316	0.0000	0.0980	0.0000
Pelvis	NM		3.75	0	32.20	3.316	0.0000	0.2190	0.0000
						Total dose (rad) to bone surface			***0.0034***

Calculation of dose to remainder

Organ/ Position	MOSFETs	mV at 80 mAs	exam mAs	mV at exam mAs	CF [mV/R]	DCF	Absorbed Dose [rad]	
Rt Arm	A5	5	3.75	0.234375	33.30	1.009	0.0062	
Lt Arm	A4	0	3.75	0	34.80	1.009	0.0000	
Esophagus	D4	2	3.75	0.09375	34.80	1.009	0.0024	
Breast	D5	1	3.75	0.046875	38.50	1.009	0.0011	
Stomach	A2	0	3.75	0	38.50	1.009	0.0000	
Liver	NM		3.75	0	32.20	1.009	0.0000	
Bladder	A4	0	3.75	0	34.80	1.009	0.0000	
Colon	NM		3.75	0	31.98	1.009	0.0000	
Average Lung							0.0020	
Rt Lung	D3	2	3.75	0.09375	32.00	1.046	0.0027	
Lt Lung	D1	1	3.75	0.046875	33.30	1.046	0.0013	
Average Ovary							0.0000	
Rt Ovary	A2	0	3.75	0	32.20	1.009	0.0000	
Lt Ovary	NM		3.75	0	31.18	1.009	0.0000	
Testes	NM		3.75	0	33.04	1.009	0.0000	
						Total dose (rad) to remainder-F		***0.0012***
						Total dose (rad) to remainder-M		***0.0008***

Calculation of dose to skin

Position	MOSFETs	mV at 80 mAs	exam mAs	mV at exam mAs	CF [mV/R]	DCF	Absorbed Dose [rad]
Entrance	A1	6	3.75	0.28125	32.90	1.009	0.0076
Exit	A2	0	3.75	0	28.80	1.009	0.0000
				Total dose (rad) to skin			***0.0038***

Subtotal Effective Dose ***0.0008*** rem

Female Effective Dose ***0.0009*** rem
Male Effective Dose ***0.0009*** rem

ESE LAT Chest 0.0189 R

	f(d)	g(b)
Leukemia	2.124E-06	132.3
Male Respiratory	5.502E-06	7.330949
Female Respiratory	5.615E-06	14.92601
Male Digestive	6.999E-06	1
Female Digestive	7.142E-06	1.74
Other	1.066E-05	1
Female Breast	1.055E-05	0.066005

Relative Risk

Leukemia	Male Respiratory	Female Respiratory	Male Digestive	Female Digestive	Other	Female Breast
1.000281	1.000040	1.000084	1.000007	1.000012	1.000011	1.000001

Table E-25. LAO Chest

Organ/ Position	MOSFETs	mV at 80 mAs	exam mAs	mV at exam mAs	CF [mV/R]	DCF	Absorbed Dose [rad]	Tissue Weighting Factor	Effective Dose [rem]
Esophagus	D4	2	3.75	0.09375	34.80	1.009	0.0024	0.05	0.0001
Thyroid	A3	1	3.75	0.046875	34.60	1.009	0.0012	0.05	0.0001
Breast	D5	0	3.75	0	38.50	1.009	0.0000	0.05	0.0000
Average Lung							0.0027	0.12	0.0003
Rt Lung	D3	3	3.75	0.140625	32.00	1.046	0.0040		
Lt Lung	D1	1	3.75	0.046875	33.30	1.046	0.0013		
Stomach	A2	1	3.75	0.046875	38.50	1.009	0.0011	0.12	0.0001
Liver	A4	1	3.75	0.046875	32.20	1.009	0.0013	0.05	0.0001
Bladder	A4	0	3.75	0	34.80	1.009	0.0000	0.05	0.0000
Colon	NM		3.75	0	31.98	1.009	0.0000	0.12	0.0000
Active Bone Marrow							0.0006	0.12	0.0001
Bone surface							0.0023	0.01	0.0000
Skin							0.0031	0.01	0.0000
Average Ovary							0.0000	0.20	0.0000
Rt Ovary	A2	0	3.75	0	32.20	1.009	0.0000		
Lt Ovary	NM		3.75	0	31.18	1.009	0.0000		
Testes	NM		3.75	0	33.04	1.009	0.0000	0.20	0.0000
Remainder-F							0.0039	0.05	0.0002
Remainder-M							0.0038	0.05	0.0002

Calculation of dose to active marrow

Organ/ Position	MOSFETs	mV at 80 mAs	exam mAs	mV at exam mAs	CF [mV/R]	DCF	Absorbed Dose [rads]	Fract. Active marrow assigned to MOSFET	Fract. * Absorbed dose [rad]
Spine middle	A1	1	3.75	0.046875	36.10	1.009	0.0011	0.1588	0.0002
Rt Arm	A5	4	3.75	0.1875	33.30	1.009	0.0050	0.0779	0.0004
Lt Arm	NM		3.75	0	34.80	1.009	0.0000	0.0779	0.0000
Pelvis	NM		3.75	0	32.20	1.009	0.0000	0.2191	0.0000
						Total dose (rad) to active marrow			***0.0006***

Calculation of dose to bone surface

Organ/ Position	MOSFETs	mV at 80 mAs	exam mAs	mV at exam mAs	CF [mV/R]	DCF	Absorbed Dose [rad]	Fract. Bone assigned to MOSFET	Fract. * Absorbed dose [rad]
Spine middle	A1	1	3.75	0.046875	36.10	3.316	0.0038	0.1850	0.0007
Rt Arm	A5	4	3.75	0.1875	33.30	3.316	0.0164	0.0980	0.0016
Lt Arm	NM		3.75	0	34.80	3.316	0.0000	0.0980	0.0000
Pelvis	NM		3.75	0	32.20	3.316	0.0000	0.2190	0.0000
						Total dose (rad) to bone surface			***0.0023***

Calculation of dose to remainder

Organ/ Position	MOSFETs	mV at 80 mAs	exam mAs	mV at exam mAs	CF [mV/R]	DCF	Absorbed Dose [rad]	
Rt Arm	A5	4	3.75	0.1875	33.30	1.009	0.0050	
Lt Arm	NM		3.75	0	34.80	1.009	0.0000	
Esophagus	D4	2	3.75	0.09375	34.80	1.009	0.0024	
Breast	D5	0	3.75	0	38.50	1.009	0.0000	
Stomach	A2	1	3.75	0.046875	38.50	1.009	0.0011	
Liver	A4	1	3.75	0.046875	32.20	1.009	0.0274	
Bladder	A4	0	3.75	0	34.80	1.009	0.0000	
Colon	NM		3.75	0	31.98	1.009	0.0000	
Average Lung							0.0027	
Rt Lung	D3	3	3.75	0.140625	32.00	1.046	0.0040	
Lt Lung	D1	1	3.75	0.046875	33.30	1.046	0.0013	
Average Ovary							0.0000	
Rt Ovary	A2	0	3.75	0	32.20	1.009	0.0000	
Lt Ovary	NM		3.75	0	31.18	1.009	0.0000	
Testes	NM		3.75	0	33.04	1.009	0.0000	
						Total dose (rad) to remainder-F		***0.0039***
						Total dose (rad) to remainder-M		***0.0038***

Calculation of dose to skin

Position	MOSFETs	mV at 80 mAs	exam mAs	mV at exam mAs	CF [mV/R]	DCF	Absorbed Dose [rad]
Entrance	A1	5	3.75	0.234375	32.90	1.009	0.0063
Exit	A2	0	3.75	0	28.80	1.009	0.0000
				Total dose (rad) to skin			***0.0031***

Subtotal Effective Dose ***0.0008*** rem

Female Effective Dose ***0.0010*** rem
Male Effective Dose ***0.0010*** rem

ESE LAO Chest 0.0113 R

	f(d)	g(b)
Leukemia	2.441E-06	132.3
Male Respiratory	6.374E-06	7.330949
Female Respiratory	6.404E-06	14.92601
Male Digestive	8.108E-06	1
Female Digestive	8.147E-06	1.74
Other	1.226E-05	1
Female Breast	1.223E-05	0.066005

Relative Risk

Leukemia	Male Respiratory	Female Respiratory	Male Digestive	Female Digestive	Other	Female Breast
1.000323	1.000047	1.000096	1.000008	1.000014	1.000012	1.000001

Table E-26. RPO Chest

Organ/ Position	MOSFETs	mV at 80 mAs	exam mAs	mV at exam mAs	CF [mV/R]	DCF	Absorbed Dose [rad]	Tissue Weigbting Factor	Effective Dose [rem]
Esophagus	D4	0	3.75	0	34.80	1.009	0.0000	0.05	0.0000
Thyroid	A3	6	3.75	0.28125	34.60	1.009	0.0072	0.05	0.0004
Breast	D5	5	3.75	0.234375	38.50	1.009	0.0054	0.05	0.0003
Average Lung							0.0013	0.12	0.0002
Rt Lung	D3	0	3.75	0	32.00	1.046	0.0000		
Lt Lung	D1	2	3.75	0.09375	33.30	1.046	0.0026		
Stomach	A2	2	3.75	0.09375	38.50	1.009	0.0022	0.12	0.0003
Liver	A4	1	3.75	0.046875	32.20	1.009	0.0013	0.05	0.0001
Bladder	A4	0	3.75	0	34.80	1.009	0.0000	0.05	0.0000
Colon	NM		3.75	0	31.98	1.009	0.0000	0.12	0.0000
Active Bone Marrow							0.0002	0.12	0.0000
Bone surface							0.0007	0.01	0.0000
Skin							0.0031	0.01	0.0000
Average Ovary							0.0000	0.20	0.0000
Rt Ovary	A2	0	3.75	0	32.20	1.009	0.0000		
Lt Ovary	NM		3.75	0	31.18	1.009	0.0000		
Testes	NM		3.75	0	33.04	1.009	0.0000	0.20	0.0000
Remainder-F							0.0036	0.05	0.0002
Remainder-M							0.0036	0.05	0.0002

Calculation of dose to active marrow

Organ/ Position	MOSFETs	mV at 80 mAs	exam mAs	mV at exam mAs	CF [mV/R]	DCF	Absorbed Dose [rads]	Fract. Active marrow assigned to MOSFET	Fract. * Absorbed dose [rad]
Spine middle	A1	1	3.75	0.046875	36.10	1.009	0.0011	0.1588	0.0002
Rt Arm	A5	0	3.75	0	33.30	1.009	0.0000	0.0779	0.0000
Lt Arm	NM		3.75	0	34.80	1.009	0.0000	0.0779	0.0000
Pelvis	NM		3.75	0	32.20	1.009	0.0000	0.2191	0.0000
							Total dose (rad) to active marrow		***0.0002***

Calculation of dose to bone surface

Organ/ Position	MOSFETs	mV at 80 mAs	exam mAs	mV at exam mAs	CF [mV/R]	DCF	Absorbed Dose [rad]	Fract. Bone assigned to MOSFET	Fract. * Absorbed dose [rad]
Spine middle	A1	1	3.75	0.046875	36.10	3.316	0.0038	0.1850	0.0007
Rt Arm	A5	0	3.75	0	33.30	3.316	0.0000	0.0980	0.0000
Lt Arm	NM		3.75	0	34.80	3.316	0.0000	0.0980	0.0000
Pelvis	NM		3.75	0	32.20	3.316	0.0000	0.2190	0.0000
						Total dose (rad) to bone surface			***0.0007***

Calculation of dose to remainder

Organ/ Position	MOSFETs	mV at 80 mAs	exam mAs	mV at exam mAs	CF [mV/R]	DCF	Absorbed Dose [rad]	
Rt Arm	A5	0	3.75	0	33.30	1.009	0.0000	
Lt Arm	NM		3.75	0	34.80	1.009	0.0000	
Esophagus	D4	0	3.75	0	34.80	1.009	0.0000	
Breast	D5	5	3.75	0.234375	38.50	1.009	0.0054	
Stomach	A2	2	3.75	0.09375	38.50	1.009	0.0022	
Liver	A4	1	3.75	0.046875	32.20	1.009	0.0274	
Bladder	A4	0	3.75	0	34.80	1.009	0.0000	
Colon	NM		3.75	0	31.98	1.009	0.0000	
Average Lung							0.0013	
Rt Lung	D3	0	3.75	0	32.00	1.046	0.0000	
Lt Lung	D1	2	3.75	0.09375	33.30	1.046	0.0026	
Average Ovary							0.0000	
Rt Ovary	A2	0	3.75	0	32.20	1.009	0.0000	
Lt Ovary	NM		3.75	0	31.18	1.009	0.0000	
Testes	NM		3.75	0	33.04	1.009	0.0000	
						Total dose (rad) to remainder-F		***0.0036***
						Total dose (rad) to remainder-M		***0.0036***

Calculation of dose to skin

Position	MOSFETs	mV at 80 mAs	exam mAs	mV at exam mAs	CF [mV/R]	DCF	Absorbed Dose [rad]
Entrance	A1	5	3.75	0.234375	32.90	1.009	0.0063
Exit	A2	0	3.75	0	28.80	1.009	0.0000
				Total dose (rad) to skin			***0.0031***

Subtotal Effective Dose ***0.0012*** rem

Female Effective Dose ***0.0013*** rem
Male Effective Dose ***0.0013*** rem

ESE RPO Chest 0.0113 R

	f(d)	g(b)
Leukemia	3.274E-06	132.3
Male Respiratory	8.569E-06	7.330949
Female Respiratory	8.569E-06	14.92601
Male Digestive	1.090E-05	1
Female Digestive	1.090E-05	1.74
Other	1.644E-05	1
Female Breast	1.644E-05	0.066005

Relative Risk

Leukemia	Male Respiratory	Female Respiratory	Male Digestive	Female Digestive	Other	Female Breast
1.000433	1.000063	1.000128	1.000011	1.000019	1.000016	1.000001

Table E-27. RAO Chest

Organ/ Position	MOSFETs	mV at 80 mAs	exam mAs	mV at exam mAs	CF [mV/R]	DCF	Absorbed Dose [rad]	Tissue Weighting Factor	Effective Dose [rem]
Esophagus	D4	0	3.75	0	34.80	1.009	0.0000	0.05	0.0000
Thyroid	A3	0	3.75	0	34.60	1.009	0.0000	0.05	0.0000
Breast	D1	5	3.75	0.234375	33.30	1.009	0.0062	0.05	0.0003
Average Lung							0.0013	0.12	0.0002
Rt Lung	D3	2	3.75	0.09375	32.00	1.046	0.0027		
Lt Lung	D4	0	3.75	0	34.80	1.046	0.0000		
Stomach	A3	2	3.75	0.09375	34.60	1.009	0.0024	0.12	0.0003
Liver	A2	2	3.75	0.09375	32.20	1.009	0.0026	0.05	0.0001
Bladder	A2	0	3.75	0	32.20	1.009	0.0000	0.05	0.0000
Colon	NM		3.75	0	31.98	1.009	0.0000	0.12	0.0000
Active Bone Marrow							0.0004	0.12	0.0000
Bone surface							0.0015	0.01	0.0000
Skin							0.0031	0.01	0.0000
Average Ovary							0.0000	0.20	0.0000
Rt Ovary	D1	0	3.75	0	33.30	1.009	0.0000		
Lt Ovary	NM		3.75	0	31.18	1.009	0.0000		
Testes	NM		3.75	0	33.04	1.009	0.0000	0.20	0.0000
Remainder-F							0.0067	0.05	0.0003
Remainder-M							0.0068	0.05	0.0003

Calculation of dose to active marrow

Organ/ Position	MOSFETs	mV at 80 mAs	exam mAs	mV at exam mAs	CF [mV/R]	DCF	Absorbed Dose [rads]	Fract. Active marrow assigned to MOSFET	Fract. * Absorbed dose [rad]
Spine middle	A1	1	3.75	0.046875	36.10	1.009	0.0011	0.1588	0.0002
Rt Arm	A4	2	3.75	0.09375	34.80	1.009	0.0024	0.0779	0.0002
Lt Arm	A3	0	3.75	0	34.60	1.009	0.0000	0.0779	0.0000
Pelvis	NM		3.75	0	32.20	1.009	0.0000	0.2191	0.0000
						Total dose (rad) to active marrow			***0.0004***

Calculation of dose to bone surface

Organ/ Position	MOSFETs	mV at 80 mAs	exam mAs	mV at exam mAs	CF [mV/R]	DCF	Absorbed Dose [rad]	Fract. Bone assigned to MOSFET	Fract. * Absorbed dose [rad]
Spine middle	A1	1	3.75	0.046875	36.10	3.316	0.0038	0.1850	0.0007
Rt Arm	A4	2	3.75	0.09375	34.80	3.316	0.0078	0.0980	0.0008
Lt Arm	A3	0	3.75	0	34.60	3.316	0.0000	0.0980	0.0000
Pelvis	NM		3.75	0	32.20	3.316	0.0000	0.2190	0.0000
						Total dose (rad) to bone surface			***0.0015***

Calculation of dose to remainder

Organ/ Position	MOSFETs	mV at 80 mAs	exam mAs	mV at exam mAs	CF [mV/R]	DCF	Absorbed Dose [rad]	
Rt Arm	A4	2	3.75	0.09375	34.80	1.009	0.0024	
Lt Arm	A3	0	3.75	0	34.60	1.009	0.0000	
Esophagus	D4	0	3.75	0	34.80	1.009	0.0000	
Breast	D1	5	3.75	0.234375	33.30	1.009	0.0062	
Stomach	A3	2	3.75	0.09375	34 60	1.009	0.0024	
Liver	A2	2	3.75	0.09375	32.20	1.009	0.0549	
Bladder	A2	0	3.75	0	32.20	1.009	0.0000	
Colon	NM		3.75	0	31.98	1.009	0.0000	
Average Lung							0.0013	
Rt Lung	D3	2	3.75	0.09375	32.00	1.046	0.0027	
Lt Lung	D4	0	3.75	0	34 80	1.046	0.0000	
Average Ovary							0.0000	
Rt Ovary	D1	0	3.75	0	33.30	1.009	0.0000	
Lt Ovary	NM		3.75	0	31.18	1.009	0.0000	
Testes	NM		3.75	0	33.04	1.009	0.0000	
						Total dose (rad) to remainder-F		***0.0067***
						Total dose (rad) to remainder-M		***0.0068***

Calculation of dose to skin

Position	MOSFETs	mV at 80 mAs	exam mAs	mV at exam mAs	CF [mV/R]	DCF	Absorbed Dose [rad]
Entrance	A1	5	3.75	0.234375	32.90	1.009	0.0063
Exit	A2	0	3.75	0	28.80	1.009	0.0000
				Total dose (rad) to skin			***0.0031***

Subtotal Effective Dose	***0.0010***	rem
Female Effective Dose	***0.0013***	rem
Male Effective Dose	***0.0013***	rem

ESE rao chest 0.0069 R

	f(d)	g(b)
Leukemia	3.196E-06	132.3
Male Respiratory	8.371E-06	7.330949
Female Respiratory	8.361E-06	14.92601
Male Digestive	1.065E-05	1
Female Digestive	1.064E-05	1.74
Other	1.605E-05	1
Female Breast	1.606E-05	0.066005

Relative Risk

Leukemia	Male Respiratory	Female Respiratory	Male Digestive	Female Digestive	Other	Female Breast
1.000423	1.000061	1.000125	1.000011	1.000019	1.000016	1.000001

LIST OF REFERENCES

Almen, A. and S. Mattsson (1996). "On the calculation of effective dose to children and adolescents." J. Radiol. Prot. **16**(2): 81-89.

Atherton, J. V. and W. Huda (1995). "CT doses in cylindrical phantoms." Phys. Med. Biol. **40**: 891-911.

Atherton, J. V. and W. Huda (1996). "Energy imparted and effective doses in computed tomography." Med. Phys. **23**(5): 735-741.

Ballinger, P. W. (1995). Merrill's Atlas of Radiographic Positions and Radiologic Procedures. St. Louis, Mosby.

BC (1998). Vital Statistics of the United States. Washington, D. C., U. S. Department of Commerce, Bureau of the Census; 1990-1998.

Beck, T. J. (1978). Quantification of current practice in the roentgenography of infants and children for absorbed dose calculations. Master's thesis, The Johns Hopkins University, Baltimore.

Beck, T. J. and M. Rosenstein (1979). Quantification of current practice in pediatric roentgenography for organ dose calculations. Rockville, MD, Food and Drug Administration.

Behrman, R. E. and V. C. Vaughan (1987). Nelson Textbook of Pediatrics. Philadelphia, PA, W.B Saunders.

BEIR (1990). Health Effects of Exposure to Low Levels of Ionizing Radiation. Washington, DC, National Research Council.

Bontrager, K. L. (1997). Textbook of Radiographic Positioning and Related Anatomy. St. Louis, Mosby.

Bouchet, L. G., W. E. Bolch, D. A. Weber, H. L. Atkins and J. W. Poston (1996). "A revised dosimetric model of the adult head and brain." J. Nucl. Med. **37**: 1226-1236.

Bouslog, J. (1935). "Roentgenologic studies of infants' gastrointestinal tract." Journal of Pediatrics **6**: 234.

Bower, M. W. (1997). A Physical Anthropomorphic Phantom of a One-Year-Old Child with Real-Time Dosimetry. Doctoral dissertation, University of Florida, Gainesville.

Bower, M. W. and D. E. Hintenlang (1998). "The characterization of a commerical MOSFET dosimeter system for use in diagnostic x-ray." Health Physics **75**(2): 197-204.

Boyd, E. (1927). "Growth of thymus; its relation to status thymicolymphaticus and thymic symptoms." American Journal of Diseases in Children **33**: 867.

Bunger, B. M., J. R. Cook, and M. K. Barrick (1981). "Life table methodology for evaluating radiation risk: An application based on occupational exposures." Health Physics **40**: 439-455.

Caffey, J. (1956a). "The first sixty years of pediatric roentgenology in the United States--1896 to 1956." The American Journal of Roentgenology Radium Therapy and Nuclear Medicine **76**: 437-454.

Caffey, J. (1956b). Pediatric X-Ray Diagnosis. Chicago, Year Book Publishers.

Cember, H. (1996). Introduction to Health Physics. New York, McGraw-Hill.

Chen, W. L., J. W. Poston, and G. G. Warner (1978). An Evaluation of the Distribution of Absorbed Dose in Child Phantoms Exposed to Diagnostic Medical X-Rays. Oak Ridge, TN, Oak Ridge National Laboratory.

Codmam, E. A. (1896). "Letter: Practical medical use of the x-ray." Boston Medical and Surgical Journal **135**: 50-51.

Cohrssen, J. J. and V. T. Covello (1989). Risk Analysis: A Guide to Principles and Methods for Analyzing Health and Environmental Risks. Washington, D.C., U.S. Council on Environmental Quality.

Constantinou, C., J. Cameron, L. DeWerd and M. Liss (1986). "Development of radiographic chest phantom." Medical Physics **13**(6): 917-921.

Conway, B. J., P. F. Butler, J. E. Duff, T. R. Fewell, R. E. Gross, R. J. Jennings, G. H. Koustenis, J. L. McCrohan, F. G. Rueter and C. K. Showalter (1984). "Beam quality independent attenuation phantom for estimating patient exposure from x-ray automatic exposure controlled chest examinations." Medical Physics **11**(6): 827-832.

Conway, B. J., J. E. Duff, T. R. Fewell, R. J. Jennings, L. N. Rothenberg and R. C. Fleischman (1990). "A patient-equivalent attenuation phantom for estimating patient exposure from automatic exposure controlled x-ray examinations of the abdomen and lumbo-sacral spine." Medical Physics **17**: 448-453.

Cox, P. (1896). "News of the week: Practical skiagraphy." Medical Record **49**: 524.

Cristy, M. (1980). Mathematical Phantoms Representing Children of Various Ages for Use in Estimates of Internal Dose. Oak Ridge, Tennessee, Oak Ridge National Laboratory.

Cristy, M. (1981). "Active bone marrow distribution as a function of age in humans." Phys. Med. Biol. **26**(3): 389-400.

Cristy, M. and K. F. Eckerman (1987). Specific Absorbed Fractions of Energy at Various Ages from Internal Photon Sources. Oak Ridge, Tennessee, Oak Ridge National Laboratory.

Davis, E. P. (1896). "Study of infant body and the pregnant womb by the roentgen ray." American Journal of Medical Science **III**: 263.

Drexler, G., W. Panzer, L. Widenmann, G. Williams and M. Zankl (1984). The Calculation of Dose from External Photon Exposures Using Reference Human Phantoms and Monte Carlo Methods. Part III: Organ Doses in X-Ray Diagnosis. Munich, Germany, Gesellschaft für Strahlenund Umweltforschung.

Eckerman, K. F., M. Cristy and J. C. Ryman (1996). The ORNL Mathematical Phantom Series, Unpublished.

Ellis, R. E., M. J. R. Healy, B. Shleien and T. Tucker (1975). A System for Estimation of Mean Active Bone Marrow Dose. Rockville, Maryland, Food and Drug Administration.

Fabrikant, J. I. (1990). "Factors that modify risks of radiation-induced cancer." Health Physics **59**(1): 77-87.

Gage, W. V. (1896). "News of the week: Need of caution in the use of Roentgen rays." Medical Record **50**: 307.

George, A. W. (1908). "Use of Roentgen ray in study of diseases in children." Boston Medical and Surgical Journal **158**: 381.

Gkanatsios, N. A. and W. Huda (1997). "Computation of energy imparted in diagnostic radiology." Med. Phys. **24**(4): 571-579.

Gladstone, D. J. and L. M. Chin (1991). "Automated data collection and analysis system for MOSFET radiation detectos." Med. Phys. **18**(3): 542-547.

Gladstone, D. J. and L. M. Chin (1995). "Real-time, in vivo measurement of radiation dose during radioimmunotherapy in mice using a miniature MOSFET dosimeter probe." Radiat. Res. **141**: 330-335.

Griscom, N. T. (1995). "The foundation and early meetings of The Society for Pediatric Radiology." Pediatric Radiology **25**: 657-660.

Griscom, N. T. (1996).In A History of the Radiological Sciences. Pediatric Radiology. R. Gagliardi and B. McClennan. Reston, Virginia, American Roentgen Ray Society: 345-367.

Griscom, N. T. and D. Jaramillo (1995). "Trends in papers presented at meetings of the Society for Pediatric Radiology." Pediatric Radiology **25**: 161-164.

Hart, D., D. Jones and B. Wall (1994). Normalized Organ Doses for Medical X-Ray Examinations Calculated Using Monte Carlo Techniques. Chilton, United Kingdom, National Radiological Protection Board.

Hart, D., D. G. Jones and B. F. Wall (1996). Coefficients for Estimating Effective Dose from Paediatric X-Ray Examinations. Chilton, United Kingdom, National Radiological Protection Board.

Haschke, F., S. J. Fomon and E. Ziegler (1981). "Body composition of a nine-year-old reference boy." Pediatric Research **15**: 847-849.

Henderson, S. G. (1942). "Gastrointestinal tract in healthy newborn infant." American Journal of Roentgenology Radium Therapy and Nuclear Medicine **48**: 302.

Henderson, S. G. and L. S. Sherman (1946). "Roentgen anatomy of skull of newborn infant." Radiology **46**: 107.

Herman, K. P., L. Geworski, T. Hatzhy, R. Lietz and D. Harder (1986). "Muscle and fat equivalent polyethylene-based phantom materials for x-ray dosimetry at tube voltages below 100 kV." Phys. Med. Biol. **31**(9): 1041-1046.

Herman, K. P., L. Geworski, M. Muth and D. Harder (1985). "Water equivalent phantom material for x-ray dosimetry from 10 to 100 kV." Phys. Med. Biol. **30**(11): 1195-1200.

Hickey, P. M. (1904). "The development of the skeleton." Transactions of the American Roentgen Ray Society: 120-127.

Hickey, P. M. (1906). "The development of the elbow." Transactions of the Americal Roentgen Ray Society: 55-61.

Hodges, P. C. (1933). "Estimation of cardiac size in children." Journal of the American Medical Association **101**: 914.

Hubbell, J. H. (1982). "Photon mass attenuation, and energy-absorption coefficients from 1 keV to 20 MeV." Int. J. Appl. Radiat. Isot. **33**: 1269-1290.

Huda, W. and J. V. Atherton (1995). "Energy imparted in computed tomography." Med. Phys. **22**(8): 1263-1269.

Huda, W., J. V. Atherton, D. Ware and W. Cumming (1997). "An approach for the estimation of effective radiation dose at CT in pediatric patients." Radiology **203**: 417-422.

Huda, W. and K. Bissessur (1990). "Effective dose equivalents, H_E, in diagnostic radiology." Med. Phys. **17**(6): 998-1003.

Huda, W. and N. A. Gkanatsios (1997). "Effective dose and energy imparted in diagnostic radiology." Med. Phys. **24**(8): 1311-1316.

Huda, W., B. Lentle, et al. (1989). "The effective dose equivalent in radiology." J. Can. Assoc. Radiol. **40**: 3-4.

Hughes, R. C., D. Huffman, J. V. Snelling, T. E. Zipperian, A. J. Ricco and C. A. Kelsey (1988). "Miniature radiation dosimeter for in vivo radiation measurements." Int. J. Radiation Oncology Biol. Phys. **14**: 963-967.

Hwang, J. M. L., R. L. Shoup and J. W. Poston (1976a). Modifications and Additions to the Pediatric and Adult Mathematical Phantoms. Oak Ridge, Tennessee, Oak Ridge National Laboratory.

Hwang, J. M. L., R. L. Shoup, G. G. Warner and J. W. Poston. (1976b). Mathematical Description of a One- and Five-Year-Old Child for Use in Dosimetry Calculations. Oak Ridge, Tennessee, Oak Ridge National Laboratory.

Hwang, J. M. L., R. L. Shoup and J. W. Poston (1976c). Mathematical Description of a Newborn Human for Use in Dosimetry Calculations. Oak Ridge, Tennessee, Oak Ridge National Laboratory.

ICRP (1975). Report on the Task Group on Reference Man. Elmsford, New York, Pergamon Press, International Commission on Radiological Protection.

ICRP (1977). Recommendations of the International Commission on Radiological Protection. Elmsford, New York, Pergamon Press, International Commission on Radiological Protection.

ICRP (1985). Quantitative Bases for Developing a Unified Index of Harm. Elmsford, New York, Pergamon Press, International Commission on Radiological Protection.

ICRP (1989). Age-Dependent Doses to Members of the Public from Intake of Radionuclides: Part I. Elmsford, New York, International Commission on Radiological Protection.

ICRP (1991). 1990 Recommendations of the International Commission on Radiological Protection. Elmsford, New York, Pergamon Press, International Commission on Radiological Protection.

ICRP (1995). Basic Anatomical and Physiological Data for Use in Radiological Protection: The Skeleton. Elmsford, New York; Pergamon Press, International Commission on Radiological Protection.

ICRU (1989). Tissue Substitutes in Radiation Dosimetry and Measurement. Bethesda, Maryland, International Commission on Radiation Units and Measurements.

ICRU (1993). Phantoms and Computational Models in Therapy, Diagnosis, and Protection. Bethesda, Maryland, International Commission on Radiation Units and Measurements.

Johnson, K. A. (1998). Measurement of Organ Doses of Pediatric Patients Undergoing Computed Tomography Examinations. Master's thesis, University of Florida, Gainesville.

Jones, D. G. and B. F. Wall (1985). Organ Doses from Medical X-Ray Examinations Calculated Using Monte Carlo Techniques, Chilton, United Kingdom, National Radiological Protection Board.

Josephi, M. G. (1935). "Measurements of size of hearts in normal children." American Journal of Diseases in Children **50**: 929.

Kirks, D. R. and N. T. Griscom (1998). Practical Pediatric Imaging: Diagnostic Radiology of Infants and Children. Philadelphia, PA, Lippincott-Raven.

Kodimer, K. A. (1995). Monte Carlo calculations of specific absorbed fractions and S values for anthropomorphic pediatric phantoms. Master's thesis, , Texas A&M University, College Station.

Kramer, R., M. Zankl, G. Williams and G. Drexler (1982). The Calculation of Dose from External Photon Exposures Using Reference Human Phantoms and Monte Carlo Methods. Part I: The Male (ADAM) and Female (EVA) Adult Mathematical Phantoms. Munich, Germany, Gesellschaft für Strahlenund Umweltforschung.

Lincoln, M. E. and R. Stillman (1928). "Studies of hearts of normal children; Roentgen-ray studies." American Journal of Diseases in Children **35**: 791.

Maresh, M. and A. H. Washburn (1940). "Paranasal sinuses from birth to late adolescence." American Journal of Diseases in Children **60**: 841.

Muirhead, C. R. and S. C. Darby (1987). "Modelling the relative and absolute risks of radiation-induced cancers." Journal of the Royal Statistical Society **A150**(Part 2): 83-118.

Murphy, G. P., W. Lawrence and R. E. Lenhard. (1995). American Cancer Society Textbook of Clinical Oncoilogy. Washington, D. C., American Cancer Society.

NCRP (1980). Influence of Dose and its Distribution in Time on Dose-Response Relationships for Low-LET Radiations. Bethesda, Maryland, National Council on Radiation Protection and Measurements

NCRP (1987). Ionizing Radiation Exposure of the Population of the United States. Bethesda, Maryland, National Council on Radiation Protection and Measurements.

NCRP (1989). Exposure of the U.S. Population from Diagnostic Medical Radiation. Bestheda, Maryland, National Council on Radiation Protection and Measurements.

Nelson, W. R. and R. H. Hirayama (1985). The EGS4 Code System. Stanford, Stanford Linear Accerlerator Center.

NRC (1983). Risk Assessment in the Federal Government: Managing the Process. Washington, D. C., National Research Council, National Academy Press.

Poston, J. W. (1993). "Application of the effective dose equivalent to nuclear medicine patients." J. Nucl. Med. **34**(4): 714-716.

Ramani, R., O'Brien (1997). "Clinical dosimetry using MOSFETs." Int. J. Radiation Oncology Biol. Phys. **37**: 959-964.

Rosenstein, M. (1976a). Handbook of Selected Organ Doses for Projections Common in Diagnostic Radiology. Rockville, Maryland, Food and Drug Administration.

Rosenstein, M. (1976b). Organ Doses in Diagnostic Radiology. Rockville, Maryland, Food and Drug Administration.

Rosenstein, M. (1988). Handbook of Selected Tissue Doses for Projections Common in Diagnostic Radiology. Rockville, Maryland, Food and Drug Administration.

Rosenstein, M., T. J. Beck and G. G. Warner (1979). Handbook of Selected Organ Doses for Projections Common in Pediatric Radiology. Rockville, Maryland, Food and Drug Administration.

Rosenstein, M., O. H. Suleiman, R. L. Burkhart, S. H. Stern and G. Williams (1992). Handbook of Selected Tissue Doses for the Upper Gastrointestinal Fluoroscopic Examination. Rockville, Maryland, Food and Drug Administration.

Seibert, J. A., G. T. Barnes and R. G. Gould (1994). Specification, Acceptance Testing and Quality Control of Diagnostic X-Ray Imaging Equipment. Woodbury, Connecticut, American Institute of Physics.

Sharko, G. A. and D. M. Wilmot (1987). Pediatric Imaging for the Technologist. New York, Springer-Verlag.

Shimizu, Y., H. Kato, W. J. Schull, D. L. Preston, S. Fujia and D. A. Pierce (1987). Life Span Study Report 11: Part 1. Comparison of Risk Coefficients for Site-Specific Cancer Mortality Based on the DS86 and T65D Shield Kerma and Organ Dose. Hiroshima, Japan, Radiation Effects Research Foundation.

Shleien, B. (1973). A Review of Determinations of Radiation Dose to the Active Bone Marrow from Diagnostic X-Ray Examinations. Rockville, Maryland, Food and Drug Administration.

Shrimpton, P. C., D. G. Jones, M. C. Hillier, B. F. Wall, J. C. Le heron and K. Faulkner (1991). Survey of CT Practice in the UK. Part 2: Dosimetric Aspects. Didcot, United Kingdom, National Radiological Protection Board.

Smith, R. M. (1951). "Medicine as science: Pediatrics." The New England Journal of Medicine **244**: 176-181.

Snyder, W. S., M. R. Ford and G. G. Warner (1978). Estimates of Specific Absorbed Fractions for Photon Sources Uniformly Distributed in Various Organs of a Heterogeneous Phantom. New York, New York, Society of Nuclear Medicine.

Snyder, W. S., M. R. Ford, G. G. Warner and H. L. Fisher (1969). Estimates of Absorbed Fractions for Monoenergetic Photon Sources Uniformly Distributed in Various Organs of a Heterogeneous Phantom. New York, New York, Society of Nuclear Medicine.

Sosman, M. C. (1951). "Fifty years of medical progress: Medicine as a science: Roentgenology." New England Journal of Medicine **244**: 552.

Soubra, M., J. Cygler and G. Mackay (1994). "Evaluation of a dual bias metal oxide-silicon semiconductor field effect transistor detector as a radiation dosimeter." Medical Physics **21**(4): 567-572.

Spiegel, P. K. (1995). "The first clinical x-ray made in America." American Journal of Radiology **164**: 241-243.

Stabin, M. G. (1996). "MIRDOSE: Personal computer software for internal dose assessment in nuclear medicine." J. Nucl. Med. **37**: 538-546.

Stern, S. H., M. Rosenstein, L. Renaud and M. Zankl (1995). Handbook of Selected Tissue Doses for Fluoroscopic and Cineangiographic Examination of the Coronary Arteries. Rockville, Maryland, Food and Drug Administration.

Swischuk, L. E. (1997). Imaging of the Newborn, Infant, and Young Child. Baltimore, Williams & Wilkins.

Thomas, D., S. Darby, F. Fagnani, P. Hubert, M. Vaeth and K. Weiss (1992). "Definition and estimation of lifetime detriment from radiation exposures: Principles and methods." Health Physics **63**: 250-272.

UNSCEAR (1977). Radiation Carcinogenesis in Man. New York, New York, United Nations Scientific Committee for the Effects of Atomic Radiation.

UNSCEAR (1986). Genetic and Somatic Effects of Ionizing Radiation. New York, New York, United Nations Scientific Committee for the Effects of Atomic Radiation.

Vaeth, M. and D. A. Pierce (1990). "Calculating excess lifetime risk in relative risk models." Environmental Health Perspectives **87**: 83-94.

Vettese, F., C. Donichak, P. Bourgeault and G. Sarrabayrouse (1996). "Assessment of a new p-MOSFET usable as a dose rate insensitive gamma dose sensor." IEEE Transactions on Nuclear Science **43**(3): 991-996.

White, D. R. (1977). "The formulation of tissue substititue materials using basic interaction data." Phys. Med. Biol. **22**: 889-999.

White, D. R., C. Constantinou and R. J. Martin (1986). "Foamed epoxy resin-based substitutes." Br. J. Radiol. **59**: 787-790.

White, D. R., R. J. Martin and R. Darlison (1977). "Epoxy resin-based tissue substitutes." Br. J. Radiol. **50**: 814-821.

Zankl, M., N. Petoussi, R. Veit, G. Drexler and H. Fendel (1989). In BIR Report No. 20. Organ Doses for a Child in Diagnostic Radiology; Comparison of a Realistic and a MIRD-Type Phantom. B. M. Moores, B. F. Wall, H. Eriskdat and H. Schibilla. London, United Kingdom, British Institute of Radiology: 196-198.

BIOGRAPHICAL SKETCH

Kathleen Marie (Buckley) Hintenlang was born in Saranac Lake, New York, in 1964 to Thomas and Barbara Buckley. She attended Saranac Lake Central High School from 1978 to 1982, graduating in 1982 with a Regent's diploma concentrated on mathematics and science. She entered Rochester Institute of Technology, Rochester, New York, in September of 1982. Following three clinical internships, she graduated from the nuclear medicine program in the College of Science with a Bachelor of Science degree in May, 1987. She entered the medical physics program in the College of Engineering's Nuclear Engineering Sciences Department at the University of Florida in January of 1988. With a research assistantship provided by the Department of Radiology and under the supervision of Dr. Clyde Williams and Dr. Libby Brateman, she graduated with a Master of Science degree in May, 1990. She accepted the position of Assistant Radiation Control Officer for the University in October, 1989. In 1992, she married Dr. David E. Hintenlang, Associate Professor in the Nuclear and Radiological Engineering Department. They have one daughter, Lauren Lea, born in March of 1994 and one son, Hunter Austin, born in August of 1997. In November of 1994, she was admitted to candidacy in the Environmental Engineering Sciences Department, with grants provided by the Children's Miracle Network Foundation and under the supervision of Dr. Emmett Bolch and Dr. Jon Williams, to perform the research leading to a Doctor of Philosophy degree. She was granted dual certification by the American Board of Radiology in the specialties of diagnostic radiological physics and medical nuclear physics in June of 1997.

I certify that I have read this study and that in my opinion it conforms to acceptable standards of scholarly presentation and is fully adequate, in scope and quality, as a dissertation for the degree of Doctor of Philosophy.

W. Emmett Bolch Jr., Chairman
Professor of Environmental
Engineering Sciences

I certify that I have read this study and that in my opinion it conforms to acceptable standards of scholarly presentation and is fully adequate, in scope and quality, as a dissertation for the degree of Doctor of Philosophy.

Jonathan L. Williams
Professor of Radiology

I certify that I have read this study and that in my opinion it conforms to acceptable standards of scholarly presentation and is fully adequate, in scope and quality, as a dissertation for the degree of Doctor of Philosophy.

Lawrence T. Fitzgerald
Associate Professor of Nuclear
and Radiological Engineering

I certify that I have read this study and that in my opinion it conforms to acceptable standards of scholarly presentation and is fully adequate, in scope and quality, as a dissertation for the degree of Doctor of Philosophy.

Randolph L. Carter
Professor of Statistics

I certify that I have read this study and that in my opinion it conforms to acceptable standards of scholarly presentation and is fully adequate, in scope and quality, as a dissertation for the degree of Doctor of Philosophy.

Thomas L. Crisman
Professor of Environmental
Engineering Sciences

This dissertation was submitted to the Graduate Faculty of the College of Engineering and to the Graduate School and was accepted as partial fulfillment of the requirements for the degree of Doctor of Philosophy.

December, 1998

Winfred M. Phillips
Dean, College of Engineering

Mihran J. Ohanian
Dean, Graduate School

LD
1780
1998
.H6666

UNIVERSITY OF FLORIDA
3 1262 06554 9474